Characterisation of Supported and Unsupported 12-Heteropolyacids

Thesis

Characterisation of Supported and Unsupported 12-Heteropolyacids

Glyn Derrick B.Sc. (Hons), M.Sc.

A Thesis Presented to The Open University for the
Degree of Doctor of Philosophy

Department of Chemistry and Analytical Sciences
September, 2008

I certify that all material in this thesis which is not my own has been identified and that no material has been previously submitted and approved for the award of a Degree by this or any other University.

Submission date: 29 Sept 2008
Date of award: 4 Feb 2009

Acknowledgements

Firstly, I would like to thank my supervisors at The Open University, Prof. Frank Berry and Dr. Michael Mortimer, for all their help and advice. Their continued support and encouragement throughout my time at The Open University has been invaluable. I would also like to thank Dr. Gordon Haining, of BP Chemicals, for his guidance during this project and supplying the catalyst samples that were investigated.

I am also grateful to Dr. J.F. Marco (Instituto de Química-Física 'Rocasolano', Consejo Superior de Investigaciones Cientificas, Serrano 119, 28006 Madrid, Spain) for recording the XPS data discussed in Chapter 6.

I would like to take this opportunity to thank the technical staff Gordon Oates, Allen Bowden, Graham Jeffs, Colin Haynes and Pravin Patel without whose help the practical aspects of this project would not have been possible.

I gratefully acknowledge the funding received for this project from EPSRC and BP Chemicals.

My studies here would not have been the same without the friends both within and outside of the chemistry department. I will always remember the great times spent with Gosia, Mike, Patrick, Sharon, Allen, Huma, Vai, Rachel, Vincenzo and Nanda.

I would also like to thank my parents, Graham and Rosalie, and my sisters, Sarah and Hayley, for all their kindness and support.

Finally, to my wife, Marielle, a special thank you for all her patience, love and encouragement over the past four years.

Abstract

Phase transformations of $H_4[SiW_{12}O_{40}]\cdot xH_2O$ in the temperature range 25 - 900 °C have been investigated and characterised by differential thermal analysis (DTA), thermogravimeteric analysis (TGA), X-ray powder diffraction (XRD), ^{29}Si MAS NMR and FT-IR spectroscopy. Dehydration occurs between 25 - 300 °C to give three crystalline hydrated states ($x = 24$, 14 and 6) and finally an anhydrous form.

Silica-supported $H_4[SiW_{12}O_{40}]$ with 25 wt % loading has been studied using DTA, TGA, XRD, FT-IR, ^{29}Si MAS NMR and X-ray photoelectron spectroscopy (XPS). It is found that the Keggin anion remains unchanged and is well dispersed on the support. A chemically distinct interfacial $H_4[SiW_{12}O_{40}]$ species is identified by XPS and is attributed to perturbed tungsten atoms within Keggin anions in direct contact with the silica-support.

Used catalysts have been characterised by DTA (under nitrogen), TGA, XRD, ^{29}Si MAS NMR, FT-IR and XPS : the basic Keggin cage structure is unaffected by standard reactor conditions and lifetimes. TGA and DTA studies carried out under flowing air revealed two forms of coke deposited on the catalyst : hard and soft coke. Extraction with dichloromethane allowed the removal of soft coke (TGA removal range 170-370 °C) but was unable to remove hard coke (TGA removal range 370-570 °C). Removal of hard coke from industrial catalysts was attempted using aerobic oxidisation at 400 °C, the complete oxidisation of the coke occurred after 6 hours.

The acidic sites of $H_4[SiW_{12}O_{40}]$, $H_3[PW_{12}O_{40}]$ and $H_4[SiW_{12}O_{40}]/H_3[PW_{12}O_{40}]$

(1 : 1 molar ratio), both silica-supported and non-supported, were characterised using solid state ^{13}C NMR experiments for adsorbed acetone. For all three solid acids CP/MAS NMR experiments revealed the presence of isolated and hydrated acidic protons. The isolated acidic protons are restricted in mobility compared to the hydrated acidic protons. A reduction in the acidity of the hydrated acidic proton was observed when the 12-heteropolyacid compounds were supported on silica.

Contents

Chapter 1

Introduction

Concern, as well as legislation, associated with environmental issues has initiated activity within the chemical and petrochemical industries to develop more environmentally friendly processes.

Until 2001, ethyl acetate was produced by BP chemicals using traditional acid-catalysed esterification of ethanol and acetic acid:

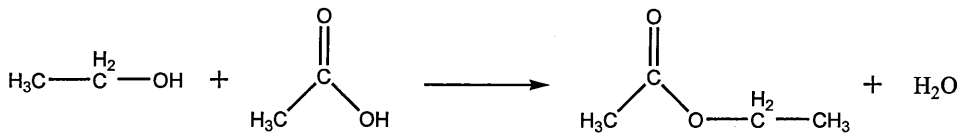

(1.1)

In 2001, a full-scale commercial plant was commissioned to prepare ethyl acetate using a continuous gas-phase process involving ethene and acetic acid over a solid catalyst. This process, known as the AdVanced Acetate esters by Direct Addition (AVADA) process, also depended on the presence of water and was catalysed by a fixed-bed solid acid catalyst composed of a strong acid on a silica support:

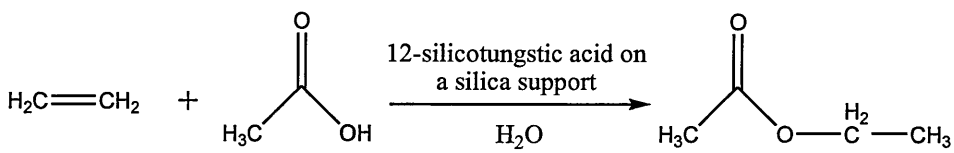

(1.2)

The AVADA process resulted in both environmental and industrial benefits. Environmentally, the issues raised by homogeneous catalysts, such as their corrosive and toxic nature, were addressed. From a commercial standpoint, the product quality was improved and the expensive ethanol feedstock was no longer required. However, the role played by the solid acid catalyst in the AVADA process still remains not well

understood. In particular, issues such as the nature of the interaction between the strong acid and the silica support, the extent of agglomeration of the strong acid on the silica support, changes in the catalyst over its lifetime and how factors such as exothermic events in the plant affect the industrial catalyst, remain the subject of uncertainty. These issues, and others, are investigated in the work reported here using techniques including thermal analysis, nuclear magnetic resonance spectroscopy, X-ray powder diffraction and FT-IR spectroscopy. As a starting point a detailed investigation is carried out for 12-silicotungstic acid and the results are compared with those reported in the literature for 12-phosphotungstic acid which is the most widely studied of the 12-heteropolyacids.

Chapter 2 starts with general comments concerning 12-heteropolyacids and this account is then followed by a specific review of 12-phosphotungstic and 12-silicotungstic acid. A brief overview of the catalytic function of 12-heteropoyacids then leads to a more detailed review of silica-supported 12-phosphotungstic acid. Information relating to silica-supported 12-silicotungstic acid, which is relatively sparse in the literature, is incorporated into this review.

The underlying principles of two of the main characterisation techniques used in the work reported in this thesis, X-ray powder diffraction (XRD) and magic-angle spinning nuclear magnetic resonance spectroscopy (MAS NMR), are described in Chapter 3. In Chapter 4, descriptions are given of the materials and the experimental procedures used in this thesis. Systematic errors[1] that are relevant to the XRD powder patterns recorded in this work are outlined.

Chapter 5 describes detailed investigations of the various hydrated phases of 12-silicotungstic acid by thermal analysis, X-ray powder diffraction, ^{29}Si MAS NMR and FT-IR spectroscopy. The results achieved provide a firm basis for the interpretation of other results in this thesis. New and used samples of industrial silica-supported 12-silicotungstic acid, obtained from BP Chemicals at Saltend in Hull, are investigated in Chapter 6. In addition to the techniques used in Chapter 5, X-ray photoelectron spectroscopy (XPS) is shown to provide unique information concerning the interaction between 12-silicotungstic acid and the silica surface on which it is supported.

In Chapter 7 the possibility of fine tuning the acidity of 12-heteropolyacids is reported through the preparation of 12-phosphotungstic acid and 12-silicotungstic acid mixed compounds followed by characterisation using thermal analysis, XRD, ^{31}P MAS NMR and FT-IR spectroscopy. The interaction between isotopically labelled 2-^{13}C-acetone (99% ^{13}C enriched) and the acidic protons of both bulk and silica-supported 12-heteropolyacids is also investigated using ^{13}C MAS and CPMAS NMR spectroscopy. Direct information on acid strength and the mobility of acid protons is obtained.

Chapter 8 provides a summary of the main findings reported in this thesis, and makes suggestions for further work.

References

(1) Shirley, R. *Accuracy in Powder Diffraction* **1980**, *567*, 361-382.

Chapter 2

Background information :

12-heteropolyacids

2.1 Introduction

A wide range of publications and patents exist with regards to polyoxometalates and their applications in fuel cells,[1] selective electrodes[2] and electrically conductive polymers.[3] However, over 80% of the polyoxometalate patent applications are concerned with catalysis[4] and this is by far the most important area of polyoxometalate chemistry. It is the structural characteristics and multi-functionality of polyoxometalates that make them such advantageous catalysts.

Polyoxometalates are a class of anionic species with structures based on metal-oxygen clusters with dimensions in the nanoscale region. They represent a diverse range of species and can be isolated as solids using an appropriate counter ion (H^+, NH_4^+, alkali metal cations). As might be expected, the chemistry and catalytic properties of polyoxometalates have been extensively reviewed, including monographs by Souchay,[5] Pope,[6] Kozhevnikov[7] and Moffat.[8]

Based on their chemical composition, polyoxometalates can be separated into two sub-groups, isopolyanions ($[M_mO_y]^{p-}$) and heteropolyanions ($[X_xM_mO_y]^{q-}$). The latter are the main subject of this review. In the general formula for heteropolyanions M represents an addenda atom, typically molybdenum or tungsten, and X represents a heteroatom which can be almost any element in the Periodic Table. Current nomenclature[6] treats heteropoly anions as quasi-coordination complexes where the heteroatom is considered as the central atom of the complex and the addenda atoms are the ligands. In the chemical formulae of heteropoly anions, the heteroatoms are placed before the addenda atoms, and the counter cations before the heteroatom. The heteropoly anion is placed in square brackets and is thus separate from the

counter cations. For example, silicotungstic acid is represented as $H_4[SiW_{12}O_{40}]$, where the heteroatom is silicon, the addenda atoms are tungsten and the counter cations are the protons.

The work in this thesis, as already indicated in the introductory chapter, is concerned with the acid forms of just two isostructural heteropoly anions which can be represented by the general formula $[XW_{12}O_{40}]^{n-}$ where X is either phosphorous ($n = 3$) or silicon ($n = 4$). The literature review that follows is thus largely restricted to these two so-called 'strong acids'; that is 12-phosphotungstic acid ($H_3[PW_{12}O_{40}]$), and 12-silicotungstic acid ($H_4[SiW_{12}O_{40}]$). These acids have a variety of hydrated forms and these are represented by indicating $\cdot xH_2O$ in the respective formulae.

2.2 A 12:1 heteropoly anion : the Keggin structure

Heteropoly salts were first discovered in 1826 by Berzelius when he prepared ammonium 12-molybdophosphate, $(NH_4)_3[PMo_{12}O_{40}]$, in a hydrated form.[9] However, the structure of this type of compound and, in particular, that of the heteropoly anion remained unsolved for more than 100 years. In 1933, the X-ray powder diffraction pattern of a hydrate of 12-phosphotungstic acid, represented as $H_3[PW_{12}O_{40}]\cdot 5H_2O$, was investigated by J.F. Keggin[10] and a structure was proposed for the $[PW_{12}O_{40}]^{3-}$ anion where WO_6 octahedra were connected through the sharing of both edges and corners. This type of structure is now known as the Keggin structure (Figure 2.1) and it is adopted by many polyoxometalates. The importance of this structure is demonstrated by the fact that approximately two-thirds of the applied polyoxometalate literature describes applications based on Keggin-type

heteropoly acids.[4]

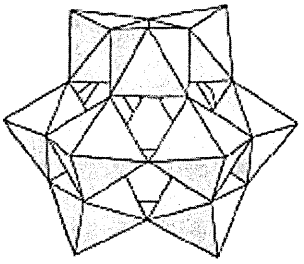

Figure 2.1 Structure of the Keggin anion.

The central heteroatom in a Keggin structure is tetrahedrally bonded to 4 oxygen atoms. Surrounding this central tetrahedron are twelve metal atoms each within an octahedron of oxygen atoms. The structure is often referred to as a 12:1 type heteropoly anion. The twelve octahedral metal-oxygen clusters are arranged in four groups, each of which corresponds to M_3O_{13}. In each of these 'triplets', the metal octahedra share one edge with each of the other two octahedra resulting in one oxygen atom common to all three octahedra. This common oxygen atom is also shared with the central tetrahedral XO_4 group.

The 40 oxygen atoms present in the Keggin structure exist in four different environments. The chemically inequivalent oxygen atoms can be discriminated by ^{17}O solution state NMR spectroscopy.[11] A schematic structure of the Keggin $[PW_{12}O_{40}]^{3-}$ anion is shown in Figure 2.2. The different oxygen environments are labelled O_a, O_b, O_c and O_d and the four W_3O_{13} 'triplets' are shown as an outline. The different oxygen environments can be described as representing i) the four internal P-O-W oxygen atoms (O_a), ii) the twelve corner-bridging quasi-linear W-O-W oxygen atoms connecting two different W_3O_{13} groups (O_b), iii) twelve edge-bridging

angular W-O-W oxygen atoms shared by the octahedra within a W_3O_{13} group (O_c), and iv) twelve terminal W=O oxygen atoms (O_d). The structure gives rise to characteristic infrared bands[6] in the range 600-1100 cm^{-1}.

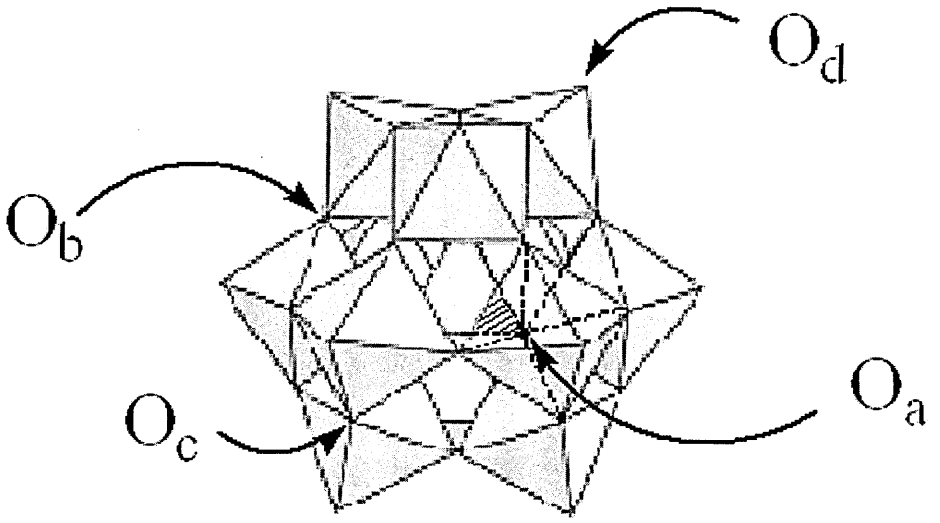

Figure 2.2 Structure of the Keggin anion $[PW_{12}O_{40}]^{3-}$, showing the central phosphorous tetrahedron (red), the four W_3O_{13} 'triplets' (grey) and the four oxygen environments. O_a : internal P-O-W, O_b : corner bridging W-O-W, O_c : edge-bridging W-O-W and O_d : terminal W=O. (Diagram modified from reference 12.)

Five possible isomers of the Keggin unit are known. The Keggin unit shown in Figure 2.2 represents the α isomer. Rotation through an angle of 60 ° of one of the W_3O_{13} groups results in the structure of the β isomer.[13] This is demonstrated in more detail by the rotation of the shaded area in Figure 2.3.[12] Three further isomers, that is, γ, δ and ε, are generated[12] by successive rotation of each of the remaining M_3O_{13} groups through 60°.

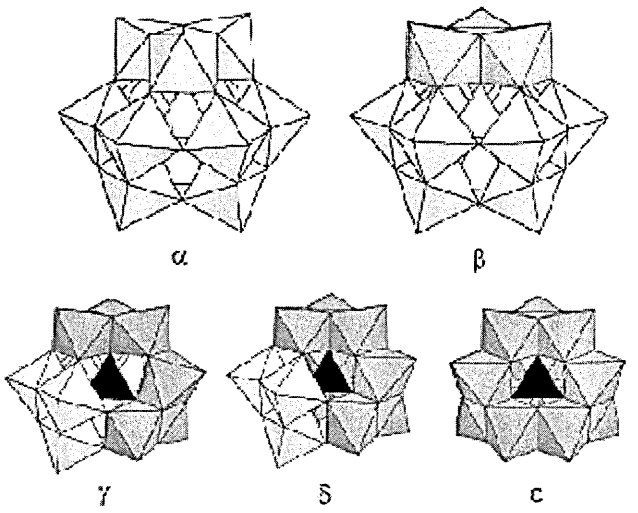

Figure 2.3 The five possible isomers of the Keggin anion structure: $[XM_{12}O_{40}]^{n-}$. (This diagram is modified from reference 12)

The α and the β isomers are considered to have similar energies, although the α isomer is probably more stable since isomerisations for Keggin heteropolytungstates and molybdates all occur in the β → α direction.[12, 13] The γ, δ and ε isomers of Keggin-type heteropoly anions are all less stable than the α and β forms.[6]

One of the key characteristics of heteropoly acids is their ability to be reversibly reduced. This reduction can be controlled through the addition of specific numbers of electrons depending on the pH and the applied potential. The partial reduction of the addenda atoms in heteropoly anions yields a characteristic intense blue colour; these species are known as "heteropoly blues". More highly reduced heteropoly anions, especially under acidic conditions, are transformed to brown species that are less sensitive to oxidation than the "blues".

2.3 Characterisation of 12-heteropolyacids

2.3.1 General features : thermal characteristics and acidity

A combination of techniques has been used in the characterisation of 12-heteropolyacids, thermal analysis being the most common. Thermal analysis profiles recorded from 12-heteropolyacids show various stable, single phases corresponding to different hydration states, the number of which depends on the acid under investigation. Once identified, these single-phase hydrated states have been studied in more detail using techniques such as X-ray and neutron diffraction, FT-IR and multinuclear solid-state NMR spectroscopy. A few general comments can be made regarding the hydrated states of 12-heteropolyacids and their thermal characteristics, although the temperatures at which transitions occur depend on the hetero- and addenda- atoms present.

The waters of hydration present in the higher hydrates of 12-heteropolyacids can be described as "zeolitic" in nature; that is, the water molecules are easily (and reversibly) removed from the solid acid at relatively low temperatures. The remaining waters of hydration are structural in nature and require a higher temperature for their removal. With the removal of the structural waters of hydration, an anhydrous phase remains consisting of the Keggin anion and protons as the counter cations. The acidic protons remain located on the Keggin unit until a temperature is reached at which an interaction occurs with one of the oxygen atoms of the Keggin anion such that protons are then lost in the form of water molecules. At temperatures not significantly higher than those for the loss of these constitutional water molecules, the Keggin unit decomposes into a mixture of its oxides.

General comments can also be made concerning the acidity of 12-heteropolyacids. The acid strength of 12-heteropolyacids have been investigated in detail using Hammett indicator tests,[14] temperature-programmed desorption (TPD)[15] and microcalorimetry.[16] It is generally accepted that the acid sites in 12-heteropolyacids are purely Brønsted in nature.[17] Hammett indicator tests[14] have also suggested that some anhydrous forms of 12-heteropolyacids are superacidic (that is, having a Hammett acidity (H_0) value exceeding that of 100% sulphuric acid). However, the use of Hammett indicators to characterise the surface acidity of solid acids has been criticised because the surface acidity function H_o, in contrast to that measured in solution, has no explicit physico-chemical meaning.[18]

In contrast to Hammett indicator tests, results obtained from H/D exchange between isobutene and anhydrous 12-heteropolyacids are consistent with the acid strengths of these species being comparable to that of a non-superacidic zeolite.[19] TPD has also been used to investigate the acid strengths of crystalline 12-heteropolyacids and these were found to decrease in the series $H_3[PW_{12}O_{40}]\cdot xH_2O > H_4[SiW_{12}O_{40}]\cdot xH_2O \geq H_3[PMo_{12}O_{40}]\cdot xH_2O > H_4[SiMo_{12}O_{40}]\cdot xH_2O$.[15] This order is identical to that found in solution as determined by the heteroconjugation (hydrogen bonding) of chloral hydrate with the heteropoly anion using NMR spectroscopy.[20] $H_3[PW_{12}O_{40}]\cdot xH_2O$ has also been found to be more acidic than $H_4[SiW_{12}O_{40}]\cdot xH_2O$ in microcalorimetry studies.[16]

2.3.2 12-Phosphotungstic acid

This acid, particularly in its hydrated form, is of interest both fundamentally and industrially and is the most studied of the 12-heteropolyacids.

Thermal analysis has been widely used, in combination with other techniques, to highlight and characterise five hydrated states of $H_3[PW_{12}O_{40}]\cdot xH_2O$ as well as an anhydrous phase.[21-23] The results from neutron diffraction,[22, 24-27] X-ray diffraction,[21] multinuclear NMR spectroscopy[28-32] and FT-IR spectroscopy[33-41] which are particularly relevant to the work in this thesis are discussed below.

Thermal analysis

Thermal analytical methods such as thermogravimeteric analysis (TGA), differential thermal analysis (DTA) and differential scanning calorimetery (DSC) have been used to investigate the thermal stability of hydrated forms of $H_3[PW_{12}O_{40}]\cdot xH_2O$.[21, 22]

Mioc and co-workers studied the effects of temperature on $H_3[PW_{12}O_{40}]\cdot 29H_2O$ from room temperature up to 1150°C using DTA and TGA methods.[21] Three events were observed in the DTA data: firstly an endothermic doublet occurred in the region of 30 to 50°C, followed by a second endothermic peak occurring between 175 and 230°C, and finally an exothermic peak was observed at a temperature in the region of 600°C. A glass transition temperature (T_g) anomaly at approximately 410°C was also noted. TGA data were used in the interpretation of these results.

The low temperature endothermic doublet observed in the region of 30 to 50°C was resolved into two components at approximately 30 and 40°C. The TGA data were consistent with the formation of $H_3[PW_{12}O_{40}]\cdot 21H_2O$ and $H_3[PW_{12}O_{40}]\cdot 14H_2O$, respectively, at these temperatures. The latter phase then rapidly lost a further eight waters of crystallisation on heating from 40 to 60°C, forming $H_3[PW_{12}O_{40}]\cdot 6H_2O$. The water molecules in this hydrate were taken to be structural in nature and the

phase was stable up to 170°C. Between 170 and 240°C, further loss of water occurred to give the anhydrous phase which was stable up to a temperature of 410°C. It was in the region of this temperature that the T_g anomaly occurred as a broad, exothermic peak in the DTA data. The anomaly was associated with the exothermic process of water formation and the endothermic process of water loss occurring simultaneously. The formation of water was taken to occur through the interaction of the acidic protons and one of the oxygen atoms of the Keggin anion. This corresponded to the loss of 1 - 1.5 constitutional water molecules in the TGA data. Decomposition of the solid anhydride occurred between 580 and 620°C followed by bronze formation; that is the formation of tungsten and phosphorous oxides.

Other TGA investigations[22] have established that a hydrated state corresponding to $H_3[PW_{12}O_{40}]\cdot 3H_2O$ can be isolated.

Neutron diffraction

In the original powder X-ray structural investigation of $H_3[PW_{12}O_{40}]$ Keggin proposed a structure based on a pentahydrate.[10] Subsequently, a re-determination of the structure using X-ray and neutron diffraction data from a single crystal was carried out by Brown, Noe-Spirlet, Busing and Levy.[24] The cubic structure with space group P*n*3*m* suggested by Keggin was confirmed through the neutron diffraction data. The cubic unit cell length of 12.140 (±0.005) Å was refined more accurately as 12.1506(5) Å. The major difference between the neutron diffraction study and Keggin's original work was that the neutron diffraction data showed the "pentahydrate" proposed by Keggin was in fact the hexahydrate of formula

$H_3[PW_{12}O_{40}]\cdot 6H_2O$. An important aspect of the structure is that the six structural water molecules are paired in nearly planar diaqua-hydrogen ions, $H_5O_2^+$, in which the acidic proton is hydrogen bonded to each of two water molecules through the oxygen atom as shown in Figure 2.4. An alternative formulation for the acid is, therefore, $[H_5O_2^+]_3[PW_{12}O_{40}]^{3-}$.

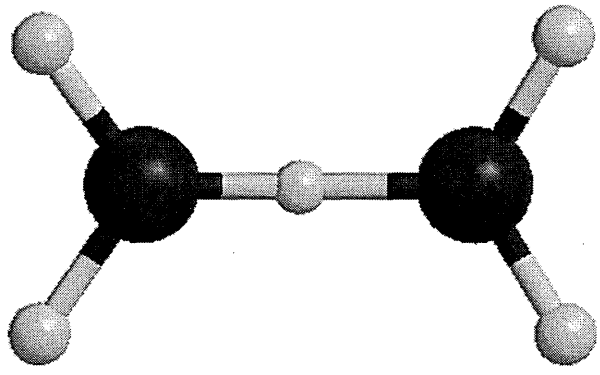

Figure 2.4 The nearly planar diaqua-hydrogen ion, $H_5O_2^+$.

The cubic unit cell of $H_3[PW_{12}O_{40}]\cdot 6H_2O$ contains two formula units ($Z = 2$) and the acidic hydrogen atoms of $H_5O_2^+$ are located at the centres of each face and each edge of the unit cell. If just the central phosphorous atoms of the Keggin anion are considered then these form a body-centred cubic array. (In this view, the central Keggin anion has a different orientation to those anions at the corners.) To describe the hydrogen bonding within the structure it is useful to consider it as consisting of two interpenetrating primitive cubic structures formed by the Keggin anions. The two cubic sub-structures have no hydrogen bonding between them; that is one structure involves hydrogen bonding with the face-centred $H_5O_2^+$ ions and the other with the edge-centred $H_5O_2^+$ ions. The details of a typical hydrogen-bonding arrangement are shown in Figure 2.5. This figure represents a view looking down the *c* axis of one sub-structure with a face-centred $H_5O_2^+$ ion. Each water molecule

in this ion is hydrogen bonded to two Keggin anions through one of the terminal W=O groups so that, overall, the acidic proton is shared between four Keggin anions. The hydrogen atoms of each water molecule are slightly twisted (~ 4 °) above and below the plane. For clarity, the figure does not show the further interconnections of the Keggin anions with $H_5O_2^+$ ions located in the centres of the vertical and horizontal (as drawn) cell faces.

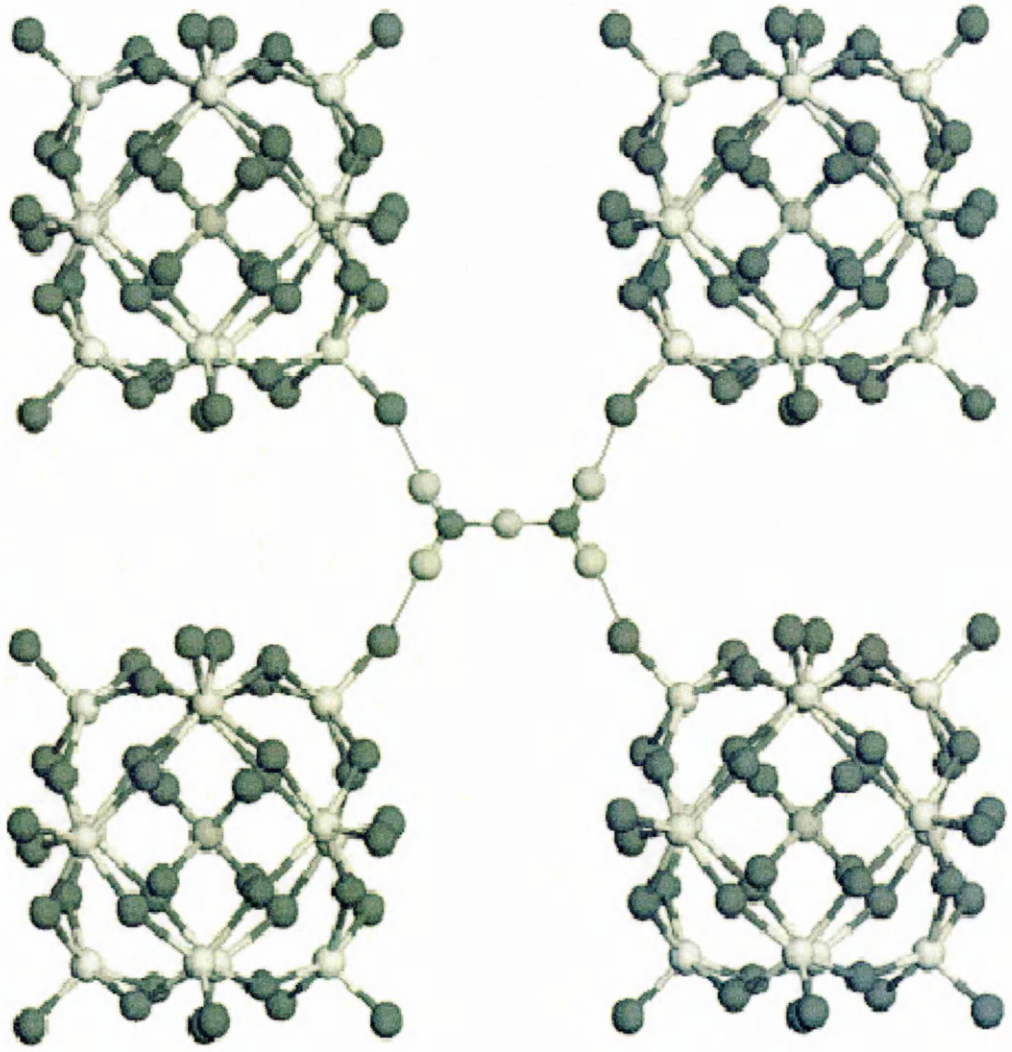

Figure 2.5 Hydrogen bonding in $H_3[PW_{12}O_{40}]\cdot 6H_2O$. (Diagram modified from reference 36.)

The $H_5O_2^+$ ions within the structure of $H_3[PW_{12}O_{40}]\cdot 6H_2O$ are disordered; in the refinement of the neutron crystallographic data the oxygen atoms of the water molecules were assigned an occupancy of 0.5. The environment around a single H^+ ion is shown schematically in Figure 2.6. The two-fold disorder of $H_5O_2^+$ does not disrupt the manner in which the Keggin anions in the structure are interconnected by hydrogen bonding as can be visualised, for example, using Figure 2.5.

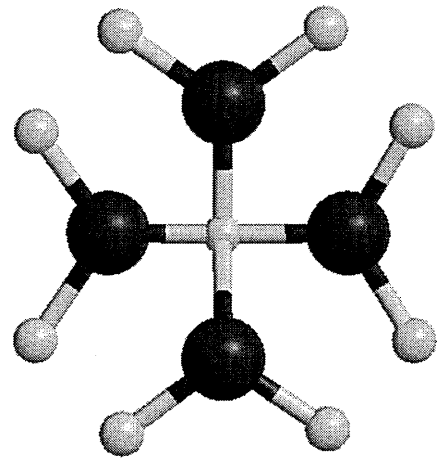

Figure 2.6 Disorder around a single acidic H^+ ion. The occupancy of each of the oxygen atoms of the water molecules is 0.5.

For hydrates with $x > 6$ the water molecules are generally[8, 17] considered to be hydrogen-bonded together and zeolitic in nature. However, neutron diffraction studies[25, 26] have found single crystalline phases for hydrates with $x = 21$ and $x = 29$. Unit cell information for these structures is summarised in Table 2.1.

Table 2.1 A comparison of unit cell information recorded from the various hydrated states of $H_3[PW_{12}O_{40}]\cdot xH_2O$ from both neutron diffraction and X-ray diffraction data.

Hydration state	**Neutron diffraction Cell length / Å Cell angle / °**		**X-ray diffraction Cell length / Å Cell angle / °**	
	Unit cell parameters	**Ref.**	**Unit cell parameters**	**Ref.**
29	$a = 23.28$ (1)	26	$a = 23.3328$ (2)	21
21	$a = 20.788$ (10)		$a = 20.825$ (2)	
	$b = 13.086$ (3)	25	$b = 13.097$ (1)	21
	$c = 18.879$ (5)		$c = 18.9266$ (4)	
14			$a = 14.075$ (4) $\alpha = 112.01$ (2)	
			$b = 14.121$ (4) $\beta = 109.62$ (2)	21
			$c = 13.525$ (3) $\gamma = 60.89$ (1)	
6	$a = 12.1506$ (5)	24	$a = 12.151$ (2)	21
3			$a = 11.78$ (1)	22
0			$a = 12.166$ (4)	21

X-ray powder diffraction

X-ray powder diffraction patterns for single crystalline phases of hydrates of $H_3[PW_{12}O_{40}]\cdot xH_2O$ corresponding to $x = 29$, 21, 14, 6 and 3 as well as the anhydrous phase ($x = 0$) have been recorded and indexed. The structures determined for the $x = 29$ and 21 hydrates[21] are in very good agreement with the neutron diffraction data

(see Table 2.1). The x = 14 hydrate was indexed[21] by analogy with $H_3[PMo_{12}O_{40}]\cdot 13H_2O$ and $NaH_2[PW_{12}O_{40}]\cdot 14H_2O$ and was suggested to have a triclinic unit cell. A summary of the unit cell information determined for all of the hydrates investigated is given in Table 2.1.

Multinuclear NMR spectroscopy

Variable temperature ^1H, ^{17}O and ^{31}P MAS NMR spectroscopy has been used[28] to investigate the states of the acidic protons in $H_3[PW_{12}O_{40}]\cdot xH_2O$ in the hydration range $0 < x < 6$. The preparation of samples was undertaken by either of two methods. The first method involved the absorption of calculated amounts of water vapour on to the anhydrous acid ($x = 0$) at room temperature. The second method, the desorption method, used a temperature range of 373 to 423 K to achieve the controlled removal of water from the hexahydrate ($x = 6$). However, it was found that the two methods produced samples that gave different NMR spectra. This was attributed to the differences in preparation temperature of the two methods. For example, it was suggested that the absorption method at room temperature may lead to inhomogeneity in a sample caused by the slow diffusion of the water molecules into the solid acid. As a consequence, the majority of the work was focussed on samples prepared by the desorption method which were taken to have a more homogeneous structure. Initial work focussed on spectra recorded from $x = 0$ and 6 samples.

A single line, with spinning sidebands, was observed in the ^1H MAS NMR spectrum of anhydrous $H_3[PW_{12}O_{40}]\cdot 0H_2O$ at both 298 and 173 K, $\delta(^1H) = 9.0$. This signal was assigned to "isolated acidic protons" which were taken to be protons randomly

distributed on the oxygen atoms of the Keggin anion and not involved in any hydrogen bonding to water molecules. The corresponding ^{31}P MAS NMR spectra consisted of a single, sharp line at $\delta(^{31}P) = -11.0$ at both temperatures. The fact that this chemical shift is sensitive to the degree of hydration was established by measuring $\delta(^{31}P)$ for the hexahydrate. The neutron diffraction crystal structure for the hexahydrate[24] indicates that all of the acidic protons are incorporated into $H_5O_2^+$ cations and so there are no acidic protons attached to the polyanions. As expected, the ^{31}P MAS NMR spectrum at both 298 and 173 K was a single line but, importantly, there was a change in the chemical shift such that $\delta(^{31}P) = -15.6$, consistent with a change in $\delta(^{31}P)$ with a change in hydration.

The ^{17}O MAS NMR spectrum recorded from the hexahydrate showed resonances corresponding to bridging and terminal oxygen atoms, (O_b, O_c and O_d in Figure 2.2). The MAS spectrum recorded from the anhydrous acid was not well resolved. It was suggested that this was probably due to the desorption process causing a reduction in crystallinity (as well as crystal symmetry) in the sample leading to enhanced quadrupolar broadening effects in the ^{17}O ($I = 5/2$) spectrum. It was therefore not possible to determine, with any certainty, the location of the isolated acidic protons on the Keggin anion. However, FT-IR,[42] LCAO-MO calculations,[43] NMR[44] and DFT calculations[45] have indicated that the isolated acidic proton is located on bridging oxygen atoms. This is in contrast to the results of ^{17}O NMR investigations of Kozhevnikov and co-workers[29] who compared the spectra recorded from solution and the solid anhydrous acid state. The results were interpreted in terms of the isolated acidic proton being located on terminal oxygen atoms. This remains an area for further investigation.

Indirect information[28] relating to the environment of the acidic protons has been revealed through variable temperature ^{31}P MAS NMR studies on $H_3[PW_{12}O_{40}]\cdot xH_2O$ with $0 < x < 6$. MAS NMR spectra recorded at 298 K indicated the presence of additional resonances in the chemical shift range -11.0 to -15.6 ppm (see Figure 2.7), however, due to motional averaging effects, the spectra were not well resolved. At 173 K, individual lines were clearly resolved; for example as shown in Figure 2.7, for $x = 2.1$ four major lines were observed ($\delta(^{31}P)$ = -10.6, -11.9, -13.5 and -14.9) as well as a further line associated with the hexahydrate ($\delta(^{31}P)$ = -15.6) indicating the presence of $H_5O_2^+$. The interpretation of the four new resonances[28] was based on previous studies of the salt $Cs_nH_{3-n}[PW_{12}O_{40}]$ ($0 < n < 3$). The resonances were assigned, in decreasing order of chemical shift, to polyanions with different numbers (3, 2, 1 and 0) of isolated acidic protons directly attached to them. Furthermore, an analysis of the integrated intensities of the ^{31}P NMR peaks demonstrated that at any value of x in the range 0 to 6 there is a random distribution of isolated acidic protons amongst the Keggin polyanions, Figure 2.7.

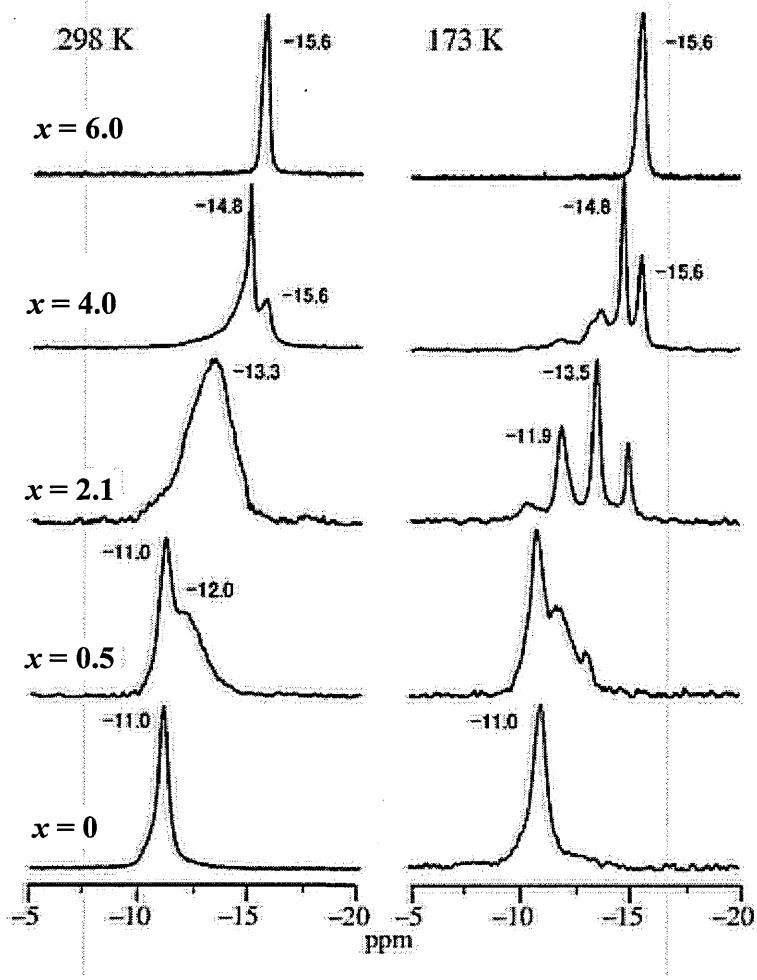

Figure 2.7 ^{31}P MAS NMR spectra recorded at 298 K from $H_3[PW_{12}O_{40}]\cdot xH_2O$ with $0 < x < 6$. (Diagram modified from reference 28.)

A key result of the ^{31}P MAS NMR studies of Misono *et al.*[28] is that the acid protons in $H_3[PW_{12}O_{40}]\cdot xH_2O$ can be divided into two types: isolated acidic protons directly attached to polyanions and those that are bonded to water molecules. The latter, from the point of view of the value of $\delta(^{31}P)$, have little influence on the nearby polyanion. Misono *et al.* also demonstrated that further information could be gained from the analysis of the integrated intensities of the observed ^{31}P resonance. They recognised that water molecules could be protonated to form different oligomers,

$(H_2O)_nH^+$, where $n = 1$ is a monomer, $n = 2$ is a dimer, and so on. For samples prepared by desorption of water from the hexahydrate, however, it is highly unlikely that oligomers with n > 2 will be formed. It was therefore assumed that both $H_5O_2^+$ and H_3O^+ were present in $H_3[PW_{12}O_{40}]\cdot xH_2O$ with $0 < x < 6$ and in this context it was noted that inelastic neutron scattering evidence had been reported[46] for the presence of the monomer in a hydrated sample with $x = 1$. The results of their analysis are summarized in Figure 2.8(a).

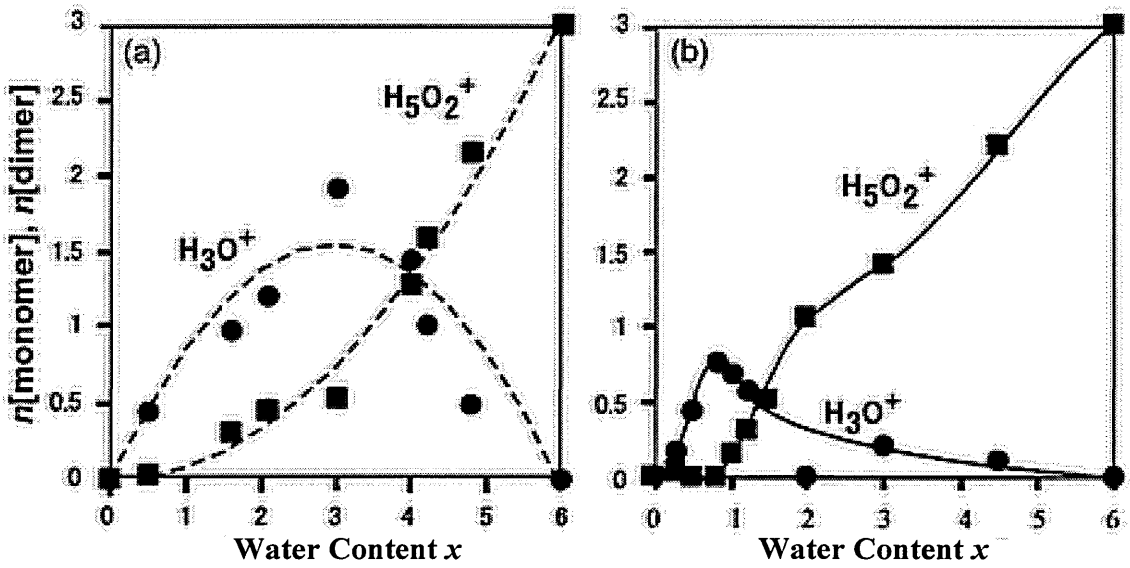

Figure 2.8 The amounts of H_3O^+ and $H_5O_2^+$, expressed as n(monomer)/n(dimer) per Keggin anion, as a function of overall water content (x) in $H_3[PW_{12}O_{40}]\cdot xH_2O$ ($0 < x < 6$) prepared by (a) the desorption and (b) the adsorption method. Solid circles represent H_3O^+ and solid squares $H_5O_2^+$. The significance of the theoretical dashed line in (a) is discussed in the text. The solid line in (b) is simply to guide the eye. (Diagram modified from reference 28.)

The dashed lines in Figure 2.8 (a) were calculated on the basis that water molecules are randomly removed from the hexahydrate structure. The good fit between model and experiment was taken as further evidence for the presence of both H_3O^+ and $H_5O_2^+$ in the structure. Figure 2.8 (b) provides a comparison with data obtained by the same type of analysis but from samples prepared by the adsorption method. There is clearly a marked difference in the behaviour with the presence of $H_5O_2^+$ more dominant at low values of x. As already discussed, it is probably the different preparation temperatures that accounts for the difference between samples. It is likely that the results would be more comparable if the samples from both methods of preparation were treated at the same high temperatures, but ensuring no water loss by desorption.

A series of ^{31}P MAS NMR experiments at a frequency of *ca.* 121 MHz have been undertaken[31] to investigate the dependence of the ^{31}P longitudinal relaxation time ($T_1(^{31}P)$) for $H_3[PW_{12}O_{40}]\cdot xH_2O$ as a function of hydration in the region $0 < x < 24$. Initially a dramatic increase in $T_1(^{31}P)$ was observed as x increased from 0 to 6; that is $T_1(^{31}P)$ increased from 50 to 210 s. This was then followed by a decrease in $T_1(^{31}P)$ such that a constant value was recorded at $x = 16$ ($T_1(^{31}P) = 30$ s) independent of any further increase in hydration state. The maximum in the value of $T_1(^{31}P)$ for the hexahydrate was attributed to the formation of a well defined hydrogen-bonded structure involving $H_5O_2^+$ ions.

The line shapes of the ^{31}P MAS NMR spectra recorded during the T_1 experiments were also analysed.[31] Two types of proton were defined : i) acidic protons which penetrate into the Keggin anion, and ii) acidic protons which exist outside the

Keggin anion which also determine the T_1 relaxation time of the ^{31}P nucleus.

FT-IR spectroscopy

FT-IR spectroscopy has been commonly used in the characterisation of 12-heteropolyacids. This is due to the characteristic band pattern displayed by the Keggin unit in the fingerprint region of the spectrum.[33] The bands have been found to be independent of hydration state[33] and are summarised in Table 2.2. FT-IR spectroscopy is widely used as a method to verify that changes to the structure of a polyanion have not taken place during a reaction or after impregnation onto a support.[47]

Table 2.2 Assignment of the characteristic bands observed in the fingerprint region of the FT-IR spectrum recorded from $H_3[PW_{12}O_{40}]\cdot xH_2O$. The oxygen atoms are labelled using the notation in Figure 2.2.

Wavenumber / cm^{-1}	Assignment
1080	$P\text{-}O_a\text{-}W$
990	$W{=}O_d$
890	$W\text{-}O_b\text{-}W$
810	$W\text{-}O_c\text{-}W$

The region of the FT-IR spectrum associated with OH vibrations and therefore the region of the spectrum most likely to yield information on the nature of individual hydrated states, has received little attention. Only two publications[34, 35] have attempted to investigate this region with respect to hydration state. Zecchina *et al.*[34] investigated hydrated states of $H_3[PW_{12}O_{40}]\cdot xH_2O$ using samples prepared by

de-gassing in ultrahigh vacuum at room and elevated temperatures. The results were discussed in terms of the presence of four different hydrated species in the form of $H_{(2n+1)}O_n^+$; that is i) fully hydrated $H_3[PW_{12}O_{40}]$, ii) $H_5O_2^+$ (n = 2) prepared after a short period of degassing, iii) $0 \leq n \leq 2$, obtained after a period of 2 hours degassing and iv) n = 0, the point at which the anhydrous acid is formed. The deprotonated anion $[PW_{12}O_{40}]^{3-}$ was also considered.

Three bands, associated with the bending and stretching modes of H_2O, were observed at 3510 (broad), 1720 and 1620 cm^{-1} in fully hydrated $H_3[PW_{12}O_{40}]$. The bands observed at 3510 and 1620 cm^{-1} were assigned to water molecules not associated with an acidic proton. The 1720 cm^{-1} band was assigned to the bending mode of the diaqua-hydrogen ion, $H_5O_2^+$. After degassing for a short period (3 minutes) the broad band observed at 3510 cm^{-1} disappeared revealing the presence of a band at 3180 cm^{-1}. The band observed at 1620 cm^{-1} also disappeared leaving two main bands at 3180 and 1710 cm^{-1} (shifted from 1720 cm^{-1}) which were assigned to the ν and δ modes of external OH groups of the $H_5O_2^+$ ion. These data suggest that two species of water molecule are present in the fully hydrated $H_3[PW_{12}O_{40}]$, i) non-interacting water molecules which absorb at 3510 and 1620 cm^{-1} and ii) water molecules interacting with the acidic protons of $H_3[PW_{12}O_{40}]$, which absorb at 3180 and 1710 cm^{-1}.

After degassing for a further two hours at room temperature the modes typically associated with water molecules in an acidic media (3180 and 1710 cm^{-1}) disappeared. A very broad band was then observed between 3400 and 1300 cm^{-1} with weak bands recorded at 3400 and 1638 cm^{-1}. These bands were assigned to the

presence of H_3O^+ species attached to the Keggin unit.

A new absorption was observed between 3500 and 2750 cm^{-1} after hydrated $H_3[PW_{12}O_{40}]$ was heated under vacuum between 433 and 523 K. This new absorption and the broad band between 3400 and 1300 cm^{-1} were assigned to two different acidic OH groups present on the Keggin unit.

Further heating between 623 and 723 K resulted in the complete disappearance of bands associated with hydroxyl groups, indicating that all water and acidic protons had been removed.

Misono,[30] however, has queried the level of hydration in some of the samples studied by Zecchina and co-workers.[34] In particular it was questioned whether an evacuation time of just three minutes would yield the hexahydrate from a fully hydrated sample.[30] It was deemed more likely that the sample evacuated for two hours was the hexahydrate, suggesting the assignment of IR bands by Zecchina was partially incorrect.[30]

A separate FT-IR study, by Misono *et al.*,[35] focused in detail on the $x = 0$ to $x = 6$ range of hydration states. After heating fully hydrated $H_3[PW_{12}O_{40}]$, under evacuation, at 343 K for one hour Misono *et al.* observed the same broad band between 3400 and 1300 cm^{-1} as Zecchina *et al.*[34] had previously reported. Misono *et al.*, however, assigned the broad band to the hydroxyl groups present in the $H_5O_2^+$ ion. Heating at an increased temperature of 373 K for the same period of time led to the observation of a broad band centred at 3200 cm^{-1}. This band continued to

increase in intensity as the temperature was increased, however, the broad band, between 3400 and 1300 cm^{-1}, decreased in intensity. The increase in the absorption at 3200 cm^{-1} was assigned to acidic OH groups or isolated acidic protons on the Keggin unit.

Acidity

Interest in the acidity of heteropoly acids has been fuelled by the need for industrial replacements for toxic H_2SO_4 and HF based catalysts.[17, 48] As a consequence, the acidity of 12-heteropolyacids have been investigated in detail by a variety of techniques in order to determine those factors which influence acid strength. The results will not be discussed here except to note that they have prompted much debate in the literature[17] as to whether or not $H_3[PW_{12}O_{40}]\cdot xH_2O$ can possess acid sites stronger than those found in 100 % H_2SO_4; that is, "superacidic" sites.

More recently a technique based on ^{13}C solid-state NMR spectroscopy has been used[49] to investigate acid sites in $H_3[PW_{12}O_{40}]\cdot xH_2O$. These investigations are of direct interest to the work in this thesis and are reviewed below.

Acid strength : adsorption of acetone and ^{13}C solid-state NMR spectroscopy

Solid state ^{13}C MAS and CPMAS NMR experiments have recently been used[49] to probe the location, mobility and strength of the acidic protons in $H_3[PW_{12}O_{40}]\cdot xH_2O$. Samples of $H_3[PW_{12}O_{40}]$ with different degrees of hydration were prepared by holding fully hydrated and purified samples of this material in vacuum at different temperatures for periods of either two or four hours. Controlled amounts of 2-^{13}C-acetone (99 % ^{13}C enriched) were then adsorbed onto these

hydrates at room temperature. The molar ratio of isotopically labelled acetone to hydrate was kept to a minimum (typically 0.3 molecules per Keggin unit) to avoid the acid catalysed condensation of acetone to diacetone alcohol followed by dehydration to mesityl oxide, Figure 2.9.

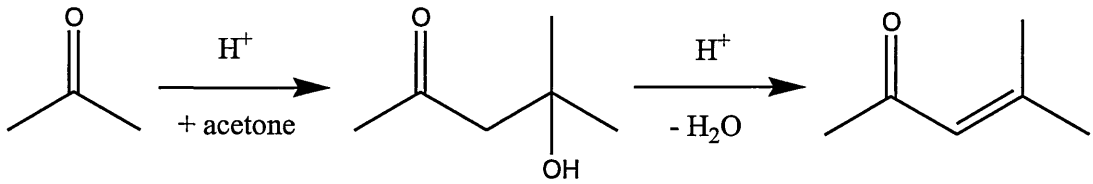

DA MO

Figure 2.9 Acid catalysed condensation of acetone to diacetone alcohol (DA) followed by dehydration to mesityl oxide (MO).

A key feature of the work was to compare the isotopic ^{13}C chemical shifts of resonances observed in the carbonyl region for the adsorbed isotopically labelled acetone with those of an acidity scale proposed by Biaglow *et al.*[50-54] This is a scale that shows that the carbonyl value of $\delta(^{13}C)$ for adsorbed acetone increases from that of pure liquid acetone (206.0 ppm) depending on the type of solid acid catalyst that is used as an adsorbate. The change in chemical shift can be qualitatively attributed to protonation of the carbonyl group and hence the presence of a partial positive charge on the carbonyl carbon. It has been demonstrated[54, 55] that this scale provides a reasonable measure of the acid strength of solid acids and the changes in chemical shift are of sufficient magnitude to distinguish between sites of different acidity. The threshold acid strength, corresponding to 100 % H_2SO_4, gives rise to a value of $\delta(^{13}C) = 245$ for adsorbed acetone.

For $H_3[PW_{12}O_{40}]\cdot xH_2O$ samples dehydrated at temperatures above 573 K for two

hours it was assumed that all the water molecules of crystallisation were removed. The observed ^{13}C carbonyl resonances at values of $\delta(^{13}C)$ = 246 and 235 were therefore assigned to acetone adsorbed on isolated acidic protons. The presence of two signals, indicating two types of adsorption site, was surprising since it was generally assumed in the literature,[28, 29] although without direct evidence, that this type of proton would be localized at only one type of oxygen atom on the Keggin unit. The acid strengths of the two sites are high with one at the threshold of superacidity. Further NMR evidence also indicated that the isolated acidic protons and the adsorbed acetone were tightly bound together with restricted mobility.

At lower dehydration temperatures, with waters of crystallisation present, a resonance at $\delta(^{13}C)$ = 219 was observed and this was assigned to acetone adsorbed on hydrated proton species. The acid strength was found to be equivalent to that of zeolites.[54, 55] Furthermore the absence of spinning sidebands and the relatively low cross-polarisation enhancement of this resonance in the CPMAS experiments, was taken as indicating considerable mobility of the adsorbed acetone and the hydrated proton. It is interesting that a resonance at $\delta(^{13}C)$ = 235 (but not 246) was also observed in these hydrated samples so that both isolated acidic protons and hydrated protons are present. The authors did not comment on this behaviour.

The use of ^{13}C solid-state NMR to study the behaviour of adsorbed isotopically labelled acetone on 12-heteropolyacids, although relatively new, offers a useful way of obtaining detailed information on the properties of acid sites particularly for well characterised samples with known hydration.

2.3.3 12-Silicotungstic acid

Comparatively little work has been carried out on 12-silicotungstic acid. Thermal analysis data have been recorded in the form of TGA and DTA.[56] There have also been limited FT-IR[33, 56, 57] and XRD[57-59] investigations.

Thermal analysis

Bielanski *et al.*[57] recorded two endothermic phase changes and an exothermic phase change in support of an FT-IR investigation of hydrated $H_4[SiW_{12}O_{40}]\cdot xH_2O$. The first endothermic phase change, corresponding to the loss of 18 water molecules in the TGA data, occurred over the temperature range 20-100°C and represented the transformation $H_4[SiW_{12}O_{40}]\cdot 24H_2O \rightarrow H_4[SiW_{12}O_{40}]\cdot 6H_2O$. The hexahydrate, as in the case of $H_3[PW_{12}O_{40}]\cdot 6H_2O$, is relatively stable so that the second endothermic phase change did not occur until 200°C. This phase change corresponded to the loss of six water molecules and thus to the formation of the anhydrous acid. The anhydrous phase was then found to be stable until 450°C where two constitutional water molecules were formed from the four acidic protons and two oxygen atoms from the Keggin unit. The formation of the anhydride (x = -2) was complete at 520°C. At 525°C an exothermic phase change was observed, and this was assigned to the decomposition of the Keggin structure into a mixture of WO_3 and SiO_2.

In a later study,[56] Bielanski *et al.* recorded a third endothermic phase change at approximately 125°C. This endothermic event was correlated with the observation of a plateau in the TGA data which had not previously been observed. This plateau corresponded to the formation of $H_4[SiW_{12}O_{40}]\cdot 17.3H_2O$. The authors, however, did not indicate the conditions under which their results were recorded or discuss this

hydrate with regards to any other technique.

FT-IR spectroscopy

$H_4[SiW_{12}O_{40}]\cdot xH_2O$ (x = 24.8, 6 and 0) has been characterised by FT-IR spectroscopy.[57] The bands observed in the fingerprint region were found to be independent of the hydrated state, as in the case of $H_3[PW_{12}O_{40}]\cdot xH_2O$ (see section 2.3.2, Table 2.2), and have been assigned[33] as shown in Table 2.3.

Table 2.3 Assignment of the characteristic $H_4[SiW_{12}O_{40}]\cdot xH_2O$ FT-IR peaks in the fingerprint region.[33] The oxygen atoms are labelled using the notation described in Figure 2.2.

Wavenumber / cm^{-1}	**Assignment**
1020	$H_2O...H$
981	$W{=}O_d$
921	$Si\text{-}O_a\text{-}W$
880	$W\text{-}O_b\text{-}W$
779	$W\text{-}O_c\text{-}W$

In a more detailed investigation, Bielański *et al.*[56] used FT-IR spectroscopy to study the dehydration of $H_4[SiW_{12}O_{40}]\cdot 15.6H_2O$ *in situ*. The determination of the hydration state of the acid involved a parallel experiment using a microbalance under the same conditions as those used in the IR chamber.

Evacuation of the IR chamber for 30 seconds at room temperature lead to the loss of loosely-bonded water molecules, characterised by bands observed at 3550 and

1616 cm^{-1}. After 30 seconds evacuation the water content was calculated to be 8.3 water molecules per Keggin unit. The bands in the fingerprint region of the spectrum remained the same as those recorded from the fully hydrated sample. The remaining absorptions outside of the fingerprint region, observed at 3445, 1710 and 1100 cm^{-1}, were assigned to the hydrogen bond between the O_d atom and the $H_5O_2^+$ ion : 3445 cm^{-1} and the $H_5O_2^+$ ion itself : 1710 and 1100 cm^{-1}.

Heating $H_4[SiW_{12}O_{40}]\cdot 8.3H_2O$ to 100°C at 0.8°C min^{-1} under vacuum led to the formation of the anhydrous acid. Treatment under these conditions resulted in the complete loss of absorptions previously observed outside the fingerprint region and the observation of a new band at 3106 cm^{-1}. The absorption at 3106 cm^{-1} was assigned to a hydrogen bond occurring between two neighbouring Keggin units $O_d\text{-}H^+\text{-}O_c$.

X-ray powder diffraction

In early work, Scroggie and Clark[58] recorded the X-ray powder diffraction pattern of a hydrated sample of $H_4[SiW_{12}O_{40}]$ which was taken to be the hexahydrate. The unit cell was confirmed to be cubic with a cell length of 12.16 Å. Illingworth and Keggin[59] later confirmed $H_4[SiW_{12}O_{40}]\cdot 6H_2O$ had a similar packing to that of the "pentahydrate" of 12-phosphotungstic acid.[24] Although detailed crystallographic studies have not subsequently been carried out, discussion in the literature[17] generally suggests that in comparison to the established structure of $H_3[PW_{12}O_{40}]\cdot 6H_2O$,[24] the extra acidic proton in $H_4[SiW_{12}O_{40}]\cdot 6H_2O$ is most likely located on a bridging oxygen atom (labelled O_b in Figure 2.2) of the Keggin polyanion.

2.4 12-Heteropolyacids as catalysts

Heteropoly acids are known for their very strong Brønsted acidity[30] and, as efficient oxidants, they exhibit fast, reversible, multi-electron redox properties which can be varied over a wide range by changing their chemical composition.[60] These properties make heteropolyacids attractive as possible replacements for current heterogeneous strong acid catalysts.[60]

2.4.1 Hierarchical structure of 12-heteropolyacids and types of catalysis

Misono and co-workers[30] have proposed that a better understanding of the catalytic activity of solid 12-heteropolyacids can be achieved if the hierarchical structures of these materials are considered. This view then leads to a classification of their catalytic mode of action into three distinct types: surface, bulk-type I (pseudo-liquid) and bulk-type II. The usefulness of this approach is demonstrated by the fact that various reactions involving solid 12-heteropolyacid catalysts, that have been published in the literature, can be classified in this way.

The hierarchical structure of solid 12-heteropolyacids is based on a division into sub-structures (or structural building blocks). The basic building block is the primary structure which is the 12-heteropolyanion or Keggin Unit (KU). The secondary structure is described as the three-dimensional arrangement of the Keggin units and counter cations. The flexibility of the secondary structure is dependent on the counter cation and structure of the heteropoly anion. In Figure 2.10 the secondary structure is represented by the acidic caesium salt of the $[PW_{12}O_{40}]^{3-}$ anion, which has catalytic properties. The tertiary structure represents the manner in which the secondary structure assembles into solid particles and relates to properties such as

particle size, surface area and pore structure and plays an important role in heterogeneous catalysis.

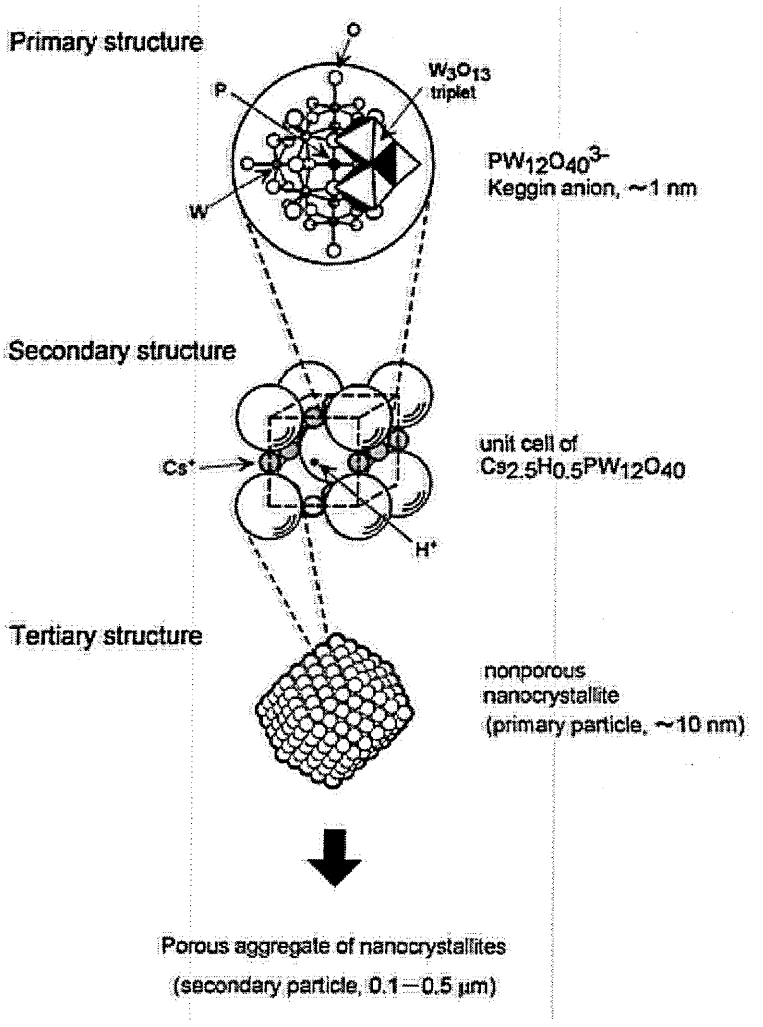

Figure 2.10 A schematic representation of the primary, secondary and tertiary structures of 12-heteropolyacids using an acidic caesium salt of $[PW_{12}O_{40}]^{3-}$ as an example. (Diagram modified from reference 61.)

Surface-type catalysis depends on tertiary structure. It is ordinary heterogeneous catalysis with the chemical reaction taking place on the outer surface. Catalytic activity depends critically on surface area and the rate of reaction is expected to depend on surface acidity: that is, the number of acidic protons on the surface.

Several reactions catalysed by acidic caesium salts, $Cs_xH_{3-x}[PW_{12}O_{40}]$ show this type of behaviour.[14, 62, 63]

The concept of bulk-type I, or pseudo-liquid phase, catalysis is now widely accepted.[28] It involves absorption of the reactant molecules into the bulk of the catalyst. The reactant molecules penetrate between the heteropoly anions that form the secondary structure. This is achieved, for example, by substitution of water molecules or by increasing the distance between the heteropoly anions in the secondary structure. In effect, the catalytic reaction takes place within a pseudo-liquid phase within the bulk catalyst; product molecules diffuse to the surface and are released to the surrounding gas phase. The 12-heteropolyacid, although a solid acid catalyst, behaves as a liquid and the catalytic activity is high because it depends on the number of acidic protons in the bulk phase. For example, in the case of catalysis using acidic sodium salts of $[PW_{12}O_{40}]^{3-}$ the bulk acidity will depend on the Na^+ content, that is the extent of neutralisation of the acid. For instance, for the dehydration of 2-propanol at 100°C, it has been found that the catalytic activity of $Na_xH_{3-x}[PW_{12}O_{40}]$ decreases monotonically with increasing value of x or, in other words, with decrease in bulk acidity.[61]

Bulk-type II catalysis is particularly relevant for oxidation reactions involving 12-heteropolyacids at high temperatures (typically 200-350°C). In this case the reactants usually remain on the surface, but the diffusion of redox carriers (protons) to the surface from the bulk is rapid and so, in effect, the whole bulk participates in the reduction-oxidation cycle. In general, if the rates of bulk-type II oxidations are plotted against a surface redox property then good correlations are found.[30, 62]

While the strong Brønsted acidity of heteropoly acids makes them ideal candidates to replace less environmentally-friendly catalysts, their very low surface area (1-5 m^2 g^{-1})[64, 65] results in very low catalytic activity for reactions occurring via surface-type catalysis. The immobilization of heteropoly acids on various supports including ZrO_2, carbon, silica-alumina and clays has therefore been investigated. Silica is, however, the most studied support[66] due to its wide availability, its neutral or mild acidity, specific (tuneable) surface areas and porosity.[64, 66] Silica supported catalysts are considered in the next section.

2.4.2 Silica-supported 12-phosphotungstic acid

Silica-supported 12-phosphotungstic acid has been characterised by thermal analysis,[64, 66] X-ray powder diffraction,[65] temperature-programmed reduction (TPR),[47, 67] FT-IR,[68] ^1H and ^{31}P MAS NMR spectroscopy,[65, 69] microcalorimetry[64] and TEM.[65] These investigations will be discussed in this section, however, due to the limited information available, the few studies involving 12-silicotungstic acid will also be included where appropriate.

Thermal analysis

Thermal analysis investigations[66] of hydrated $H_3[PW_{12}O_{40}]$ supported on silica demonstrated differences when compared to the thermal data recorded from the unsupported heteropoly acid.[21]

Supported samples were prepared, with loadings in the range of 3.6 to 63 % by weight, using an impregnation technique where a solution of $H_3[PW_{12}O_{40}]$ was mixed with silica powder (Fisher 100 Å) and dried at 60°C over night.

TGA data for unsupported $H_3[PW_{12}O_{40}]\cdot xH_2O$ was compared with that for a supported sample with a loading of 43.5 wt %. A significant difference in the total weight percentage lost between the two samples was observed. This discrepancy was attributed to the difference in density of the silica supported sample coupled with the loss of physisorbed water associated with the silica. Physisorbed, or zeolitic, water molecules from both the silica and the hydrated $H_3[PW_{12}O_{40}]$ were lost at approximately 90 - 100°C. After this initial weight loss the TGA data recorded from the supported acid was similar to that of unsupported $H_3[PW_{12}O_{40}]\cdot 6H_2O$ and two further distinct weight losses, which corresponded to 3.3 and 0.7 wt %, were observed. These weight losses were found to be equivalent to the loss of 6 structural and 1.5 constitutional water molecules, respectively. However, the loss of the constitutional waters in the supported sample occurred at a lower temperature, approximately 380 to 390°C, than observed for the unsupported sample, approximately 410°C.

TGA data recorded from all the silica-supported samples were similar. The authors suggested[66] that the differences observed between silica-supported and non-supported $H_3[PW_{12}O_{40}]$ are caused be the presence of "common supported species".

DTA data were also recorded from the silica-supported samples between 540 and 660°C, the region in which bulk $H_3[PW_{12}O_{40}]$ decomposes (*ca.* 620°C). These data showed the exothermic peak, associated with the decomposition of the Keggin unit, to move to a significantly lower temperature compared to that for bulk $H_3[PW_{12}O_{40}]$. For a sample with a loading of 10.3 wt % the exothermic peak was observed at 580°C, as the loading was increased to 62.5 wt % the observed peak moved to

595°C. This shift in temperature of the exothermic phase change was taken to indicate that the Keggin unit was destabilised at low coverages by the interaction with the silica support.

In another study, Chuvaeu *et al.*[70] suggested that the decomposition of silica-supported $H_3[PW_{12}O_{40}]$ can occur at a temperature as low as 465°C. This study also investigated the thermal analysis of fully hydrated $H_4[SiW_{12}O_{40}]$ supported on silica the decomposition of which was found to occur at 445°C.

The reduced thermal stability of silica-supported heteropoly acids has had industrial consequences. Some 12-heteropolyacids have been used as catalysts at moderately high temperatures, up to 300-350°C. However, regeneration of these catalysts after long periods of use is hindered by their low thermal stability. The regeneration of used catalysts is discussed in the next section.

Coking of the catalyst

The importance of the thermal stability of silica-supported $H_3[PW_{12}O_{40}]$ is brought into focus when considering the problem of catalyst regeneration. Silica-supported $H_3[PW_{12}O_{40}]$ is known to be deactivated by coke formation in acid-catalysed organic conversions.[71, 72] Regeneration of alternative solid acid catalysts such as SiO_2-Al_2O_3 or zeolites has been successfully achieved by burning off the deposited coke in the presence of O_2 at relatively high temperatures : 450-550°C.[71] Silica-supported $H_3[PW_{12}O_{40}]$, however, has insufficient thermal stability to make this a viable method since the catalytic activity of heteropolyacid catalysts would probably be lost with the removal of the acidic protons, well before the decomposition of the Keggin

unit itself.

A relatively low-temperature solution has been pursued to remove coke, formed through gas-phase conversion of hydrocarbons, deposited on silica-supported $H_3[PW_{12}O_{40}]$. In this context, the oligomerisation of propene[71, 72] has been studied as a model reaction to investigate the deposition of coke. The nature of the coke deposited on the surface of the supported catalyst was analysed using TGA and DTA. The coke was found to exist in two forms: i) high boiling point hydrocarbons, or "soft" coke, and, ii) polynuclear aromatics, or "hard" coke.[72] The "soft" coke was found to have a TGA removal range of 170-370°C and the "hard" coke a removal range of 370-570°C, well above the decomposition temperature of silica-supported $H_3[PW_{12}O_{40}]$.[72] The regeneration of silica supported $H_3[PW_{12}O_{40}]$ after coke deposition was investigated using three separate methods.

Firstly, the coked catalyst was refluxed in dichloromethane, since $H_3[PW_{12}O_{40}]$ is not soluble in dichloromethane, for 3hrs followed by filtration. This solvent extraction technique resulted in 19% of the total deposited coke being removed. The composition of the removed coke was found by the authors[72] to be 19% of the total hard coke and 14% of the total soft coke (Only a small amount of soft coke was present on the catalyst under investigation).

Secondly, the coked catalyst was regenerated in a fixed bed flow reactor, heated to 150°C, using a gas flow containing 6% ozone. Using this approach, decoking of heavily-coked catalysts was achieved such that there was complete removal of hard and soft coke. This method, however, was deemed to be of little practical interest,

due to the volatile nature of ozone.

The final method of regeneration involved doping the catalyst, prior to the deposition of coke, with palladium. Coke was then deposited on the palladium-doped catalyst using the same process as in the first two methods. The modification of the catalyst with palladium prevented the formation of the hard coke so that only soft coke was formed. The regeneration of the soft-coked catalyst was then achieved by aerobic burning of the coke at 350°C in air over 2 hours. This allowed the regeneration of the catalyst at temperatures lower than that required to fully dehydrate the Keggin unit, thus keeping its catalytic activity. However, the costs associated with palladium-doping on an industrial scale would be significant.

FT-IR spectroscopy

The interaction between a silica support and hydrated $H_3[PW_{12}O_{40}]$ has been studied using FT-IR spectroscopy.[68]

FT-IR spectra were recorded from the silica support, hydrated $H_3[PW_{12}O_{40}]$ and silica-supported $H_3[PW_{12}O_{40}]$ with loadings of 10, 20, 30, 40, 50 and 60 weight percent. The silica-supported samples were prepared using an impregnation technique, where a solution of $H_3[PW_{12}O_{40}]$ was mixed with the solid silica (S = 321 m^2 g^{-1}) then dried at 110°C under vacuum. The prepared samples were then stored in a desiccator to avoid re-hydration.

The FT-IR spectrum recorded from the silica support showed the presence of two main absorptions around 1100 and 806 cm^{-1} and a weak absorption, related to

surface OH groups, at 974 cm^{-1}. As previously discussed, Section 2.3.2, absorptions observed for $H_3[PW_{12}O_{40}]$ occurred at approximately 1080, 990, 890 and 810 cm^{-1}. The spectra recorded from the silica-supported $H_3[PW_{12}O_{40}]$ showed absorptions associated with the silica support and two absorptions, typically associated with $H_3[PW_{12}O_{40}]$, at 983 and 892 cm^{-1}. The absorptions, typical of $H_3[PW_{12}O_{40}]$, at approximately 1080 and 810 cm^{-1} overlapped with the strong absorptions of the silica. The absorption at approximately 1080 cm^{-1} was, however, observed when the sample loading was increased to 60 wt %. Overall, the results led the authors to conclude, consistent with a body of other work, that when supported on silica $H_3[PW_{12}O_{40}]$ retains the Keggin structure.

FT-IR spectroscopy has also been used to show that mechanical mixtures of hydrated $H_3[PW_{12}O_{40}]$ and silica cannot be distinguished from silica-supported $H_3[PW_{12}O_{40}]$.[47]

X-ray powder diffraction

The interaction between a silica-support and hydrated $H_3[PW_{12}O_{40}]$ has been investigated using X-ray powder diffraction.[15, 65, 68]

X-ray powder diffraction patterns were recorded from the silica support, $H_3[PW_{12}O_{40}]$ and silica-supported $H_3[PW_{12}O_{40}]$ with loadings of 10, 20, 30, 40, 50 and 60 weight percent : the same as those used for the FT-IR investigation as described in the previous sub-section. The XRD pattern recorded from the silica support showed a broad diffraction peak centred around 2θ = 22 °, typical of that expected for amorphous silica.

The pattern recorded from the sample with 10 wt % loading showed two very weak, diffraction peaks at $2\theta = 10^{o}$ and 25^{o} superimposed on the characteristic peak of amorphous silica. This indicated the presence of $H_3[PW_{12}O_{40}]\cdot 6H_2O$. On increasing the loading to 20 wt % more diffraction peaks consistent with the presence of $H_3[PW_{12}O_{40}]\cdot 6H_2O$ became observable. The intensity of the diffraction peaks continued to increase as the loading was increased although all peaks were broader than those for crystalline $H_3[PW_{12}O_{40}]\cdot 6H_2O$. These results, however, are not consistent with those obtained by Izumi *et al.*[15] or Kozhevnikov *et al.*,[65] where no diffraction peaks were observed until 20 wt % loading was exceeded. These apparent inconsistencies in results from different groups may well be associated with differences in preparation conditions.

X-ray powder diffraction has been used to differentiate between mechanical mixtures of $H_3[PW_{12}O_{40}]$ and silica, and $H_3[PW_{12}O_{40}]$ supported on silica.[47] XRD patterns were recorded from mechanical mixtures of silica and $H_3[PW_{12}O_{40}]\cdot 6H_2O$ and compared to samples, with exactly the same ratio of silica to $H_3[PW_{12}O_{40}]$, prepared using the impregnation technique. The diffraction peaks recorded from the mechanical mixture were shown to be more intense and less broad than those recorded from the impregnated sample.

^{31}P MAS NMR spectroscopy

Lefebvre[69] has demonstrated that ^{31}P MAS NMR spectroscopy can be used to probe the interaction of hydrated $H_3[PW_{12}O_{40}]$ with a silica surface. Two distinct types of $[PW_{12}O_{40}]^{3-}$ were identified corresponding to the polyanion in both a bulk hydrated phase and in a surface phase involving silanol groups.

Samples with hydrated $H_3[PW_{12}O_{40}]$ loadings in the range 13 to 87 % by weight were prepared using an impregnation technique, where a solution of $H_3[PW_{12}O_{40}]$ was mixed with solid SiO_2 (Aerosil: $S = 380\ m^2\ g^{-1}$) and then dried at 100°C for 24 hours. The individual products were stored in a desiccator to avoid re-hydration. Powder XRD evidence suggested that $H_3[PW_{12}O_{40}]\cdot 6H_2O$ was present on the silica surface. This result is consistent with that expected from thermal analysis studies[21] of hydrated $H_3[PW_{12}O_{40}]$ (see Section 2.3.2).

The ^{31}P MAS NMR spectra recorded from all of the samples showed two overlapping resonances at -15.1 and -14.6 ppm. A typical spectrum corresponding to 50% loading of silica is shown in Figure 2.11. It can be noted that Misono *et al.*,[28] as discussed in Section 2.3.2, reported a single resonance for unsupported $H_3[PW_{12}O_{40}]\cdot 6H_2O$ at -15.6 ppm.

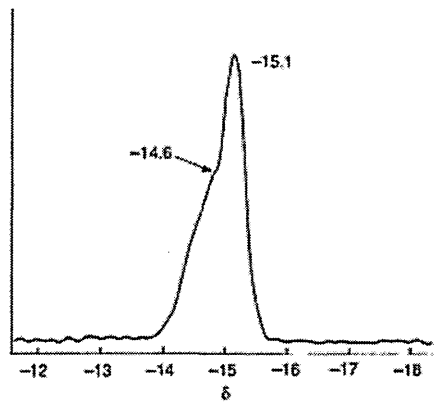

Figure 2.11 ^{31}P MAS NMR spectrum recorded from $H_3[PW_{12}O_{40}]\cdot 6H_2O/SiO_2$ catalyst. (Diagram modified from reference 69.)

The contribution of the resonance at -14.6 ppm, expressed as a percentage of the total ^{31}P NMR signal intensity, was found to vary with the loading of the hydrated

$H_3[PW_{12}O_{40}]$ on the silica. As this loading was increased from 13 to 50%, the proportion was found to be roughly constant at a value of approximately 70% (within experimental uncertainty). At loadings greater than 50% there was a marked decrease, reducing to a value of about 20 % at the highest loading of 87%.

These results can be explained in terms of the presence of two distinct types of phase on the silica surface. One of these, which is dominant at high loadings, corresponds to hydrated $H_3[PW_{12}O_{40}]$ present in the form of crystallites dispersed amongst, or on the surface of silica particles; there is no specific interaction with the silica surface. This bulk phase gives rise to the ^{31}P resonance signal at -15.1 ppm. The other phase is due to $H_3[PW_{12}O_{40}]$ units interacting directly with silanol groups on the silica surface and gives rise to the resonance at -14.6 ppm. It was suggested[69] that on initial impregnation an ionic cluster was formed with a silanol group, via simple proton transfer, to give the species $(\equiv SiOH_2)^+(H_2PW_{12}O_{40})^-$. Overall, the results suggest that, at approximately 50 wt % loading of silica, the silanol groups present on the surface (≈ 3 for 10 nm^2) are fully saturated.

At higher loadings, various $H_3[PW_{12}O_{40}]\cdot xH_2O$ forms have been observed on the silica surface by transmission electron microscopy (TEM) including discrete molecules, clusters around 5 nm, and crystals around 50 nm.[65]

Other ^{31}P MAS NMR data have been recorded[65, 73] and it has been suggested that $H_6P_2W_{18}O_{62}$ or $H_6P_2W_{21}O_{71}$, instead of $(\equiv SiOH_2)^+(H_2PW_{12}O_{40})^-$, are the species responsible for the resonance recorded at $\delta(^{31}P) = -14.6$.

Surface studies

A surface study involving the use of XPS, Raman, FT-IR and XRD investigated the evolution of $H_3[PW_{12}O_{40}]\cdot xH_2O$ adlayers over a porous, hydroxylated silica.[66, 74] A fully dispersed $H_3[PW_{12}O_{40}]\cdot xH_2O$ layer was found to cover the silica surface up to a loading of approximately 44 wt % $H_3[PW_{12}O_{40}]\cdot xH_2O$. Higher loadings resulted in a dramatic loss of surface area and associated pore blockage, indicating a change in growth mode and bulk $H_3[PW_{12}O_{40}]\cdot xH_2O$ agglomeration. These data are in agreement with ^{31}P MAS NMR data recorded from silica supported $H_3[PW_{12}O_{40}]$ (Section 2.4.2) where it was suggested that a loading of up to approximately 50 wt % forms a monolayer of the Keggin units. After *ca.* ≈ 50 wt % accumulation, it was suggested[74] that the Keggin units could form agglomerates or an adlayer and were therefore not perturbed by an interaction with the silica surface. The $H_3[PW_{12}O_{40}]$ present in these agglomerates or adlayers should therefore possess bulk-like properties.

Depending on the loading, various forms of 12-heteropolyacid have been observed using TEM on a silica surface.[75] Both $H_3[PW_{12}O_{40}]\cdot xH_2O$ and $H_4[SiW_{12}O_{40}]\cdot xH_2O$ form finely dispersed species on the surface and above 20 wt % loading a crystal phase is reported to form.[15, 75]

Acidity

The proton sites in bulk anhydrous $H_3[PW_{12}O_{40}]\cdot 0H_2O$ have been reported to be evenly distributed due to the pseudo-liquid nature of 12-heteropolyacids.[76] By contrast, the proton sites on the silica-supported $H_3[PW_{12}O_{40}]\cdot xH_2O$ (20 wt %) have been shown by microcalorimetry[76] to become less acidic and less uniformly

distributed. Only 20% of the proton sites retain the strength observed in bulk $H_3[PW_{12}O_{40}]\cdot xH_2O$. The remaining 80% of the proton sites have a differential heat of ammonia adsorption of about 120 kJ mol^{-1}, close to that of the acid sites in HX and HY zeolites. The differential heat of ammonia adsorption on silica-supported $H_3[PW_{12}O_{40}]\cdot xH_2O$, like that for bulk $H_3[PW_{12}O_{40}]\cdot xH_2O$, is found to depend strongly on the pre-treatment temperature of the acid.

References

(1) Staiti, P.; Hocevar, S.; Giordano, N. *International Journal of Hydrogen Energy* **1997**, *22*, 809-814.

(2) Campiglio, A. *Analyst* **1994**, *119*, 2209-2212.

(3) Cho, K.; Chung, S. D.; Ryu, K. S.; Kim, Y.; Choy, J. H.; Kim, H. *Synthetic Metals* **1995**, *69*, 481-482.

(4) Katsoulis, D. E. *Chemical Reviews* **1998**, *98*, 359-387.

(5) Souchay, P. *Polyanions et Polycations*; Gauthier-Villars: Paris, 1963.

(6) Pope, M. T. *Heteropoly and Isopoly Oxometalates*; Springer-Verlag: Berlin, 1983.

(7) Kozhevnikov, I. V. *Catalysis Reviews-Science and Engineering* **1995**, *37*, 311-352.

(8) Moffat, J. B. *Metal-Oxygen Clusters*; Kluwer Academic/Plenum Publishers: New York, 2001.

(9) Berzelius, J. J. *Poggendorfs Ann. Phys.* **1826**, *6*, 369-380.

(10) Keggin, J. F. *Proceedings of the Royal Society of London* **1934**, *144*, 75-100.

(11) Kozhevnikov, I. V.; Sinnema, A.; Jansen, R. J. J.; Vanbekkum, H. *Catalysis Letters* **1994**, *27*, 187-197.

(12) Weinstock, I. A.; Cowan, J. J.; Barbuzzi, E. M. G.; Zeng, H. D.; Hill, C. L. *Journal of the American Chemical Society* **1999**, *121*, 4608-4617.

(13) Matsumoto, K. Y.; Kobayashi, A.; Sasaki, Y. *Bulletin of the Chemical Society of Japan* **1975**, *48*, 3146-3151.

(14) Okuhara, T.; Nishimura, T.; Watanabe, H.; Misono, M. *Journal of Molecular Catalysis* **1992**, *74*, 247-256.

(15) Izumi, Y.; Hasebe, R.; Urabe, K. *Journal of Catalysis* **1983**, *84*, 402-409.

(16) Liu-Cai, F. X.; Sahut, B.; Faydi, E.; Auroux, A.; Herve, G. *Applied Catalysis A - General* **1999**, *185*, 75-83.

(17) Kozhevnikov, I. V. *Catalysts for Fine Chemical Synthesis: Catalysis by*

Polyoxometalates; John Wiley & Sons Ltd: West Sussex, 2002.

(18) Corma, A. *Chemical Reviews* **1995**, *95*, 559-614.

(19) Essayem, N.; Coudurier, G.; Vedrine, J. C.; Habermacher, D.; Sommer, J. *Journal of Catalysis* **1999**, *183*, 292-299.

(20) Izumi, Y.; Matsuo, K.; Urabe, K. *Journal of Molecular Catalysis* **1983**, *18*, 299-314.

(21) Mioc, U. B.; Dimitrijevic, R. Z.; Davidovic, M.; Nedic, Z. P.; Mitrovic, M. M.; Colomban, P. *Journal of Materials Science* **1994**, *29*, 3705-3718.

(22) Marosi, L.; Platero, E. E.; Cifre, J.; Arean, C. O. *Journal of Materials Chemistry* **2000**, *10*, 1949-1955.

(23) Rode, E. J. *Doklady Akademii Nauk Sssr* **1958**, *119*, 953-956.

(24) Brown, G. M.; Noespirlet, M. R.; Busing, W. R.; Levy, H. A. *Acta Crystallographica Section B - Structural Science* **1977**, *33*, 1038-1046.

(25) Spirlet, M. R.; Busing, W. R. *Acta Crystallographica Section B - Structural Science* **1978**, *34*, 907-910.

(26) Noespirlet, M. R.; Brown, G. M.; Busing, W. R.; Levy, W. A. *Acta Crystallographica Section A* **1975**, *31*, S80-S80.

(27) Fournier, M.; Feumijantou, C.; Rabia, C.; Herve, G.; Launay, S. *Journal of Materials Chemistry* **1992**, *2*, 971-978.

(28) Uchida, S.; Inumaru, K.; Misono, M. *Journal of Physical Chemistry B* **2000**, *104*, 8108-8115.

(29) Kozhevnikov, I. V.; Sinnema, A.; Vanbekkum, H. *Catalysis Letters* **1995**, *34*, 213-221.

(30) Misono, M. *Chemical Communications* **2001**, *1*, 1141-1152.

(31) Chidichimo, G.; Golemme, A.; Imbardelli, D.; Iannibello, A. *Journal of the Chemical Society - Faraday Transactions* **1992**, *88*, 483-487.

(32) Stepanov, A. G.; Shegai, T. O.; Luzgin, M. V.; Essayem, N.; Jobic, H. *Journal of Physical Chemistry B* **2003**, *107*, 12438-12443.

(33) Thouvenot, R.; Rocchiccioli-Deltcheff, C.; Fournier, M.; Franck, R. *Inorganic Chemistry* **1983**, *22*, 207-216.

(34) Zecchina, A.; Paze, C.; Bordiga, S. *Langmuir* **2000**, *16*, 8139-8144.

(35) Koyano G; Saito T; Hashimoto M; Misono M *Studies in Surface Science and Catalysis* **2000**, *130*, 3077-3082.

(36) Janik, M. J.; Campbell, K. A.; Bardin, B. B.; Davis, R. J.; Neurock, M. *Applied Catalysis A - General* **2003**, *256*, 51-68.

(37) Thouvenot, R.; Fournier, M.; Franck, R.; Rocchiccioli-Deltcheff, C. *Inorganic Chemistry* **1984**, *23*, 598-605.

(38) Mioc, U.; Davidovic, M.; Tjapkin, N.; Colomban, P.; Novak, A. *Solid State Ionics* **1991**, *46*, 103-109.

(39) Mioc, U.; Colomban, P.; Novak, A. *Journal of Molecular Structure* **1990**, *218*, 123-128.

(40) Kearley, G. J.; White, R. P.; Forano, C.; Slade, R. C. T. *Spectrochimica Acta Part A-Molecular and Biomolecular Spectroscopy* **1990**, *46*, 419-424.

(41) Hashimoto, M.; Koyano, G.; Mizuno, N. *Journal of Physical Chemistry B* **2004**, *108*, 12368-12374.

(42) Lee, K. Y.; Mizuno, N.; Okuhara, T.; Misono, M. *Bulletin of the Chemical Society of Japan* **1989**, *62*, 1731-1739.

(43) Taketa, H.; Katsuki, S.; Eguchi, K.; Seiyama, T.; Yamazoe, N. *Journal of Physical Chemistry* **1986**, *90*, 2959-2962.

(44) Ueda, T.; Tatsumi, T.; Nakamura, N. *38th NMR Discussion* **1998**, P104.

(45) Bardin, B. B.; Bordawekar, S. V.; Neurock, M.; Davis, R. J. *Journal of Physical Chemistry B* **1998**, *102*, 10817-10825.

(46) Mioc, U. B.; Colomban, P.; Davidovic, M.; Tomkinson, J. *Journal of Molecular Structure* **1994**, *326*, 99-107.

(47) Dias, J. A.; Caliman, E.; Dias, S. C. L.; Paulo, M.; de Souza, A. *Catalysis Today* **2003**, *85*, 39-48.

(48) Misono, M.; Okuhara, T. *Chemtech* **1993**, *23*, 23-29.

(49) Yang, J.; Janik, M. J.; Ma, D.; Zheng, A. M.; Zhang, M. J.; Neurock, M.; Davis, R. J.; Ye, C. H.; Deng, F. *Journal of the American Chemical Society* **2005**, *127*, 18274-18280.

(50) Biaglow, A. I.; Gorte, R. J.; Kokotailo, G. T.; White, D. *Journal of Catalysis* **1994**, *148*, 779-786.

(51) Biaglow, A. I.; Gorte, R. J.; White, D. *Journal of Physical Chemistry* **1993**, *97*, 7135-7137.

(52) Biaglow, A. I.; Gorte, R. J.; White, D. *Journal of Catalysis* **1994**, *150*, 221-224.

(53) Biaglow, A. I.; Sepa, J.; Gorte, R. J.; White, D. *Journal of Catalysis* **1995**, *151*, 373-384.

(54) Haw, J. F.; Nicholas, J. B.; Xu, T.; Beck, L. W.; Ferguson, D. B. *Accounts of Chemical Research* **1996**, *29*, 259-267.

(55) Xu, T.; Munson, E. J.; Haw, J. F. *Journal of the American Chemical Society* **1994**, *116*, 1962-1972.

(56) Bielanski, A.; Datka, J.; Gil, B.; Malecka-Lubanska, A.; Micek-Ilnicka, A. *Catalysis Letters* **1999**, *57*, 61-64.

(57) Bielanski, A.; Pozniczek, J.; Hasik, M. *Journal of Thermal Analysis* **1995**, *44*, 717-723.

(58) Scroggie, A. G.; Clark, G. L. *Proceedings of the National Academy of Sciences of the United States of America* **1929**, *15*, 1-8.

(59) Illingworth, J. W.; Keggin, J. F. *Journal of the Chemical Society* **1935**, 575-580.

(60) Kozhevnikov, I. V. *Chemical Reviews* **1998**, *98*, 171-198.

(61) Okuhara, T.; Kasai, A.; Hayakawa, N.; Yoneda, Y.; Misono, M. *Journal of Catalysis* **1983**, *83*, 121-130.

(62) Misono, M.; Mizuno, N.; Mori, H.; Lee, K. Y.; Jiao, J.; Okuhara, T. In

Structure-Activity and Selectivity Relationships in Heterogeneous Catalysis, 1991; Vol. 67, pp 87-97.

(63) Essayem, N.; Coudurier, G.; Fournier, M.; Vedrine, J. C. *Catalysis Letters* **1995**, *34*, 223-235.

(64) Kozhevnikova, E. F.; Kozhevnikov, I. V. *Journal of Catalysis* **2004**, *224*, 164-169.

(65) Kozhevnikov, I. V.; Kloetstra, K. R.; Sinnema, A.; Zandbergen, H. W.; van Bekkum, H. *Journal of Molecular Catalysis A - Chemical* **1996**, *114*, 287-298.

(66) Newman, A. D.; Brown, D. R.; Siril, P.; Lee, A. F.; Wilson, K. *Physical Chemistry Chemical Physics* **2006**, *8*, 2893-2902.

(67) Lefebvre, F.; Jouguet, B. *Comptes Rendus De L'Academie Des Sciences Serie II* **1992**, *315*, 1475-1479.

(68) Kuang, W. X.; Rives, A.; Fournier, M.; Hubaut, R. *Applied Catalysis A - General* **2003**, *250*, 221-229.

(69) Lefebvre, F. *Journal of the Chemical Society-Chemical Communications* **1992**, 756-757.

(70) Chuvaev, V. F.; Popov, K. I.; Spitsyn, V. I. *Doklady Akademii Nauk Sssr* **1980**, *255*, 892-895.

(71) Vaughan, J. S.; O'Connor, C. T.; Fletcher, J. C. Q. *Journal of Catalysis* **1994**, *147*, 441-454.

(72) Kozhevnikov, I. V.; Holmes, S.; Siddiqui, M. R. H. *Applied Catalysis A - General* **2001**, *214*, 47-58.

(73) Chang, T. H. *Journal of the Chemical Society - Faraday Transactions* **1995**, *91*, 375-379.

(74) Newman, A. D.; Lee, A. F.; Wilson, K.; Young, N. A. *Catalysis Letters* **2005**, *102*, 45-50.

(75) Kulikov, S. M.; Timofeeva, M. N.; Kozhevnikov, I. V.; Zaikovskii, V. I.;

Plyasova, L. M.; Ovsyannikova, I. A. *Izvestiya Akademii Nauk SSSR Seriya Khimicheskaya* **1989**, *4*, 763-768.

(76) Kapustin, G. I.; Brueva, T. R.; Klyachko, A. L.; Timofeeva, M. N.; Kulikov, S. M.; Kozhevnikov, I. V. *Kinetika i Kataliz* **1990**, *31*, 1017-1020.

Chapter 3

Principles of the main experimental techniques

3.1 Introduction

The main experimental techniques that have been used for the characterisation of the materials examined in this thesis are X-ray powder diffraction (XRD) and Magic-Angle-Spinning Nuclear Magnetic Resonance (MAS NMR) spectroscopy.

The purpose of this chapter is to describe these two techniques and to outline the underlying physical theory in each case. Details of the equipment used and experimental procedures are described in Chapter 4. Other characterisation techniques used in this work are discussed in the appropriate chapters.

3.2 X-ray diffraction

X-ray diffraction provides information on the structure of crystalline solids and a number of detailed accounts of the technique are available.[1-7] This section provides a brief description of the method, followed by an account of the important properties of X-rays and crystalline solids that permit the diffraction phenomenon to be observed and used for the determination of crystal structure.

3.2.1 Properties of X-rays

The proposal that a crystal could act as a three-dimensional diffraction grating for incident electromagnetic radiation with a wavelength of the order of the spacing between the atoms was put forward in 1912 by the German physicist Max von Laue. Electromagnetic radiation that lies in the X-ray region satisfies this criterion and the subsequent extensive use of X-rays with wavelengths between 0.5 and 2.5 Å in the investigation of crystal structures is testimony to von Laue's original insight.

X-rays are produced when any electrically-charged body is rapidly decelerated. An X-ray tube maintains a high voltage (20 - 50 kV) across its electrodes causing electrons to be drawn away from the cathode and rapidly accelerated across the tube where they impact on a metal target or anode. It is at the point of impact that X-rays are generated and they radiate in all directions. There is a continuous range of wavelengths corresponding to Bremstrahlung radiation (literally 'braking radiation') due to the incident electrons not all being stopped upon impact but giving up their energies in stages.

The intensity of the emitted spectrum depends on the accelerating voltage applied. However, spikes are produced above a certain threshold level and their wavelength depends upon the type of metal used for the anode. These spikes are superimposed upon the continuous spectrum as shown in Figure 3.1 for copper and molybdenum anodes. For a given metal, the spikes give rise to characteristic, well defined, radiation.

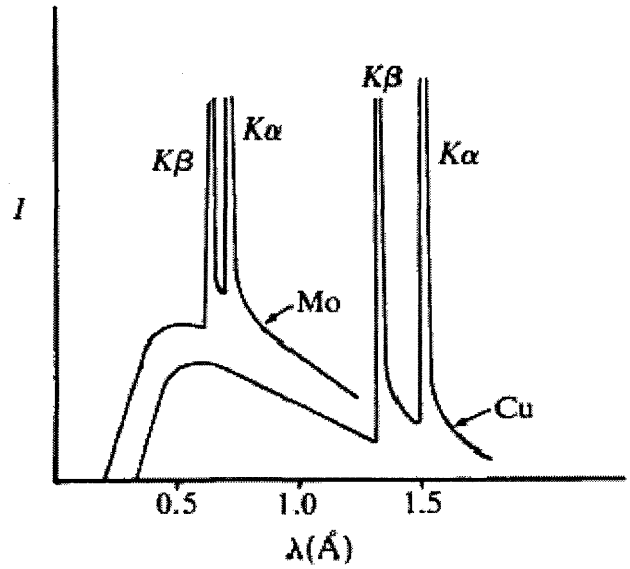

Figure 3.1 K_α and K_β peaks superimposed on the continuous spectrum of X-ray radiation for copper and molybdenum targets.

In an atomic level description, the characteristic radiation arises due to the interaction of high-energy photons with the core electrons of the metal atoms making up the target. When an incident electron knocks out a core electron from the *K*-shell, the lowest energy shell, the atom is left in an excited state and electrons from a higher shell (*L*, *M*, ...) cascade down into the vacancy. This process results in the emission of radiation with characteristics determined by the difference in energy between two given levels. In a copper target, as shown in Figure 3.1, there are two distinct emissions, K_α and K_β, with wavelengths in the region of 1.5 Å. A schematic mechanism for the production of K_α and K_β X-ray emissions is shown in Figure 3.2.

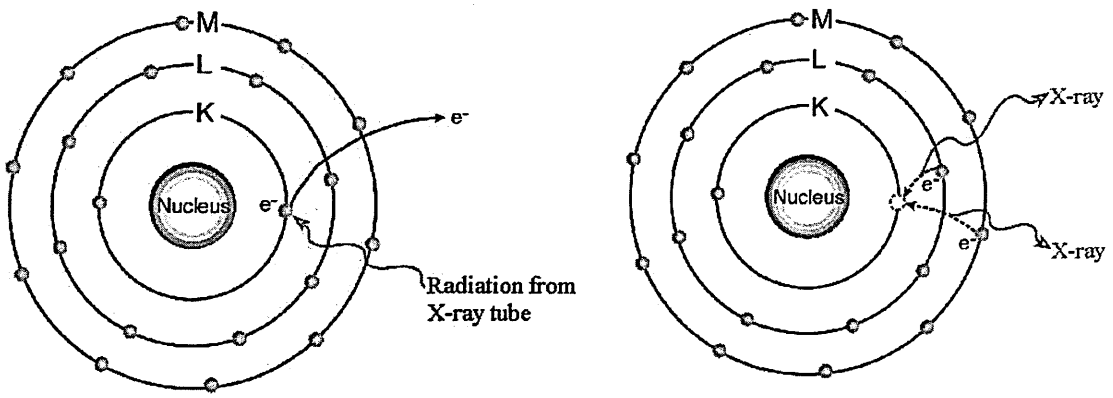

Figure 3.2 A schematic mechanism showing the production of K_α and K_β X-ray emission.

Further fine structure can arise in the X-ray emissions and this leads to a refined notation. The principal quantum number of the vacancy (n = 1, 2, 3, ...) is designated by K, L, M, ... respectively, and the number of the upper level of the transition, relative to the vacancy, is indicated by a subscript α, β, γ, ... Any fine structure levels are indicated by a further numerical subscript. In the case of copper, K_α is a doublet and the individual components are labelled $K_{\alpha 1}$ and $K_{\alpha 2}$. The emitted X-ray are due to vacancies in the lowest core level (n = 1) being filled by a transition from the next level (n = 2), specifically from either the $P_{3/2}$ or $P_{1/2}$ angular momentum states of n = 2. Without specific filtering, the diffraction patterns produced using Cu K_α irradiation will show double diffraction peaks and these become more separated as the diffraction angle increases. The wavelengths for copper are:

$K_{\alpha 1}$	1.540598 Å
$K_{\alpha 2}$	1.544426 Å
K_{β}	1.392334 Å

Although it is possible to produce monochromatic X-rays using a cyclotron, this is an extremely expensive process and for most applications it is more practical to use filters. The *K*-absorption-edge wavelength for nickel, corresponding to the energy required to promote an electron from the *K*-shell to continuum threshold, is at 1.488 Å. As a consequence, nickel will absorb Cu K_{β} radiation much more strongly than Cu K_{α} radiation. A nickel foil in an incident X-ray beam absorbs Cu K_{β} and most of the continuous radiation while allowing approximately 40 % of K_{α} radiation to pass.

3.2.2 Crystal structure

A defining feature of a crystal is that it consists of a periodic arrangement of atoms, ions or molecules packed together in three dimensions. To describe a crystal structure it is only necessary to consider the basic unit cell. The unit cell is characterised by three distances and three angles as shown in Figure 3.3.

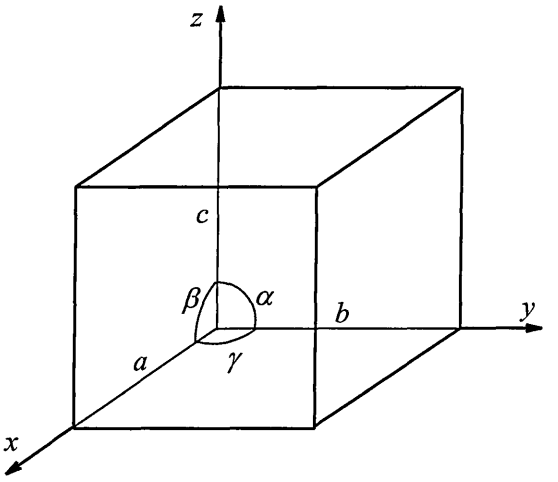

Figure 3.3 A unit cell showing the cell dimensions *a, b, c* and the angles α, β, γ.

Unit cells can be classified in terms of seven crystal systems and these are summarised in Table 3.1. A unit cell with lattice points only at the corners is referred to as primitive (P). It is also possible, depending on the unit cell system, to have additional lattice points: at the centre of the unit cell referred to as body-centred (I); at the centres of six faces referred to as face-centred (F) and at the centre of opposite faces referred to as side-centred (A, B, or C). In total, there are fourteen distinct types of unit cell and these give rise to fourteen types of lattices called the Bravais lattices.

Table 3.1 The seven crystal systems.

System	Unit cell	
	Lengths	**Angles**
Cubic	$a = b = c$	$\alpha = \beta = \gamma = 90°$
Tetragonal	$a = b \neq c$	$\alpha = \beta = \gamma = 90°$
Orthorhombic	$a \neq b \neq c$	$\alpha = \beta = \gamma = 90°$
Monoclinic	$a \neq b \neq c$	$\alpha = \gamma = 90°$, $\beta \neq 90°$
Triclinic	$a \neq b \neq c$	$\alpha \neq \beta \neq \gamma \neq 90°$
Hexagonal	$a = b \neq c$	$\alpha = \beta = 90°$; $\gamma = 120°$
Rhombohedral	$a = b = c$	$\alpha = \beta = \gamma \neq 90°$

The symmetry elements of a three-dimensional crystalline arrangement include those arising due to translations through space. This leads to an extensive set of groups referred to as space groups. Based on the Bravais lattices there are 230 space groups that can be used to classify crystal structures. Space groups are tabulated in the International Tables for Crystallography[8] and in other standard reference works.

In terms of a crystal structure represented by lattice points it is possible to define different families of planes. Several examples are shown in Figure 3.4 which, for convenience, only considers a two-dimensional lattice point array.

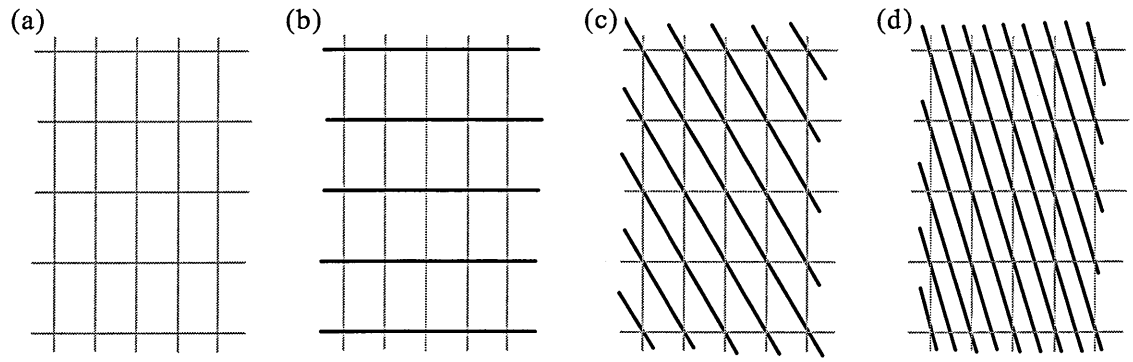

Figure 3.4 Three planes (b, c, d) based on a crystal lattice (a).

Each of the three families of planes (b), (c) or (d), is based on the same underlying lattice (a) but the spacing between planes is different for each set. It is this difference in spacings that can be exploited by diffraction techniques to give information on a crystal structure. In terms of nomenclature, diffraction planes are labelled by their Miller indices for which the general form is (*hkl*). The indices *hkl*, which can be negative, specify the orientation of the plane with respect to the unit cell edges.

3.2.3 The basic diffraction condition

When monochromatic X-rays strike an atom, its electrons interact with the X-rays and the X-radiation is scattered, normally at the same wavelength. In the model case of a single atom, the scattered waves can be viewed as a spherical wavefront. The three-dimensional array of atoms in a crystal results in the individual spherical wavefronts interfering with one another. The condition for detecting diffracted radiation, assuming elastic scattering, from the array is that the waves interfere constructively with one another; that is, they must be in phase. This requirement is illustrated in Figure 3.5 which considers an array of lattice points as a reflection

rather than a diffraction grating. This approach is due to the original work of William and Lawrence Bragg (1913) and leads to their well-known crystallographic equation.

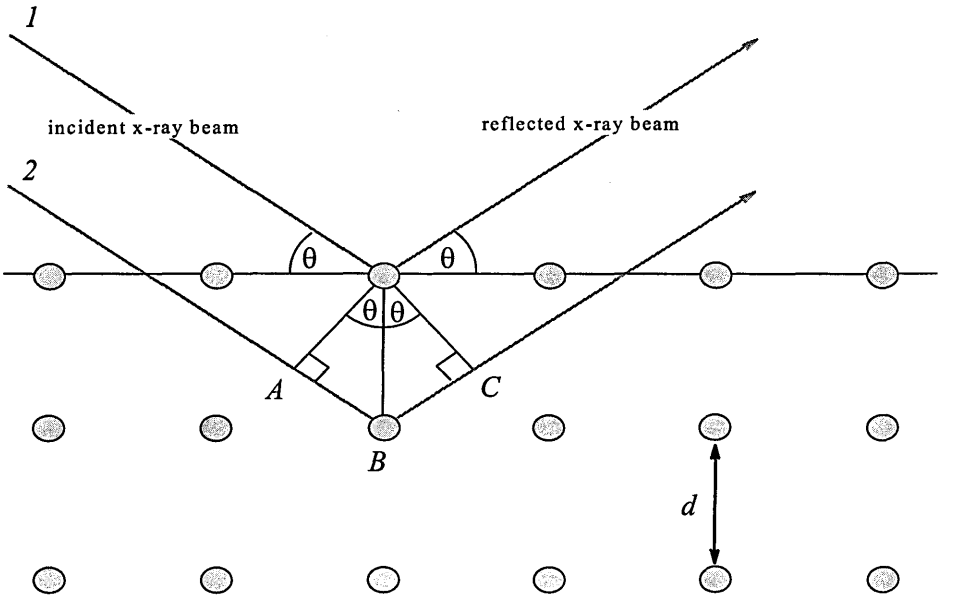

Figure 3.5 Schematic representation of the specular reflection of a monochromatic X-ray beam from parallel lattice planes with interplanar spacing, *d*.

The X-ray beam strikes the surface of the crystal at an angle θ, and part of the beam interacts with the electrons of the atoms in the top layer and is reflected at the same angle; that is, specular reflection. A similar situation applies to the X-rays that penetrate to the second and subsequent layers. In order for a peak to be observed in the 'diffractogram', X-rays reflected from the various layers must arrive in-phase at the detector. For this condition to be met the extra path length travelled by the X-ray reflected from the second layer must equal a whole number of wavelengths. The path difference between beams *1* and *2* in Figure 3.5 is the length $AB + BC$ and this can be written as:

$$AB + BC = 2d \sin \theta \tag{3.1}$$

For constructive interference, the path difference must be equal to an integral number of wavelengths, so that

$$n\lambda = 2d \sin \theta \tag{3.2}$$

This is the Bragg law where n is the order of diffraction and θ is known as the Bragg angle. Depending on the values of λ and d, there may be a number of angles for which the Bragg conditions applies. In practice, Equation (3.2) is usually written in the form

$$\lambda = 2d_{hkl} \sin \theta \tag{3.3}$$

In this case, each reflection from a three-dimensional lattice occurring at a net scattering angle of 2θ from the incident beam is related to the interplanar spacing for a given set of planes (hkl). For example, for a cubic unit cell with cell length a

$$d^2_{hkl} = a^2 / (h^2 + k^2 + l^2) \tag{3.4}$$

so that

$$\sin \theta = \lambda (h^2 + k^2 + l^2)^{1/2} / 2a \tag{3.5}$$

Equation 3.3 is the basis of all methods for obtaining geometrical information for a unit cell from a diffraction pattern.

In the case of a single crystal, the diffraction pattern is recorded as a series of 'diffraction spots' by rotating the crystal in the monochromatic X-ray beam. It will only be at certain orientations that the basic diffraction condition represented by Equation 3.3 will be satisfied. As already indicated, the geometry of this pattern is directly related to the geometry of the unit cell. The intensities of the individual spots, however, will vary markedly with some too weak to observe. Basically, the intensity of a given spot will depend upon the intensity of the source radiation and,

critically, the density of reflecting electrons and their relationship to the particular plane. It is the analysis of reflection intensities, although complex, that leads to information concerning the positions of atoms within a unit cell.

3.2.4 Powder diffraction methods

An ideal powder sample consists of crystallites that are oriented at random over all space. If this ideal sample is irradiated with monochromatic X-ray radiation then some of the crystallites will be oriented such that a given family of planes $\{hkl\}$ will satisfy the Bragg condition. This is the basis of the Debye-Scherrer method of powder diffraction. As shown schematically in Figure 3.6, the method gives rise to cones of diffracted intensity. This is because for a given family of planes there will be a continuous collection of crystallites with orientations around the direction of the incident beam for which the Bragg condition can be satisfied.

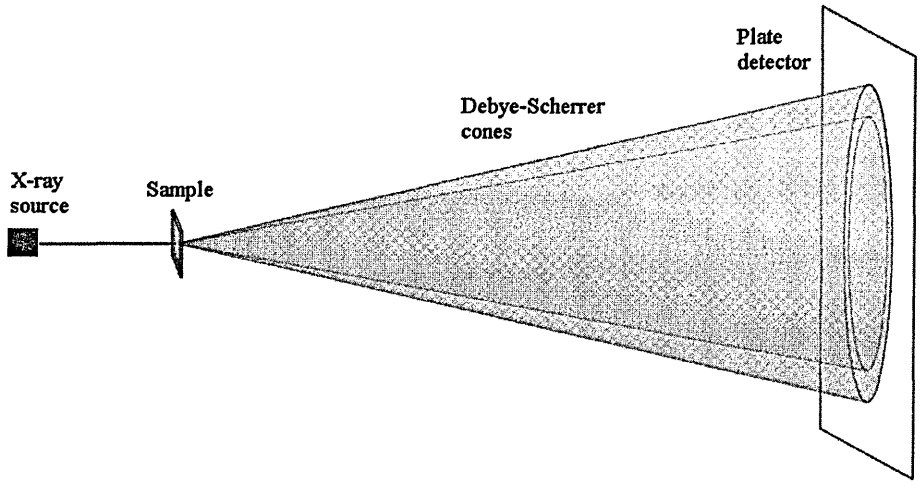

Figure 3.6 The Debye-Scherrer method produces cones of diffraction intensity.

Modern X-ray diffraction studies of polycrystalline samples are usually recorded on computer-controlled diffractometers (Figure 3.7). The sample to be investigated is rotated through the Bragg angle (θ) and the detector is rotated simultaneously through 2θ, essentially a cut is taken through the diffraction cones. In addition, the sample is rotated about the axis of its container at constant speed in order to compensate for any preferred orientations of the crystallites.

The detector for the instrument converts X-rays into small flashes of light (scintillations) which are counted over a set period of time, the total count being proportional to the intensity of the diffracted beam. An X-ray diffraction pattern is recorded in the form of scintillation counts (representing X-ray intensity) versus 2θ, the recorded data is then stored in a digital file.

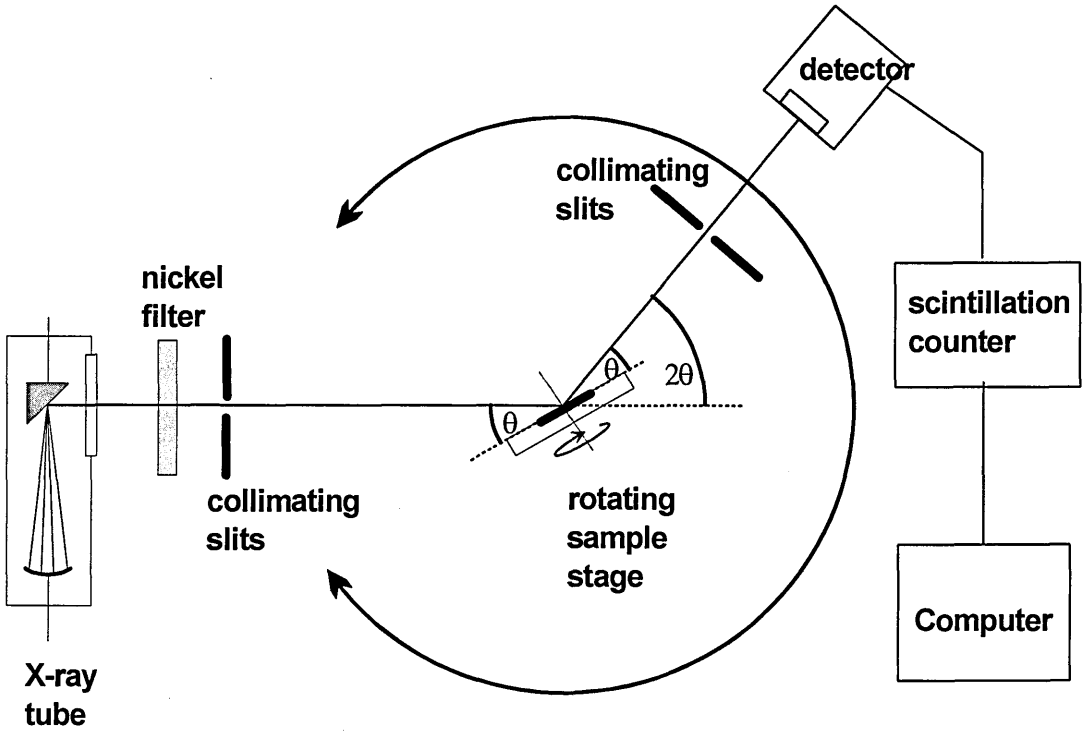

Figure 3.7 A schematic representation of a modern X-ray powder diffractometer.

3.3 Nuclear magnetic resonance (NMR) spectroscopy

NMR spectroscopy is a powerful technique that has widespread applications throughout all branches of science and, as a consequence, there is a considerable NMR literature relating to both the development of the technique and its applications to a wide range of materials. The content of this section is intended only to provide sufficient background to support the NMR investigations described in this thesis. More detailed information can be found in a wide range of textbooks and review papers, including the selection given in the reference list at the end of this chapter.[9-13]

3.3.1 Basic theory of NMR

The phenomenon of nuclear magnetic resonance is restricted to those isotopes whose nuclei possess the properties of nuclear spin. These nuclei have magnetic properties and as a consequence will interact with an applied magnetic field. It is this interaction that forms the basis of all NMR experiments.

In quantum mechanical terms an atomic nucleus is characterised by a nuclear spin quantum number, I. This is often referred to as just 'spin'.

The value of I for a given nucleus depends upon its mass number as well as its atomic number. For protons and neutrons the value of $I = ½$. For the nuclei of atoms, other than the hydrogen atom, the situation is more complex since the protons and neutrons couple within the nucleus to give an overall nuclear spin. In general, the value of I is a fundamental property of all nuclei and it may be integer, half-integer or zero; that is, it can only take values, 0, $^1/_2$, 1, $^3/_2$, 2, $^5/_2$, and so on.

There is no simple means of predicting the value of I for the nucleus of a given isotope. However, a few generalizations can be made. All nuclei with even mass number and even charge number have $I = 0$ and so these nuclei are NMR inactive, common examples of this situation are ^{12}C and ^{16}O. In the case of even mass number but an odd charge number, the nucleus has an integral nuclear spin quantum number. Only seven permanent nuclei fall into this category; ^{2}H and ^{14}N both with $I = 1$ are the most studied. All nuclei with odd mass numbers have half-intergral nuclear spin which can be expressed as $I = {}^{n}/_{2}$ where n is an odd integer. In total there are 33 permanent nuclei with $I = ½$, including ^{1}H, ^{13}C, ^{29}Si and ^{31}P, and 88 permanent nuclei possess $I > ½$. The latter are known as quadrupolar nuclei, because they possess a nuclear electric quadrupole moment and represent 74% of all NMR active nuclei. Various NMR properties of a few selected isotopes relevant to the work in this thesis are given in Table 3.2.

Table 3.2 NMR properties of selected isotopes.

Nucleus	Natural abundance / %	I	*Resonance frequency / MHz	†γ / 10^7 rad s^{-1} T^{-1}
^{1}H	99.985	$\frac{1}{2}$	399.99	26.7522
^{13}C	1.108	$\frac{1}{2}$	100.66	6.7283
^{29}Si	4.70	$\frac{1}{2}$	79.43	– 5.3190
^{31}P	100	$\frac{1}{2}$	161.83	10.8394

*Values quoted are for a field strength of 9.400 T.
†Magnetogyric ratio (see text).

The magnitude of nuclear spin angular momentum is given by

$$\tilde{N} = \hbar[I(I+1)]^{\frac{1}{2}} \tag{3.6}$$

where $\hbar = h/2\pi$ and h is Plank's constant.

From classical electromagnetism, it is known that a circulating electric charge in a magnetic field has an associated magnetic dipole moment. In the particular case of nuclei that possess spin angular momentum

$$\mu = \gamma P \tag{3.7}$$

where μ is the nuclear magnetic dipole moment and is a vector quantity. The quantity γ is the magnetogyric ratio of the nucleus and is defined as the ratio of the magnitude of the magnetic moment to that of the spin angular momentum. The value of γ varies from nuclide to nuclide and may be positive or negative; for example, see Table 3.2. From equations 3.6 and 3.7 the magnitude of the nuclear magnetic dipole moment is given by

$$\mu = \gamma\hbar[I(I+1)]^{\frac{1}{2}} \tag{3.8}$$

In the absence of a magnetic field, the energy of an isolated nucleus is independent of its orientation and all orientations have the same energy. However, if a strong magnetic field is applied, a nucleus of spin I can only adopt one of $2I+1$ possible orientations such that the component of the nuclear magnetic dipole moment that is observable along the z axis, that is μ_z, is given by

$$\mu_z = -\gamma\hbar m_I \tag{3.9}$$

where m_I is the magnetic quantum number. The allowed magnetic energy levels are then given by

$$E = -\gamma\hbar m_I B_0 \tag{3.10}$$

where B_0 is the magnitude of the applied magnetic field. For a nucleus of spin $I = {}^1/_2$, there are just two allowed magnetic energy levels characterised by $m_I = +{}^1/_2$ and $m_I = -{}^1/_2$. The two energy levels are separated by $|\gamma\hbar B_0|$ which is referred to as the Zeeman splitting. In general terms, the NMR selection rule is $\Delta m_I = \pm 1$ so that

allowed transitions are between those levels that are adjacent in energy. In the case of an isolated spin $I = {}^1/_2$ nucleus, transitions between the two levels can be induced by electromagnetic radiation in the radio-frequency (rf) regime, such that

$$\nu = \left|\frac{\gamma}{2\pi}\right| B_0 \tag{3.11}$$

This equation gives the fundamental resonance condition and applies to all NMR experiments irrespective of the spin of the nuclide. It must be noted, however, that it applies only to an isolated nucleus.

3.3.2 NMR spectroscopy in solids

High resolution NMR spectroscopy in the liquid state tends to produce spectra with very narrow resonance lines from which chemical shift and spin-spin coupling information can be extracted with considerable precision. This in turn allows highly accurate correlations of the measured NMR parameters with those of known nuclear environments in model compounds so that detailed chemical information about the material under investigation can be obtained. By contrast, the NMR spectra of solids are generally broad and poorly resolved, if measured by conventional techniques.

The main reason for the difference between the spectra of liquid and solid materials can be attributed to the presence of a rapid, usually isotropic, molecular motion in the liquid state. In these circumstances, there is complete averaging of the anisotropic nuclear spin interactions, with the result that the isotropic chemical shifts of resonance lines are well resolved in the NMR spectrum. By contrast, the motion of atoms, ions or molecules in solids is often restricted and the anisotropic characteristics of the NMR interactions dominate the spectra. These interactions vary in magnitude depending upon orientation with respect to the applied magnetic

field and, in powder (polycrystalline or amorphous) samples, the resulting spectra represent a distribution over all orientations. Thus, the solid-state NMR spectra of powder samples are generally quite broad and often appear to have very little definition. Nonetheless, in principle, they contain a considerable amount of information relating to the detailed nature of the crystallographic and electronic environment of the resonant nucleus under investigation.

There are difficulties in both the acquisition and interpretation of solid-state NMR spectra. Furthermore, nuclei in solids, particularly those with spin $I = ½$, usually have long spin-lattice relaxation times (T_1). However, a number of techniques are now available that allow the acquisition of solid-state NMR spectra while selectively removing the influence of anisotropic nuclear spin interactions. A number of these are based on magic-angle-spinning (MAS) NMR spectroscopy and applications have been used on a wide range of materials.[10,12] MAS is able to reduce, or remove, the influence of both chemical shielding and magnetic dipole-dipole coupling anisotropic effects. The basic MAS NMR experiment involves compressing a polycrystalline sample into a cylindrical form within a rotor. This rotor is then placed in the main magnetic field (see Figure 3.8). The rotor is then rapidly rotated about its own axis. Further details are given below in the separate discussions of chemical shielding anisotropy and magnetic dipole-dipole interactions. A further important technique in the solid-state is cross-polarisation. For example, cross polarisation MAS NMR (CPMAS NMR) plays a key role in ^{13}C solid-state NMR spectroscopy. Cross-polarisation is also discussed in more detail below.

Chemical shielding anisotropy

When a nucleus is placed in an external magnetic field, the electrons surrounding it interact with this field and their motion is affected so that a secondary magnetic field arises which generally opposes the external field. Overall, there is a shielding effect due to the surrounding electrons. The magnitude of the effective magnetic field, B, at the nucleus is written as

$$B = B_0(1 - \sigma) \tag{3.12}$$

where the dimensionless number σ is called the chemical shielding constant and is usually quoted in parts per million (ppm). The resonance frequency for a nucleus i is obtained by combining equations 3.11 and 3.12 so that:

$$\nu_i = \left|\frac{\gamma}{2\pi}\right| B_0(1-\sigma) \tag{3.13}$$

The value of ν_i is sensitive to the chemical environment of the nucleus.

In general, chemical shielding is a tensor property with principal components σ_{11}, σ_{22} and σ_{33}. In the case of rapid and isotropic molecular tumbling in solution, there is averaging of the tensor so that only the isotropic value is observed. This is conventionally labelled σ_{iso} and takes the value $1/3(\sigma_{11} + \sigma_{22} + \sigma_{33})$. In a polycrystalline sample, with random packing of crystallites, all orientations of the chemical shielding tensor with respect to the main magnetic field are present. As a consequence, there is absorption over a range of frequencies giving rise to a broad resonance line with a shape characteristic of the relative values of the components of the chemical shielding tensor. In practice, these shapes can be characterised by a corresponding chemical shift tensor with principal values δ_{11}, δ_{22} and δ_{33}, where $\delta_{11} \geq \delta_{22} \geq \delta_{33}$. The isotropic chemical shift is defined as $\delta_{iso} = 1/3(\delta_{11} + \delta_{22} + \delta_{33})$ and

the lineshape can then represented by the chemical shift anisotropy $\Delta = (\delta_{11} - \delta_{iso})$ and the asymmetry $\eta = (\delta_{33} - \delta_{22})/\Delta$. The chemical shift anisotropy provides a measure of the largest extent of the lineshape from its centre of gravity.

The lineshapes characteristic of polycrystalline samples, which are broadened due to chemical shielding anisotropic effects, can be simplified by MAS. In general, chemical shielding interactions have an angular dependence that depends on the term $(3\cos^2\theta - 1)$ where θ describes the orientation of a given nuclear environment with respect to the main magnetic field. If a polycrystalline sample is packed into a cylindrical form and then spun at an angle ϕ to this main magnetic field, see Figure 3.8, then the angle θ becomes time dependent. It is then necessary to consider the time average of the following angular term:

$$\left\langle 3\cos^2\theta(t) - 1 \right\rangle_{spinning} \tag{3.14}$$

For rapid spinning, at frequencies greater than those characterising the anisotropy, this average reduces to an expression containing the following angular term as an overall multiplier

$$\frac{1}{2}\left(3\cos^2\phi - 1\right) \tag{3.15}$$

If the angle ϕ equals 54.7356°, the so-called 'magic angle', this term, and consequently the whole expression, becomes zero: in effect, broadening due to chemical shielding anisotropy is removed from the NMR spectrum.

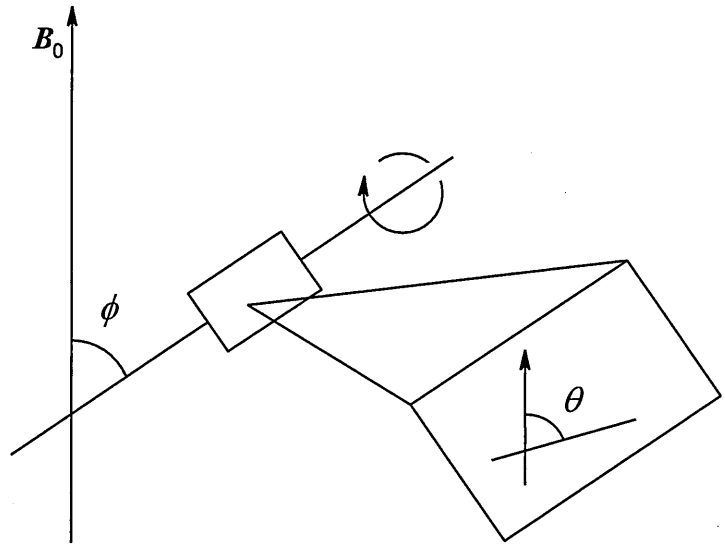

Figure 3.8 A view of a polycrystalline sample in a rotor which has its cylindrical axis inclined at an angle ϕ to the direction of the applied magnetic field. At any point in the sample, as shown by the schematic inset, there will be a particular orientation of the environment surrounding a given nucleus and this is characterised by the angle θ.

In practice, the sample is often not spun at sufficiently high speeds for the anisotropy to be completely averaged. In this case the time-dependence is evident in the appearance of spinning sidebands; that is additional peaks separated from the isotropic peak, and each other, by the rotor spinning frequency. As an example, the effects of different spinning frequencies on ^{31}P MAS NMR experiments for $CaBPO_5$ are shown in Figure 3.9.[14] (As indicated in the figure caption, a small amount of an impurity, identified as $Ca_2P_2O_7$, is also detected). The total signal intensity measured across the spectral range is approximately the same for each spinning frequency and the spacing between spinning sidebands increases linearly with this

frequency. The asymmetry of the side bands about the isotropic peak can be used to retrieve information about the chemical shielding anisotropy using standard analysis programs, such as dmfit.[15]

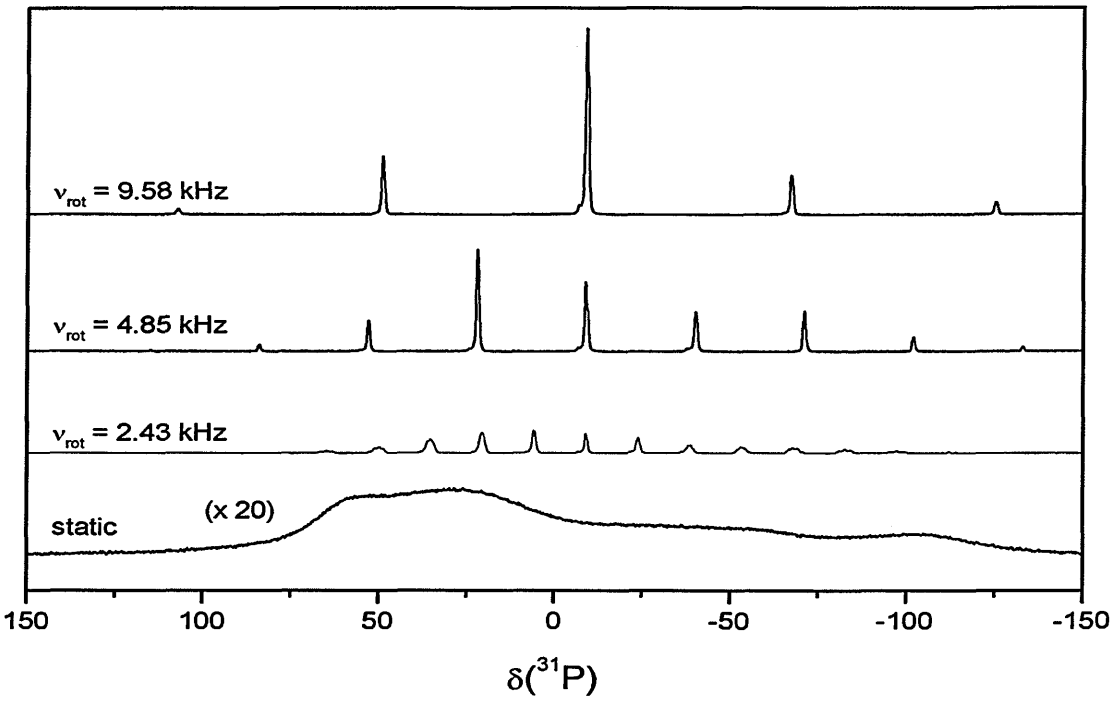

Figure 3.9 Static and ^{31}P MAS NMR spectra for $CaBPO_5$ measured at 161.8 MHz and at different spinning frequencies. (The presence of a small amount of impurity, identified as $Ca_2P_2O_7$, is clearly seen in the MAS NMR spectrum obtained at ν_{rot} = 9.58 kHz. This would not be detected in the static spectrum.) (Diagram modified from reference 14.)

Magnetic dipole-dipole interactions

A second important factor affecting the total magnetic field experienced by an observed nucleus is that due to the presence of the magnetic dipole moments of

neighbouring nuclei. These interactions can be either homonuclear or heteronuclear, in origin.

The z component of the magnetic field produced by a neighbouring nucleus with spin $I \neq 0$ and magnetic dipole moment μ at an observed nucleus is

$$B_z = \frac{\pm \mu(3\cos^2\theta - 1)}{r^3} \tag{3.16}$$

where r is the internuclear distance and θ is the angle between r and the main magnetic field in the z direction (Figure 3.10). This direct coupling is usually several orders of magnitude stronger than the scalar coupling transmitted through chemical bonds.

As with chemical shielding anisotropy, magnetic dipole-dipole interactions are made time-dependent under sample spinning conditions; depending on their strength, they are either partially or totally averaged. For many nuclei, sample rotation in the range 3 kHz to 5 kHz is sufficient to remove magnetic dipolar broadening. However, this is not the case for samples containing ^{1}H or ^{19}F nuclei which have relatively large magnetic dipole moments. In these cases, very high spinning frequencies are required or high-power decoupling sequences are necessary.

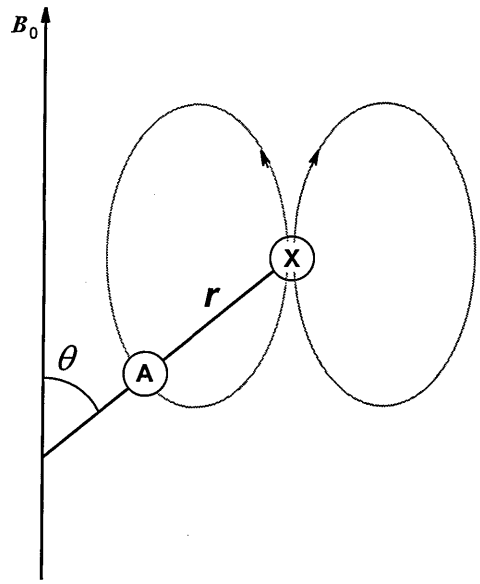

Figure 3.10 The magnetic dipolar interaction between two nuclei, A and X, where A is the observed nucleus. Light grey lines represent the magnetic field generated by X.

Cross polarization

Nuclei with low natural abundances, for example ^{13}C, are often referred to as dilute or rare spins. Two problems which arise in recording spectra from these nuclei, particularly in the solid state, are as follows. Firstly, because of the low natural abundance, the signal to noise ratio is usually low. Secondly, the spin-lattice relaxation times tend to be very long. This is largely because of the absence of strong homonuclear magnetic dipolar interactions which can stimulate relaxation transitions. Long relaxation times mean that the delay time between acquisitions are long so that the accumulation of sufficient scans to obtain a reasonable signal-to-noise ratio takes an excessive amount of time.

Both of these problems can be solved using a process known as polarisation transfer, or cross polarisation (CP). The essence of the process is to use a particular form of

pulse sequence that results in transfer of magnetisation from neighbouring abundant nuclei (often ^{1}H) to the rare spins. The resulting enhancement of signal is of the order of γ_I/γ_S where I represents the abundant spin and S the rare spin. In addition, the repetition rate for the cross polarisation experiment is now determined by the relaxation processes for the abundant spins and these are considerably more efficient than those for the rare spin. Cross polarisation can be incorporated into MAS NMR experiments. CPMAS NMR experiments, for example ^{13}C-^{1}H, are widely used in solid-state NMR.

References

(1) Klug, H. P.; Alexander, L. E. *X-ray Diffraction Procedures for Polycrystalline and Amorphous Materials*; John Wiley & Sons: New York, London, Sydney, 1954.

(2) Azaroff, L. V.; Buerger, M. J. *The Powder Method in X-ray Crystallography*: New York, Toronto, London, 1958.

(3) Jeffery, J. W. *Methods in X-ray Crystallography*; Academic Press: London, 1971.

(4) Wormald, J. *Diffraction Methods*; Clarendon Press: Oxford, 1973.

(5) Cullity, B. D. *Elements in X-ray Diffraction*, 2nd ed.; Addison-Wesley Publishing Co. Inc.: London, 1978.

(6) Whiston, C. *X-ray Methods*; John Wiley and Sons Inc.: London, 1987.

(7) Laing, M. *An Introduction to the Scope, Potential and Applications of X-ray Analysis*; University College Cardiff Press: Cardiff, 1981.

(8) *International tables for crystallography*; Kluwer Academic Publishers: Dordrecht, 1995.

(9) Harris, R. K. *Nuclear Magnetic Resonance Spectroscopy*; Longman: Harlow, 1983.

(10) Engelhardt, G.; Dieter, M. *High-Resolution Solid-State NMR of Silicates and Zeolites.*; Wiley, Chichester, 1987.

(11) Farrar, T. C.; Becker, E. D. *Pulse and Fourier Transform NMR*; Academic Press: New York and London, 1971.

(12) Duer, M. J. *Solid-state NMR Spectroscopy*; Blackwell Publishing Ltd: Oxford, 2004.

(13) Hore, P. J. *Nuclear Magnetic Resonance*; Oxford Chemistry Primers 32, Oxford University Press: Oxford, 1995.

(14) Creamer, N. *Fundamental and industrial aspects of the crystallisation of amorphous silica* **2003**, *The Open University*.

(15) Massiot, D.; Fayon, F.; Capron, M.; King, I.; Le Calve, S.; Alonso, B.; Durand, J.-O.; Bujoli, B.; Gan, Z.; Hoatson, G. *Magnetic Resonance in Chemistry* **2002**, *40*, 70-76.

Chapter 4

Experimental : materials and techniques

4.1 Materials

12-Heteropolyacids

12-Phosphotungstic acid was obtained from Sigma-Aldrich Chemicals and 12-silicotungstic acid was obtained from Japan New Metals Co., Ltd. Both materials were provided in hydrated states although details were not provided.

Authentic catalyst samples

Authentic catalyst samples were supplied by the BP Chemicals plc (Saltend, Hull) in the form of pellets of various sizes. Further details are provided in Table 4.1. Details of the original catalyst preparation are subject to confidentiality agreements. In outline it involved the addition of a 12-silicotungstic acid solution to the solid silica support which was in the form of pellets. Excess water was removed from the mixture and the resulting solid was dried in air at 120°C.

Table 4.1 Histories of the catalysts used in this thesis.

Catalyst sample	Sample history
Authentic unused catalyst	12-Silicotungstic acid, 25 wt %, supported on silica pellets with a 3-6 mm particle diameter.
Used catalyst : JM2	Used in the catalytic reactor and provided in the form of pellets 3-6 mm in size. The sample was removed from the reactor after a major heating event had taken place. It is known that the activity of this catalyst has been significantly reduced.
Used catalyst : JM3	Used in the catalytic reactor and provided in the form of pellets 3-6 mm in diameter. This catalyst did not experience any significant harmful event during its lifetime in the reactor.

Other materials used

Other materials used in this work include isotopically labelled 2-^{13}C-acetone (99% ^{13}C enriched) used as supplied by Sigma-Aldrich, ultra-high purity water (prepared using a Millipore Elix 3 combined with a Millipore Synergy 185, electrical resistivity = 18.2 MΩ cm^{-1}) and dichloromethane.

4.2 Methods of preparation

Preparation of the hydrated states of $H_4[SiW_{12}O_{40}]\cdot xH_2O$

These states were all prepared by allowing the hydration of the hexahydrate. This particular hydrate was prepared from hydrated, as received, 12-silicotungstic acid by heating at 150°C for 2 hours. Analysis using various techniques (Thermal analysis, XRD, ^{29}Si MAS NMR and FT-IR spectroscopy) confirmed the hexahydrate.

Figure 4.1 shows the weight gain observed for $H_4[SiW_{12}O_{40}]\cdot 6H_2O$ as it stands in air on an open balance. There are significant weight changes, corresponding to hydration effects, over timescales measured in minutes. Once prepared, it is important that the hexahydrate is stored in a sealed container.

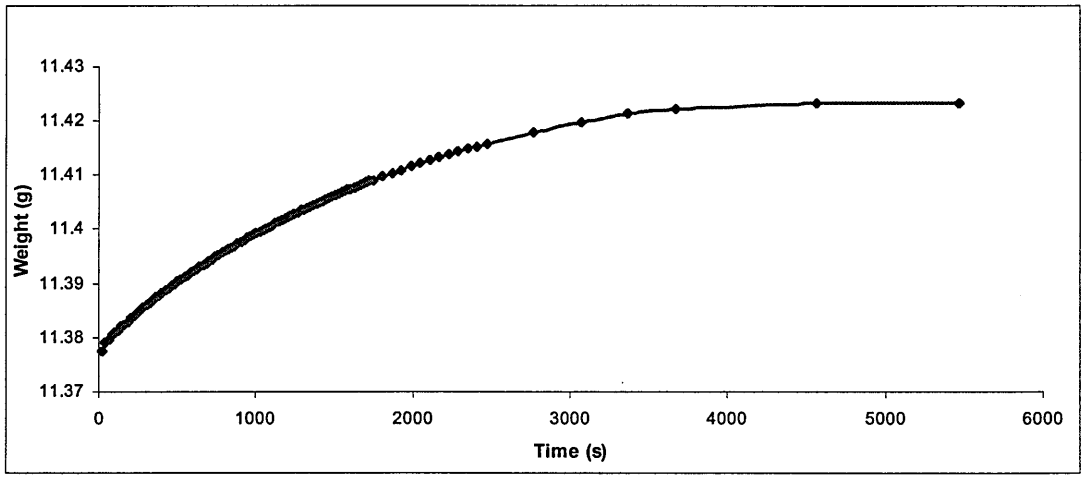

Figure 4.1 Weight gained by $H_4[SiW_{12}O_{40}]\cdot 6H_2O$ on standing in air.

The method of preparing higher hydrates was as follows. The hexahydrate was allowed to absorb water molecules directly in a sealed container containing water. To ensure the process of absorption was as homogeneous as possible, the sample was spread out thinly over the surface of a watch glass. The progression of the absorption process was followed by quickly removing the sample and watch glass

from the container and weighing. Provided this activity was carried out in 1-2 minutes there was little effect on the hydration state of the sample (see Figure 4.1). The gain in weight of the sample was monitored until a target weight corresponding to a particular hydrate was achieved. The sample was then removed from the container and sealed in an air tight container.

Preparation of mixed hydrates of 12-silicotungstic acid and 12-phosphotungstic acid.

A solution of 12-silicotugstic acid was prepared by dissolving $H_4[SiW_{12}O_{40}]\cdot 6H_2O$ (3 g) in ultrahigh purity water (25 ml). The use of ultra-high purity water is discussed in Section 4.3. This solution was then added to a solution of 12-phosphotungstic acid (25 ml) prepared from $H_3[PW_{12}O_{40}]\cdot 6H_2O$ (3 g) under the same conditions. The resulting mixed solution was stirred for five minutes and allowed to evaporate to dryness to give a white powder which was characterised by thermal analysis, XRD, ^{29}Si MAS NMR and FT-IR spectroscopy.

The preparation method discussed above is for a 1 : 1 mixed compound. Mixed compounds with other ratios (1 : 3 and 3 : 1) were prepared using the same method.

4.3 Extraction procedures

Aqueous extraction of 12-silicotungstic acid from the authentic unused catalyst

The extent to which 12-silicotungstic acid could be extracted from the authentic unused catalyst using water was investigated. For this purpose it was necessary to use ultra-high purity water. This was because preliminary experiments revealed

contamination of extracted $H_4[SiW_{12}O_{40}]$ if water from other, less pure, sources was used.

The aqueous extraction procedure was as follows. A sample of catalyst (3g) was placed in a beaker with ultra-high purity water (40 ml). The solution was stirred for five minutes and filtered. The material that is water insoluble is left as a residue in the filter paper and can subsequently be characterised. Evaporation of the filtrate allows the original water soluble material to be investigated.

Dichloromethane extraction of coke deposited on the surface of the used catalysts

Soxhlet extraction, with dichloromethane (200 ml) as the solvent, was used to remove any soluble carbon deposits on the used catalyst. Dichloromethane extraction has previously been used to remove soluble carbon present on silica-supported $H_3[PW_{12}O_{40}]$ catalysts[1]. The filtrate was initially dark green in colour, but after several extractions became lighter green in colour. This process was continued until no further colour was observed in the filtrate. This process took approximately 4 hours to complete. The residue was then allowed to dry before characterisation.

4.4 Thermal removal of deposited coke

Used catalysts were heated at a temperature of 400°C for between 0 - 48 hours in air. The remaining material was subjected to aqueous extraction procedures (see Section 4.3) for further investigation.

4.5 Adsorption of acetone

Adsorption of isotopically-labelled 2-^{13}C-acetone (99%, ^{13}C enriched) was used to investigate the acid sites in $H_4[SiW_{12}O_{40}]\cdot 6H_2O$, $H_3[PW_{12}O_{40}]\cdot 6H_2O$ and $H_4[SiW_{12}O_{40}]/H_3[PW_{12}O_{40}]\cdot 6H_2O$ mixed compounds. The general procedure was as follows.

The material (2 g) to be investigated was placed in a 25ml round-bottomed flask. Isotopically labelled 2-^{13}C-acetone (99% ^{13}C enriched) (0.2 g, 0.3 mol) was placed in a second round-bottomed flask. The two round bottomed flasks were then interconnected through a T joint which was subsequently connected to a Schlenk line. The isotopically-labelled acetone was frozen by lowering the flask into liquid nitrogen. Following this the complete system was evacuated for 5 minutes and the acetone was then allowed to thaw so that the vapour could be adsorbed onto the material under investigation. Optimum results were achieved when the system was left closed for three days. The resulting pale yellow solid was then characterised by ^{13}C MAS NMR and ^{13}C CPMAS NMR spectroscopy, adamantane was used as an external reference prior to each experiment. The results were compared to those reported for $H_3[PW_{12}O_{40}]\cdot 6H_2O$ by Yang *et al.*[2]

4.6 Characterisation techniques

4.6.1 X-ray powder diffraction

Instrumentation

X-ray powder diffraction patterns were recorded at room temperature using a

Siemens D5000 diffractometer linked directly to a PC equipped with DIFFRAC.AT software for storing and displaying recorded data. A copper metal target was used to produce X-rays using an X-ray tube incorporating a tungsten filament with 400 mA current and 40 kV electron acceleration voltage. X-rays exited the tube via a beryllium window and were collimated using a 2 mm slit. K_β radiation and most of the continuous X-ray radiation was removed by a nickel filter to produce an almost pure K_α beam. A scintillation detector equipped with three collimating slits (2 mm, 0.2 mm and 6 mm) recorded the diffracted X-ray beam.

Experimental procedure

Samples were ground to a fine powder to ensure an even size of crystallite. Powders were loaded into the centre of a sample holder and a glass slide was used to distribute the crystallites evenly and ensure that the surface of the sample was as flat as possible while avoiding excessive pressure which could induce preferred orientation. To prevent any further hydration of the sample a thin layer of grease was applied to the edge of the sample holder to form an air tight seal with a thin polyethylene sheet which was used to cover the sample. Sample preparation is discussed in more detail in Section 4.7.

Typical diffractometer settings were a 0.01° step every 8 seconds over the 2θ range 10° to 80°. Total scan time was approximately 15 hours unless otherwise stated.

Preparation of samples for X-ray powder diffraction analysis of 12-heteropolyacids with a standard included

Hydrated 12-heteropolyacid was prepared, as described in Section 4.2, and mounted into a sample holder as described above. The end of a small spatula was used to measure out and add a small amount of a known standard to the sample under investigation. The standard used was fluorophlogopite mica obtained from the National Bureau of Standards, Standard Reference Material 675, $d(001)$ = 9.98104(7) Å. The sample as a whole was then smoothed over again with the edge of a glass slide to give a flat surface and to avoid any preferred orientation. The XRD pattern of the 'spiked' sample was then recorded. The diffraction peaks observed from the standard sample were fitted and indexed, so that the zero correction could be determined for the recorded XRD pattern as a whole.

4.6.2 Multinuclear nuclear magnetic resonance spectroscopy

Instrumentation

NMR spectra were recorded on a JEOL JNM-EX400 FT NMR spectrometer equipped with a JEOL EX Solid NMR facility. The nominal field strength was 9.4 T and the instrument was coupled to a Doty Scientific Inc. MAS NMR probe (5 mm, high-speed 14 kHz, double-tuned, multinuclear, CP/MAS). Rotors were made of either silicon nitride or zirconia and fitted with polyimide end caps. A compressed air system was used for sample spinning. The probe used two air streams: one for bearing gas to prevent the rotor colliding with the walls of the stator and the other as a drive to spin the rotor. Careful setting of these streams was required to ensure stable rotor spinning. For the acquisition of both ^{31}P and ^{29}Si MAS NMR spectra samples were packed in zirconia rotors and spun at typically 5 kHz. For the

acquisition of ^{13}C NMR spectra samples were packed in silicon nitride rotors and spun between frequencies in the range 3 - 6 kHz, depending on the sample.

Sample preparation

Samples were ground to a fine powder prior to loading into an NMR rotor. Powders were carefully packed to ensure even spinning of the rotor, particularly at high frequencies. This was achieved using accurately machined plastic tools. Small amounts of sample were carefully placed in the rotor with one end cap removed and compacted using a plastic ram before adding more sample. This procedure was repeated until the rotor was full then, using a calibrated plastic tool, a portion of the sample was removed to the depth of the end cap and the second cap fitted.

Acquisition parameters

Typical parameters used for acquisition of spectra are summarised in Table 4.2.

Table 4.2 Typical parameters for the acquisition of NMR spectra.

Nucleus	Resonance frequency MHz	Pulse width μs	Pulse delay s	Typical number of scans	External reference standard
^{13}C MAS	100.525	5.5	60	800	adamantane
^{13}C CPMAS	100.525	5.5	30	256	adamantane
^{29}Si	79.426	4.0	20	1500	$Si(CH_3)_4$
^{31}P	161.830	3.0	10	100	H_3PO_4 (85 %)

Accumulated NMR signal data were transferred to a PC and processed using Delta software for the production of spectra and dmfit98[3] for spectral modelling.

4.6.3 Thermal analysis

Instrumentation

Simultaneous thermogravimeteric analysis (TGA) and differential scanning calorimetery (DSC) were carried out under a flow of dry air (50 ml min^{-1}) using a Rheometric Scientific STA 1500. This analyser combines a sensitive balance with a heat flux DSC hangdown. Samples, typically in the order of 50 mg, were held in Al_2O_3 pans. Scan rates were set, depending on the experiment, in the temperature range 20 - 1000°C.

Experimental procedure

A sample was ground to a fine powder and loaded into the Al_2O_3 pan. The pan was then positioned carefully on the balance located inside the furnace. The acquisition of the data was typically achieved through heating from 25°C to 900°C at ramp rates of 10 or 20°C min^{-1}.

4.6.4 FT-IR spectroscopy

Instrumentation

Infrared spectra were obtained using a Perkin-Elmer 1710 Infrared Fourier Transform (FT) spectrometer. Samples were prepared by incorporation into potassium bromide discs.

Experimental procedure

The finely ground sample was mixed with finely-ground, dried, potassium bromide in a ratio of 1:100 to give 1% dilutions of the sample to achieve maximum absorptions of no more than 70% in the resulting spectra. 8 scans were carried out

per sample over a range of 4000 cm^{-1} to 500 cm^{-1}. A background spectrum was run at the start of each session of acquisition.

4.7 Systematic errors in X-ray powder diffraction patterns

An understanding of systematic errors in XRD powder diffraction patterns is important for the work in this thesis.

There are three potential issues to consider :

1) preferred orientation,
2) zero shift of the instrument,
3) displacement of the sample out of the focusing circle of the diffractometer.

It is the latter two that are important in the present work.

The preferred orientation of crystallites can produce large variations in the intensities of observed peaks. This error is considerably reduced by ensuring minimum pressure is used to obtain a flat sample (for example, by using the edge of a glass slide for this purpose.). Rotation of the sample about the axis of its holder also 'averages out' preferred orientation effects.

A significant error present in XRD is caused by small systematic offset errors that are unique to each machine, this error is called the zero shift. A relatively small zero shift can lead to the observed peak positions being incorrectly indexed and this can hinder the indexing of powder patterns.

The zero shift of the diffractometer was obtained by recording the powder pattern of a standard sample. The standard used in this work was fluorophlogopite mica and the powder diffraction pattern is shown in Figure 4.2.

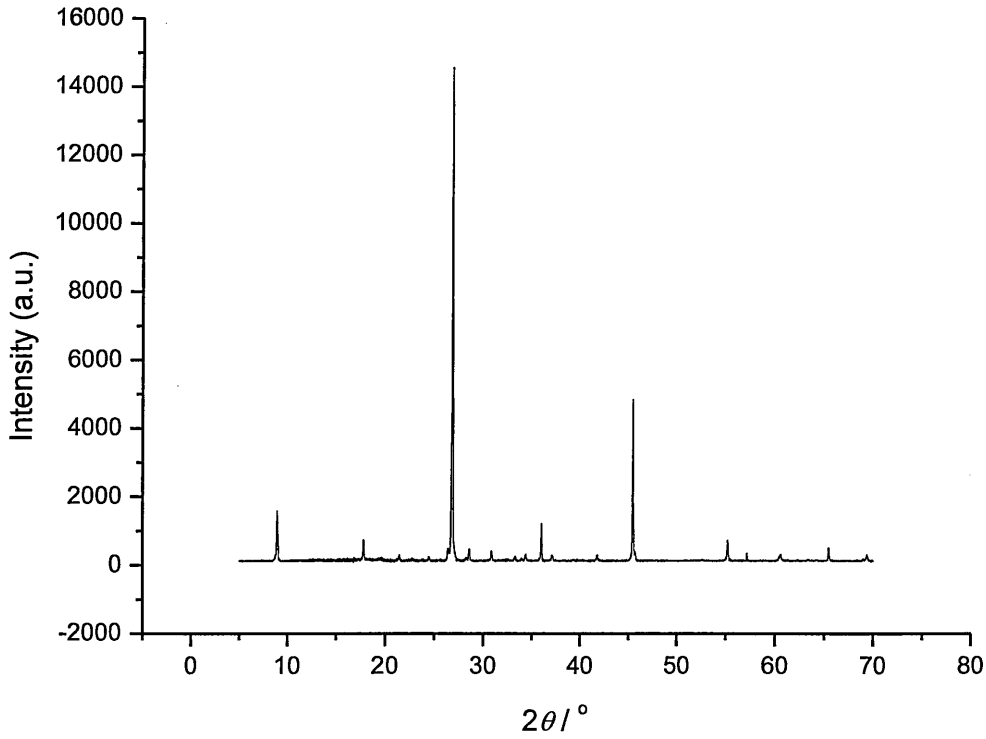

Figure 4.2 X-ray powder diffraction pattern of fluorophlogopite mica (National Bureau of Standards, Standard Reference Material 675, $d(001) = 9.98104(7)$ Å).

Analysis of the XRD pattern, given the value of $d(100) = 9.98104(7)$ Å, gives a zero correction of 0.047 ° in 2θ. This value is typical for a properly adjusted X-ray diffractometer. In principle, this value can be used as a starting parameter in such programs as Chekcell[4]. However, in the present work sample (height) displacement was also a significant problem.

Sample displacement

Due to the moisture sensitive nature of hydrated 12-heteropolyacids and the time required to record an XRD pattern a sealed sample was required. An air tight seal was formed by applying a thin layer of grease to the edge of an ordinary sample followed by covering the sample with a thin polyethylene sheet, Figure 4.3.

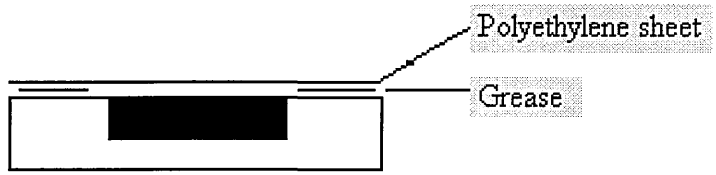

Figure 4.3 A schematic representation of a covered sample.

Sealing the sample did not, however, only stabilise the hydration state of the 12-heteropolyacid. The addition of the grease and the polyethylene sheet results in the presence of a thin layer between the sample and the sample holder. This additional layer caused the sample to become displaced out of the focusing circle of the X-ray beam causing a usually insignificant error to become substantial. The displacement of the sample can lead to a considerable shift in the observed powder pattern.

Sample (or height) displacement contributes to the zero shift of an instrument with the magnitude of the effect depending on $\cos \theta^5$. For scans over a limited 2θ range (10 to 40 °), the influence of the angular dependence is relatively small. On this basis an angular independent zero shift (which includes that of the instrument) can be determined. In the present work, depending on circumstances, three approaches were used.

The first approach was to simply spike the sample with the standard fluorophlogopite mica. The second approach was used in the case that accurate single crystal diffraction data were available; specifically this was for $H_3[PW_{12}O_{40}]\cdot 6H_2O$. The Bragg peaks were fitted (as for other samples in this work) using X-fit[6] : peaks in the 2θ range 10^o - 30^o were fitted using a split Pearson (PV II) function and greater angle peaks to a Pseudo Voight (PV) function. This data, in combination with the known single crystal unit cell parameters, was sufficient to determine a starting value for the overall zero shift correction. The final approach used was the 'reflection-pair method' of Dong *et al.*[7]

The reflection pair method was developed in order to determine the zero shift correction for powder patterns without the need for prior indexing. The method is based on considering reflection pairs of the form (*hkl*) and (*h'k'l'*). In the present work, the method is only applied to cubic diffraction patterns and it can be shown that the zero correction ($2\theta_z$) is given by :

$$2\theta_z = 2\arctan[(\sin\theta' - n\sin\theta)/(n\cos\theta - \cos\theta')] \qquad (4.1)$$

where $n = [(h'^2 + k'^2 + l'^2)/(h^2 + k^2 + l^2)]^{1/2}$ and θ and θ' characterise the angular positions of the selected Bragg peaks.

As an aside and a point of interest, sample displacement is demonstrated by inserting sheets of paper between a standard sample and the sample support to deliberately displace the sample out of the focusing circle of the X-ray beam, Figure 4.4.

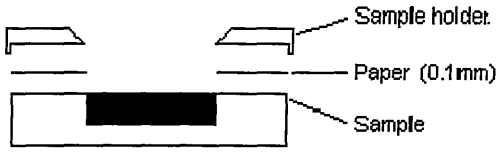

Figure 4.4 Displacement of a crystalline sample by sheets of paper. (A sheet of paper has a thickness of ~ 0.1 mm.)

Significant shifts are observed for the Bragg peak in the region of $2\theta = 26.7^{\circ}$ as shown in Figure 4.5.

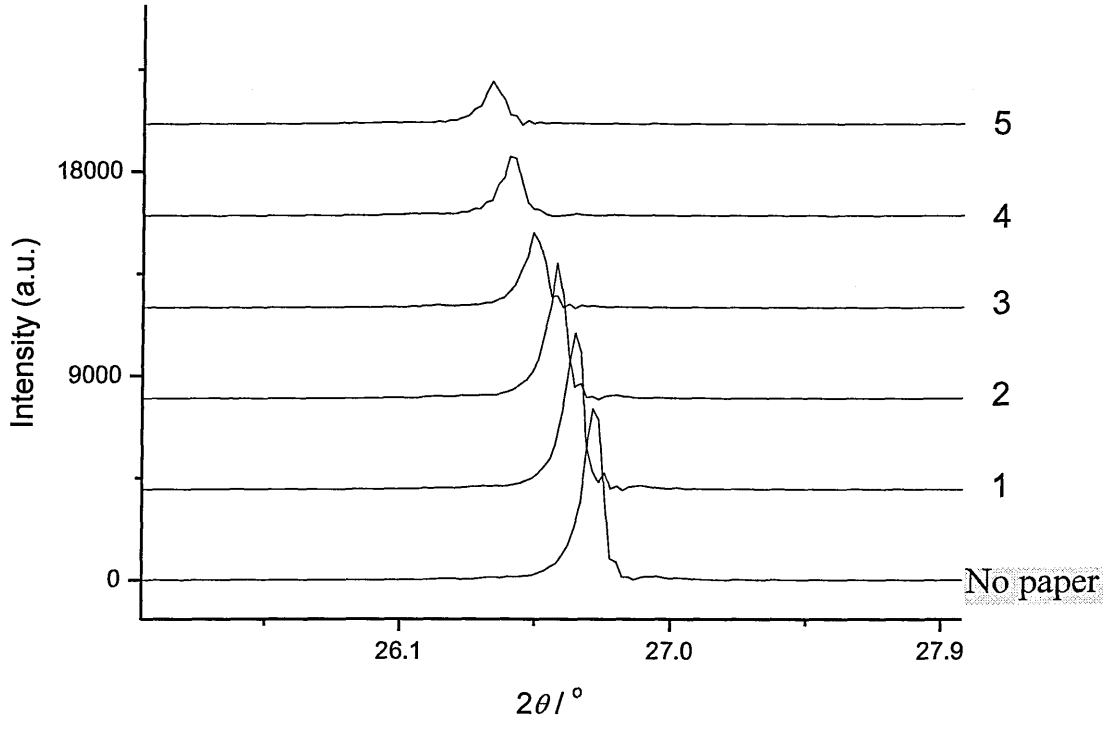

Figure 4.5 Shift of Bragg peaks as the sample (Figure 4.4) is displaced from the focusing circle.

References

(1) Kozhevnikov, I. V.; Holmes, S.; Siddiqui, M. R. H. *Applied Catalysis A - General* **2001**, *214*, 47-58.

(2) Yang, J.; Janik, M. J.; Ma, D.; Zheng, A. M.; Zhang, M. J.; Neurock, M.; Davis, R. J.; Ye, C. H.; Deng, F. *Journal of the American Chemical Society* **2005**, *127*, 18274-18280.

(3) Massiot, D.; Fayon, F.; Capron, M.; King, I.; Le Calve, S.; Alonso, B.; Durand, J. O.; Bujoli, B.; Gan, Z. H.; Hoatson, G. *Magnetic Resonance in Chemistry* **2002**, *40*, 70-76.

(4) Laugier, J.; Bochu, B., pp WWW: http://www.inpg.fr/LMGP and http://www.ccp14.ac.uk/tutorial/lmgp/.

(5) Atkins, P. W. *Physical chemistry*, Sixth edition ed.; Oxford University Press: Oxford, 1998.

(6) Cheary, R. W.; Coelho, A. A.; deposited in CCP14 Powder Diffraction Library, Engineering and Physical Sciences Research Council, Daresbury Laboratory, Warrington, England. (http://www.ccp14.ac.uk/tutorial/xfit-95/xfit.htm), 1996.

(7) Dong, C.; Wu, F.; Chen, H. *Journal of Applied Crystallography* **1999**, *32*, 850-853.

Chapter 5

Characterisation of hydrates of 12-silicotungstic acid

5.1 Introduction

A number of industrial processes use 12-heteropolyacids, usually in a hydrated form, as acid catalysts.[1,2] Since 12-phosphotungstic acid possesses the highest acidity, it is often the favoured catalyst and this is reflected in the number of industrial patents which involve its use.[3] It is not surprising, therefore, that there have been a number of detailed investigations aimed at characterising the form, structure and properties of this acid and its hydrated states (see Chapter 2, Section 2.3.2). By contrast, 12-silicotungstic acid has not been as widely patented or studied, even though it is the second most acidic of the 12-heteropolyacids.[4] Nonetheless, it still remains of fundamental as well as of industrial interest to carry out more detailed studies of the hydrated forms of this acid. It is also to be expected that useful comparisons with the corresponding hydrated states of 12-phosphotungstic acid will be informative.

The main content of this chapter is concerned with a detailed investigation, using thermal analysis, X-ray powder diffraction, ^{29}Si MAS NMR spectroscopy and FT-IR spectroscopy, of 12-silicotungstic acid in various hydrated forms. The results are compared and contrasted with those reported for hydrates of 12-phosphotungstic acid.

5.2 Thermal analysis

Simultaneous TGA and DTA results recorded at heating rates of 10 °C min^{-1} and 20 °C min^{-1} for hydrated, as received, $H_4[SiW_{12}O_{40}]\cdot xH_2O$ are shown in Figures 5.1(A) and (B), respectively. In both cases, the sample (approximately 50 mg) was held under a flow of dry air (50 ml min^{-1}). The TGA and DTA behaviour is

comparable to that reported in other work[5-8] although differences in detail occur because of the different experimental conditions and masses of samples that have been used in the various studies. Analysis of the TGA results in Figures 5.1(A) and (B), as well as results from repeat studies, gives the hydration state of the starting material as $x = 23.5$ (± 0.3). The TGA plateau in the region of 300 to 400 °C corresponds to the anhydrous material, $H_4[SiW_{12}O_4]$.

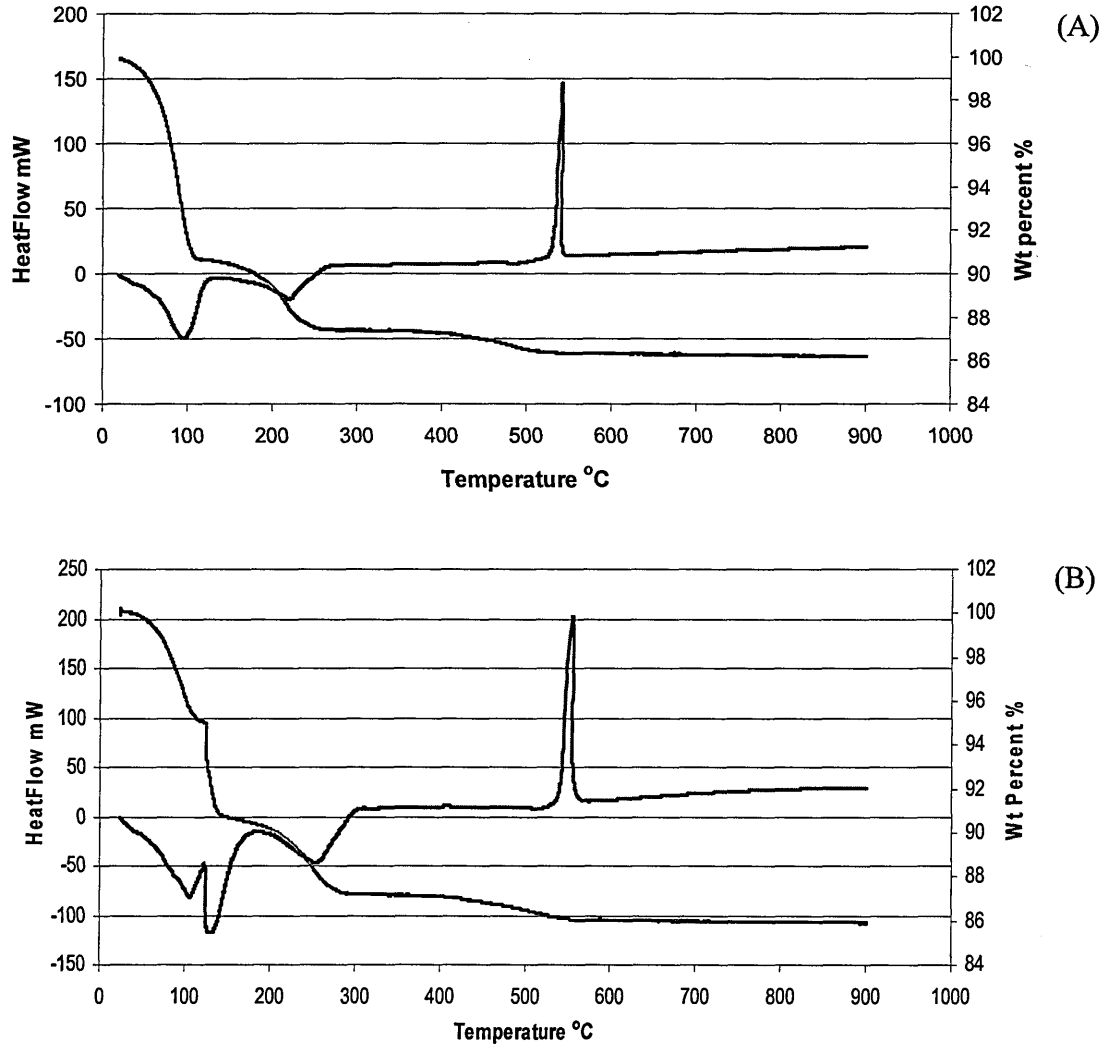

Figure 5.1 TGA (pink) and DTA (blue) data recorded from a hydrated sample of $H_4[SiW_{12}O_{40}]\cdot xH_2O$ with a heating rate of (A) 10 °C min^{-1} and (B) 20 °C min^{-1}; other experimental details are given in the text.

As is more clearly seen in Figure 5.2, which represents an amplified version of Figure 5.1(A) in the temperature range 400 to 600 °C, anhydrous $H_4[SiW_{12}O_{40}]$ undergoes a transition in the region of 465 °C. The associated mass change in the TGA is equivalent to the loss of two water molecules. These water molecules can be referred to as 'constitutional' since they result from a reaction between protons in the anhydrous acid and oxygen atoms within the Keggin units so that the denuded species $[SiW_{12}O_{38}]$ remains. Similar behaviour has been observed for anhydrous $H_3[PW_{12}O_{40}]$ which looses 1.5 constitutional water molecules to give a so-called D-phase[9]. In comparison with this study, it is reasonable to assume that the $[SiW_{12}O_{38}]$ units maintain a Keggin-like cage structure. The observed transition in Figure 5.2 is relatively weak and broad because of the simultaneous occurrence of the exothermic reaction to form water and the endothermic process of dehydration.

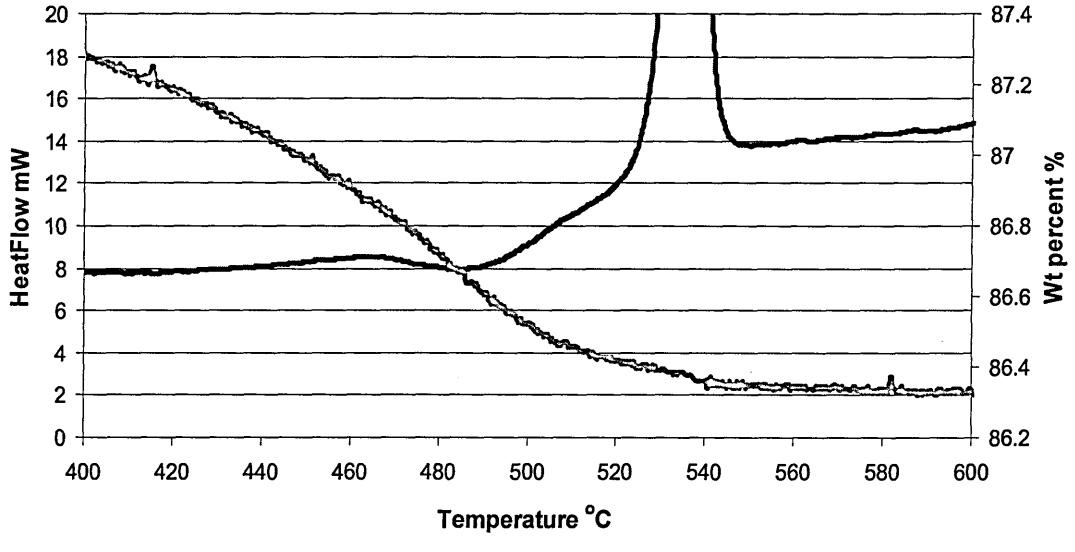

Figure 5.2 An amplified view of the data in Figure 5.1(A) in the temperature range 400 to 600 °C

The final sharp and relatively intense exothermic transition at 535 °C in Figure 5.1(A) (550 °C in Figure 5.1(B)) is attributed to a decomposition reaction to form silicon and tungsten oxides. This type of reaction has been observed in other DTA

investigations[6-8] although the observed temperature of the transition varies depending on the experimental conditions: values in the range 520 to 545°C have been reported. The corresponding decomposition temperature for $[PW_{12}O_{38.5}]$ has been reported as 602°C[9] and 600°C,[10] although a much lower value of 553°C has also been recorded.[11] On the basis of this data, it seems that the decomposition of anhydrous 12-silicotungstic acid occurs at a lower temperature than that for 12-phosphotungstic acid, although for an exact comparison results carried out under equilibrium conditions would be required.

The results in Figures 5.1(A) and (B) at temperatures below 300°C reflect the loss of water from the starting hydrate. The observed endothermic transitions have peak maxima at temperatures that correspond (to a good approximation) to the maximum rate of mass loss between plateaus in the TGA data. A key difference between the two sets of results is that, at the lower heating rate, only two endothermic transitions are observed compared to three at the higher heating rate. This behaviour is probably related to the heat conduction properties of the sample. It can also be noted in both figures that the DTA data in the temperature regime from 30 to 90°C do not evolve as a smooth curve. The small 'shoulders' in the data can be attributed to dissolution of dehydrated sample in released water of crystallization. As to be expected, there is no effect observed in the TGA data.

The TGA data in Figure 5.1(A) is consistent with the loss of 17 - 18 water molecules from the starting hydrate to form $H_4[SiW_{12}O_{40}]\cdot 6H_2O$ at a temperature in the region of 100 °C. This hexahydrate is then relatively stable with no further significant mass loss up to approximately 150 °C. As will be discussed in more detail in Section 5.3,

the hexahydrate has a well-defined crystal structure directly comparable to that of $H_3[PW_{12}O_{40}]\cdot 6H_2O$.[12] A stable hexahydrate is also formed at the higher heating rate (Figure 5.1(B)), but on a temperature scale increased by approximately 25°C compared to that for the lower heating rate.

The observation of an additional endothermic transition in Figure 5.1(B) is attributed to the formation of an 'intermediate hydrate' with $x \approx 14$. This result is consistent with reports (reference 11, and references therein) that heteropolyacids of the type $H_{3+n}PM_{12-n}V_nO_{40}$ (M = Mo, W; n = 0 - 1) have intermediate hydrates, although usually of poor crystallinity, with x = 13 - 14. The result, however, is not in such good agreement with the work of Bielański *et al.*[7] on $H_4[SiW_{12}O_{40}]\cdot 23.7H_2O$. These authors found a plateau in their TGA data in the region of 84 °C which they attributed to a hydrate with x = 17.3. Overall, an intermediate hydrate with $x \approx 14$ seems the more reasonable result, as will be discussed further in Section 5.3.3.

The results described above indicate that 12-silicotungstic acid can form distinct hydrated phases of the form $H_4[SiW_{12}O_{40}]\cdot xH_2O$ with x = 24, 14 and 6; in addition, there is a well defined anhydrous phase (x = 0). The properties of these phases are investigated in more detail in the following sections.

5.3 X-ray powder diffraction (XRD)

5.3.1 $H_4[SiW_{12}O_{40}]\cdot 6H_2O$

The XRD pattern recorded from a sample of $H_4[SiW_{12}O_{40}]\cdot 6H_2O$ is shown in Figure 5.3 compared with that recorded from $H_3[PW_{12}O_{40}]\cdot 6H_2O$. Both samples were prepared in a similar manner by heating to 120°C for 5 hours. In order to prevent re-hydration during the XRD measurements, the samples were covered with a thin polyethylene sheet which was sealed to the sample container using grease (see Chapter 4, Section 4.7).

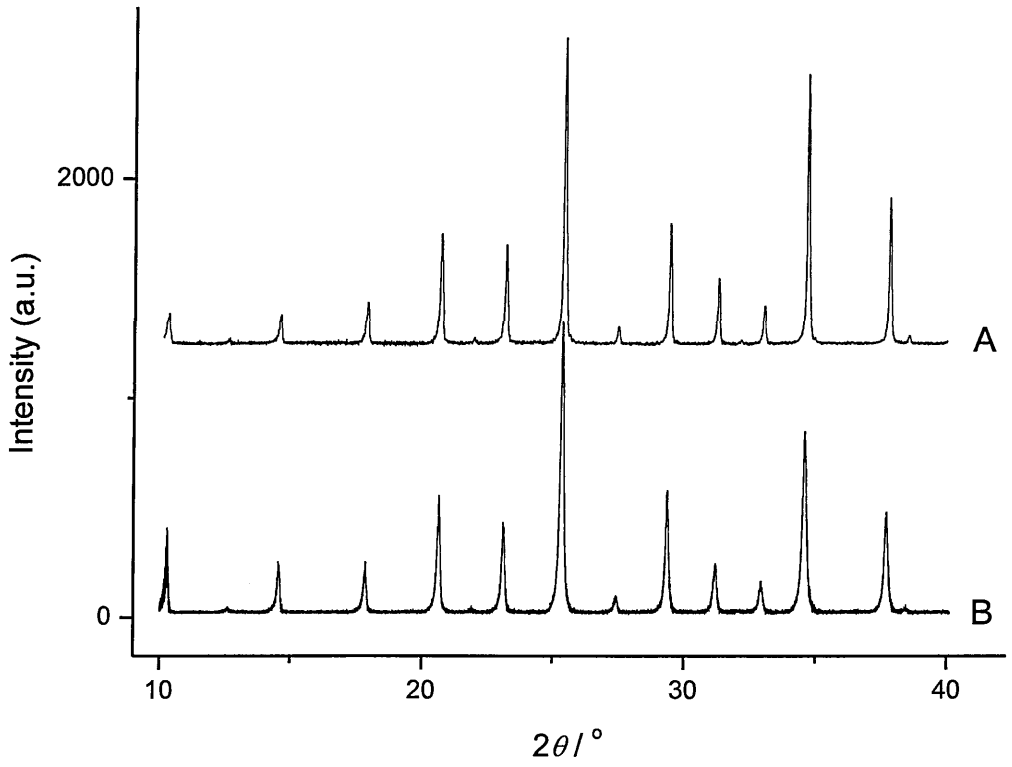

Figure 5.3 XRD patterns recorded over the 2θ range of 10° - 40° for A) $H_4[SiW_{12}O_{40}]\cdot 6H_2O$ and B) $H_3[PW_{12}O_{40}]\cdot 6H_2O$ (step size = 0.01°; step time = 8 s).

It is clear in Figure 5.3 that the two diffraction patterns are very similar to one another both in terms of the positions of the Bragg peaks and their relative

intensities. X-ray and neutron diffraction studies of a single crystal of $H_3[PW_{12}O_{40}]\cdot 6H_2O$ have shown[12] that this hydrate has a cubic unit cell with a cell constant of 12.1506(5) Å : the value determined in this work is 12.1521(12) Å. It is reasonable to conclude, without the need for further analysis, that $H_4[SiW_{12}O_{40}]\cdot 6H_2O$ also has a cubic unit cell. This conclusion is also in agreement with early diffraction studies.[13, 14] Analysis of the powder pattern, in Figure 5.3(A), gives a value of 12.1183(5) Å for the cubic cell constant. This value is less than that for $H_3[PW_{12}O_{40}]\cdot 6H_2O$ and the slight contraction in the unit cell may be associated with the presence of the 'additional' acidic proton. In addition, it is also possible that there could be small differences in the dimensions of the Keggin units, $[SiW_{12}O_{40}]^{4-}$ and $[PW_{12}O_{40}]^{3-}$. It can be noted that in their original work Scroggie and Clark[14] found the unit cell constant for $H_4[SiW_{12}O_{40}]\cdot 6H_2O$ to be equal to 12.16(1) Å.

The form of the XRD pattern for $H_3[PW_{12}O_{40}]\cdot 6H_2O$ can be predicted using the detailed structural information provided in the single crystal study of Brown *et al.*[12] and the standard program Powdercell.[15] The simulated pattern is shown in Figure 5.4(A). The corresponding pattern for $H_4[SiW_{12}O_{40}]\cdot 6H_2O$, simulated using the same data but with P replaced by Si and the cell constant set to the experimental value (12.1183 Å), is shown in Figure 5.4(B). It should be noted that the simulation does not take into account the additional acidic proton but any effect on the intensities of the Bragg peaks in the X-ray powder pattern should be minimal. The experimental X-ray powder diffraction pattern recorded for $H_4[SiW_{12}O_{40}]\cdot 6H_2O$ is shown in Figure 5.4(C). Overall, all three patterns are directly comparable with one another and this provides further confirmation that $H_3[PW_{12}O_{40}]\cdot 6H_2O$ and

$H_4[SiW_{12}O_{40}]\cdot 6H_2O$ are isostructural. Furthermore, it can be concluded that $H_4[SiW_{12}O_{40}]\cdot 6H_2O$ has a crystal structure in which diaquahydrogen ions, $H_5O_2^+$, are hydrogen bonded to the terminal oxygen atoms of four separate Keggin units (see Chapter 2, Section 2.3.2). The acid can be formulated, alternatively, as $[H_5O_2^+]_3H^+[SiW_{12}O_{40}]^{4-}$, although the exact location of the acidic, non-hydrated H^+ ion is not determined.

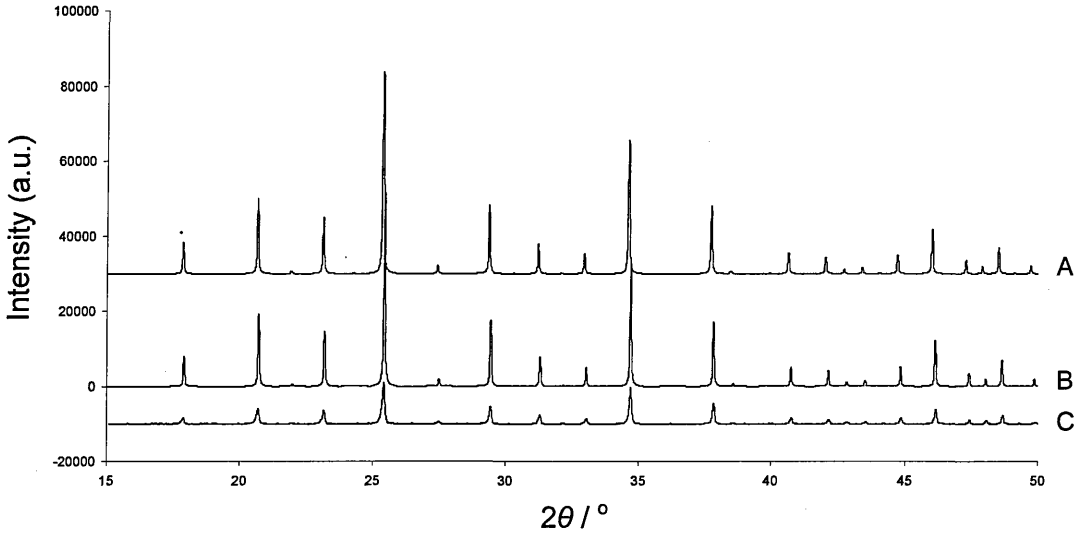

Figure 5.4 Simulated XRD powder patterns (see the text for details) for A) $H_3[PW_{12}O_{40}]\cdot 6H_2O$ and B) $H_4[SiW_{12}O_{40}]\cdot 6H_2O$. The experimental XRD powder pattern for the latter hexahydrate is shown in C.

It is useful to comment further on the details of the analysis of the XRD powder patterns in Figure 5.3. In particular, some of the comments are relevant to later work in this chapter. The requirement to keep the samples sealed under a thin sheet of polyethylene introduces a degree of sample displacement because of the manner in which the sample holder is held in the sample mount of the instrument in order to achieve the desired reflection geometry. This is illustrated schematically in

Figure 5.5. The X-ray diffraction instrument used in this work was available only in reflection mode.

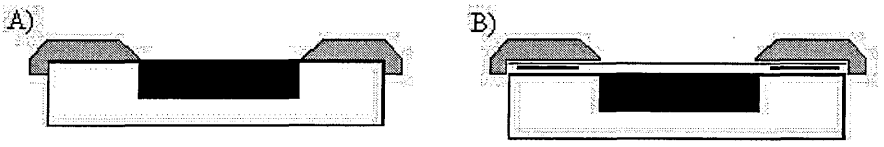

Figure 5.5 A schematic view of the sample arrangement for recording XRD patterns A) without and B) with a polyethylene cover. The thin layer of polyethylene sheet, sealed to the sample holder using grease, results in the sample being displaced downwards when the sample holder is held in the sample mount of the instrument. Effectively, the sample is slightly displaced from the focusing circle of the X-ray beam.

Sample displacement, as already discussed in Chapter 4, Section 4.7, contributes to the zero shift of the XRD instrument. The diffraction patterns in Figure 5.3 were analysed using an angular independent zero shift correction. The approach taken initially was to determine the zero shift for the recorded pattern using the reflection-pair method.[16] The application of this method to cubic systems has already been described in Chapter 4, Section 4.7. This zero shift was then applied to the pattern prior to use of the program Chekcell.[17] Both the zero shift and the cubic cell parameter were then refined so that the minimum mean squared deviation between experiment and fit was determined. In the case of $H_4[SiW_{12}O_{40}]\cdot 6H_2O$ the zero shift found by the reflection-pair method was 0.117(32)°. Refinement of the corrected

pattern using Chekcell,[17] gave a new zero correction of 0.030(2)°. The corresponding values for $H_3[PW_{12}O_{40}]\cdot 6H_2O$ were 0.1201(55)° and 0.002(5)°. As to be expected, the refined zero corrections for the corrected X-ray diffraction patterns are close to zero.

5.3.2 Anhydrous $H_4[SiW_{12}O_{40}]$

The work in this thesis is generally concerned with hydrated 12-silicotungstic acid but, nonetheless, it is useful to briefly comment on results obtained for the anhydrous phase. The XRD powder pattern recorded at room temperature for a sealed sample of anhydrous $H_4[SiW_{12}O_{40}]$ is shown in Figure 5.6.

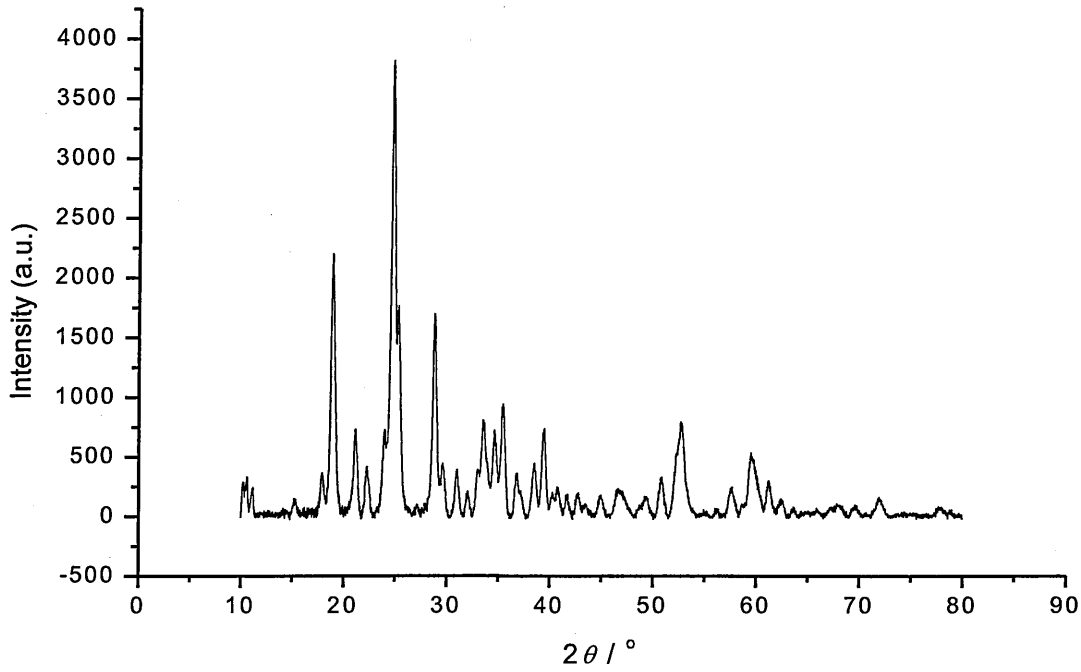

Figure 5.6 XRD pattern recorded over the 2θ range of 10° - 80° for anhydrous $H_4[SiW_{12}O_{40}]$ (step size = 0.01°; step time = 8 s).

Fournier *et al.*[11] have used *in-situ* XRD powder diffraction to follow the dehydration of both $H_3[PMo_{12}O_{40}]\cdot 13H_2O$ and $H_3[PW_{12}O_{40}]\cdot 14H_2O$ as a function of temperature. In both cases a single anhydrous phase, which indexed in the tetragonal system, was observed at a temperature of 350°C. It is important to note, however, that a later study by Marosi *et al.*[18] found anhydrous $H_3[PMo_{12}O_{40}]$ (at 380°C) to have a rhombohedral unit cell with the parameters $a = 11.48(0)$ Å, $\alpha = 87.46(0)$ ° and $Z = 2$. This unit cell is close to cubic and in this respect is very similar in dimensions to the cubic unit cells found in detailed studies of anhydrous ammonium and potassium salts of 12-molybdophosphate.[19] Marosi *et al.*[18] also noted that anhydrous $H_3[PW_{12}O_{40}]$ is isostructural with anhydrous $H_3[PMo_{12}O_{40}]$. In the context of this work, the reported XRD pattern for anhydrous $H_3[PMo_{12}O_{40}]$[18] is qualitatively very similar to that in Figure 5.6 for anhydrous $H_4[SiW_{12}O_{40}]$. This powder pattern was, therefore, indexed using the cell parameters of anhydrous $H_3[PMo_{12}O_{40}]$ as a starting point for the refinement. The final best fit parameters were found to be $a = 11.551(29)$ Å, $\alpha = 87.0(2)$ °, $Z = 2$. The volume of the rhombohedral unit cell, space group $R3$, was found to be $V = 1535$ Å^3. In comparison with the hexahydrate ($V = 1795$ Å^3) there is a decrease in volume of 260 Å^3. Given that $Z = 2$ for the unit cell, then this corresponds to a decrease of approximately 22 Å^3 per water molecule of hydration. In qualitative terms, this may not be unreasonable given that the hydrogen-bonded structural network has been broken down in the dehydration process.

5.3.3 $H_4[SiW_{12}O_{40}]\cdot 14H_2O$

12-Heteropolyacids containing 13-14 H_2O are generally referred to as intermediate hydrates and have not been widely investigated since they tend to have poor

crystallinity when prepared by dehydration methods from higher hydrates.[11] In the present case, $H_4[SiW_{12}O_{40}]\cdot 14H_2O$ was prepared by controlled hydration of the hexahydrate (see Chapter 4, Section 4.2). However, as indicated by the XRD powder pattern, shown in Figure 5.7, the intensities of the diffracted Bragg peaks are relatively weak.

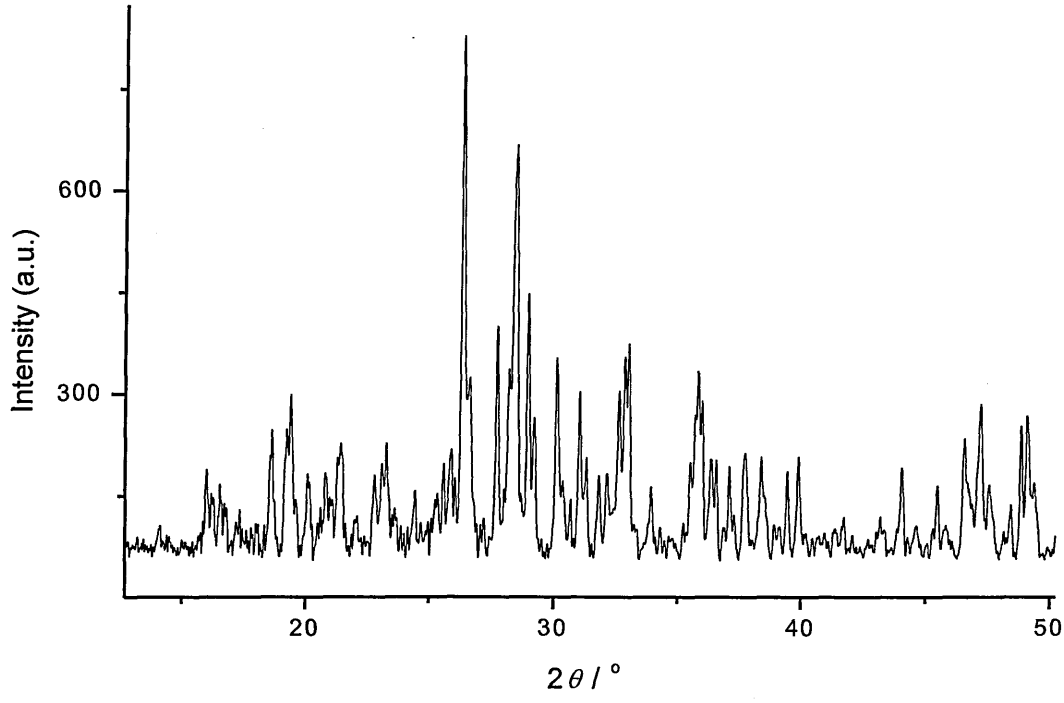

Figure 5.7 XRD pattern recorded over the 2θ range of 10° - 50° for $H_4[SiW_{12}O_{40}]\cdot 14H_2O$ (step size = 0.01°; step time = 8 s).

In order to analyse the diffraction pattern it was necessary to obtain a good estimate of the zero shift correction. The reflection-pair method could not be used since the pattern is complex. For this purpose, therefore, the sample was spiked with a standard compound (fluorophlogopite mica, $d(001)$ = 9.98104(7) Å). Diffraction peaks due to the standard have been removed from the diffraction pattern in Figure 5.7 since their intensities significantly eclipse those of the sample peaks. The zero shift correction was found to be 0.124(6) °.

D'Amour and Allmann[20] have carried out a single crystal X-ray diffraction study for $H_3[PMo_{12}O_{40}]\cdot(13\text{-}14)\ H_2O$ and found a triclinic structure for which details are given in Table 5.1. The XRD powder pattern simulated using this data, and generated using the Inorganic Crystal Structure Database (ICSD)[21] is shown in Figure 5.8. The diffracted peaks simulated in this pattern occur at angles comparable to those observed in Figure 5.7 for $H_4[SiW_{12}O_{40}]\cdot 14H_2O$. This is most evident over the 2θ range of 25° - 30°. The intensities of the diffracted peaks, however, are noticeably affected by the different addenda atoms present in the Keggin anions.

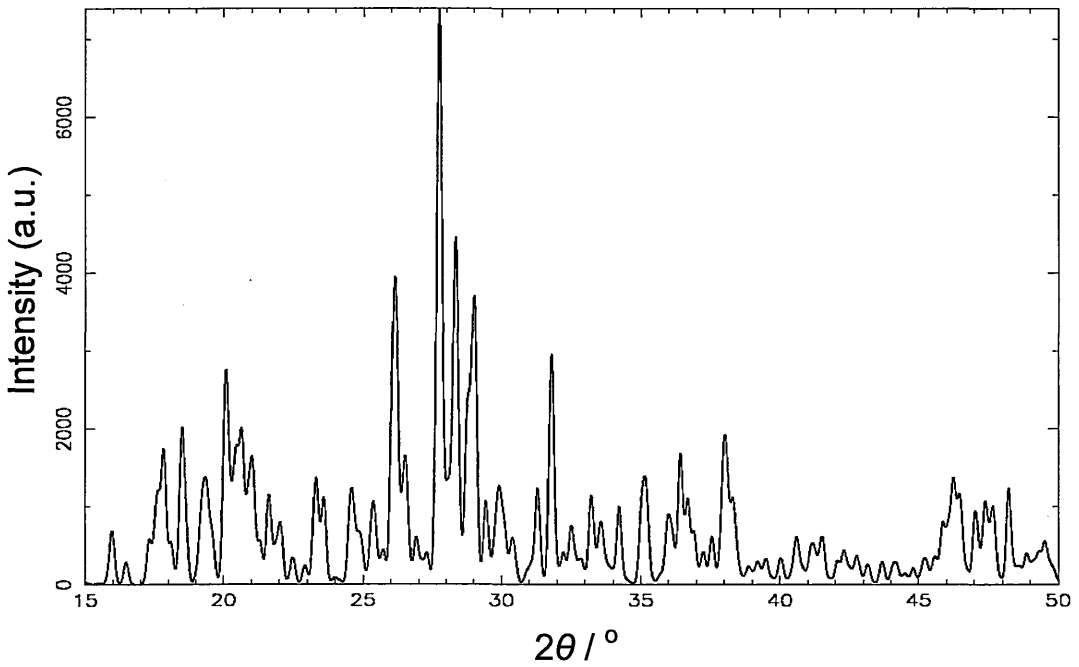

Figure 5.8 The simulated XRD powder pattern for $H_3[PMo_{12}O_{40}]\cdot(13\text{-}14)\ H_2O$ based on single crystal data.

Fournier *et al.*[11] have measured XRD powder patterns at room temperature for four 12-heteropolyacids which can be classified as intermediate hydrates: $H_3[PMo_{12}O_{40}]\cdot 13H_2O$, $H_4[PMo_{11}VO_{40}]\cdot 13H_2O$, $H_3[PW_{12}O_{40}]\cdot 14H_2O$, and $H_4[PW_{11}VO_{40}]\cdot 14H_2O$. Using information from the single crystal study of D'Amour

and Allmann for $H_3[PMo_{12}O_{40}]\cdot(13\text{-}14)H_2O$, all four powder patterns were indexed with triclinic symmetry and the unit cell parameters were found to be very similar. The cell parameters for $H_3[PW_{12}O_{40}]\cdot 14H_2O$ are summarised in Table 5.1. It can be noted that the cell volumes are close to 2100 Å^3 which is generally recognized as being at the upper limit for indexing cells using powder patterns recorded on typical laboratory powder X-ray diffractometers.[22]

Table 5.1 Triclinic unit cell parameters determined by XRD for $H_3[PMo_{12}O_{40}]\cdot(13\text{-}14)H_2O$ (single crystal) and $H_3[PW_{12}O_{40}]\cdot 14H_2O$ (powder) at room temperature.

$H_3[PMo_{12}O_{40}]\cdot 13H_2O$		**$H_3[PW_{12}O_{40}]\cdot 14H_2O$**	
Cell lengths/Å	**Cell angles/°**	**Cell lengths/Å**	**Cell angles/°**
$a = 14.\ 10(1)$	$\alpha = 112.1(3)$	$a = 14.26(1)$	$\alpha = 113.95(8)$
$b = 14.13(1)$	$\beta = 109.8(3)$	$b = 14.25(1)$	$\beta = 110.86(7)$
$c = 13.55(1)$	$\gamma = 60.7(3)$	$c = 13.79(1)$	$\gamma = 59.51(8)$
Cell volume, $V = 2141$ Å^3		Cell volume, $V = 2168$ Å^3	

The XRD powder pattern for $H_4[SiW_{12}O_{40}]\cdot 14H_2O$ was indexed using the triclinic cell parameters for $H_3[PMo_{12}O_{40}]\cdot(13\text{-}14)\ H_2O$ as a starting point for the refinement. The final best fit parameters are given in Table 5.2. The volume of the unit cell is $V = 2155$ Å^3. In comparison with the hexahydrate ($V = 1795$ Å^3) there is an increase in volume of 360 Å^3. Given that Z = 2 for the unit cell, then this corresponds to an increase of approximately 23 Å^3 per additional water molecule. This can be compared, for example, with an average volume of approximately 30 Å^3 for a water molecule in liquid water at 0°C (density 0.9998 g cm^{-3})[23]. D'Amour and Allmann[20]

describe the waters of hydration in $H_3[PMo_{12}O_{40}]\cdot(13\text{-}14)\ H_2O$ as "zeolitic-like" and find various short H_2O - H_2O distances typical of hydrogen bonding. They also suggest the presence of $H_7O_3^+$ and $H_5O_2^+$ within the unit cell. However, given the low symmetry of the structure there is no simple arrangement of the water molecules. It can be expected that similar comments apply to $H_4[SiW_{12}O_{40}]\cdot 14H_2O$ although this could only be confirmed using single crystal X-ray and neutron diffraction studies.

Table 5.2 Triclinic cell parameters for $H_4[SiW_{12}O_{40}]\cdot 14H_2O$ at room temperature.

$H_4[SiW_{12}O_{40}]\cdot 14H_2O$	
Cell lengths / Å	**Cell angles / °**
$a = 14.15(3)$	$\alpha = 111.9(1)$
$b = 14.13(3)$	$\beta = 110.0(1)$
$c = 13.60(3)$	$\gamma = 60.6(1)$
Cell volume, $V = 2155$ Å^3	

5.3.4 $H_4[SiW_{12}O_{40}]\cdot 24H_2O$

The XRD powder pattern recorded from $H_4[SiW_{12}O_{40}]\cdot 24H_2O$ is shown in Figure 5.9. The pattern is well defined and typical of that for a crystalline material.

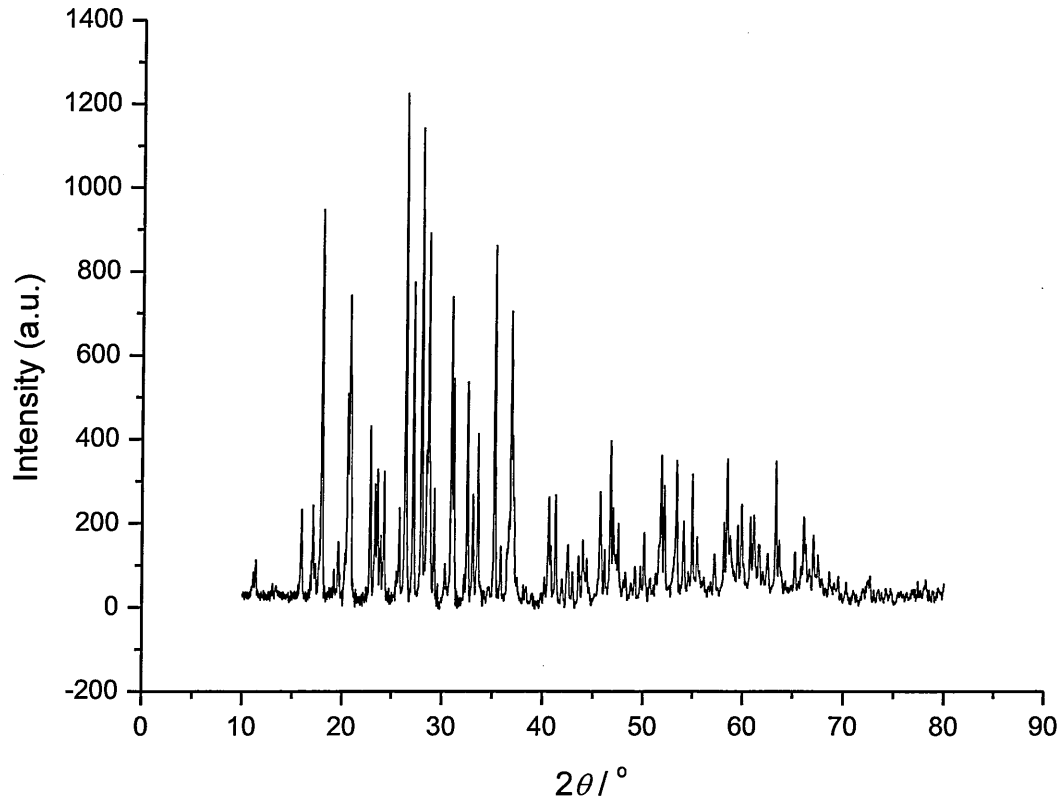

Figure 5.9 XRD powder pattern recorded over the 2θ range of 10° - 80° for $H_4[SiW_{12}O_{40}]\cdot 24H_2O$ (step size = 0.01°; step time = 8 s).

To obtain a good estimate of the zero shift correction, as described for $H_4[SiW_{12}O_{40}]\cdot 14H_2O$, the sample was spiked using the standard fluorophlogopite mica. The diffraction peaks recorded from the standard have been removed from the diffraction pattern in Figure 5.9 since their intensities eclipse those of the sample peaks. The zero shift correction was found to be 0.1172(1) °.

The XRD powder pattern in Figure 5.9 was indexed in orthorhombic symmetry. The final best fit parameters are given in Table 5.3.

Table 5.3 Cell parameters for $H_4[SiW_{12}O_{40}]\cdot 24H_2O$, at room temperature.

$H_4[SiW_{12}O_{40}]\cdot 24H_2O$
Cell lengths/Å
$a = 20.826$ (14)
$b = 13.091$ (6)
$c = 18.870$ (13)
cell volume, $V = 5145$ Å^3

Hydrated single phases, higher than x = 14, have been investigated for 12-phosphotungstic acid using neutron diffraction techniques; although no stable phase with x = 24 has been reported. Spirlet and Busing[24] studied $H_3[PW_{12}O_{40}]\cdot 21H_2O$ and reported the unit cell to be orthorhombic, *Pcca*, Z = 4, a = 20.788 (10), b = 13.086 (3) and c = 18.879 (5) Å. Studies of $H_3[PW_{12}O_{40}]\cdot 29H_2O$ by Noe-Spirlet *et al.*[25] revealed a cubic unit cell with $a = 23.28$ (1) Å.

5.3.5 Hydration occurring in the range : $H_4[SiW_{12}O_{40}]\cdot 14H_2O$ to $H_4[SiW_{12}O_{40}]\cdot 24H_2O$

Hydrated states occurring between the single hydrated states x = 14 and 24 were investigated and a typical XRD powder pattern for an x = 16.7 hydrate is shown in Figure 5.10.

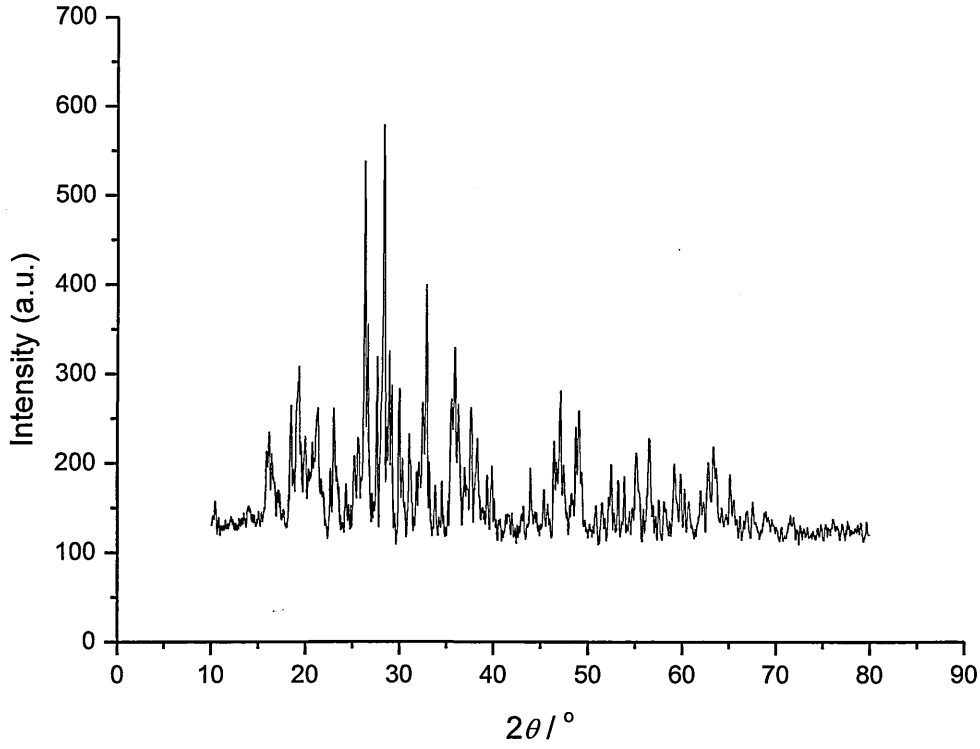

Figure 5.10 XRD pattern recorded over the 2θ range of 10° - 80° for $H_4[SiW_{12}O_{40}]\cdot 16.7H_2O$ (step size = 0.01°; step time = 8 s).

Diffraction peaks characteristic of $H_4[SiW_{12}O_{40}]\cdot 14H_2O$ and $H_4[SiW_{12}O_{40}]\cdot 24H_2O$ account for all the peaks present in the powder pattern. This suggests that hydrated states in the region x = 14 and x = 24 are not single phases but rather a simple combination of the stable hydrated states at the extremes of the range. Thus, a hydrate with x = 16.7 corresponds to a 30 : 70 molar mixture of $H_4[SiW_{12}O_{40}]\cdot 24H_2O$ and $H_4[SiW_{12}O_{40}]\cdot 14H_2O$. This is verified in Figure 5.11 which compares the experimental XRD pattern for $H_4[SiW_{12}O_{40}]\cdot 16.7H_2O$ with that formed (using the XRD software EVA) by adding together the experimental patterns for the x = 24 and x = 14 single phases in the ratio 30 % to 70 %.

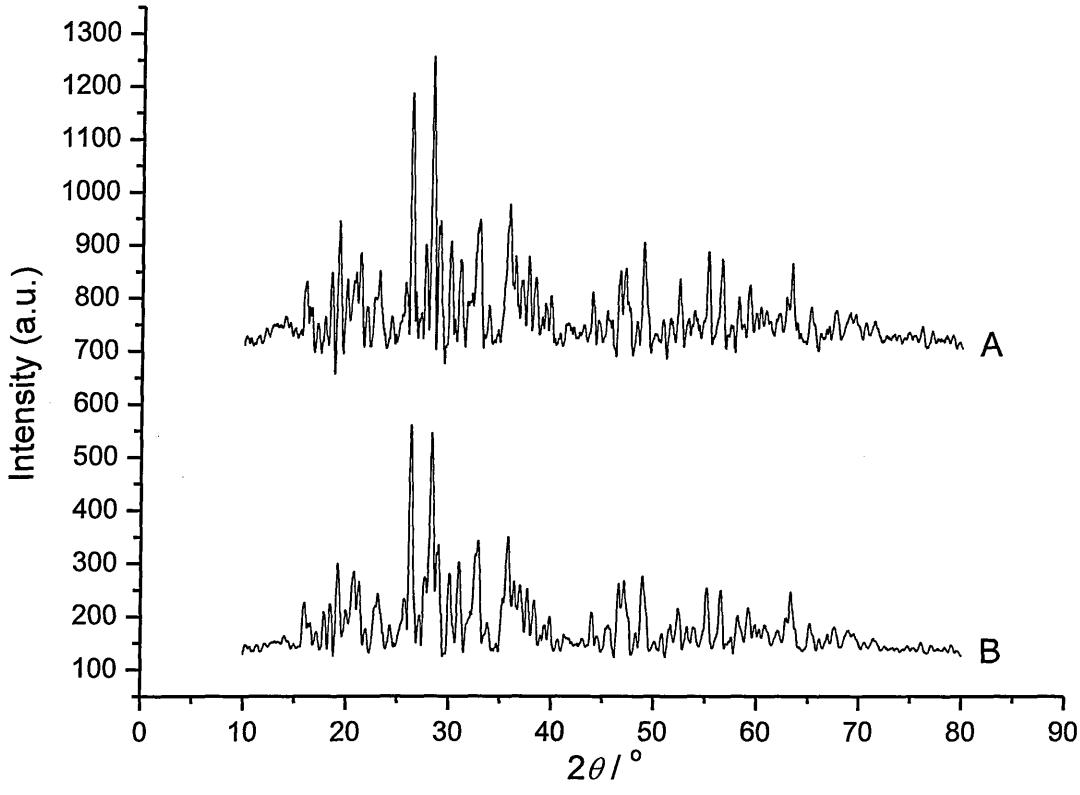

Figure 5.11 XRD patterns recorded over the 2θ range of 10° - 80° for A) $H_4[SiW_{12}O_{40}]\cdot 16.7H_2O$ and B) generated from the addition of experimental patterns for $H_4[SiW_{12}O_{40}]\cdot 24H_2O$ and $H_4[SiW_{12}O_{40}]\cdot 14H_2O$ in the ratio 30 % to 70 %.

Although not shown here, it was found that all XRD diffraction patterns for hydrates in the range $x = 14$ to $x = 24$ could be generated by simple weighted additions of the two single phases.

5.3.6 Hydration occurring in the range : $H_4[SiW_{12}O_{40}]\cdot 6H_2O$ to $H_4[SiW_{12}O_{40}]\cdot 14H_2O$

XRD powder patterns recorded for $H_4[SiW_{12}O_{40}]\cdot 6H_2O$ to $H_4[SiW_{12}O_{40}]\cdot 8H_2O$ are shown in Figure 5.12.

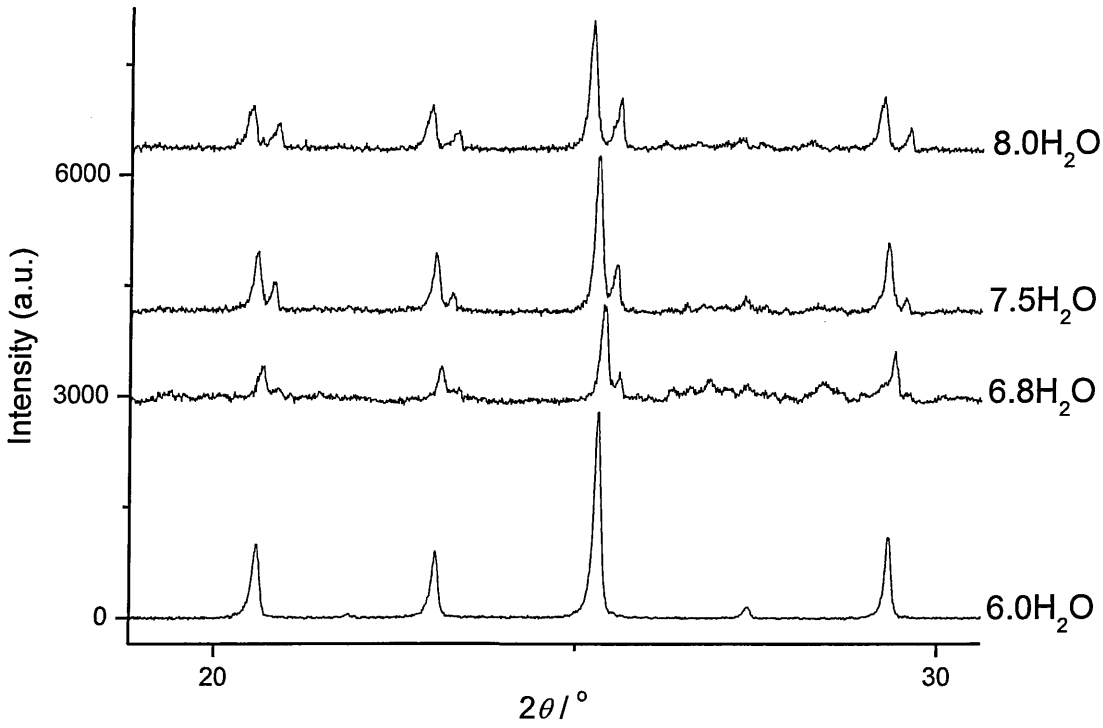

Figure 5.12 XRD patterns recorded over the 2θ range of 20° - 30° for $H_4[SiW_{12}O_{40}]\cdot xH_2O$ (where $6 \leq x \leq 8$) (step size = 0.01°; step time = 8 s).

Weak diffraction peaks characteristic of $H_4[SiW_{12}O_{40}]\cdot 14H_2O$ are observed for the samples with $x > 6$. This suggests that a mixture of stable phases is present. However, it is also noticeable that Bragg peaks in positions corresponding to those observed for the $x = 6$ sample are split. The splitting in each pattern is the same for each Bragg peak and is summarised in Table 5.4. It is clear that the splitting increases as the level of hydration increases. This splitting behaviour is not observed in samples with $x > 8$; although reasons for this are not clear.

Table 5.4 Observed splittings ($\Delta 2\theta$) for the Bragg peaks in the XRD patterns recorded from $H_4[SiW_{12}O_{40}]\cdot xH_2O$ where $6 < x \leq 8$.

Hydrated state	$\Delta 2\theta$ / °
$H_4[SiW_{12}O_{40}]\cdot 8H_2O$	0.3868 (3)
$H_4[SiW_{12}O_{40}]\cdot 7.5H_2O$	0.2383 (4)
$H_4[SiW_{12}O_{40}]\cdot 6.8H_2O$	0.2213 (3)

The nature of the splitting of the observed Bragg peaks strongly suggests that it is an artefact of the experimental method. This can be shown to be the case, for example, by means of the XRD powder pattern for the x = 8 sample (Figure 5.12). If it is assumed that the Bragg peaks in the x = 6 positions are influenced by two separate sample displacements then, in effect, there are two different diffraction patterns (1 and 2) present. The result of an analysis on this basis, using the reflection-pair method, are summarised in Table 5.5. The key outcome is that, within experimental uncertainty, the cubic unit cell parameter derived from each pattern is the same. Furthermore, the value is not significantly different to that determined for $H_4[SiW_{12}O_{40}]\cdot 6H_2O$; that is a = 12.1183(5) Å. It can be concluded that only the hexahydrate is present, although the diffraction pattern is distorted in a specific way due to the manner in which the sample behaves in the sealed sample holder of the XRD instrument. Further supporting, and more extensive, detail is given in Appendix A.

Table 5.5 Zero correction and cubic unit cell parameters calculated for the two sets of peaks observed in the XRD pattern recorded from $H_4[SiW_{12}O_{40}]\cdot 8H_2O$.

	Zero correction / °	***a* / Å**
Pattern 1	0.409(4)	12.047(10)
Pattern 2	0.0956(15)	12.016(42)

Figure 5.13 shows the XRD pattern for $H_4[SiW_{12}O_{40}]\cdot 10H_2O$ in comparison with the experimental XRD patterns for the $x = 6$ and $x = 14$ hydrates. It is clear that it is a mixed phase. Other hydrates in the range between these two single phases behave in a similar manner; that is, they are mixed phases. Overall, the behaviour is comparable to that already discussed (Section 5.3.5) for hydrates in the range $x = 14$ to $x = 24$.

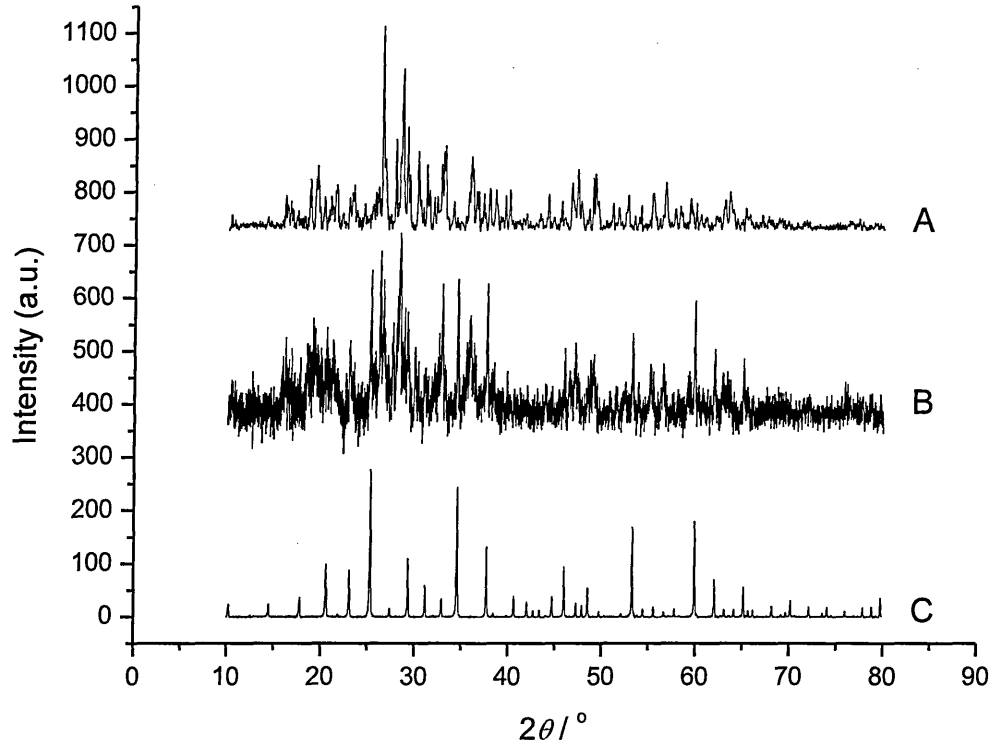

Figure 5.13 XRD patterns recorded over the 2θ range of 10° - 80° for A) $H_4[SiW_{12}O_{40}]\cdot 14H_2O$, B) $H_4[SiW_{12}O_{40}]\cdot 10H_2O$ and C) $H_4[SiW_{12}O_{40}]\cdot 6H_2O$ (step size = 0.01°; step time = 8 s).

5.3.7 A comparison of $H_4[SiW_{12}O_{40}]\cdot xH_2O$ ($6 \leq x \leq 8$) with $H_3[PW_{12}O_{40}]\cdot xH_2O$ ($6 \leq x \leq 12$)

It is interesting to compare the results for $H_4[SiW_{12}O_{40}]\cdot xH_2O$ ($6 \leq x \leq 8$) with XRD patterns recorded from $H_3[PW_{12}O_{40}]\cdot xH_2O$ ($6 \leq x \leq 12$) under the same conditions. A set of results recorded for $H_3[PW_{12}O_{40}]\cdot xH_2O$ in the range $6 \leq x \leq 7.5$ is shown in Figure 5.14. In all cases, except for the $x = 6.00$ and $x = 7.50$ samples (A and F, respectively) the Bragg peaks in the typical cubic diffraction patterns are split. The reason for the splitting of the individual Bragg peaks is ascribed to the manner in which the samples are held in the their sample holders, as already discussed in the

previous Section (5.3.6) and Appendix A. Analysis, for example, of the x = 6.72 sample (D) on the basis of the presence of two separate sample displacements gives :

- pattern 1 with a zero correction of 0.208(3)° and a = 12.150(2) Å, and
- pattern 2 with a zero correction of -0.248(2)° and a = 12.159(13) Å.

The value determined for the cubic unit cell parameter for $H_3[PW_{12}O_{40}]\cdot 6H_2O$ in Section 5.3.1 was a = 12.1521(12) Å.

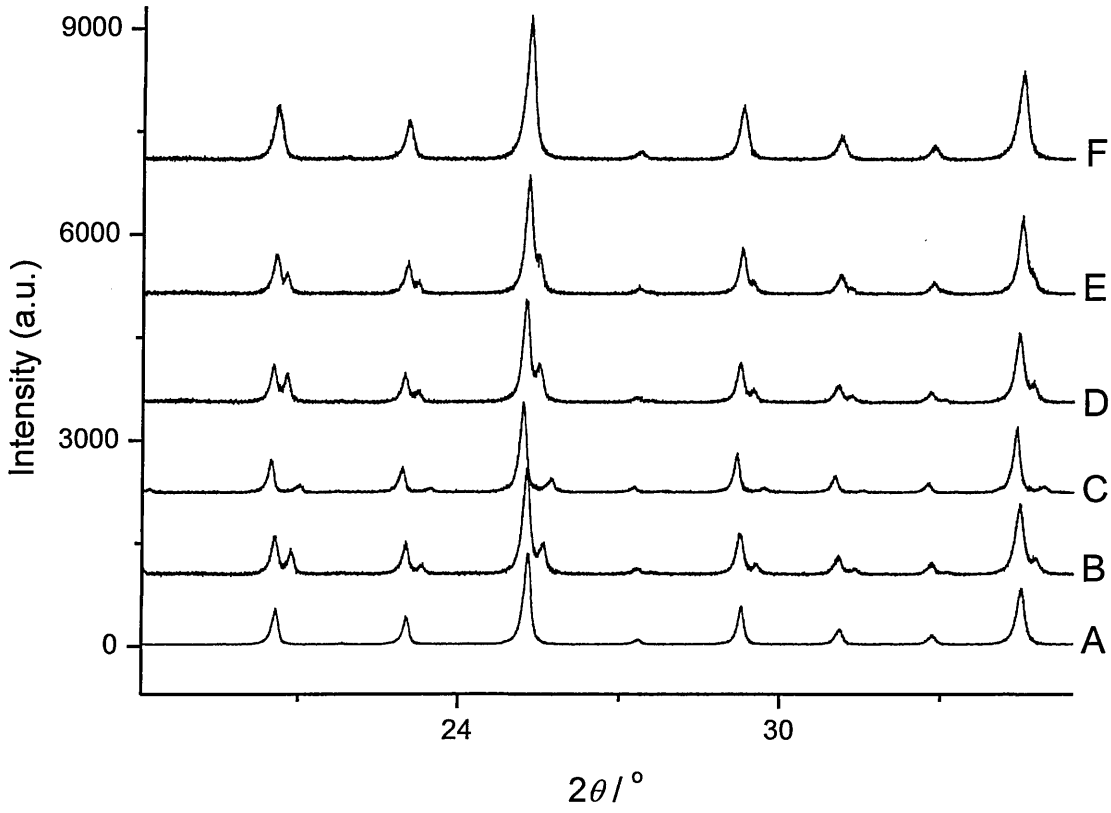

Figure 5.14 XRD patterns (A-F) recorded over the 2θ range of 20° - 35° for $H_3[PW_{12}O_{40}]\cdot xH_2O$ x = 6.00, 6.39, 6.66, 6.72, 7.10 and 7.50 (step size = 0.01°; step time = 8 s).

A major difference between the XRD patterns recorded for $H_4[SiW_{12}O_{40}]\cdot xH_2O$ ($6 \leq x \leq 8$) and the hydrates of $H_3[PW_{12}O_{40}]\cdot xH_2O$ ($6 \leq x \leq 12$) is that no splitting of

individual Bragg peaks is observed for the x = 7.5 sample. In fact it is also found experimentally that this is also the case for samples with x = 9.0, 10.5 and 12.0. Analysis of the XRD patterns for these samples (including x = 7.5) is summarised in Table 5.6.

Table 5.6 Zero correction and cubic unit cell parameters (a) calculated from the XRD patterns for $H_3[PW_{12}O_{40}]\cdot xH_2O$ samples with x = 7.50, 9.00, 10.5 and 12.0.

	***a* / Å**	**Zero correction / °**
$H_3[PW_{12}O_{40}]\cdot 7.5H_2O$	12.1413(82)	0.068(4)
$H_3[PW_{12}O_{40}]\cdot 9.0H_2O$	12.17(1)	-0.119(19)
$H_3[PW_{12}O_{40}]\cdot 10.5H_2O$	12.1508(55)	-0.122(31)
$H_3[PW_{12}O_{40}]\cdot 12.0H_2O$	12.148(5)	-0.073(9)

A tentative model for the behaviour in Table 5.6 and the associated diffraction patterns involves the filling of empty vacancies present in the unit cell of $H_3[PW_{12}O_{40}]\cdot 6H_2O$ (See Chapter 2, Figure 2.5 and 2.6). The 'non-split patterns' occur every 1.5 water molecules per Keggin unit or, as Z = 2, every 3 water molecules per unit cell. This corresponds, on average, to filling one vacancy on each of the faces of the cubic unit cell. This suggests that vacancies are only filled when an even distribution of the water molecules over the unit cell is possible. For reasons which are not clear, these samples must be stable and do not reduce in volume over the timescale of the XRD experiment.

Considering the strong similarities in the crystal structures recorded for both the $x = 6$ and $x = 14$ single phases of $H_3[PW_{12}O_{40}]$ and $H_4[SiW_{12}O_{40}]$, the markedly different behaviour for hydrated samples in the range $x = 6$ and $x = 14$ is striking. The key difference between the two acids is the extra acidic proton associated with $H_4[SiW_{12}O_{40}]$ which is thought to be located on the Keggin unit itself. The presence of this extra acidic proton may result in additional competition for adsorbed water molecules with consequences for the evolution of hydrated phases.

5.4 ^{29}Si MAS NMR spectroscopy

A single sharp resonance at $\delta(^{29}Si)$ = -84.5 (±0.1) was observed in the spectrum recorded from $H_4[SiW_{12}O_{40}]\cdot 24H_2O$ indicating, as expected, that only a single silicon environment is present. Details for the resonances observed in the spectra recorded from other stable single phases are given in Table 5.7. It should be noted that in order to observe a resonance signal for the hexahydrate with reasonable signal-to-noise ratio it was necessary to use an experimental relaxation delay of 400 s.

Table 5.7 ^{29}Si MAS NMR chemical shifts recorded from $H_4[SiW_{12}O_{40}]\cdot 24H_2O$, $H_4[SiW_{12}O_{40}]\cdot 14H_2O$, $H_4[SiW_{12}O_{40}]\cdot 6H_2O$ and $H_4[SiW_{12}O_{40}]\cdot 0H_2O$, at room temperature.

	$\delta(^{29}Si)$
$H_4[SiW_{12}O_{40}]\cdot 24H_2O$	-85.1 ±0.1
$H_4[SiW_{12}O_{40}]\cdot 14H_2O$	-85.0 ±0.1
$H_4[SiW_{12}O_{40}]\cdot 6H_2O$	-84.5 ±0.1
$H_4[SiW_{12}O_{40}]\cdot 0H_2O$	-81.6 ±0.1

The resonance recorded from the anhydrous acid ($\delta(^{29}Si)$ = -81.6 ±0.1) shows an increase in chemical shift (deshielding) compared to the other hydrates. In this respect, there are parallels with ^{31}P MAS NMR studies[26] of $H_3[PW_{12}O_{40}]\cdot xH_2O$. A chemical shift change of 4.6 ppm corresponding to deshielding, was observed between $x = 6$ ($\delta(^{31}P)$ = -15.6 ±0.1), and $x = 0$ ($\delta(^{31}P)$ = -11.0 ±0.1). It was suggested that this change in chemical shift was associated with the removal of structural water resulting in the acidic protons being directly bonded to individual Keggin units (See Chapter 2, Section 2.3.2). It seems reasonable to suggest that similar behaviour occurs in 12-silicotungstic acid.

A broadening of the ^{29}Si MAS NMR resonance for $H_4[SiW_{12}O_{40}]\cdot 0H_2O$ was also observed compared to the resonances for the hydrates. This is also consistent with results[27] recorded from $H_3[PW_{12}O_{40}]\cdot 0H_2O$. This broadening may well be due to the presence of acidic protons which have penetrated into the Keggin cage, as suggested in the interpretation of the ^{31}P NMR results.[27]

The ^{29}Si spin-lattice relaxation time (T_1) of $H_4[SiW_{12}O_{40}]\cdot 6H_2O$ is greater in magnitude than that of the other hydrates as evidenced by the need to significantly increase the relaxation delay during signal accumulation. This result suggests that the structural water molecules in the hexahydrate have less mobility than the zeolitic-type water molecules in the higher hydrates and so provide a less efficient pathway for magnetic dipolar relaxation of the central silicon nucleus. Chidichimo *et al.*[27] observed an almost identical result in ^{31}P MAS NMR investigations of $H_3[PW_{12}O_{40}]\cdot xH_2O$. Spin-lattice relaxation measurements (see Chapter 2, Section 2.3.2), showed the hexahydrate to have the largest value of $T_1(^{31}P)$. As x decreased from 6 to 0, the value of $T_1(^{31}P)$ decreased from 210 to 50 s; a value slightly larger than observed for the higher hydrated states; for example, $T_1(^{31}P) = 30$ s for $x > 16$.

5.5 FT-IR spectroscopy

The FT-IR spectra recorded from the four single phases of $H_4[SiW_{12}O_{40}]\cdot xH_2O$, $x = 0$, 6, 14 and 24, are presented in Figure 5.15.

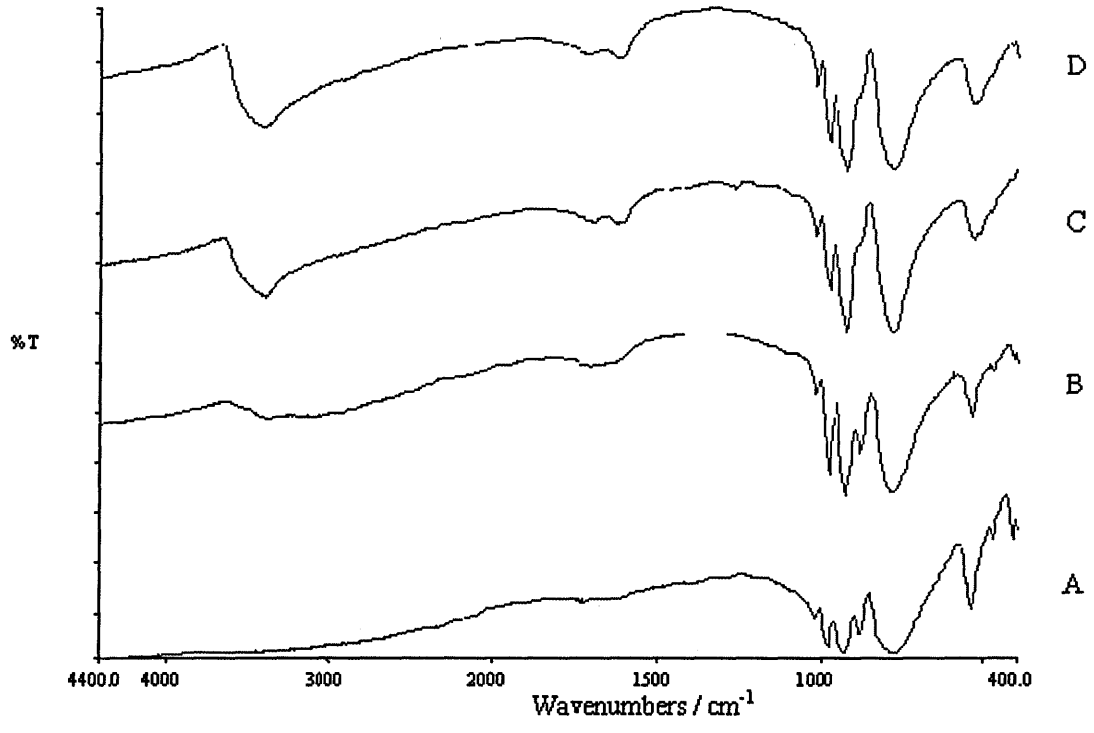

Figure 5.15 FT-IR spectra recorded from A) $H_4[SiW_{12}O_{40}]\cdot 0H_2O$, B) $H_4[SiW_{12}O_{40}]\cdot 6H_2O$, C) $H_4[SiW_{12}O_{40}]\cdot 14H_2O$ and D) $H_4[SiW_{12}O_{40}]\cdot 24H_2O$.

Five absorptions are observed in the finger-print region of the recorded FT-IR spectra at 1020 (w), 981 (s), 921 (s), 880 (m) and 779 (s) cm^{-1} for each of the single hydrated phases, as well as the anhydrous phase. These absorptions correspond to those previously reported[28] for $H_4[SiW_{12}O_{40}]\cdot 17H_2O$ as summarised in Table 5.8.

Table 5.8 Assignments (taken from reference [28]) in the fingerprint region of the FT-IR spectrum of $H_4[SiW_{12}O_{40}]\cdot 17H_2O$. The oxygen atoms are labelled using the notation in Figure 2.2.

Wavenumber / cm^{-1}	Association
1020(w)	$H_2O...H$
981(s)	$W=O_d$
928(s)	$Si-O_a-W$
880(m)	$W-O_b-W$
785(s)	$W-O_c-W$

In the region 4000-1500 cm^{-1} differences in the FT-IR spectra of the single hydrated states are observed. Three absorptions are observed in the FT-IR spectrum recorded for $H_4[SiW_{12}O_{40}]\cdot 24H_2O$ (Figure 5.15(D)); 3510 (broad), 1720 and 1620 cm^{-1}. Similar absorptions were also observed by Zecchina *et al.*[29] and Misono *et al.*[30] for $H_3[PW_{12}O_{40}]\cdot xH_2O$ and were associated with the OH bending and stretching modes of water molecules.[29, 30] In particular the bands occurring at 3510 and 1620 cm^{-1} were associated with "neutral" or zeolitic type water molecules.[29]

Dehydration to $H_4[SiW_{12}O_{40}]\cdot 14H_2O$, Figure 5.15(C), results in a reduction in the intensity of the band occurring at 3510 cm^{-1}. Further dehydration to the hexahydrate, Figure 5.15(B), does not affect the band occurring at 1720 cm^{-1}, however, the absorptions observed at 3510 and 1620 cm^{-1} are significantly reduced in intensity. The removal of the broad band occurring at 3510 cm^{-1} reveals the presence of a band in the region of 3300 cm^{-1}. FT-IR investigations[29] for $H_3[PW_{12}O_{40}]\cdot 6H_2O$ also

showed a band at 1710 cm^{-1} to be unaffected by the dehydration process from a higher hydrate, as well as the presence of an absorption at 3180 cm^{-1} which was originally obscured by a broad band at 3510 cm^{-1}. These two bands were associated[29] with water molecules interacting with acidic protons. A broad band centred at approximately 3000 cm^{-1} between the 3300 and 1720 cm^{-1} bands is also observed in Figure 5.15(B). This absorption was also observed[29, 30] for $H_3[PW_{12}O_{40}]\cdot 6H_2O$. On complete dehydration of the Keggin unit, Figure 5.15(A), no distinct absorptions are observed in the 4000-1500 cm^{-1} region.

Overall the FT-IR results indicate that the OH modes associated[29] with the acidic proton in $H_3[PW_{12}O_{40}]\cdot 6H_2O$ (3180 and 1720 cm^{-1}) are comparable to those of $H_4[SiW_{12}O_{40}]\cdot 6H_2O$ (3300 and 1720 cm^{-1}). Absorptions characteristic of zeolitic type water molecules (3510 and 1620 cm^{-1}) observed in the FT-IR spectrum recorded from $H_4[SiW_{12}O_{40}]\cdot xH_2O$, where $x > 6$, are also consistent with values observed for the corresponding 12-phosphotungstic acid hydrate.[29, 30]

5.6 Summary

Characterisation of single hydrated phases of $H_4[SiW_{12}O_{40}]$ have been undertaken using thermal analysis, XRD, ^{29}Si MAS NMR and FT-IR spectroscopy. The results, as might be expected, compare favourably with similar studies of hydrated phases of $H_3[PW_{12}O_{40}]$, although the presence of the additional acidic proton in $H_4[SiW_{12}O_{40}]$ has an influence.

Three hydrated single phases (x = 6, 14 and 24), as well as an anhydrous phase, have been identified by thermal analysis and their unit cell parameters confirmed by X-ray powder diffraction data. ^{29}Si MAS NMR confirms a single silicon environment for each of the hydrated states. The increased value of $T_1(^{29}Si)$ for the hexahydrate indicates that the water molecules are highly ordered and are more restricted, therefore, in influencing the magnetic relaxation of the silicon environment. Deshielding (in the order of 3 ppm) was observed as the hydration state was lowered from $x = 6$ to $x = 0$. This deshielding is most likely caused by the acidic protons of the anhydrous acid being located randomly on the oxygen atoms of the Keggin unit instead of being associated with water molecules.

FT-IR spectroscopy demonstrated that the hydration state of $H_4[SiW_{12}O_{40}]\cdot xH_2O$ has no influence on the vibrational frequencies associated with the Keggin anion itself. However, the bending and stretching vibrations of the zeolitic type water molecules (3510 and 1620 cm^{-1}) decrease in spectral intensity as the water molecules are removed between $6 < x < 24$. Vibrations associated with water molecules interacting with acidic protons (3300 and 1720 cm^{-1}) were found to decrease in spectral intensity between $0 < x < 6$.

Appendix A

The splitting of Bragg peaks in the XRD powder patterns recorded from samples in the range $H_4[SiW_{12}O_{40}]\cdot 6H_2O$ to $H_4[SiW_{12}O_{40}]\cdot 8H_2O$ is associated with the behaviour of this particular range of hydrated samples in their sample holders. The general manner in which samples are held has already been described and illustrated

in Figure 5.5. Close inspection (by eye) of an $x = 6$ to $x = 8$ sample following the recording of a diffraction pattern showed two features : (i) a thin layer of sample 'attached' to the covering polyethylene sheet and (ii) a 'shrinkage' of the remaining bulk sample. The situation is shown schematically in Figure A.1. In effect, there are two layers of sample present each with its own sample displacement. It is not clear why this behaviour was not observed for samples with $x > 8$.

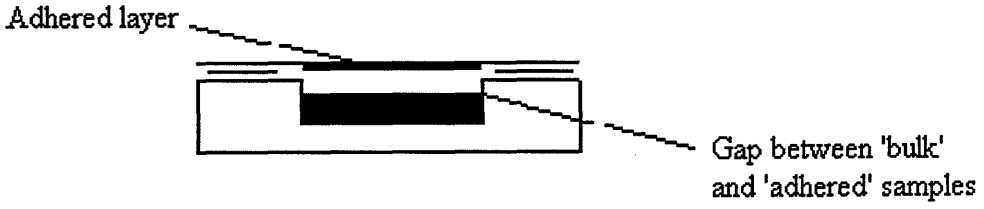

Figure A.1 A schematic representation of a sample following the recording of an X-ray diffraction pattern. The sample is present in two distinct layers in the covered sample holder.

A series of experiments were carried out to confirm the observations reported above. The polyethylene sheet was removed from a covered $H_4[SiW_{12}O_{40}]\cdot 8H_2O$ sample and XRD patterns were recorded from both the polyethylene sheet containing adhered sample and the bulk sample. A single set of diffraction peaks was observed in each case characteristic of the hexahydrate ($x = 6$).

The shrinkage of a sample in the sample holder was also monitored using XRD. The diffraction peak at approximately $2\theta = 25^\circ$ (004) was recorded from freshly prepared

$H_4[SiW_{12}O_{40}]\cdot 7.5H_2O$ every ten minutes for an hour. These results are shown in Figure A.2.

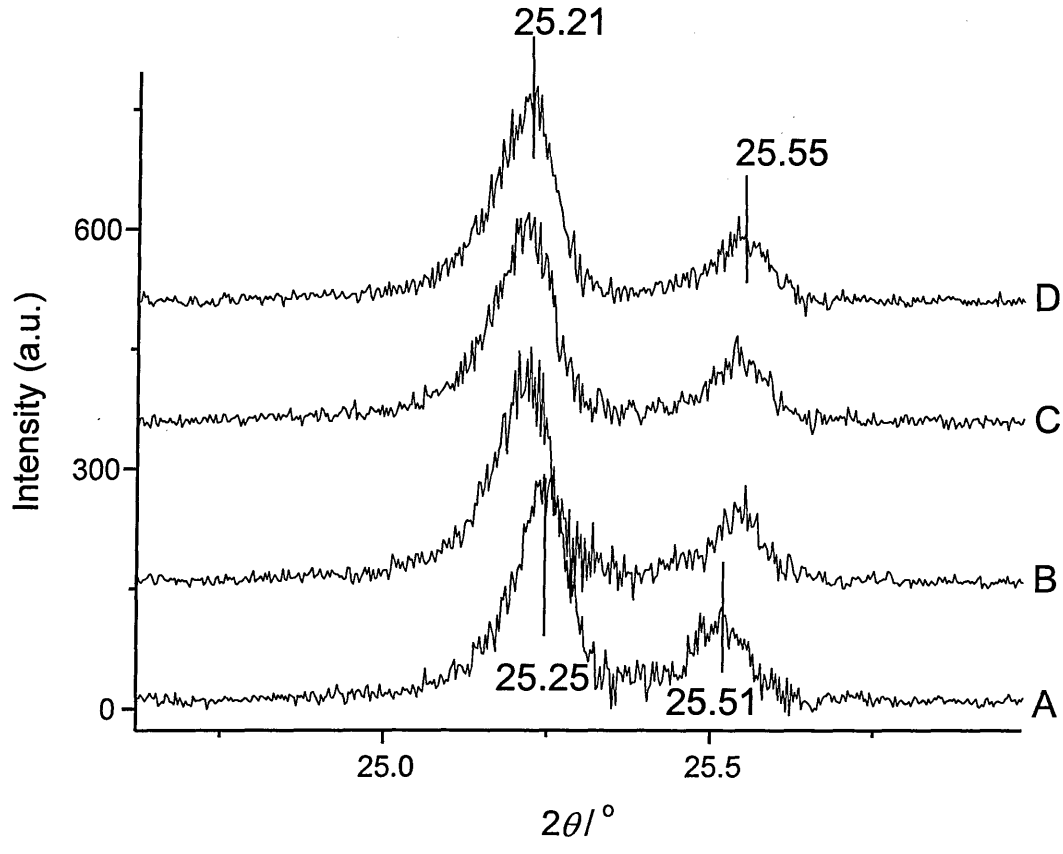

Figure A.2 XRD pattern recorded over the 2θ range of 24.5° - 26.5° (step size = 0.03° and step time = 7 s) every ten minutes from 10-40 minutes A-D, following preparation of the sample.

After approximately 30 minutes, the splitting remains approximately constant at $2\theta = 0.34°$. The increase in splitting over time clearly shows the sample volume is reducing in the sealed holder. A possible reason for this behaviour is that the sample may not have been completely homogeneous when sealed.

References

(1) Moffat, J. B. *Metal-Oxygen Clusters*; Kluwer Academic/Plenum Publishers: New York, 2001.

(2) Kozhevnikov, I. V. *Catalysts for Fine Chemical Synthesis: Catalysis by Polyoxometalates*; John Wiley & Sons Ltd: West Sussex, 2002.

(3) Katsoulis, D. E. *Chemical Reviews* **1998**, *98*, 359-387.

(4) Bardin, B. B.; Bordawekar, S. V.; Neurock, M.; Davis, R. J. *Journal of Physical Chemistry B* **1998**, *102*, 10817-10825.

(5) Mioc, U.; Davidovic, M.; Tjapkin, N.; Colomban, P.; Novak, A. *Solid State Ionics* **1991**, *46*, 103-109.

(6) Bielanski, A.; Pozniczek, J.; Hasik, M. *Journal of Thermal Analysis* **1995**, *44*, 717-723.

(7) Bielanski, A.; Datka, J.; Gil, B.; Malecka-Lubanska, A.; Micek-Ilnicka, A. *Catalysis Letters* **1999**, *57*, 61-64.

(8) Sun, J. Z.; MacFarlane, D. R.; Forsyth, M. *Electrochimica Acta* **2001**, *46*, 1673-1678.

(9) Mioc, U. B.; Dimitrijevic, R. Z.; Davidovic, M.; Nedic, Z. P.; Mitrovic, M. M.; Colomban, P. *Journal of Materials Science* **1994**, *29*, 3705-3718.

(10) Vaughan, J. S.; O'Connor, C. T.; Fletcher, J. C. Q. *Journal of Catalysis* **1994**, *147*, 441-454.

(11) Fournier, M.; Feumijantou, C.; Rabia, C.; Herve, G.; Launay, S. *Journal of Materials Chemistry* **1992**, *2*, 971-978.

(12) Brown, G. M.; Noespirlet, M. R.; Busing, W. R.; Levy, H. A. *Acta Crystallographica Section B - Structural Science* **1977**, *33*, 1038-1046.

(13) Illingworth, J. W.; Keggin, J. F. *Journal of the Chemical Society* **1935**, 575-580.

(14) Scroggie, A. G.; Clark, G. L. *Proceedings of the National Academy of Sciences of the United States of America* **1929**, *15*, 1-8.

(15) Kraus, W.; Nolzeb, G. *Journal of Applied Crystallography* **1996**, *29*, 301-303.

(16) Dong, C.; Wu, F.; Chen, H. *Journal of Applied Crystallography* **1999**, *32*, 850-853.

(17) Laugier, J.; Bochu, B. *"CHECKCELL : A Software Performing Automatic Cell/Space Group Determination"; Collaborative Computational Project, Number 14 (CCP14), Laboratory of Materials and Phyisical Engineering, School of Physics, University of Grenoble, France* **2000**.

(18) Marosi, L.; Platero, E. E.; Cifre, J.; Arean, C. O. *Journal of Materials Chemistry* **2000**, *10*, 1949-1955.

(19) Boeyens, J. C. A.; McDougal, G. J.; Smit, J. V. R. *Journal of Solid State Chemistry* **1976**, *18*, 191-199.

(20) D'Amour, V. H.; Allmann, R. *Zeitschrift fuer Kristallographie* **1976**, *143*, 1-13.

(21) Bergerhoff, G.; Hundt, R.; Sievers, R.; Brown, I. D. *Journal of Chemical Information and Computer Sciences* **1983**, *23*, 66-69.

(22) Farkas, L.; Werner, P. E. *Zeitschrift fuer Kristallographie* **1980**, *151*, 141-152.

(23) Liu, L. J.; Quillin, M. L.; Matthews, B. W. *Proceedings of the National Academy of Sciences of the United States of America* **2008**, *105*, 14406-14411.

(24) Spirlet, M. R.; Busing, W. R. *Acta Crystallographica Section B - Structural Science* **1978**, *34*, 907-910.

(25) Noespirlet, M. R.; Brown, G. M.; Busing, W. R.; Levy, W. A. *Acta Crystallographica Section A* **1975**, *31*, S80-S80.

(26) Uchida, S.; Inumaru, K.; Misono, M. *Journal of Physical Chemistry B* **2000**, *104*, 8108-8115.

(27) Chidichimo, G.; Golemme, A.; Imbardelli, D.; Iannibello, A. *Journal of the Chemical Society - Faraday Transactions* **1992**, *88*, 483-487.

(28) Thouvenot, R.; Rocchiccioli-Deltcheff, C.; Fournier, M.; Franck, R. *Inorganic Chemistry* **1983**, *22*, 207-216.

(29) Zecchina, A.; Paze, C.; Bordiga, S. *Langmuir* **2000**, *16*, 8139-8144.

(30) Koyano G; Saito T; Hashimoto M; Misono M *Studies in Surface Science and Catalysis* **2000**, *130*, 3077-3082.

Chapter 6

Characterisation of silica-supported 12-silicotungstic acid

6.1 Introduction

The preparation of ethyl acetate through the AVADA process, discussed in Chapter 1, uses a strong acid catalyst consisting of 12-silicotungstic acid (in a hydrated form) supported on silica. The silica support, which has neutral or mild acidity (See Chapter 2, Section 2.4.1), increases the surface area and, consequently, the activity of the 12-heteropolyacid catalyst. 12-Silicotungstic acid is selected as the solid acid due to its high acidity (Chapter 2, Section 2.3) and an overall contribution to environmental issues. Whilst the acidity of 12-phosphotungstic acid has been shown to be greater than that of 12-silicotungstic acid,[1, 2] the high number of patents associated with this acid[3] restrict its commercial use; hence, the selection by BP Chemicals of the less acidic 12-silicotungstic acid for use in their AVADA process.

The lifetime of the catalyst used in the AVADA process, which is a property of key commercial concern, depends on a variety of factors. One of these relates to the production of by-products (such as methyl ethyl ketone) as the catalyst ages. Once the level of by-products reaches a pre-designated level, the industrial reactor has to be decommissioned. A key area of investigation, therefore, is to understand the processes involved in the 'ageing' of the catalyst since these may be linked to the production of excess by-products. A comparison between authentic unused catalysts with catalysts that have spent time in the reactor (used catalysts) is important in this area of research.

Once a used catalyst has been removed from an industrial reactor the 12-silicotungstic acid is recovered, through extraction with water, so that it can be

reused. However, it has been found in studies by BP Chemicals[4] that complete recovery of all of the solid acid present is not possible. This finding has been correlated with evidence relating to carbon deposition (coking) on the catalyst during its lifetime in the reactor. It was found that there was a linear relationship between the increase in percentage (by weight) of carbon deposited on the catalyst and the percentage of tungsten that could not be removed by washing with water; this is referred to as 'insoluble tungsten'. However, it was not determined whether this insoluble tungsten was in the form of 12-silicotungstic acid or decomposition products of the acid. From an industrial perspective, it is important to gain more information in this area. In particular, if the insoluble tungsten is not in the form 12-silicotungstic acid it would be of interest to characterise the compounds present and assess their role in the deactivation of the catalyst. By contrast, an insoluble 12-silicotungstic acid residue would require examination of the reasons for this insolubility with a view to developing methods for recovery of this valuable acid.

6.2 The authentic unused catalyst

The characterisation of an authentic unused catalyst (which will also be referred to as silica-supported 12-silicotungstic acid) is discussed in this section, particularly with respect to the properties of the unsupported acid. The preparation of the industrial catalyst has already been described in Chapter 4.1. The loading of 12-silicotungstic acid corresponds to 25.5 wt %.

6.2.1 Thermal analysis

Simultaneous TGA and DTA results recorded from silica-supported 12-silicotungstic acid are shown in Figure 6.1(A). The experimental conditions corresponded to a

flow of dry air at 50 ml min^{-1}, a heating rate of 20 °C min^{-1} and a sample mass of approximately 30 mg. These conditions are similar to those used previously (Chapter 5, Section 5.2) for the investigation of the unsupported hydrated acid, the results for which are reproduced in Figure 6.1 (B). Figure 6.1(C) shows the thermal analysis results for the silica support under the same conditions.

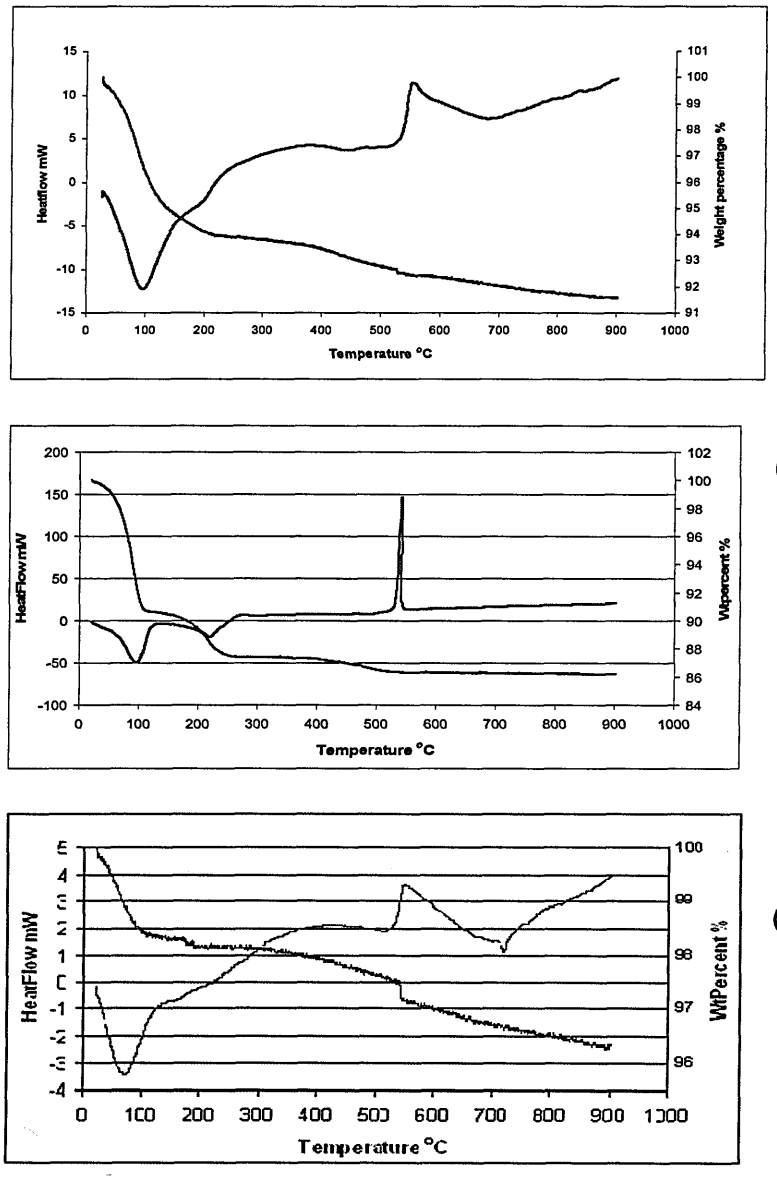

Figure 6.1 Thermal analysis recorded from (A) silica-supported 12-silicotungstic acid, (B) $H_4[SiW_{12}O_{40}]\cdot xH_2O$ ($x \approx 24$), and (C) the silica-support. Further information is provided in the text.

Below 300 °C two relatively weak endothermic transitions are observed with peak maxima in the temperature regions of 90 and 190 °C for the silica-supported 12-silicotungstic acid, Figure 6.1(A). The first of the transitions is in the region in which a strong endothermic transition is observed in the DTA results for the silica support itself (Figure 6.1 (C)). It is thus not clear from these results alone whether fully hydrated crystallites of 12-silicotungstic acid are present on the silica support. Indeed, later XRD results (Section 6.2.2) are consistent with the presence of mainly the hexahydrate. The observed transition at approximately 190 °C corresponds to the loss of water molecules from this hydrate. The TGA data recorded from the silica-supported 12-silicotungstic acid at temperatures below 300 °C, show weight loss in two stages between 25 - 100 °C and 100 - 200 °C. Between 200 - 400 °C a plateau is observed which is consistent with the formation of the anhydrous unsupported acid as also observed in Figure 6.1(B). Between 430 - 490 °C a weak transition is observed in the DTA recorded from the unsupported 12-silicotungstic acid which can be attributed to the loss of two constitutional water molecules. This transition is also observed in the DTA recorded from the silica-supported 12-silicotungstic acid in a similar temperature range. Overall, the less well-defined character of the thermal analysis data in the temperature range 25 °C to 500 °C for the silica-supported 12-silicotungstic acid can be attributed to contributions from the silica support itself. As shown in Figure 6.1 (C) there is significant water loss from silica in this temperature range.

The sharp exothermic transition, corresponding to the decomposition of the Keggin unit[5], observed at 535 °C in Figure 6.1(B) is not readily apparent in the DTA data recorded from the silica-supported 12-silicotungstic acid (Figure 6.1(A)). It is

suggested that this is a result of two factors : i) there is less 12-silicotungstic acid present in the sample under investigation, and ii) the broad exothermic transition present in the thermal analysis recorded from the silica support occurs in the same temperature range and dominates the output. The broad exothermic peak for silica is probably due to a transition temperature[6] in the silica support. By contrast, thermal investigations carried out for silica-supported 12-phosphotungstic acid[7] have revealed an exothermic event characteristic of the decomposition of the acid but at a higher temperature of 595 °C for a loading of 62.5 wt %. When compared with data for the unsupported 12-phosphotungstic acid,[8] the observed exothermic peak was found to be broader, less intense and, depending on loading, the decomposition temperature of the acid was reduced by 20 - 40 °C. At a loading equivalent to that of the silica-supported 12-silicotungstic acid (~25 wt %), the exothermic event observed for silica-supported 12-phosphotungstic acid was very broad and significantly reduced in intensity when compared with the unsupported acid[7]. It is reasonable to conclude that, as to be expected, 12-silicotungstic acid does decompose on silica at a temperature close to that for the unsupported acid. However, the exothermic event, which is probably broad, is obscured in the DTA.

Overall, the thermal analysis data show that hydrated 12-silicotungstic acid is present on the silica support and that it dehydrates in a similar manner to that of the unsupported acid : in the temperature regions 100 - 200 °C and 200 - 400 °C the hexahydrate and the anhydrous acid, respectively, are present. Decomposition of 12-silicotungstic acid occurs in a similar temperature region (535 °C) to that of the unsupported acid.

6.2.2 X-ray powder diffraction

The X-ray powder diffraction pattern recorded from silica-supported 12-silicotungstic acid (as received) is shown in Figure 6.2; XRD powder patterns for $H_4[SiW_{12}O_{40}]\cdot 6H_2O$ and the silica support itself are also included in this figure for comparison.

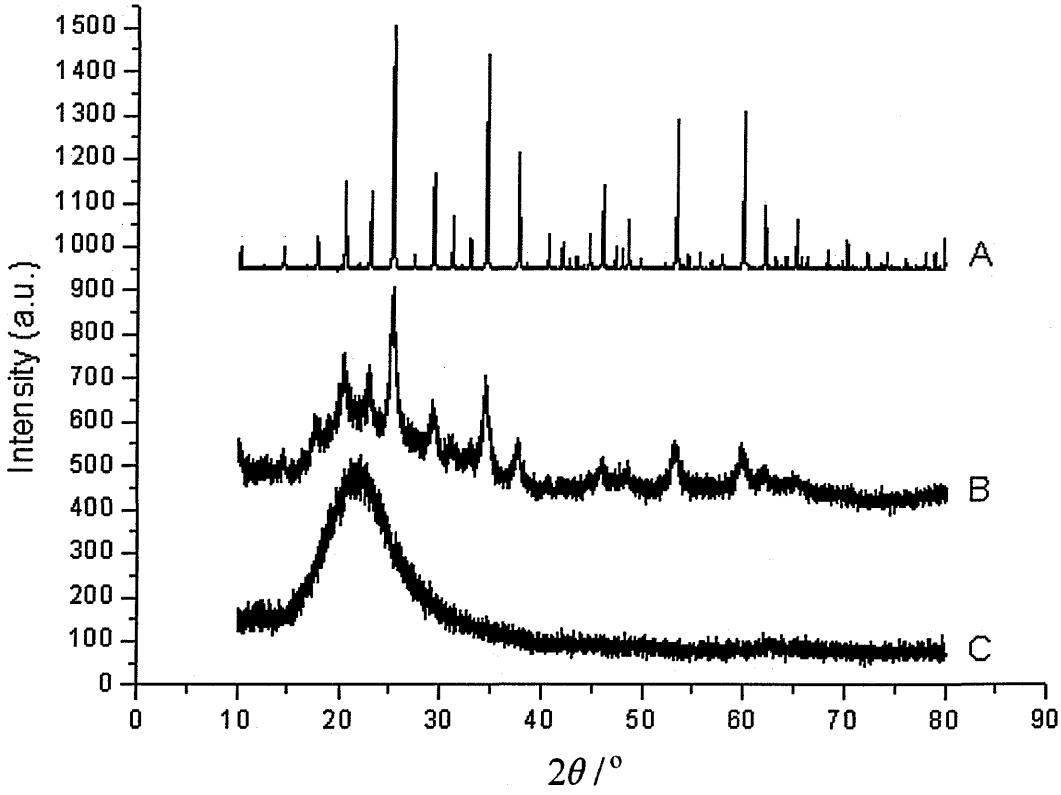

Figure 6.2 XRD patterns recorded for A) $H_4[SiW_{12}O_{40}]\cdot 6H_2O$, B) silica-supported 12-silicotungstic acid and C) the silica support over the 2θ range of 10° - 80° (step size = 0.01°, step time = 8 s).

The characteristic broad peak, centred at approximately 2θ = 22°, for amorphous silica is clearly present in the XRD pattern recorded from the supported acid. It is also clear in this powder pattern that diffraction peaks characteristic of

$H_4[SiW_{12}O_{40}]\cdot 6H_2O$ are present. This suggests that a large fraction of the crystallites present on the surface of the silica-support are in the form of the hexahydrate. This suggests that the majority of water loss observed in the thermal analysis data in the temperature range 25 - 100 °C (Section 6.2.1, Figure 6.1 (A)) was as a result of water molecules present on the silica support and was not due to the presence of a higher hydrate.

The diffraction peaks observed in the XRD pattern recorded for silica-supported 12-silicotungstic acid are much broader than those recorded from $H_4[SiW_{12}O_{40}]\cdot 6H_2O$. The broadening is consistent with X-ray diffraction investigations carried out by Newman *et al.*[7] on pure and silica-supported (26 wt %) $H_3[PW_{12}O_{40}]\cdot 6H_2O$. This broadening effect was shown, through application of the Scherrer equation,[9] to be a result of a reduction in particle size from 48 nm (±1 nm) to 6 nm (±1 nm). Similar calculations based on the diffraction patterns in Figures 6.2 (A) and (B) also indicate a reduction in particle size, although from 89 nm (±4 nm) to 10 nm (±0.5 nm). Characterisation of silica-supported $H_3[PW_{12}O_{40}]$ by Kuang *et al.*,[10] using X-ray powder diffraction, showed results consistent with those reported by Newman *et al.*[7] Samples with a loading of between 30-60 wt % were found to have a particle size of between 24-27 nm leading to the conclusion that the majority of $H_3[PW_{12}O_{40}]$ present is in the form of small crystalline particles. Broadening of diffraction peaks characteristic of $H_3[PW_{12}O_{40}]\cdot 6H_2O$ supported on silica has also been observed by Kozhevnikov *et al.*[11] and Izumi *et al.*[12]

Thermal analysis of silica-supported 12-silicotungstic acid, Figure 6.1(A), indicated that the anhydrous acid could be prepared by heating the sample between 200 -

400°C. The XRD pattern recorded from a sample heated to 350 °C is compared with that recorded from anhydrous $H_4[SiW_{12}O_{40}]$ in Figure 6.3.

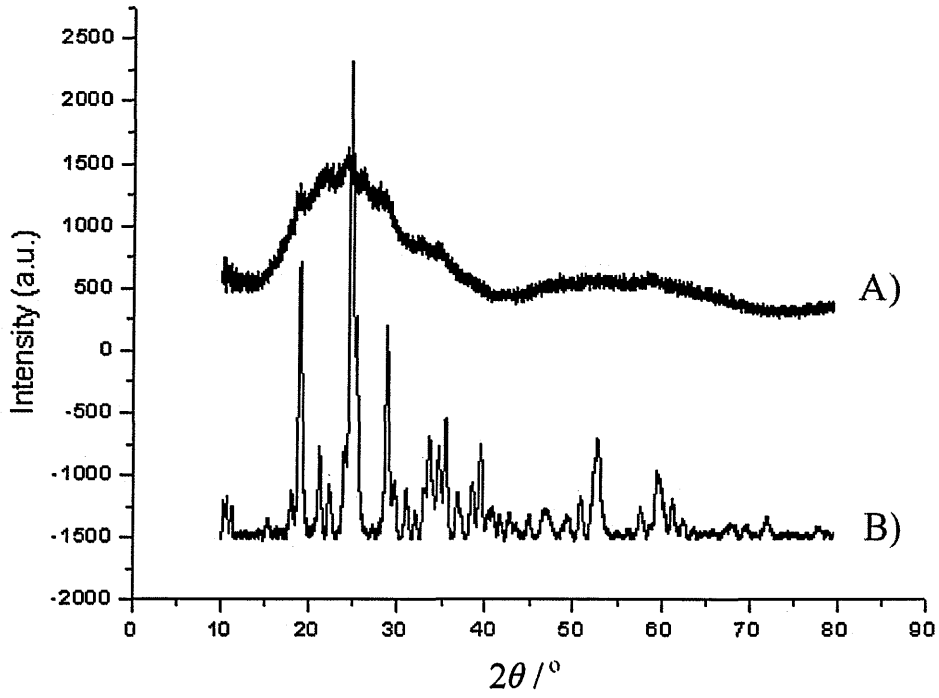

Figure 6.3 XRD patterns recorded for A) silica-supported 12-silicotungstic acid heated to 350 °C and B) anhydrous $H_4[SiW_{12}O_{40}]$ over the 2θ range of 10° - 80° (step size = 0.01°, step time = 8 s).

The three most intense peaks present in the powder diffraction pattern of anhydrous $H_4[SiW_{12}O_{40}]$ occur at 2θ = 18.9°, 24.7° and 28.8°. While the intensities of the peaks in the diffraction pattern recorded from the silica-supported 12-silicotungstic acid heated to 350 °C are much weaker, broad peaks centred around 2θ = 18°, 25° and 28° are observed. This suggests that small crystallites, probably in poorly crystalline form, of the anhydrous acid are present on the silica-support. As already suggested by the results of thermal analysis, the silica support has little influence on the

dehydration behaviour of 12-silicotungstic acid, even though the crystallite sizes are smaller.

Due to both the 12-silicotungstic acid and the silica support being susceptible to hydration, it was difficult to prepare silica-supported samples with a known hydration state of the adsorbed 12-silicotungstic acid. However, it can be noted that a sample that was allowed to stand in open air for several months gave the diffraction pattern shown in Figure 6.4. The XRD patterns for $H_4[SiW_{12}O_{40}]\cdot 14H_2O$ and silica are also given for comparative purposes.

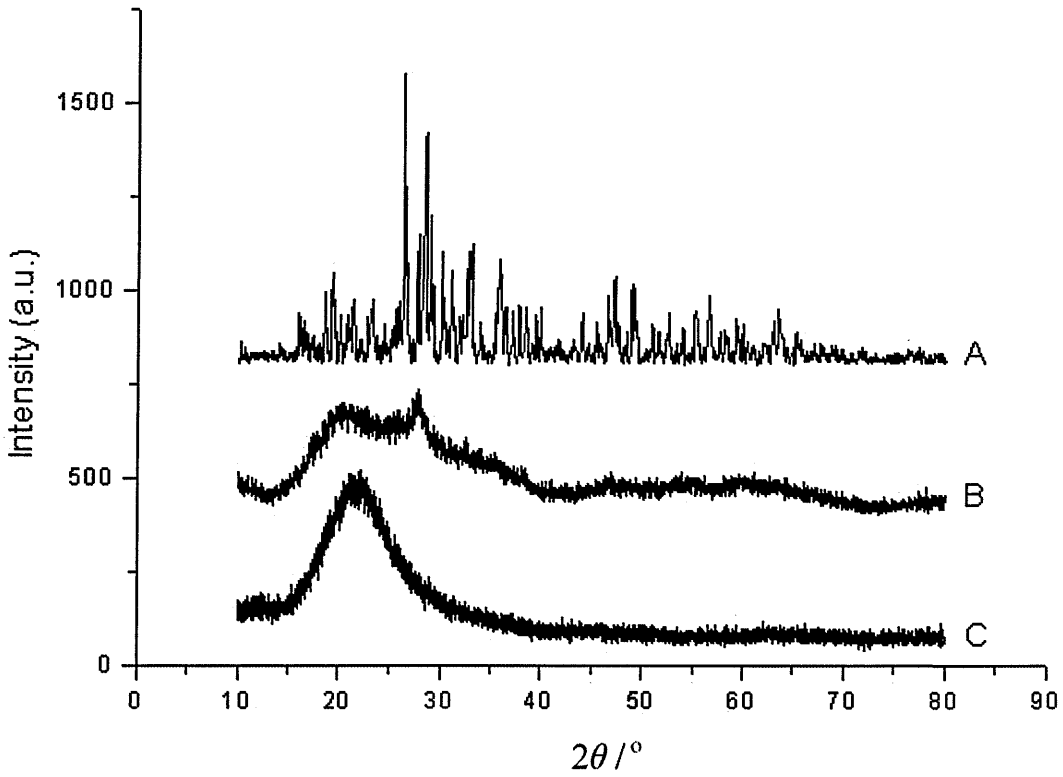

Figure 6.4 XRD patterns recorded for A) $H_4[SiW_{12}O_{40}]\cdot 14H_2O$, B) silica-supported 12-silicotungstic acid which has been left to stand in the open air for several months and C) silica over the 2θ range of 10° - 80° (step size = 0.01°, step time = 8 s).

The XRD pattern recorded from silica-supported 12-silicotungstic acid after hydration from the open air shows a significant change compared to the diffraction pattern recorded from the same sample where hydration had not been allowed to take place (see Figure 6.2(B)). One major peak is observed at approximately $2\theta = 28^{\circ}$. On examination of the powder pattern recorded from $H_4[SiW_{12}O_{40}]\cdot 14H_2O$ four relatively intense peaks are grouped together around this diffraction angle. This strongly suggests that crystallites of $H_4[SiW_{12}O_{40}]\cdot 14H_2O$ are present on the silica support; but as small crystallites in a poorly crystalline form. The presence of the silica does not inhibit the formation of this intermediate hydrate.

6.2.3 ^{29}Si MAS NMR spectroscopy

The ^{29}Si MAS NMR spectrum recorded from the silica-supported 12-silicotungstic acid which was allowed to hydrate in the open air is shown in Figure 6.5.

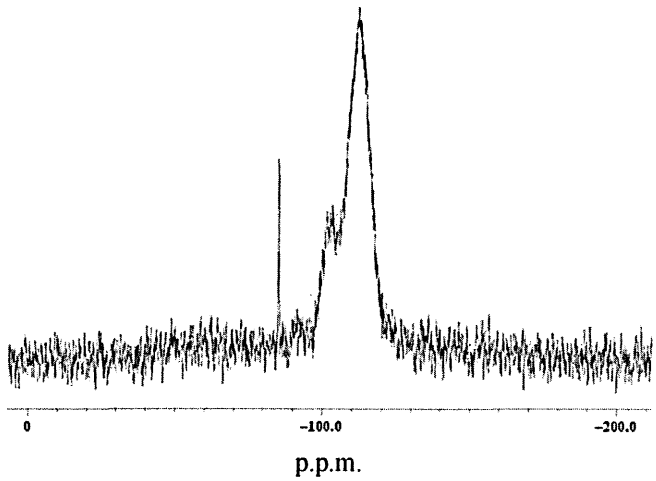

Figure 6.5 ^{29}Si MAS NMR spectrum recorded from silica-supported 12-silicotungstic acid hydrated in the open air.

A single, sharp resonance at $\delta(^{29}Si)$ = -84.5 (±0.1) is observed, as well as a broad resonance at $\delta(^{29}Si)$ = -112.0 (±0.1) with a shoulder at $\delta(^{29}Si)$ = -110.0 (±0.1)

characteristic of the silica support.[13] The silicon resonance observed at -84.5 ppm corresponds to that observed for $H_4[SiW_{12}O_{40}]\cdot xH_2O$, where $6 \leq x < 14$, indicating the presence of hydrated crystallites of the acid on the silica surface, consistent with the thermal analysis and XRD results.

In the context of the present results, it is useful to review the investigations carried out by several different groups on silica-supported 12-phosphotungstic acid, using ^{31}P MAS NMR, in which different numbers of resonances are reported. Kozhevnikov *et al.*[14] and Mohana Rao *et al.*[15] both observed single resonances at $\delta(^{31}P)$ = -15.4 and $\delta(^{31}P)$ = -15.1, respectively, which are consistent within experimental uncertainty with the resonance observed for pure $H_3[PW_{12}O_{40}]\cdot 6H_2O$.[16] However, Lefebvre[17] observed two resonances in the ^{31}P MAS NMR spectrum recorded for silica-supported 12-phosphotungstic acid at -14.6 and -15.1 ppm The resonance observed at $\delta(^{31}P)$ = -15.1 was attributed to pure $H_3[PW_{12}O_{40}]\cdot 6H_2O$[16] and that at $\delta(^{31}P)$ = -14.6 to an interaction of the Keggin anion with the silica-support. Lefebvre[17] suggested this interaction led to the formation of $(SiOH_2)^+(H_2PW_{12}O_{40})^-$. Investigations carried out by Chang[18] in the range 4 - 30 weight percent, however, resulted in the observation of three resonances : $\delta(^{31}P)$ = -15.2, -11.7 and 3.2. The -15.2 and -11.7 ppm resonances were attributed, through comparison with the literature,[19] to $H_3[PW_{12}O_{40}]\cdot 6H_2O$ and to 'partially dehydrated 12-phosphotungstic acid', respectively. The resonance at 3.2 ppm, which was dominant at a low loading, was assigned to anions of 12-phosphotungstic acid interacting with the silica-support. It seems that the differences in the number of observed resonances reported in the literature can be attributed to differences in preparation conditions. Kozhevnikov *et al.*[14] heated the catalyst at 120°C overnight, Mohana Rao *et al.*[15]

heated the catalyst for several hours at 87°C, the conditions used by Lefebvre[17] involved heating at 100°C for 24 hours followed by placement of the sample in a desiccator, and Chang[18] heated the sample at 300°C for a period of 4 hours. It would appear that the multiple resonances observed after heating to 300°C[18] are the result of the presence of hexahydrate and lower hydrates.[19] Heating silica-supported 12-phosphotungstic acid at 100°C is insufficient to form the lower hydrates[7] suggesting the resonance observed at -14.6 ppm is due to the presence of the $(SiOH_2)^+(H_2PW_{12}O_{40})^-$ species. Finally, single resonances appear to be observed where the heating conditions used were less harsh, and possibly the samples were not stored in desiccators, suggesting that the hexahydrate and higher hydrates are present.

The ^{29}Si MAS NMR recorded in the present work is comparable to the ^{31}P MAS NMR spectra recorded from silica-supported 12-phosphotungstic acid investigated by Kozhevnikov *et al.*[14] and Mohana Rao *et al.*[15] It is important to recognise, however, that this result is sensitive to the manner in which the sample is treated.

6.2.4 FT-IR spectroscopy

The FT-IR spectrum recorded from the silica-supported 12-silicotungstic acid is compared with FT-IR spectra recorded of the silica support and $H_4[SiW_{12}O_{40}]\cdot 6H_2O$ in Figure 6.6.

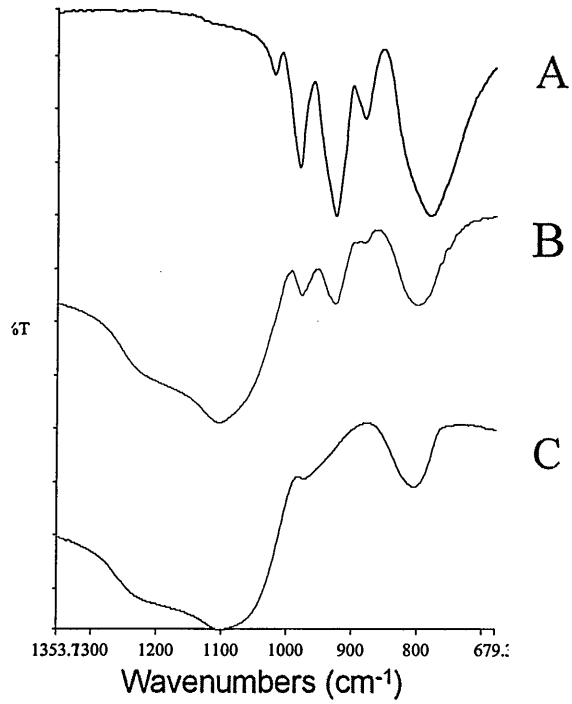

Figure 6.6 FT-IR spectra recorded from A) $H_4[SiW_{12}O_{40}]\cdot 6H_2O$, B) silica-supported 12-silicotungstic acid and C) silica support.

The FT-IR spectrum recorded from the silica-supported 12-silicotungstic acid, Figure 6.6(B), shows absorptions characteristic of the silica support occurring at 1106.5 and 799.2 cm^{-1} (Figure 6.6(C)). Absorptions characteristic of 12-silicotungstic acid[20] (Figure 6.6(A)), are also observed at 981, 928, 880 and 785 cm^{-1}, however, the peak expected at 1020 cm^{-1} is obscured by the broad silica absorption occurring in this region. It can be concluded that the fingerprint region of the 12-silicotungstic acid FT-IR spectrum is largely unaffected by the presence of the silica support.

6.2.5 X-ray photoelectron spectroscopy

The interaction between 12-phosphotungstic acid and a silica support has been studied by a variety of techniques, including thermal analysis,[21] XRD,[11] FT-IR,[10] TEM,[11] ^{31}P MAS NMR spectroscopy[14, 15, 17, 18] and XPS.[7, 22] Of these techniques, the two that have shown significant differences between supported and unsupported 12-phosphotungstic acid have been ^{31}P MAS NMR spectroscopy[14, 15, 17, 18] and XPS.[7, 22] In the present work, ^{29}Si MAS NMR spectroscopy has not provided evidence of direct interaction between 12-silicotungstic acid and the silica support, although it has been noted that any such observation may depend on sample treatment. This Section, therefore, extends the study to an XPS investigation including results for a low-loaded sample and the effect of reducing the silanol content of the support.

Initial studies

The XPS data recorded from unsupported 12-silicotungstic acid is shown in Figure 6.7. The exact hydrated state of the sample is difficult to determine since it is held under vacuum conditions in the XPS instrument.

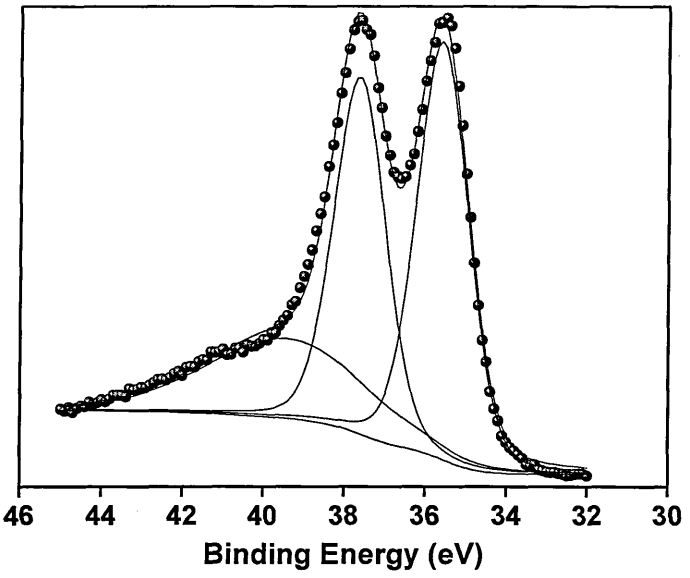

Figure 6.7 W 4*f* spectrum recorded from 12-silicotungstic acid.

The W 4*f* XP spectrum is composed of a well-resolved spin-orbit doublet with binding energies for the W $4f_{7/2}$ and W $4f_{5/2}$ core levels of 35.7 and 37.7 eV, respectively. These values are typical[23] for the presence of W(VI). The spectrum also shows a broad component on the high binding energy side (39.7 eV) which might be associated with energy loss and was not observed in the spectra recorded from the silica-supported samples. It should be noted that unsupported 12-phosphotungstic acid also gives a well-resolved spin-orbit doublet with a reported value for the binding energy for the W $4f_{7/2}$ core level equal to 35.3 eV and a spin-orbit splitting of 2.2 eV.[7, 22] The shift in binding energies (0.4 eV) between the two acidic compounds may be associated with the presence of the additional acidic proton in 12-silicotungstic acid. It has been suggested[24] that the additional acidic proton is randomly distributed over the twelve oxygen atoms of the $[SiW_{12}O_{40}]^{4-}$ Keggin unit.

The W 4*f* XP spectrum recorded from the silica-supported 12-silicotungstic acid, with a loading of 25.5 wt%, (Figure 6.8) is less well-resolved than that for the pure acid.

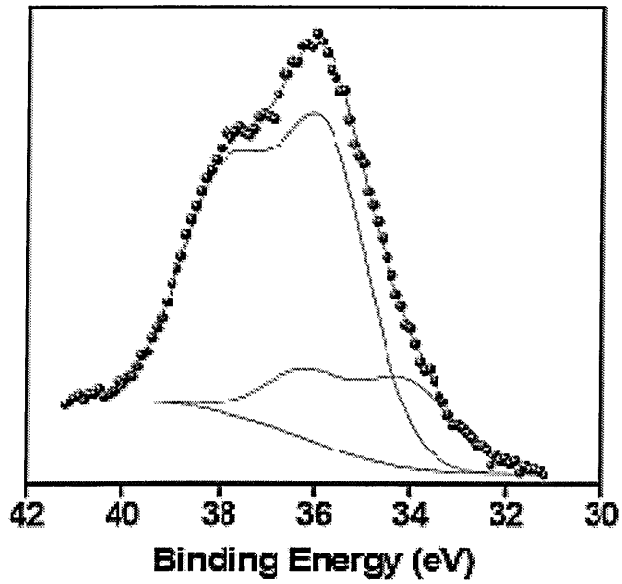

Figure 6.8 W 4*f* spectrum recorded from the silica-supported 12-silicotungstic acid with a loading of 25.5 wt %.

The shape of the spectrum suggests the presence of more than one tungsten-containing contribution and, in this respect, resembles the W 4*f* XP spectrum recorded from silica-supported 12-phosphotungstic acid at a comparable loading where two different chemical states of W were observed.[7, 22] In the present case, the W 4*f* XP spectrum was also fitted on the basis of two different W contributions: a spin-orbit doublet at 35.7 eV ($4f_{7/2}$ component) which accounts for approximately 80% of the total spectral area, and a second doublet at 34.4 eV ($4f_{7/2}$ component) accounting for the remaining area. The major component has a binding energy that corresponds directly with that observed in pure 12-silicotungstic acid and is therefore associated with the existence of 'unperturbed' Keggin units on the silica surface. The

minor component, appearing at lower binding energy, may represent the partial decomposition of silicotungstic acid on the silica surface and the formation of an oxide of the type WO_x in which W has an oxidation state lower than VI. Alternatively, it could indicate the existence of "perturbed tungstate environments" in otherwise intact Keggin units. The minor component is consistent with that reported by Hollinger *et al.*[25] for W^{5+}. However, reduced 12-heteropolyacids are highly coloured[26] and the silica-supported acid is white so this would appear unlikely. The more likely cause of the minor component is perturbed environments corresponding to tungsten atoms in terminal W=O bonds that directly coordinate to the silica surface; tungsten atoms in other terminal W=O bonds retain their bulk characteristics. Thus, the minor component corresponds to 'interfacial' Keggin anions; for example, ion pairs of the form $(\equiv SiOH_2)^+(H_3[SiW_{12}O_{40}])^-$ may be present. The latter model is similar to that put forward by Newman *et al.*[22] in their investigation of silica-supported phosphotungstic acid samples at loadings corresponding to less than monolayer coverage (< 44 wt%) and to recent studies of silica-supported 12-silicotungstic acid by Nguyen *et al.*[27] To gain further information on the interaction between 12-silicotungstic acid and the silica support, XPS investigations were carried out on both a low-loaded sample and a sample prepared from a silica with a low silanol content.

Interaction of 12-silicotungstic acid with the silica support at low loadings

The W 4*f* XPS spectrum recorded from a silica supported 12-silicotungstic acid at low loading (3.2 wt %), see Figure 6.9, can also be analysed in terms of the contribution of two spin-orbit doublets. However, the reduction in loading causes significant changes in both the relative contributions of the spin-orbit doublets and

their binding energies. Analysis gives spin-orbit doublets at 36.4 eV and 35.3 eV ($4f_{7/2}$ components) with contributions to the total spectral area of 58% and 42%, respectively. It can be noted that this type of behaviour was not observed for silica-supported 12-phosphotungstic acid, although specific catalytic experiments at low loadings (< 6 wt%) have indicated that the acidic sites are weaker.[7] The latter finding has been attributed to site isolation of individual Keggin units and stronger interaction with the support. This view is supported by the present results which suggest that on initial loading $[SiW_{12}O_{40}]^{4-}$ Keggin anions occupy highly active sites on the silica surface such that the influence of surface interactions on tungsten environments within the isolated individual units is enhanced. With increased loading, the relative contribution of these tightly bound units to the observed XPS spectrum will be reduced, and, as a consequence, will not be easily observed.

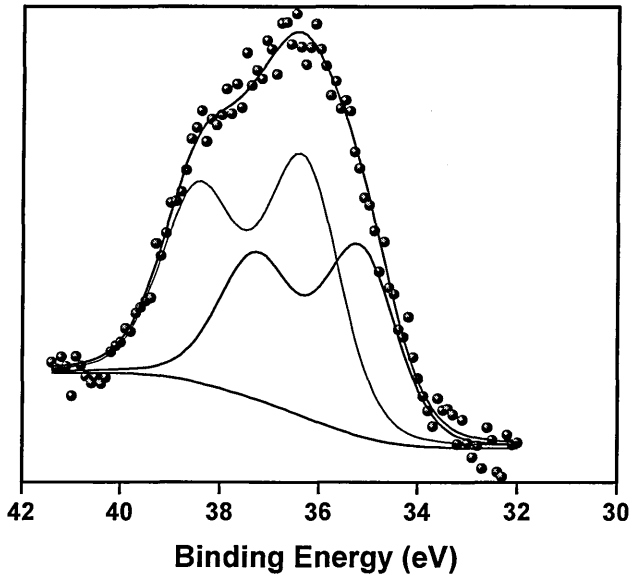

Figure 6.9 W 4*f* XPS spectrum recorded from silica-supported 12-silicotungstic acid with a loading of 3.2 wt %.

Interaction of 12-silicotungstic acid with a silica support containing a reduced number of silanol groups

The W 4*f* spectrum recorded from 12-silicotungstic acid (loading 25.9 wt %) supported on a silica with a low-silanol content is shown in Figure 6.10. This spectrum is very similar to that shown in Figure 6.8 with comparable binding energies and relative spectral areas of the bulk and interfacial species of 76% and 24%, respectively.

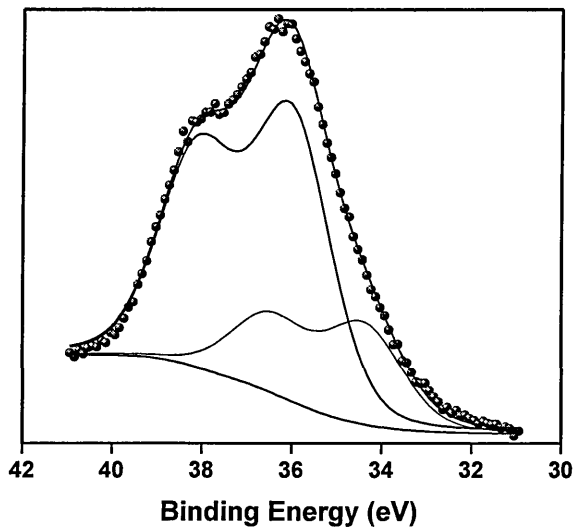

Figure 6.10 W 4*f* XPS spectrum recorded from 12-silicotungstic acid supported on a low-silanol silica support.

The approximate silanol content of the low-silanol silica is 1.5 groups per 100 $Å^2$ compared with 3 groups per 100 $Å^2$ for the silica used in the preparation of the authentic catalyst. Given an individual Keggin unit occupies[28] an average surface area of 144 $Å^2$, then it is clear that in both cases there are sufficient surface -OH groups for interaction. In the case of the authentic unused catalyst, Figure 6.8, the adsorption geometry could involve individual Keggin units binding to silanol groups on the silica surface through three terminal W=O bonds and this would be consistent

with the observed contributions of 80% and 20% of the bulk and interfacial species, respectively, to the overall spectral area. The low-silanol catalyst does not have sufficient silanol groups to satisfy binding of three terminal W=O bonds from an individual Keggin unit to the silica surface in a complete monolayer. However, since the loading of the sample corresponds to roughly 0.6 of a monolayer, it is possible that there can be selective ordering of silanol groups and this would be consistent with the experimental observations.

6.2.6 Summary

The authentic unused catalyst consists of 12-silicotungstic acid supported on silica which has a silanol content of approximately 1.5 groups per 100 $Å^2$. The acid loading is 25.5 wt %. X-ray powder diffraction measurements indicate that the hexahydrate of 12-silicotungstic acid is present in the form of small crystallites (10 nm (±0.5 nm)) dispersed over the silica surface. Depending on conditions, the $H_4[SiW_{12}O_{40}]\cdot 14H_2O$ hydrate can also be present. The most direct evidence for an interaction between the 12-silicotungstic acid and the silica-support is provided by XPS. This technique suggests that interfacial species are present in which intact, individual Keggin anions interact with the silica surface via terminal W=O bonds. The strongest interactions are observed at low loadings. For the samples used in the present work, ^{29}Si MAS NMR spectroscopy was not able to detect the presence of these interfacial species although the chemical shift differences between the bulk and interfacial species would be expected to be small and subject to averaging by motional effects. In addition, sample preparation may have an influence.

6.3 Used industrial catalysts

As already indicated the useful lifetime of the industrial catalyst in the reactor depends on the level of by-products (primarily methyl ethyl ketone) produced; above certain levels of by-products the process is no longer commercially viable. Once pre-designated limits are reached the reactor is decommissioned and a new catalyst is introduced. An understanding of the ageing of a catalyst, and whether or not it can be regenerated, is of both scientific and commercial interest.

Coke is deposited on the catalyst[4] during its time in the reactor. Coking is also observed in acid-catalysed organic conversions where silica-supported 12-phosphotungstic acid is the catalyst involved[14] and has been found to cause deactivation of the catalyst.[14] This, as will be shown, would appear to be the main reason for the deactivation of the silica-supported 12-silicotungstic acid catalyst used in the AVADA process by BP Chemicals.

To gain more information about the behaviour of industrial catalysts, two used catalysts with different histories have been investigated; these are designated as JM2 and JM3 by BP Chemicals. JM2 was decommissioned after a thermal event led to a significant reduction in the activity of the catalyst. JM3 was decommissioned after 1.5 years in the reactor and had an uneventful lifetime. Comparisons will be made with the results for the authentic unused catalyst described in Section 6.2.

6.3.1 JM3

Simultaneous TGA and DTA data recorded for JM3 are shown in Figure 6.11. In comparison to that for the silica-supported 12-silicotungstic acid (Figure 6.1 (A)) the data are less well-defined. Weight loss in the region of 100°C to 230°C is suggestive of the presence of the hexahydrate and the characteristic exothermic phase change, between 500-590°C, for the silica support is present in the DTA data. Overall, the thermal analysis data suggest that 12-silicotungstic acid is still present in the used catalyst. This suggestion is confirmed by XRD, ^{29}Si MAS NMR spectroscopy, FT-IR and XPS as briefly described below.

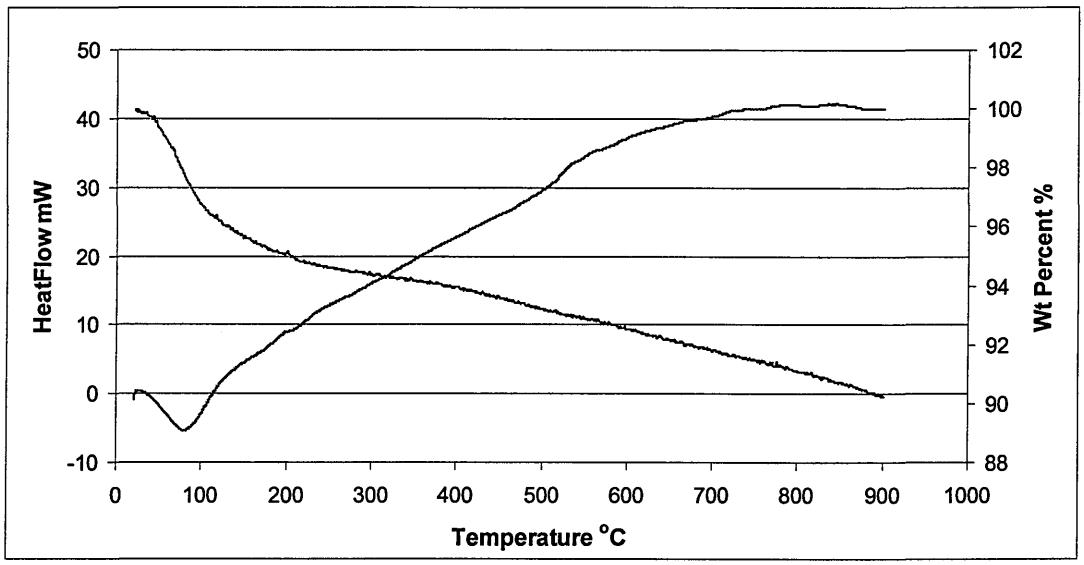

Figure 6.11 Thermal analysis of JM3 (approximately 20 mg) recorded under a flow of dry nitrogen (50 ml min^{-1}) with a ramp rate of 20°C min^{-1}.

The X-ray powder diffraction pattern recorded for JM3 is shown in Figure 6.12 and shows broad peaks occurring at $2\theta = 26.0°$, 27.8 °, 35.7° and 46.7°. These peaks can be reasonably compared with the more intense diffraction peaks recorded from

unsupported $H_4[SiW_{12}O_{40}]\cdot 14H_2O$; 2θ = 26.4°, 28.4°, 35.9° and 47.2° as can be seen from Figure 6.12 (B).

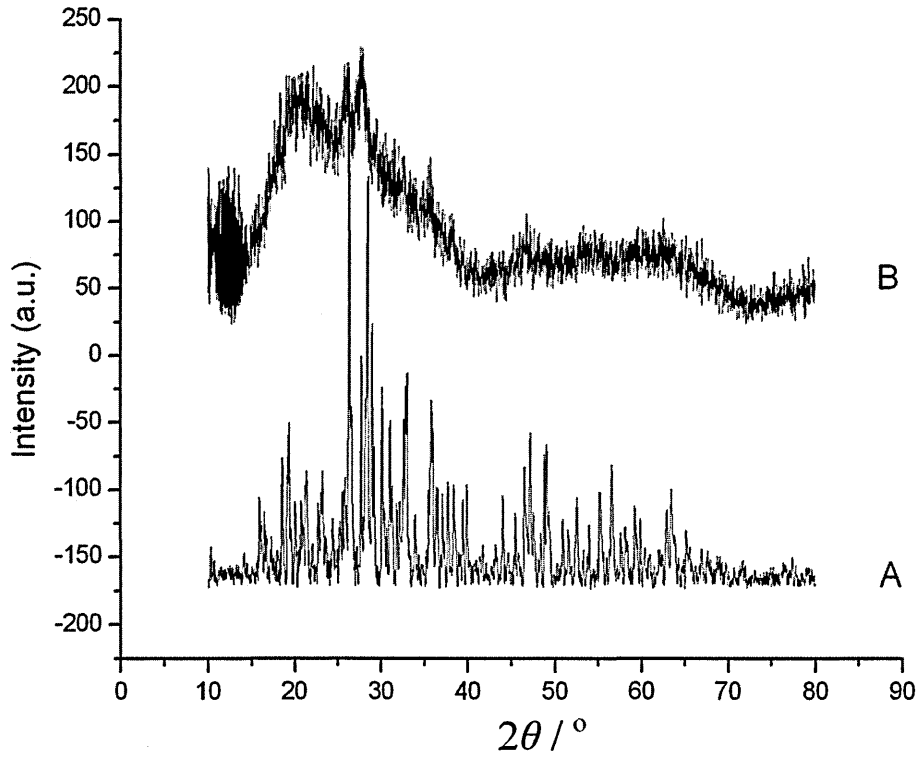

Figure 6.12 XRD patterns recorded from A) $H_4[SiW_{12}O_{40}]\cdot 14H_2O$ and B) the used catalyst JM3 over the 2θ range 10° - 80° (step size = 0.01°, step time = 8 s).

The presence of 12-silicotungstic acid is further highlighted by heating JM3 at 120°C for 5 hours. The resulting XRD powder pattern is shown in Figure 6.13 (B) and unequivocally indicates the presence of crystalline $H_4[SiW_{12}O_{40}]\cdot 6H_2O$ as can be seen by comparison with Figure 6.13 (A). The initial presence of the $H_4[SiW_{12}O_{40}]\cdot 14H_2O$ hydrate may reflect the manner in which JM3 has been stored before its study in this work.

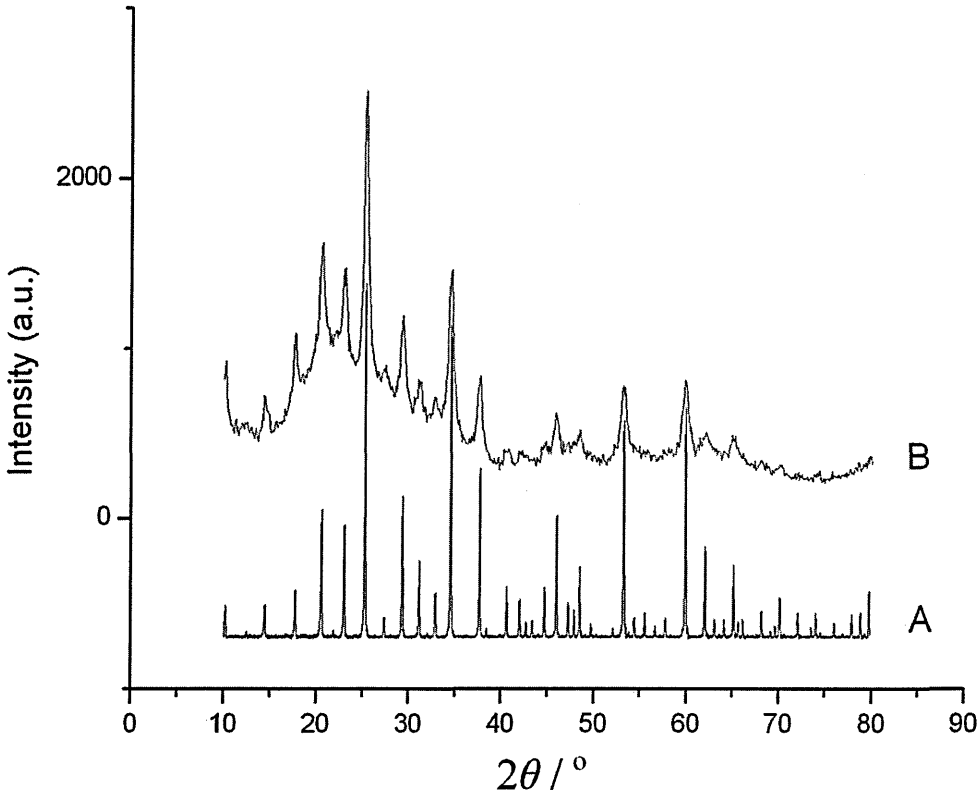

Figure 6.13 XRD patterns recorded for A) $H_4[SiW_{12}O_{40}]\cdot 6H_2O$ and B) JM3 after heating at 120°C for 5 hours over the 2θ range 10° - 80° (step size = 0.01°, step time = 8 s).

It can also be noted that the powder diffraction pattern recorded from JM3 after heating resembles that recorded from silica-supported 12-silicotungstic acid, Figure 6.2(B). This suggests heating the hydrated JM3 for 5 hours at 120°C leads to the formation of well-formed crystallites on the silica surface.

The ^{29}Si MAS NMR spectrum recorded from JM3 is shown in Figure 6.14. As expected, a ^{29}Si MAS NMR resonance, $\delta(^{29}Si)$ = -84.5, is observed consistent with the presence of $H_4[SiW_{12}O_{40}]\cdot xH_2O$ with $x \geq 6$.

Figure 6.14 The ^{29}Si MAS NMR spectrum recorded from JM3.

The FT-IR spectrum recorded from JM3 was very similar to that recorded for silica-supported 12-silicotungstic acid, Figure 6.6. Absorptions characteristic of both 12-silicotungstic acid and the silica support were observed.

The XPS data recorded from JM3 is shown in Figure 6.15.

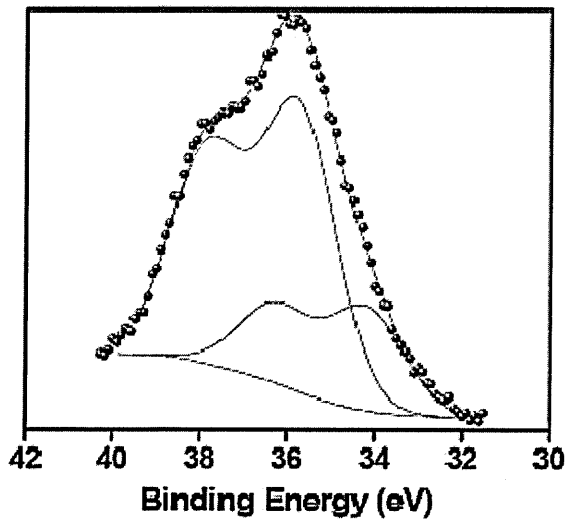

Figure 6.15 W 4*f* spectrum recorded from the catalyst JM3.

The W 4*f* spectrum is directly comparable to that recorded from the silica-supported 12-silicotungstic acid, Figure 6.8. This indicates that interfacial species in which individual Keggin anions interact with the silica surface via terminal W=O bonds are still present, despite the considerable lifetime of the catalyst in the reactor.

Overall, on the basis of the results of the various characterisation techniques it is clear that 12-silicotungstic acid in a hydrated form is still present in JM3. Furthermore, within the limits of detection of these techniques, there is no evidence for decomposition of the 12-silicotungstic acid. The reasons for the deactivation of the catalyst are thus not revealed by this type of structural characterisation. Although the evidence is limited, this suggests that the process may be due to another type of factor. It would seem likely that this could be due to coking blocking the physical access of reactants to 12-silicotungstic acid.

6.3.2 JM2

Simultaneous TGA and DTA data recorded from JM2 are shown in Figure 6.16. The data are comparable to that obtained from JM3 (Figure 6.11) up to a temperature of 300°C.

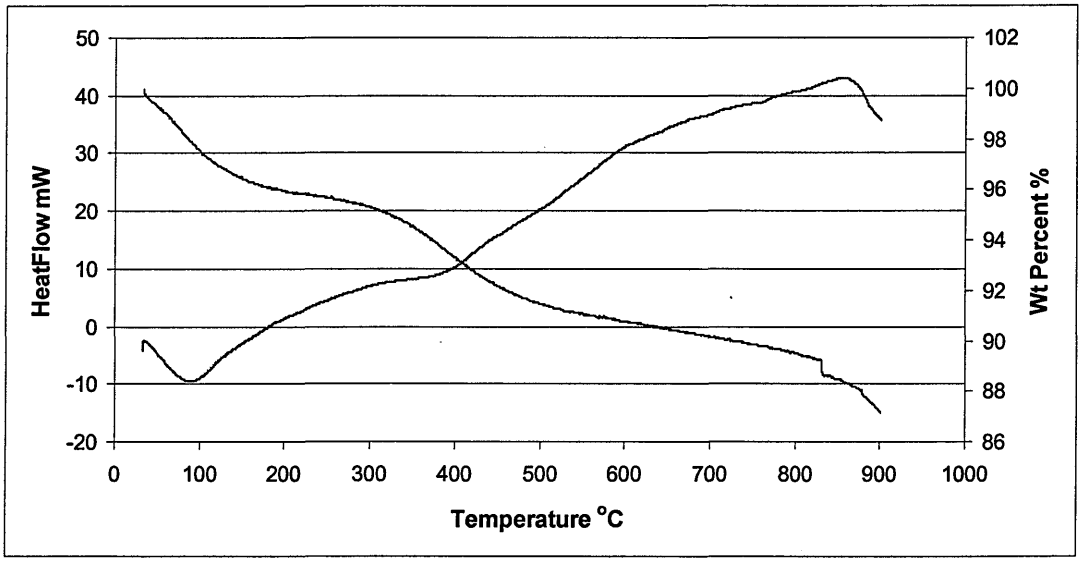

Figure 6.16 Thermal analysis recorded for JM2 (approximately 30 mg) under a flow of dry nitrogen (50 ml min^{-1}) with a ramp rate of 20°C min^{-1}.

Between 300-550°C there is a distinct weight loss corresponding to approximately 5% of the total weight of the catalyst. This weight loss is characterised by a broad, but weak, exothermic phase transition centred at approximately 425°C in the DTA data. The behaviour can be attributed to the presence of a small amount of oxygen in the flowing nitrogen gas reacting with carbon present on the catalyst,[4] in the form of coke, and forming gaseous carbon dioxide. The presence of significant amounts of coke on this catalyst is not unexpected since it experienced a strong thermal event in the industrial reactor.

The XRD powder pattern recorded from JM2 is show in Figure 6.17.

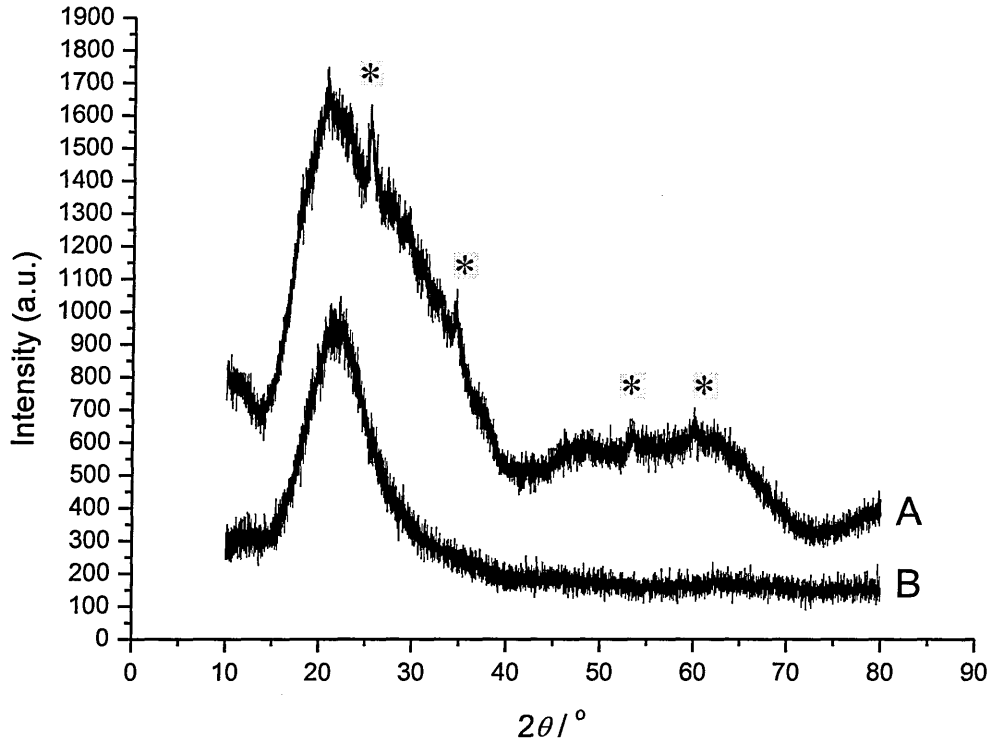

Figure 6.17 The XRD pattern recorded over the 2θ range of 10° - 80° for A) JM2 and B) silica (step size = 0.01°, step time = 8 s).

A shoulder, centred at approximately 2θ = 30 ° is observed, on the characteristic amorphous peak of silica and weak diffraction peaks at approximately 2θ = 25°, 35°, 53° and 60° (*) are also observed. The latter compare well with the most intense diffraction peaks observed in the diffraction pattern recorded for $H_4[SiW_{12}O_{40}]\cdot 6H_2O$. This result suggests that crystallites of $H_4[SiW_{12}O_{40}]\cdot 6H_2O$ remain intact on the silica-support after the thermal event has taken place that contributes to the deactivation of the catalyst. The origin of the shoulder at $2\theta \approx 30°$ is not clear.

The ^{29}Si MAS NMR spectrum recorded from JM2 showed only the presence of the silica support. This may reflect a reduction in the amount of 12-silicotungstic acid

that is present or a significant reduction in intensity associated with NMR saturation effects in the experiment. This was not pursued further.

Absorptions characteristic of both 12-silicotungstic acid and the silica support were observed in the FT-IR spectrum recorded from JM2. The spectrum was similar in nature to those recorded for both JM3 and silica-supported 12-silicotungstic acid, Figure 6.6. XPS data recorded from JM2 are shown in Figure 6.18. The W 4*f* spectrum is consistent with the presence of 12-silicotungstic acid, including an interfacial form. There is a slight, but not significant, increase in the component appearing at higher binding energy (82 % of the total spectral area).

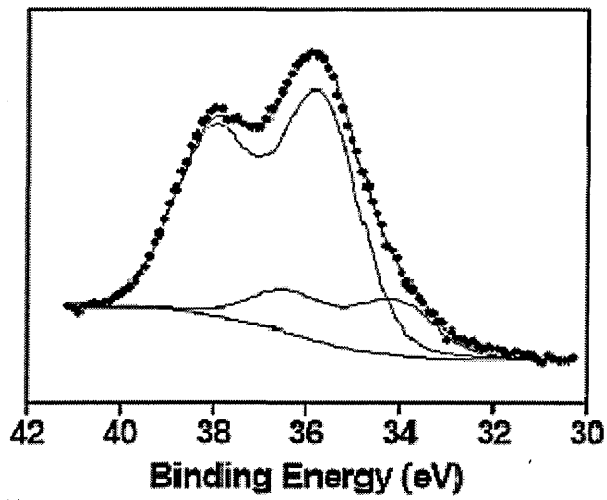

Figure 6.18 W 4*f* spectrum recorded from the used catalyst JM2.

Overall, the thermal analysis, XRD, FT-IR and XPS data provide evidence that hydrated 12-silicotungstic acid is also present in JM2 even though it suffered a major thermal event in the reactor. There is also evidence of significant coking. Although it is difficult to quantify, it may also be the case that the percentage by weight of the hydrated 12-silicotungstic acid in the catalyst has been reduced.

6.3.3 Coking of JM3 and JM2

Evidence supplied by BP Chemicals[4] (Section 6.1) indicated that as levels of carbon or 'coke' deposited on the industrial, silica-supported, 12-silicotungstic acid catalyst increase, then the levels of tungsten that are amenable to extraction from the used catalyst by aqueous methods decreases. In terms of the used catalysts JM2 and JM3, it has been established in the previous two sections, that hydrated 12-silicotungstic acid is still present in these catalysts. Both of these catalysts may presumed to be 'coked'; in particular, JM2 which suffered a major thermal event when in the reactor shows direct evidence of significant coking (Section 6.3.2.). It can be inferred, therefore, that the 'insoluble tungsten' in these catalysts is probably associated with 12-silicotungstic acid (the solubility of which has been restricted by coke deposition in the pores of the silica support). It is thus of direct interest to characterise the coking of these used catalysts in more detail. The approach taken in the work of Kozhevnikov *et al.*[14] can be used for this purpose. These authors found that increasing levels of carbon or coke formation caused deactivation in silica supported 12-phosphotungstic acid in studies of the oligomerisation of propene.[14] Thermal analysis, carried out under flowing air, showed the presence of two exothermic phase changes with peak maxima at approximately 320 and 500°C. The exothermic phase change, occurring at approximately 320°C, was associated with oxidation of high boiling point hydrocarbons or "soft" coke and was found to have a broad TGA removal range of between 170 and 370°C. The exothermic phase change centred at approximately 500°C was associated with the oxidation of polynuclear aromatics or "hard" coke and was found to have a TGA removal range of between 370 and 570°C.

JM3 coking

The thermal analysis of this catalyst was repeated in flowing air instead of flowing nitrogen and the results are shown in Figure 6.19.

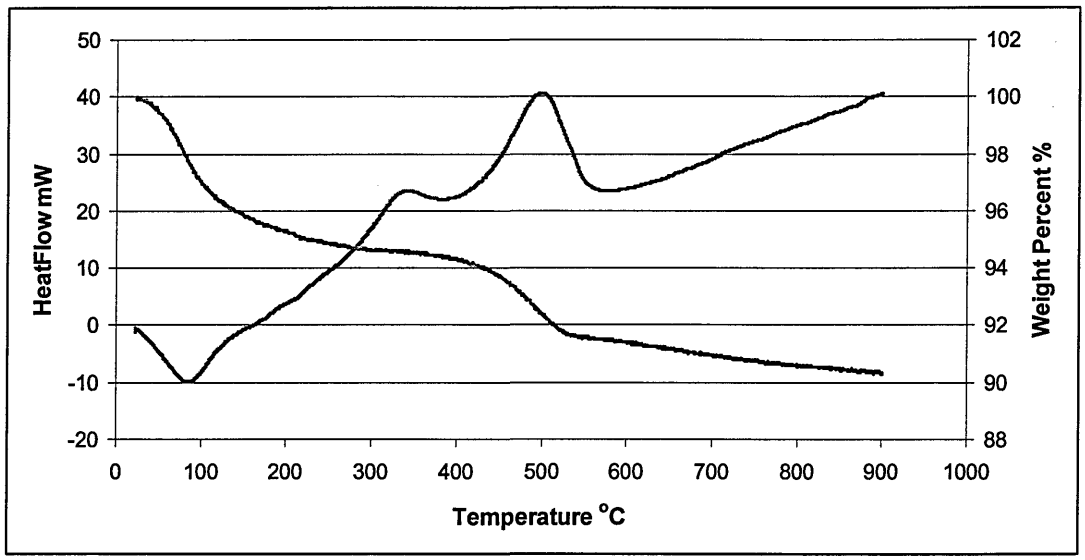

Figure 6.19 Thermal analysis of the catalyst JM3 (approximately 30 mg) recorded under a flow of dry air (50 ml min^{-1}) with a ramp rate of 20°C min^{-1}.

The DTA show an endothermic phase change characteristic of the loss of water, between 25 - 130°C, followed by two broad, exothermic changes with peak maxima at approximately 320 and 500°C. These changes can be compared with those observed by Kozhevnikov *et al.*[14] for a coked silica-supported 12-phosphotungstic acid catalyst under similar experimental conditions and can be assigned to the oxidation of soft and hard coke, respectively.

The TGA data is similar to that observed in flowing nitrogen to approximately 400°C (see Figure 6.11). However, between 400 and 525°C a weight loss of approximately 3% is observed. Since the weight loss observed for the exothermic

event corresponding to the removal of soft coke is too small to detect, this suggests that the majority of coke deposited on the used catalyst during its lifetime is hard in nature. It can be noted Jeong *et al.*[29] have made similar observations in investigating the deactivation of a caesium-containing 12-heteropolyacid, $Cs_{2.5}H_{0.5}PW_{12}O_{40}$ in the catalytic isomerisation reaction of *endo*-tetrahydrodicylcopentadiene (*endo*-THDCPD) on a laboratory scale.

JM2 coking

Results of the thermal analysis in flowing air for this catalyst are shown in Figure 6.20.

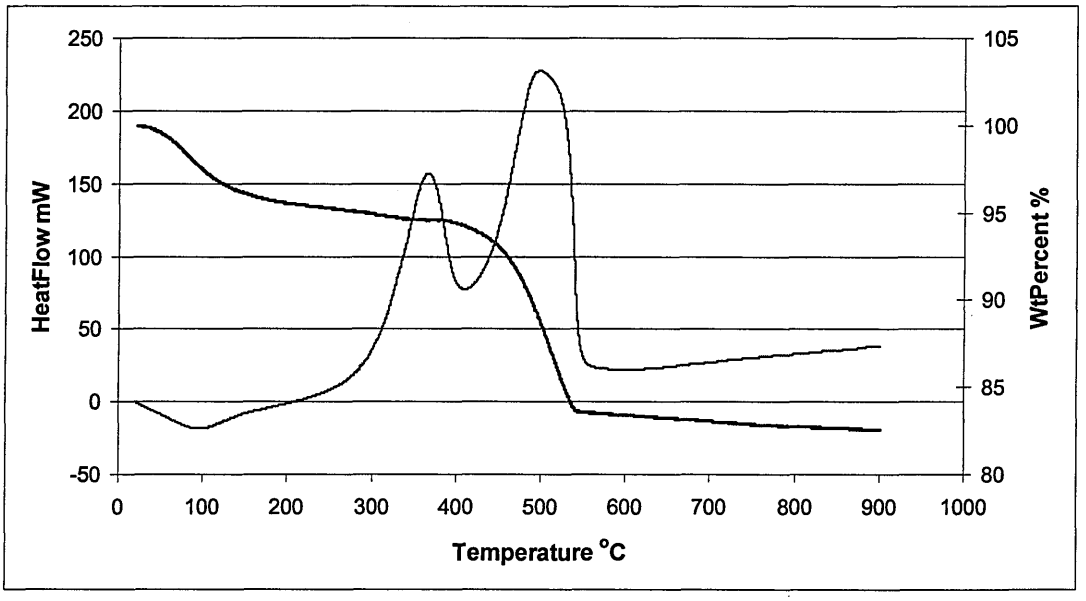

Figure 6.20 Thermal analysis of the catalyst JM2 (approximately 30 mg) recorded under a flow of dry air (50 ml min^{-1}) with a ramp rate of 20°C min^{-1}.

One endothermic and two exothermic phase changes occur between approximately 25-140, 280-400 and 400-560°C, respectively. The endothermic event is consistent with the loss of water molecules whereas the two exothermic events correspond to

the decomposition of soft and hard coke, respectively.[14] Overall, the DTA curve is comparable to that recorded for JM3 heated in flowing air (Figure 6.19); however, the exothermic events are more intense. The TGA data are similar to those recorded in flowing nitrogen up to approximately 350°C (see Figure 6.16). The weight loss occurring between 400-540°C corresponds to 11.5% of the total catalyst. It can be concluded that JM2 contains a significant amount of hard coke.

Summary

The thermal analysis data recorded for JM2 and JM3 show that the nature of the coke deposited to be similar on each catalyst. This suggests the history of the catalyst has little effect on the nature of the coke deposited. However, the amount of hard coke deposited is significantly different between JM2 and JM3. For JM3, which had an uneventful lifetime in the reactor, approximately 3% of the total weight loss is related to hard coke. For JM2, which experienced a thermal event during its lifetime, approximately 11.5% of the total weight loss was found to be hard coke. It is reasonable to conclude that the deactivation of both JM2 and JM3 is associated with coking involving both hard and soft coke. This being the case, both of the used catalysts contain hydrated 12-silicotungstic acid, with restricted solubility, which accounts for the 'insoluble tungsten'.

6.4 Decoking of used industrial catalysts

The removal of both soft and hard coke without causing the decomposition of any of the 12-silicotungstic acid that is present is relevant to industrial interest in terms of regenerating a used catalyst. Furthermore, if the regeneration of the catalyst is not

possible decoking of the catalyst is still of interest as a method of reclaiming any remaining 12-silicotungstic acid from the decommissioned catalyst.

Kozhevnikov *et al.*[14] have considered methods for decoking catalysts. One approach is preventative in that palladium is used as an inhibitor of hard coke formation. Another involves heating of the coked catalyst in a flow of 6 % ozone in oxygen to specifically remove hard coke. Neither of these approaches is practical in an industrial context. In the present work two approaches are considered :

- the removal of soft coke using a Soxhlet extraction method with dichloromethane as solvent. This method has been used previously by Kozhevnikov *et al.*,[14] and
- the removal of hard coke by direct heating in air.

6.4.1 Soft coke

JM3

The Soxhlet extraction of JM3 with dichloromethane resulted in an initial dark green solution similar in colour to the solid catalyst. Extraction was continued until the dichloromethane solution was colourless on the assumption that no further removal of soft coke was possible.

^{1}H NMR data (see Appendix B, Table B.1) recorded from the extracted soft coke indicated the presence of various carbon-hydrogen and carbon-oxygen groups belonging to several different chemical species. However, due to the complexity of the spectrum detailed assignments were not attempted. The ^{13}C NMR data (see Appendix B, Table B.2) recorded from the same sample revealed eleven distinct

resonances, again consistent with the presence of different chemical species. It is useful to note that studies carried out by Kozhevnikov *et al.* on a similarly coked catalyst found the soft coke to consist of high boiling point hydrocarbons.[14]

Thermal analysis of JM3 after extraction with dichloromethane is shown in Figure 6.21. The data compares with that prior to extraction (see Figure 6.19) except that the ratio of the soft coke; hard coke exothermic peak areas has reduced; as to be expected.

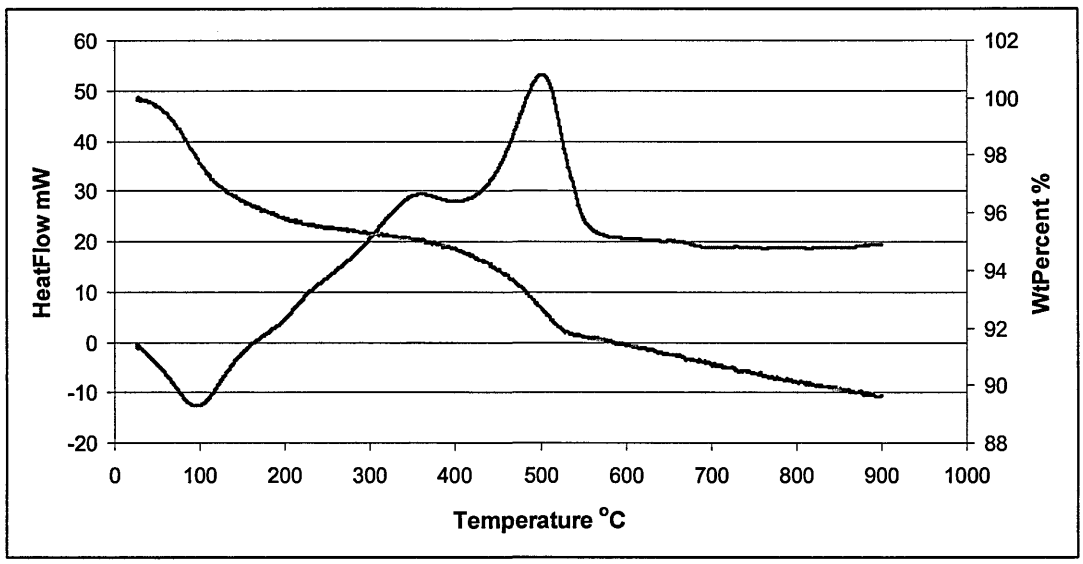

Figure 6.21 Thermal analysis of JM3 after extraction with dichloromethane recorded under a flow of dry air (50 ml min^{-1}) with a ramp rate of 20°C min^{-1}.

The FT-IR spectrum recorded from the catalyst JM3 following extraction with both dichloromethane and ultra high purity water, Figure 6.22 (B), shows only the most intense of the absorptions characteristic of 12-silicotungstic acid (929 cm^{-1}) (see Section 5.5) as a shoulder on the silica absorption at 975 cm^{-1}. The characteristic 12-silicotungstic acid absorption is, however, reduced in intensity in comparison to

that observed if the extraction of JM3 is carried out using only ultra-high purity water, Figure 6.22 (A). This result provides evidence that the presence of soft coke on the catalyst restricts the dissolution of the supported acid. Images recorded from the silica-supported 12-silicotungstic acid, JM3 and JM2 using scanning electron microscopy (see Appendix C) did not provide any further information relating to the manner in which soft coke prevents the 12-silicotungstic acid from entering the aqueous phase. However, removal of some of this soft coke by dissolution in dichloromethane was found to 'expose' the 12-silicotungstic acid so that it could then be extracted by aqueous methods.

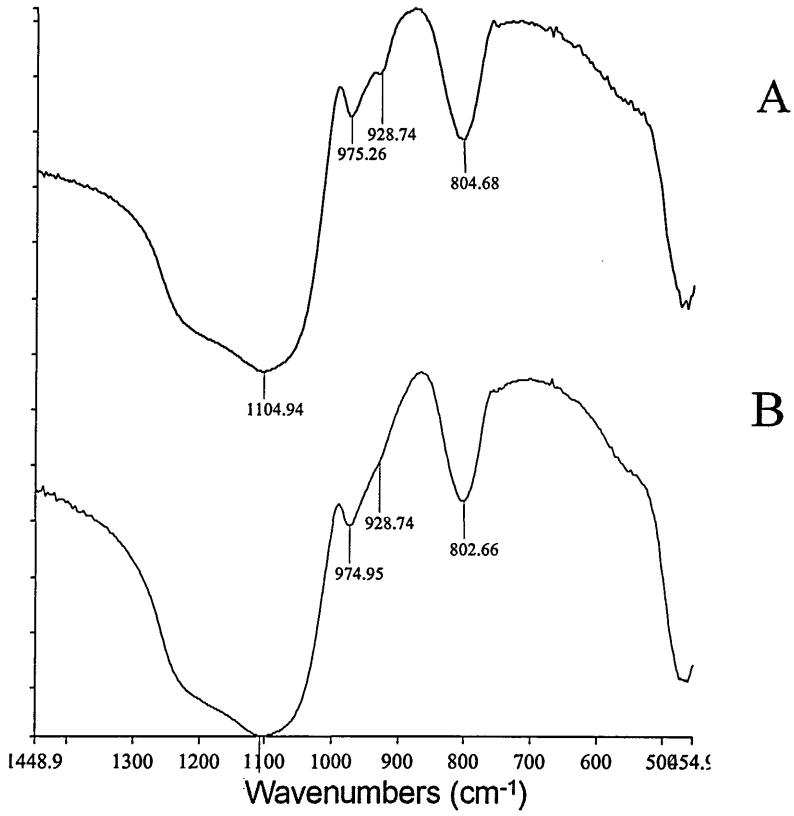

Figure 6.22 FT-IR spectra recorded from JM3 after A) extraction with ultra high purity water and B) extraction with dichloromethane followed by washing with ultra high purity water.

JM2

Thermal analysis data recorded from the residue of JM2 after Soxhlet extraction with dichloromethane is shown in Figure 6.23. The exothermic peak associated with the presence of soft coke, between 280-400°C, is clearly reduced in intensity when compared with that observed prior to extraction with dichloromethane (See Figure 6.20). This reduction is consistent with the study by Kozhevnikov *et al.*[14] in which dichloromethane led to the removal of 22% of the soft coke present on a silica-supported 12-phosphotungstic acid.

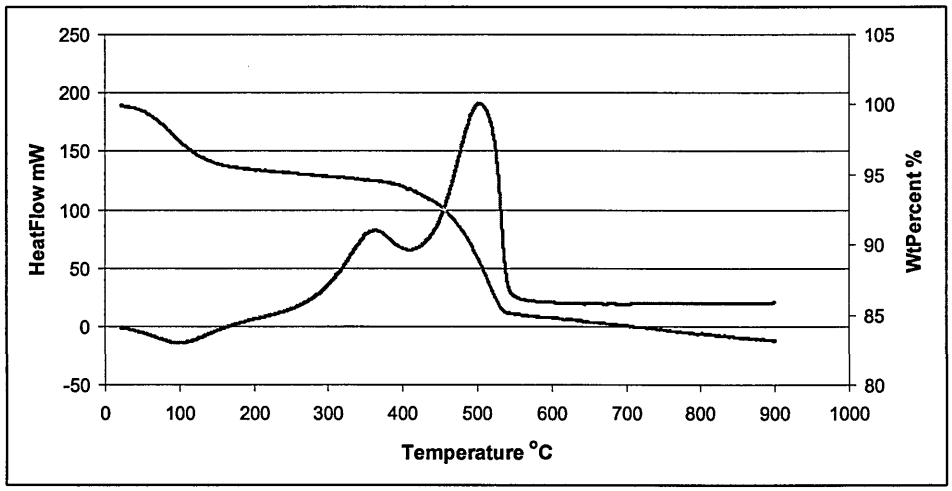

Figure 6.23 Thermal analysis of JM2 (approximately 30 mg) after extraction with dichloromethane recorded under a flow of dry air (50 ml min^{-1}) with a ramp rate of 20°C min^{-1}.

The FT-IR spectra recorded for JM2 after extraction with ultra high purity water and after extraction with both dichloromethane and ultra high purity water are shown in Figure 6.24.

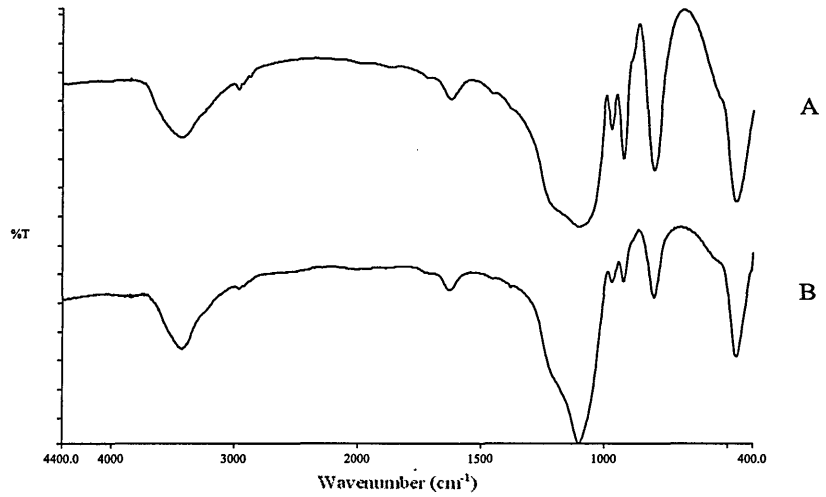

Figure 6.24 FT-IR spectra recorded from JM2 after A) extraction with ultra high purity water and B) extraction with dichloromethane followed by extraction with ultra high purity water.

The same general trends as already discussed for JM3 are observed; that is a reduction in intensity of the absorptions associated with 12-silicotungstic acid following extraction with dichloromethane followed by washing with ultra-high purity water. However, in both FT-IR spectra the absorptions characteristic of 12-silicotungstic acid are far more prominent. This suggests that the increased levels of hard coke present in JM2 play a role in restricting the solubility of the 12-silicotungstic acid within the pores of the silica support.

6.4.2 Hard coke

When supported on silica the decomposition temperature of 12-phosphotungstic acid has been shown[7] to decrease by up to 40°C. The exothermic peak associated with the decomposition of bulk 12-silicotungstic acid occurs between 530 and 550°C (Chapter 5, Section 5.2, Figure 5.1) depending on the heating rate. This would

suggest heating silica-supported 12-silicotungstic acid at a temperature lower than 490°C, to remove the hard coke present, would avoid causing the decomposition of the acid. Hard coke is known to oxidise to volatile compounds when heated in the temperature range 370-550°C,[14] therefore a temperature of 400°C was chosen to remove hard coke from the catalysts JM3 and JM2 by heating in air.

JM3

JM3 was heated for intervals between 4 and 48 hours at 400°C in air and the XRD pattern recorded for each sample is shown in Figure 6.25.

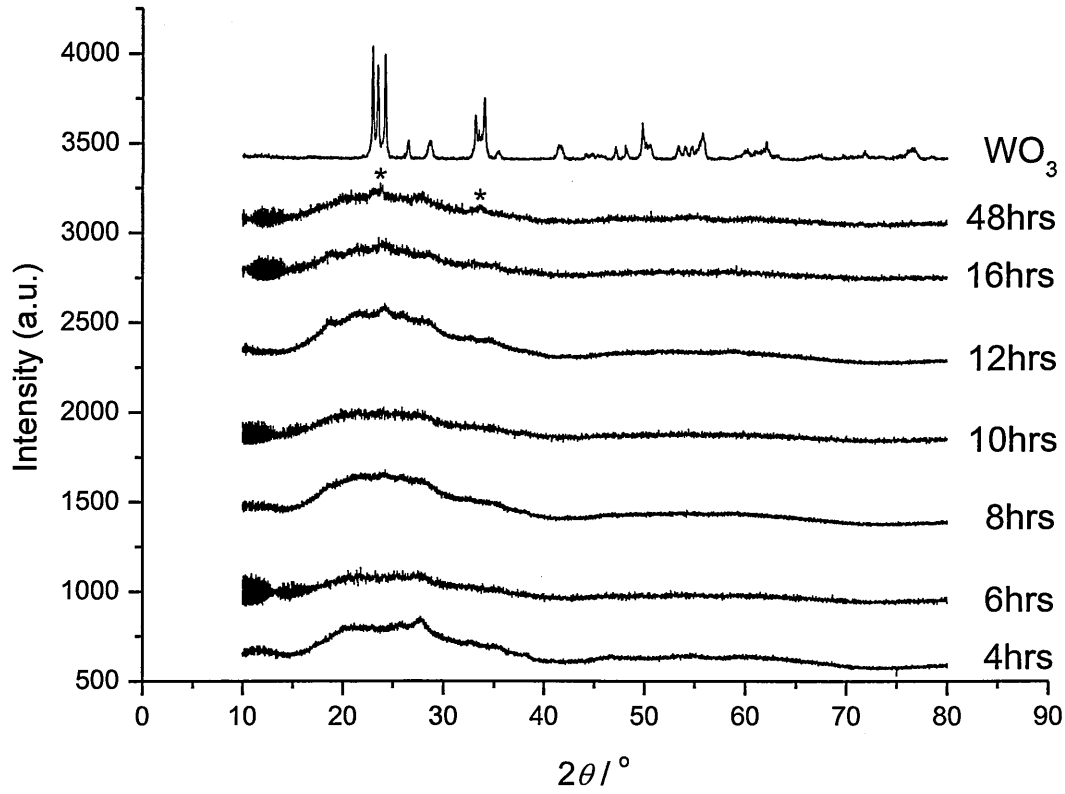

Figure 6.25 The XRD patterns recorded over the 2θ range of 10° - 80° for JM3 after heating at 400°C between 4 and 48 hours (step size = 0.01°, step time = 8 s).

Diffraction patterns, although not well defined, are consistent with the presence of $H_4[SiW_{12}O_{40}]\cdot 14H_2O$, Figure 6.4, and anhydrous $H_4[SiW_{12}O_{40}]$, Figure 6.3, on the silica support are observed after 4 and 8 hours, respectively. The anhydrous acid still remains present after heating for 16 hours at 400°C. After 48 hours of heating, characteristic peaks of the decomposition product WO_3(*) are observed. The appearance of WO_3 is surprising and indicates that some decomposition of supported 12-silicotungstic acid can occur after prolonged heating at the relatively low temperature of 400°C (compared to a temperature of 530°C for the unsupported acid).

FT-IR spectra recorded for JM3 after heating to 400°C in air show characteristic absorptions associated with 12-silicotungstic acid and the silica support. There is no evidence of absorptions characteristic of WO_3 in the spectrum recorded after 48 hours. However, the 937(b) and 812(b) cm^{-1} absorptions of WO_3 occur in the same region as those of 12-silicotungstic acid and the silica support. It is possible, therefore, that any weak absorptions are obscured.

Thermal analysis experiments revealed that significant removal of coke can be achieved in several hours when the catalyst JM3 is heated in air at 400°C. Particular examples corresponding to heating for 4 and 6 hours, respectively are shown in Figures 6.26 and 6.27.

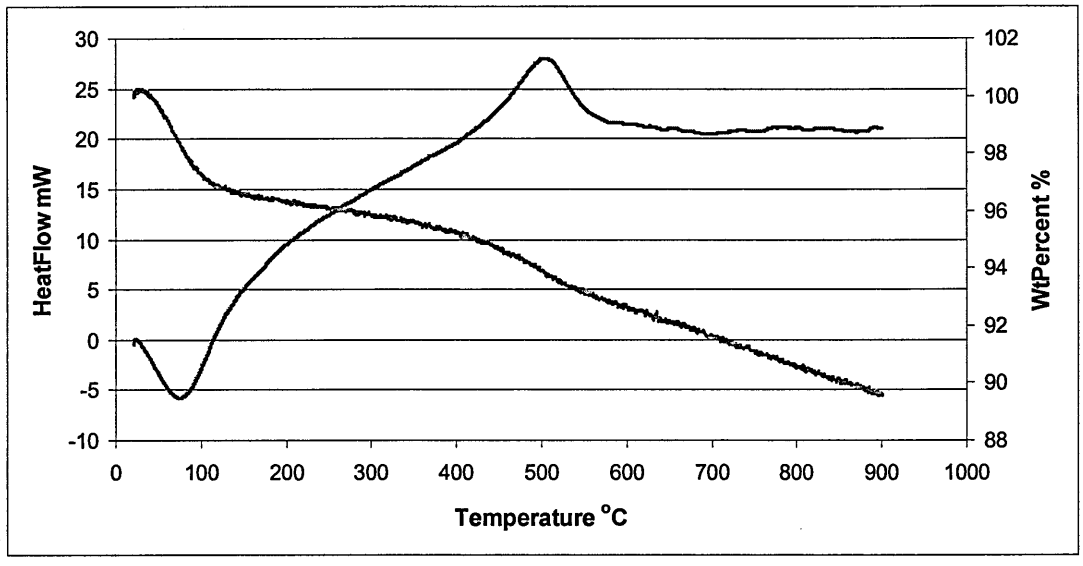

Figure 6.26 Thermal analysis of JM3 (approximately 30 mg) after heating at 400°C in air for 4 hours recorded under a flow of dry air (50 ml min^{-1}) with a ramp rate of 20°C min^{-1}.

An exothermic transition, characteristic of hard coke, with a peak maximum of 505°C is observed in Figure 6.26, although there is no evidence of the presence of a transition corresponding to the oxidation of soft coke which would be expected to occur in the temperature region 275-375°C. It must be concluded that heating in air for the relatively short period of 4 hours removes the soft coke completely. It can also be noted that the exothermic transition of the hard coke is reduced in area suggesting that some of the hard coke constituents have also been removed. Heating for 6 hours in flowing air, as shown in Figure 6.27, results in removal of a significant proportion of the hard coke present.

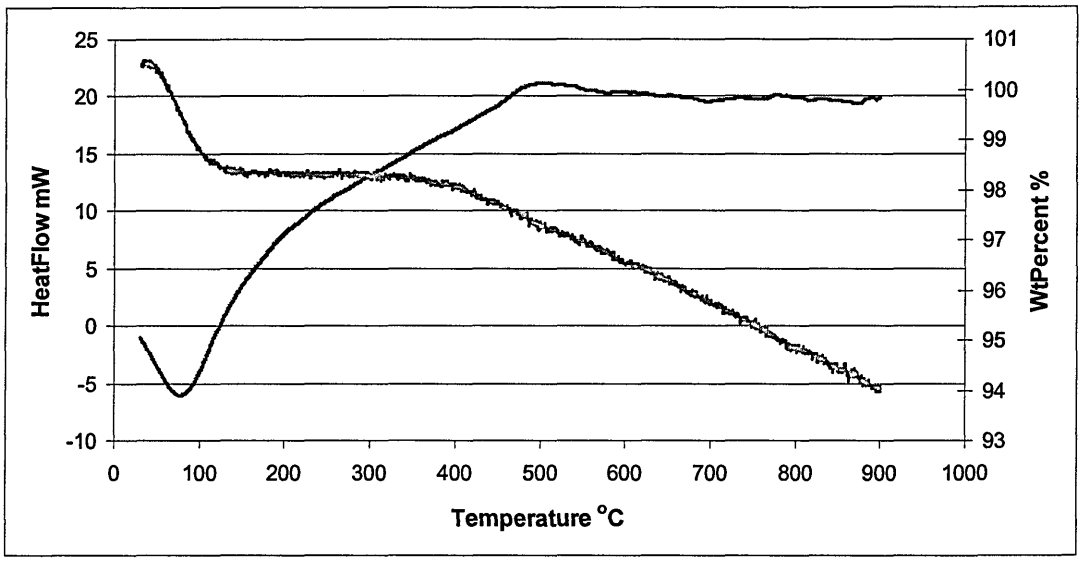

Figure 6.27 Thermal analysis recorded, under a flow of dry air (50 ml min^{-1}) with a ramp rate of 20°C min^{-1}, for JM3 (approximately 30 mg) after heating at 400°C in air for 6 hours.

The residues remaining after JM3 was heated in air at 400°C for different time intervals were characterised as follows. Firstly the residues were thoroughly washed with ultra-high purity water and then subjected to FT-IR and XRD examination. Neither the FT-IR spectra, or the XRD patterns, provided evidence of the presence of 12-silicotungstic acid for any of the residues. However, it is possible that the residues corresponding to relatively short periods of heating contain the acid but in quantities that could not be detected by the techniques used. The XRD data also shows the presence of WO_3 for the sample heated for 48 hours. This is consistent with the fact that this oxide would not be expected to be removed by aqueous extraction. As found previously, it was not possible to detect WO_3 in the FT-IR spectra due to the dominance of absorptions associated with the silica support.

Overall, the results for JM3 indicate that soft coke and a significant amount of hard coke can be removed by heating in air at 400°C for a period in the order of 6 hours. This process then allows 12-silicotungstic acid, with restricted solubility, to be recovered by aqueous extraction. However, it appears that if the heating period is extended then decomposition of the 12-silicotungstic acid may occur. More detailed investigations using more sensitive analytical techniques would be required to refine the outlined results. It should be noted that the results are relevant to an industrially-used catalyst that has had an uneventful lifetime in the reactor.

JM2

Thermal analysis data recorded for JM2 after heating at the optimum conditions found for JM3 (6 hours at 400°C in air) are shown in Figure 6.28. The behaviour is comparable to that observed for JM3 in that it is clear that the soft coke has been removed and that there is a significant reduction in the amount of hard coke present.

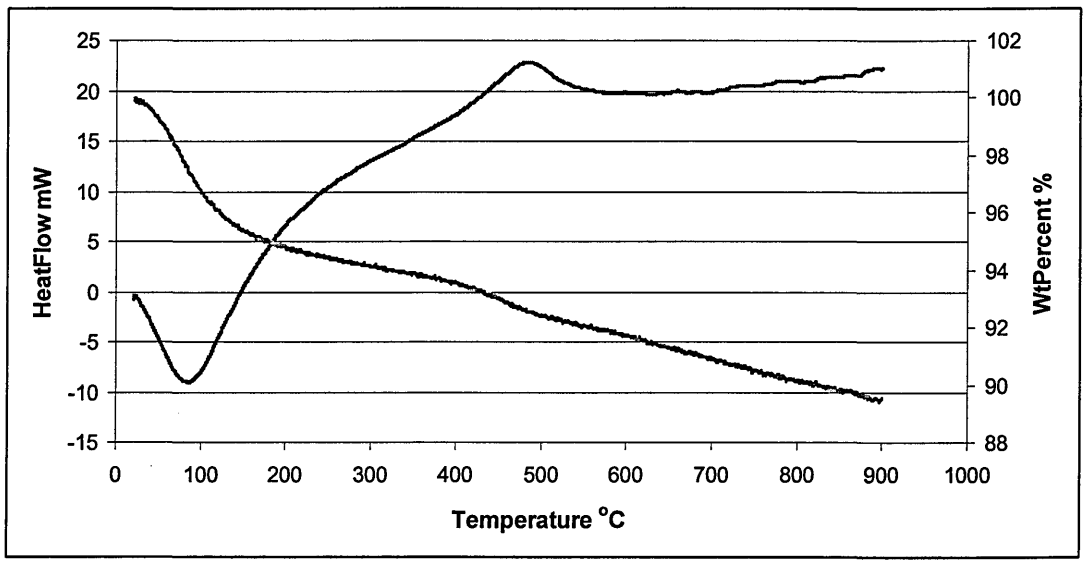

Figure 6.28 Thermal analysis of JM2 (approximately 30 mg) after heating at 400°C in air for 6 hours recorded under a flow of dry air (50 ml min^{-1}) with a ramp rate of 20°C min^{-1}.

Samples of JM2 heated at 400°C in air over periods of between 6-167 hours were characterised by XRD and FT-IR spectroscopy. The XRD patterns are shown in Figure 6.29. For all of the samples there is no evidence in the patterns for the presence of 12-silicotungstic acid. However, the formation of the decomposition product WO_3 is observed after only 6 hours of heating. It may also be the case that this decomposition product was present in the original sample, but in an amount not detectable by XRD.

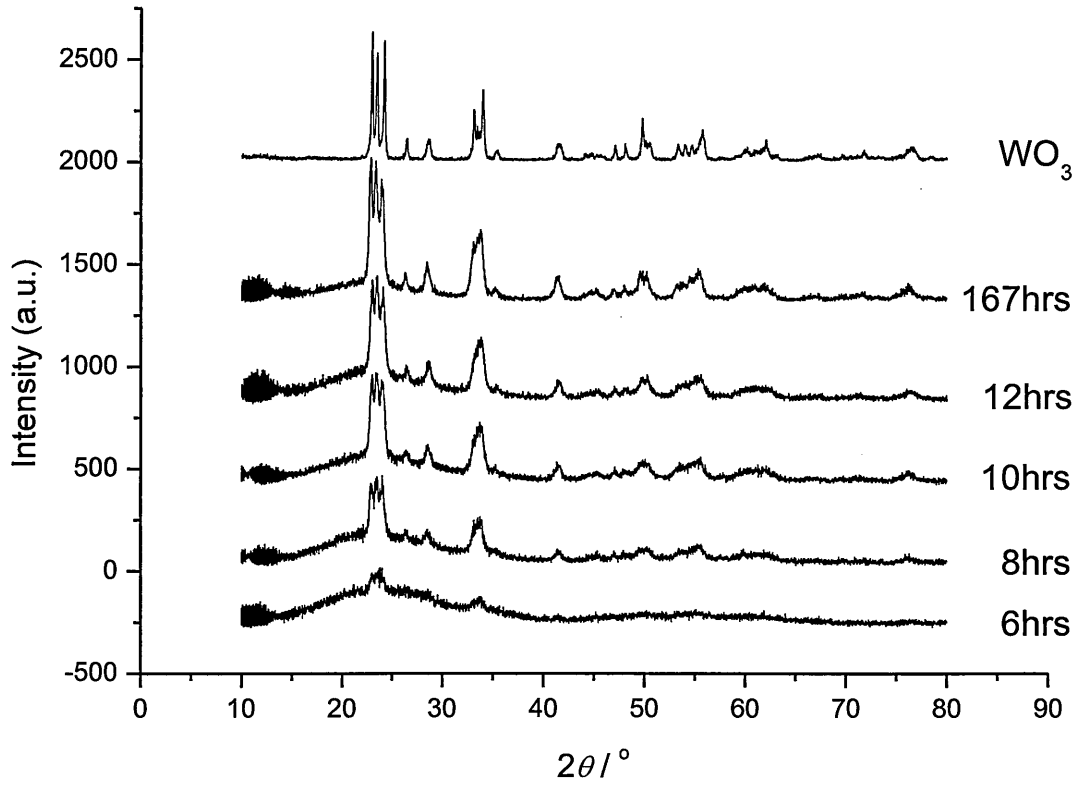

Figure 6.29 The XRD patterns recorded over the 2θ range 10° - 80° for JM2 after heating at 400°C for periods between 6 and 167 hours (step size = 0.01°, step time = 8 s).

In contrast to the data observed in the XRD patterns weak absorptions characteristic of 12-silicotungstic acid are observed in the FT-IR spectra after heating for between

6 - 12 hours. However, after heating for 8 hours the formation of a new absorption, characteristic of WO_3, on the shoulder of the characteristic silica peak at 805 cm^{-1} is observed. After heating for 167 hours, the absorptions characteristic of 12-silicotungstic acid are no longer observed and only those characteristic of silica and WO_3 remain. This indicates that prolonged heating at 400°C in air leads to the complete decomposition of 12-silicotungstic acid when supported on silica.

Aqueous extraction of 12-silicotungstic acid from the heated JM2 samples was also undertaken. Examination of the residues using XRD showed no difference from the XRD patterns in Figure 6.29. This is as expected since WO_3 is insoluble in water. FT-IR analysis of the residues again showed the presence of the silica support and WO_3 superimposed on one another with the intensity of the WO_3 absorptions increasing with heating time. However, no weak absorptions characteristic of 12-silicotungstic acid were observed suggesting all the insoluble 12-silicotungstic acid within the pores of the silica support had been removed.

These results indicate that the significant difference in the volume of hard coke caused by the different histories of JM2 and JM3 does not affect the optimum conditions for oxidation of this coke. Thus, the same decoking process can be applied to catalysts which have low and significant levels of hard coke. Oxidation of the coke results in the unblocking of previously blocked pores allowing any insoluble 12-silicotungstic acid to be removed. However, there is evidence to suggest that prolonged heating at 400°C leads to the decomposition of 12-silicotungstic acid. Therefore, to remove the maximum amount of 12-silicotungstic

acid from the catalyst, the soluble acid should be extracted first by aqueous methods, followed by heating at 400°C and a second extraction.

6.5 Summary

Characterisation of JM3 has demonstrated that, after a 1.5 year uneventful lifetime, the catalyst is almost identical to the authentic unused catalyst except for the presence of coke on the catalyst. Thermal analysis data showed the presence of soft and hard coke of which the hard coke was found to be the major component. This being the only difference would suggest that the coking of the catalyst is the primary cause of its deactivation.

Characterisation of the used catalyst JM2, which underwent a significant deactivation during its lifetime in the reactor, revealed 12-silicotungstic acid to be present as well as a significant level of coke. The quantity of hard coke present on JM2 was significantly higher than that found on JM3, 11.5 and 3%, respectively. Deactivation of JM2 is, therefore, most likely caused by very high levels of hard coke.

The results indicate that the 'insoluble tungsten' characterised by BP Chemicals is primarily 12-silicotungstic acid, within the pore structure of silica, which is restricted by a combination of soft and hard coke. The removal of soft coke, by dichloromethane extraction, allows the majority of the insoluble 12-silicotungstic acid in the pores of the silica to become water soluble on a lightly-coked catalyst. However, dichloromethane extraction on a heavily-coked catalyst makes little

difference to the solubility of the 12-silicotungstic acid with restricted solubility. Hard coke can be removed from a used catalyst by heating at 400°C in air for 6 hours. Insoluble 12-silicotungstic acid can then be extracted in aqueous solution.

Appendix B

Table B.1 ^{1}H NMR chemical shifts recorded from soft coke extracted from JM3.

$\delta(^1H)$	group
0.00(s)	R-H
0.80(m)	R-H
1.06(s)	R-H or R-OH
1.12(m)	R-H or R-OH
1.33(q)	R-H or R-OH
1.44(s)	R-H or R-OH
1.77(s)	R-H or R-OH or R_2C=CR-CH
1.96(m)	R-H or R-OH or R_2C=CR-CH
2.10(s)	R-OH or RC≡CH or R_2C=CR-CH or R-(C=O)-CH
2.20(s)	R-OH or Ar-CH or R-(C=O)-CH or RC≡CH
2.58(s)	R-OH or Ar-CH or R-(C=O)-CH or RC≡CH
2.67(s)	R-OH or Ar-CH or RC≡CH
2.79(m)	R-OH or Ar-CH
2.90(m)	R-OH or Ar-CH
5.25(m)	R-OH or Ph-OH or RCH=CHR or R_2C=CH_2
7.28(s)	Ph-OH or aromatics
7.95(t)	Ph-OH or aromatics

Table B.2 ^{13}C NMR chemical shifts recorded from soft coke extracted from JM3.

$\delta(^{13}C)$	group
0.62	C-H
8.20	C-H
20.47	C-H or C-C=C
28.00	C-(C=O)-R or C-C=C
30.50	C-(C=O)-R or C-C=C
31.29	C-(C=O)-R or C-C=C
35.84	C-(C=O)-R or C-C=C
36.48	C-(C=O)-R or C-C=C
53.34	C-OH
163.05	R-CO_2H or R-CO_2R'
175.35	R-CO_2H or R-CO_2R'

Appendix C

Scanning electron microscopy images recorded from the silica support (Figure C.1), silica-supported 12-silicotungstic acid (Figure C.2), JM3 (Figure C.3) and JM2 (Figure C.4).

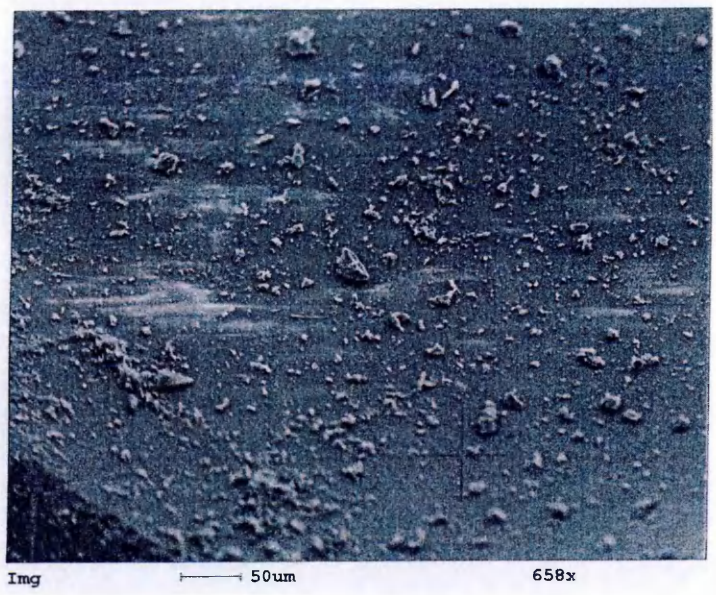

Figure C.1 SEM image recorded from the silica support.

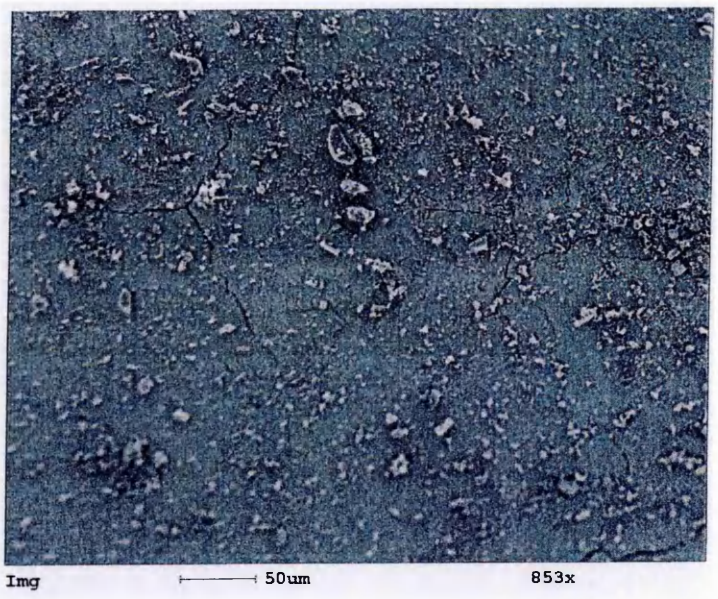

Figure C.2 SEM image recorded from the authentic unused catalyst.

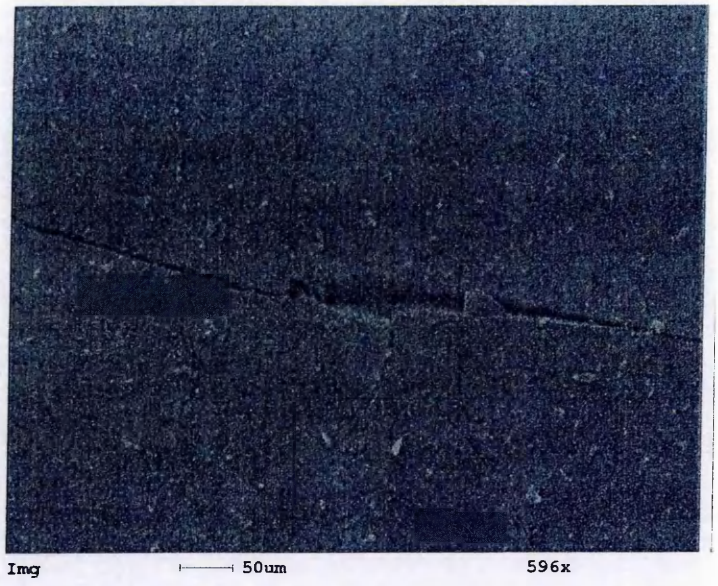

Figure C.3 SEM image recorded from JM3.

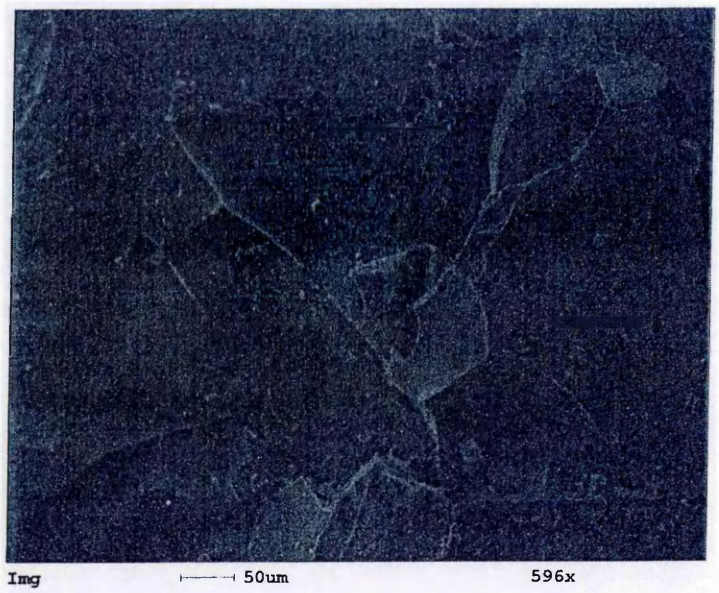

Figure C.4 SEM image recorded from JM2

References

(1) Okuhara, T.; Mizuno, N.; Misono, M. *Advances in Catalysis* **1996**, *41*, 113-252.

(2) Bardin, B. B.; Bordawekar, S. V.; Neurock, M.; Davis, R. J. *Journal of Physical Chemistry B* **1998**, *102*, 10817-10825.

(3) Katsoulis, D. E. *Chemical Reviews* **1998**, *98*, 359-387.

(4) Haining, G. *(BP Chemicals) personal communication* **2004**.

(5) Bielanski, A.; Pozniczek, J.; Hasik, M. *Journal of Thermal Analysis* **1995**, *44*, 717-723.

(6) Wong, J.; Angell, C. A. *Glass Structure by Spectroscopy*; Marcel Dekker Inc: New York, 1976.

(7) Newman, A. D.; Brown, D. R.; Siril, P.; Lee, A. F.; Wilson, K. *Physical Chemistry Chemical Physics* **2006**, *8*, 2893-2902.

(8) Mioc, U. B.; Dimitrijevic, R. Z.; Davidovic, M.; Nedic, Z. P.; Mitrovic, M. M.; Colomban, P. *Journal of Materials Science* **1994**, *29*, 3705-3718.

(9) Scherrer, P. *Nachrichten von der Köngl. Gesellschaft der Wissenschaften zu Göttingen, Mathematisch-Physikalische Klasse* **1918**, *2*, p. 98.

(10) Kuang, W. X.; Rives, A.; Fournier, M.; Hubaut, R. *Applied Catalysis A - General* **2003**, *250*, 221-229.

(11) Kozhevnikov, I. V.; Kloetstra, K. R.; Sinnema, A.; Zandbergen, H. W.; van Bekkum, H. *Journal of Molecular Catalysis A - Chemical* **1996**, *114*, 287-298.

(12) Izumi, Y.; Hasebe, R.; Urabe, K. *Journal of Catalysis* **1983**, *84*, 402-409.

(13) Engelhardt, G.; Dieter, M. *High-Resolution Solid-State NMR of Silicates and Zeolites*; Wiley, Chichester, 1987.

(14) Kozhevnikov, I. V.; Holmes, S.; Siddiqui, M. R. H. *Applied Catalysis A - General* **2001**, *214*, 47-58.

(15) Mohana Rao, K.; Gobetto, R.; Iannibello, A.; Zecchina, A. *Journal of Catalysis* **1989**, *119*, 512-516.

(16) Uchida, S.; Inumaru, K.; Misono, M. *Journal of Physical Chemistry B* **2000**, *104*, 8108-8115.

(17) Lefebvre, F. *Journal of the Chemical Society-Chemical Communications* **1992**, 756-757.

(18) Chang, T. H. *Journal of the Chemical Society - Faraday Transactions* **1995**, *91*, 375-379.

(19) Kanda, Y.; Lee, K. Y.; Nakata, S.; Asaoka, S.; Misono, M. *Chemistry Letters* **1988**, *17*, 139-142.

(20) Bielanski, A.; Datka, J.; Gil, B.; Malecka-Lubanska, A.; Micek-Ilnicka, A. *Catalysis Letters* **1999**, *57*, 61-64.

(21) Kozhevnikova, E. F.; Kozhevnikov, I. V. *Journal of Catalysis* **2004**, *224*, 164-169.

(22) Newman, A. D.; Lee, A. F.; Wilson, K.; Young, N. A. *Catalysis Letters* **2005**, *102*, 45-50.

(23) Turek, W.; Pomarzanska, E. S.; Pron, A.; Harber, J. *Journal of Catalysis* **2000**, *189*, 297-313.

(24) Brown, G. M.; Noespirlet, M. R.; Busing, W. R.; Levy, H. A. *Acta Crystallographica Section B - Structural Science* **1977**, *33*, 1038-1046.

(25) Hollinger, G.; Duc, T. M.; Deneuville, A. *Physical Review Letters* **1976**, *37*, 1564-1567.

(26) Pope, M. T. *Heteropoly and Isopoly Oxometalates*; Springer-Verlag: Berlin, 1983.

(27) Nguyen, T.-V.; Kim, K.-J.; Yang, O.-B. *Journal of Photochemistry and Photobiology, A: Chemistry* **2005**, *173*, 56-63.

(28) Kaba, M. S.; Song, I. K.; Duncan, D. C.; Hill, C. L.; Barteau, M. A. *Inorganic Chemistry* **1998**, *37*, 398-406.

(29) Jeong, B. H.; Han, J. S.; Ko, S. W.; Lee, J. H.; Lee, B. J. *Journal of Industrial and Engineering Chemistry* **2007**, *13*, 310-313.

Chapter 7

Acidity and fine-tuning of the acidic proton

7.1 Introduction

The hierarchical structure of 12-heteropolyacids proposed by Misono and co-workers[1] describes three sub-structures : the primary structure being the heteropolyanion or Keggin unit, the secondary structure consisting of the three-dimensional arrangement of the Keggin units and their counter cations and, finally, the tertiary structure comprising of nanocrystallites. Attempts to 'fine-tune' the acidity of 12-heteropolyacids have focused on the modification of the Keggin unit : that is, the primary structure. Over 65 elements have been used as heteroatoms,[2] tungsten addenda atoms have been systematically replaced by up to 3 vanadium atoms[3] and the acidic protons have also been systematically replaced by alternative counter cations such as caesium.[1,4,5] Due to the similar sizes of 12-heteropolyanions and their similar behaviour with respect to the presence of water molecules (see Chapter 5) it seems reasonable to presume that 'fine-tuning' of the acidity can also be achieved through modification of the secondary structure. It is feasible that combining two 12-heteropolyacids with different acidities could lead to a modification of the acidity to somewhere between those of the two contributing acids. This chapter reports an experimental investigation of the results of combining 12-silicotungstic acid and 12-phosphotungstic acid in different molar ratios. ^{13}C MAS and CPMAS NMR spectroscopy of adsorbed ^{13}C-labelled acetone is used to investigate the acidity in the prepared compounds.

7.2 Mixed 12-heteropolyacids

Preliminary experiments showed that mixing of aqueous solutions of 12-silicotungstic acid and 12-phosphotungstic acid followed by evaporation yielded

white crystalline residues. These experiments were repeated with quantitative ratios of the two components. Specifically, molar ratios of $H_4[SiW_{12}O_{40}]$: $H_3[PW_{12}O_{40}]$ with values of 1 : 3, 1 : 1 and 3 : 1 were used.

Characterisation experiments, which are described in detail below, confirmed that the individual residues were single phase materials. For convenience in the discussions that follow, these materials will be referred to as 'mixed compounds'.

7.2.1 Thermal analysis

The mixed compounds all showed similar thermal analytical behaviour. Thus only the results of the 1 : 1 compound are described in detail here. The thermal analysis recorded from the 1 : 1 mixed compound is shown in Figure 7.1.

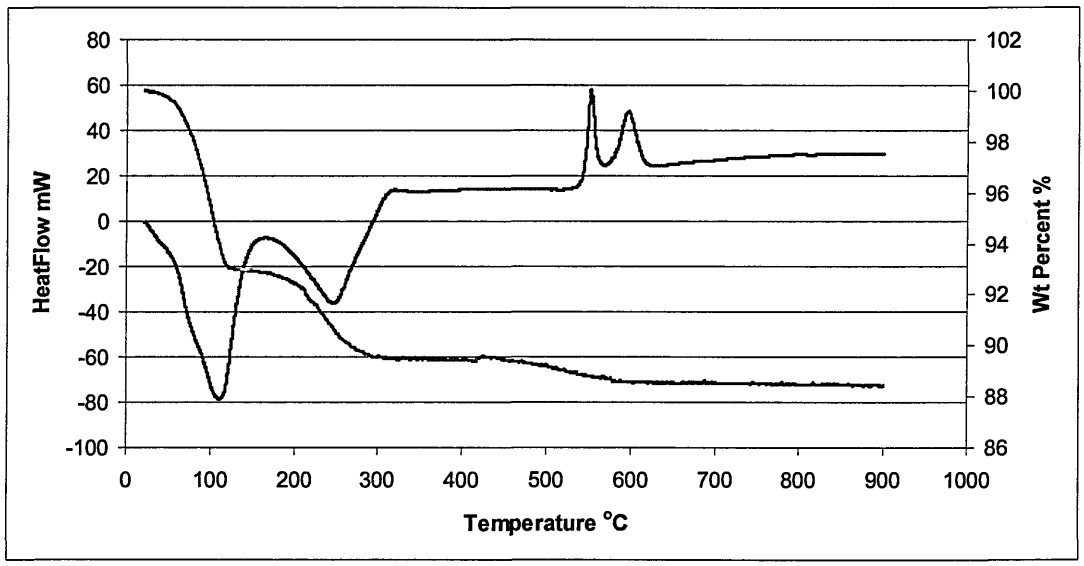

Figure 7.1 Thermal analysis recorded under a flow of dry air (50 ml min^{-1}) and at a heating rate of 10°C min^{-1} from $H_4[SiW_{12}O_{40}]$: $H_3[PW_{12}O_{40}]$ in a 1 : 1 molar ratio (approximately 50 mg).

The TGA data show similar weight loss behaviour to that observed for hydrated $H_4[SiW_{12}O_{40}]$ (see Chapter 5, Figure 5.1(A)) and the DTA data are also broadly comparable up to approximately 500°C; however, above this temperature two exothermic events are observed. The first of these centred at approximately 550°C corresponds to the decomposition of the anhydride $[SiW_{12}O_{38}]$. The second exothermic event, centred at approximately 595°C, can be attributed to the decomposition of the anhydride $[PW_{12}O_{38.5}]$. The latter assignment is confirmed by the thermal analysis of hydrated $H_3[PW_{12}O_{40}]$ reported by Mioč *et al.*[6] and Vaughan *et al.*[7] where the exothermic phase change was observed in the region of 600°C.

The observation of the decomposition of the individual silicon and phosphorous based Keggin units indicates the presence of these anions in the mixed compound. Strictly, however, the observed thermal analysis behaviour does not confirm the presence of a single, as opposed to a multi-component, phase. It is the XRD investigations to be described in Section 7.2.3 that provide direct evidence for single phase behaviour.

The thermal analysis data in Figure 7.1 are consistent with the formation of a hexahydrate at temperatures above 120°C. This is also the case for other mixed compounds with different molar ratios. In order to make comparisons between samples prepared using different molar ratios it is useful to ensure that they are all in the same hydrated form. For this purpose, the hexahydrate is the most convenient. Thus, for all subsequent investigations samples were heated at 150°C for 2 hours to prepare this specific hydrated form.

7.2.2 FT-IR spectroscopy

FT-IR spectra recorded from $H_4[SiW_{12}O_{40}]/H_3[PW_{12}O_{40}]$ compounds in the molar ratios 3 : 1, 1 : 1 and 3 : 1 are shown in Figure 7.2. In addition, FT-IR spectra for the pure acids are included in this figure for comparison. All compounds are in the form of hexahydrates.

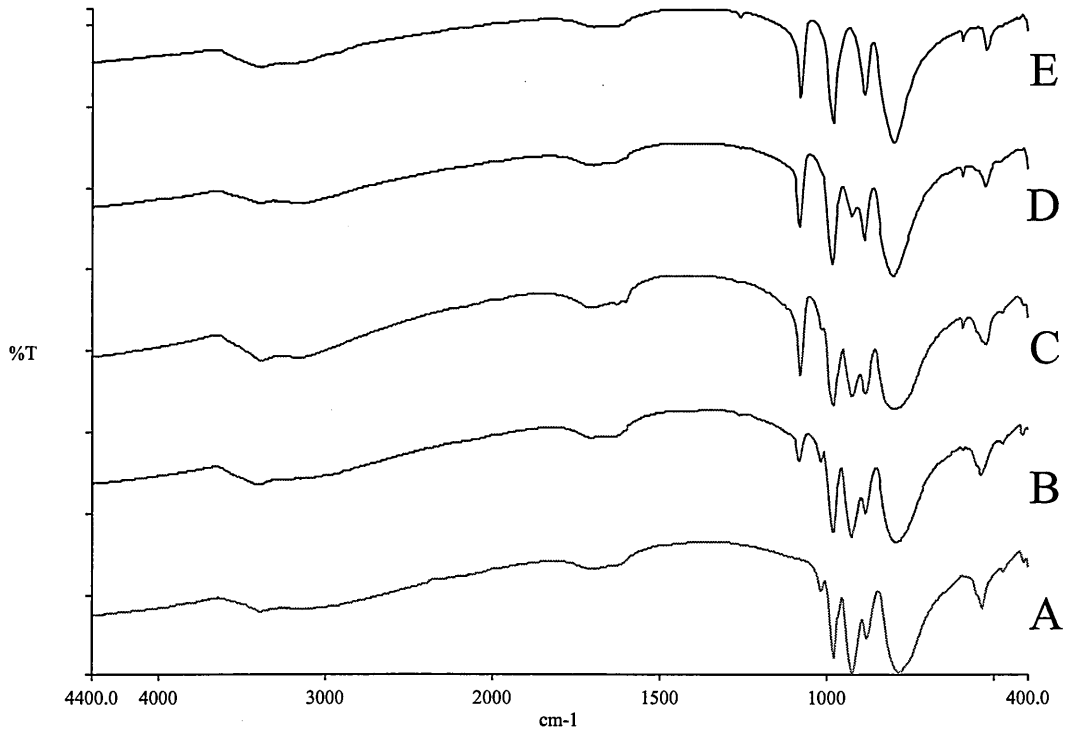

Figure 7.2 FT-IR spectra recorded from A) $H_4[SiW_{12}O_{40}]\cdot 6H_2O$, $H_4[SiW_{12}O_{40}]/H_3[PW_{12}O_{40}]\cdot 6H_2O$ compounds in the molar ratios B) 3 : 1, C) 1 : 1, D) 1 : 3, and E) $H_3[PW_{12}O_{40}]\cdot 6H_2O$.

The absorptions characteristic of $H_4[SiW_{12}O_{40}]$ (1020 (w), 981 (s), 921 (s), 880 (m) and 779 (s) cm^{-1}) gradually decrease in intensity as the $H_4[SiW_{12}O_{40}]/H_3[PW_{12}O_{40}]$ molar ratio decreases. This is best observed for the most intense, 921(s) cm^{-1}, absorption. Conversely, the absorptions characteristic of $H_3[PW_{12}O_{40}]$ (1080, 990,

890 and 810 cm^{-1}) increase, which is clearly shown by the 1080 cm^{-1} absorption. The observed peaks are comparable to those recorded from the pure 12-heteropolyacids[8,9] suggesting that neither of the Keggin units is affected by the presence of the other. The absorptions associated with the water molecules interacting with the acidic protons, 3180 and 1710 cm^{-1} (see Chapter 5, Section 5.5.1), are also unaffected by the mixing of the two 12-heteropolyacids.

7.2.3 X-ray powder diffraction

The XRD pattern recorded from a mechanical mixture, in a molar ratio of 1 : 1, of $H_4[SiW_{12}O_{40}]\cdot 6H_2O$ and $H_3[PW_{12}O_{40}]\cdot 6H_2O$ in the 2θ region of 50 - 65 ° is shown in Figure 7.3(B).

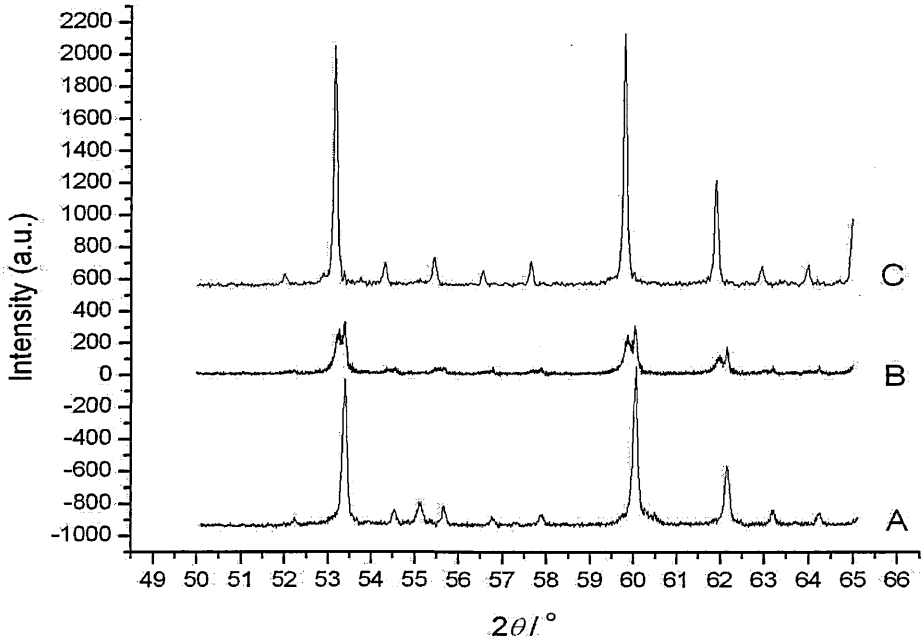

Figure 7.3 X-ray powder diffraction patterns recorded for A) $H_4[SiW_{12}O_{40}]\cdot 6H_2O$, B) mechanical mixture, in a molar ratio 1 : 1, $H_4[SiW_{12}O_{40}]\cdot 6H_2O$ and $H_3[PW_{12}O_{40}]\cdot 6H_2O$ and C) $H_3[PW_{12}O_{40}]\cdot 6H_2O$ over the 2θ range 50° - 65° (step size = 0.01°; step time = 8 s).

The XRD patterns of the pure acid hexahydrates in the same region of 2θ are shown for comparison. The cubic unit cell parameters for $H_4[SiW_{12}O_{40}]$ and $H_3[PW_{12}O_{40}]$ measured in this work are 12.1183(5) Å and 12.1521(12) Å, respectively. These unit cell parameters are very similar and so, as confirmed in Figure 7.7, it is only at relatively high angles of 2θ that the Bragg peaks are resolved for the individual acids in the mixture. This observation provides a means of testing whether the mixed compounds of $H_4[SiW_{12}O_{40}]$ and $H_3[PW_{12}O_{40}]$, when prepared as hexahydrates, correspond to well-defined single cubic phases.

The XRD powder pattern recorded in the 2θ range of 50° - 65° for the 1 : 1 $H_4[SiW_{12}O_{40}]/H_3[PW_{12}O_{40}]$ mixed compound, in the form of the hexahydrate, is shown in Figure 7.4. Significantly, there is no evidence of contributions from the individual pure acids. A single set of Bragg peaks is observed corresponding to a single phase compound with a cubic unit cell. Furthermore, the Bragg peaks for this compound occur at intermediate values of 2θ compared to the observed peaks for the individual acids.

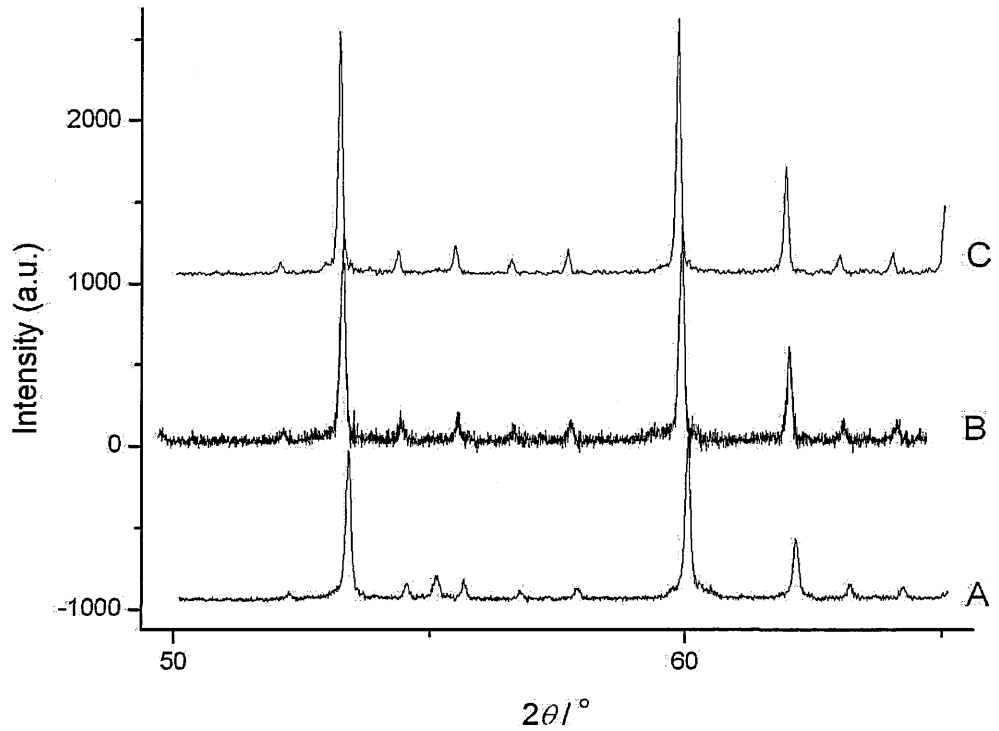

Figure 7.4 The XRD patterns recorded for A) $H_4[SiW_{12}O_{40}]\cdot 6H_2O$, B) mixed compound $H_4[SiW_{12}O_{40}]/H_3[PW_{12}O_{40}]\cdot 6H_2O$ in a 1 : 1 molar ratio and C) $H_3[PW_{12}O_{40}]\cdot 6H_2O$ over a 2θ range of 50° - 65° (step size = 0.01°; step time = 8 s).

The XRD patterns recorded from mixed compounds with different molar ratios were fitted in the X-fit program[10] and the zero shift calculated using the reflection-pair method,[11] these results were then refined in the Chekcell program[12] (as described in Chapter 5). The refined cubic cell parameters are summarised in Table 7.1, and a plot of cubic unit cell parameter *versus* percentage of 12-phosphotungstic acid is shown in Figure 7.5.

Table 7.1 The refined cubic unit cell parameters calculated from the XRD powder patterns recorded for i) $H_3[PW_{12}O_{40}]\cdot 6H_2O$, ii) $H_4[SiW_{12}O_{40}]/H_3[PW_{12}O_{40}]\cdot 6H_2O$ mixed compounds in the molar ratios 1 : 3, 1 : 1, and 3 : 1, and iii) $H_4[SiW_{12}O_{40}]\cdot 6H_2O$.

Compounds	Cubic unit cell parameter / Å
$H_3[PW_{12}O_{40}]\cdot 6H_2O$	12.1521(12)
$H_4[SiW_{12}O_{40}]/H_3[PW_{12}O_{40}]\cdot 6H_2O$ (1 : 3)	12.1496(36)
$H_4[SiW_{12}O_{40}]/H_3[PW_{12}O_{40}]\cdot 6H_2O$ (1 : 1)	12.1396(13)
$H_4[SiW_{12}O_{40}]/H_3[PW_{12}O_{40}]\cdot 6H_2O$ (3 : 1)	12.1243(10)
$H_4[SiW_{12}O_{40}]\cdot 6H_2O$	12.1183(5)

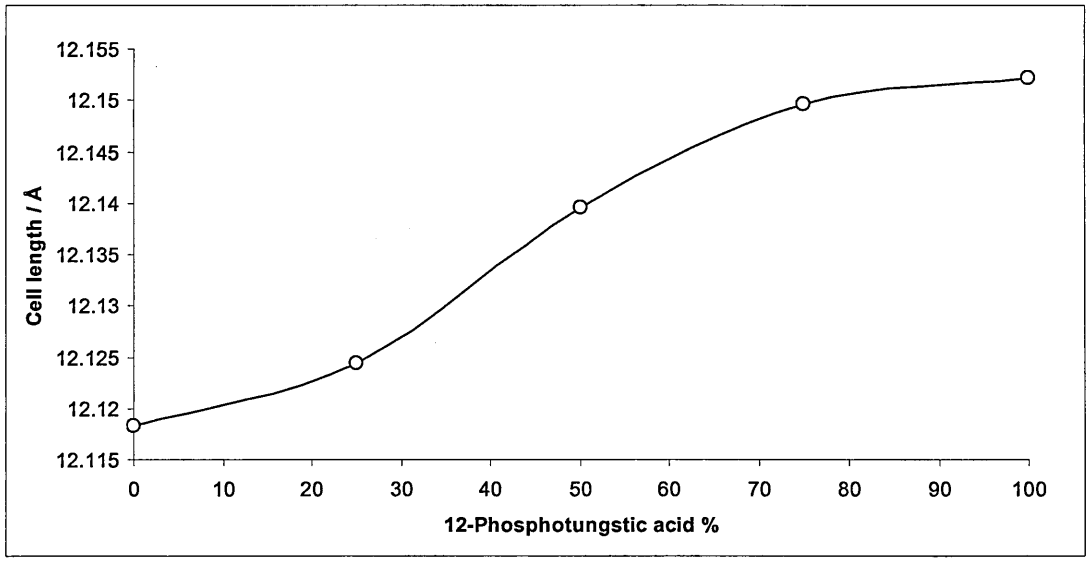

Figure 7.5 A plot of cubic unit cell parameter values calculated from the XRD patterns recorded from the mixed $H_4[SiW_{12}O_{40}]$ / $H_3[PW_{12}O_{40}]$ compounds against the percentage of 12-phosphotungstic acid present.

The data, as expected, show an increase in cubic unit cell parameter as the percentage of 12-phosphotungstic acid in the mixed compound increases. The experimental uncertainties for the individual measurements represent, on average, less than 5% of the overall change in cell parameter. On this basis, it is seen that the increase in cell parameter is distinctly non-linear. This is an area for further study and the system may be a model for understanding more about the structural properties of doped materials in which one species is replaced by another which has slightly different dimensions.

7.2.4 ^{31}P MAS NMR spectroscopy

A single resonance was observed in the ^{31}P MAS NMR spectra recorded from each of the mixed compounds and values of $\delta(^{31}P)$ are summarized in Table 7.2.

Table 7.2 The ^{31}P MAS NMR spectra recorded from $H_4[SiW_{12}O_{40}]/H_3[PW_{12}O_{40}]\cdot 6H_2O$ mixed compounds.

Compound	$\delta(^{31}P)$ / ppm (± 0.4)
$H_4[SiW_{12}O_{40}]/H_3[PW_{12}O_{40}]\cdot 6H_2O$ (1 : 3)	-15.2
$H_4[SiW_{12}O_{40}]/H_3[PW_{12}O_{40}]\cdot 6H_2O$ (1 : 1)	-15.1
$H_4[SiW_{12}O_{40}]/H_3[PW_{12}O_{40}]\cdot 6H_2O$ (3 : 1)	-15.2

The values of $\delta(^{31}P)$ are, within experimental uncertainty, equal to that recorded for $H_3[PW_{12}O_{40}]\cdot 6H_2O$ ($\delta(^{31}P)$ = -15.1), independent of the molar ratio. This behaviour is consistent with a relatively simple physical distribution of the $[PW_{12}O_{40}]^{3-}$ Keggin unit over the available cubic sites rather than any significant chemical interaction influencing the distribution.

7.3 Acid sites

As discussed in Chapter 2, the pseudo-liquid nature of 12-heteropolyacids[13] leads, in principle, to the even distribution of the acidic proton sites in bulk anhydrous $H_3[PW_{12}O_{40}]$. In contrast, the acidic proton sites of silica-supported $H_3[PW_{12}O_{40}]\cdot xH_2O$ (20 wt %) become less acidic and less uniformly distributed than in the bulk form. It has been reported that only 20% of the proton sites retain the strength observed in bulk $H_3[PW_{12}O_{40}]\cdot xH_2O$.[13]

The strength and distribution of the acidic protons in $H_3[PW_{12}O_{40}]$, both in anhydrous and hydrated states, have recently been investgated[14] using isotopically labelled acetone adsorption in conjunction with solid state ^{13}C MAS and CPMAS NMR spectroscopy. The acidity scale developed by Biaglow *et al.*[15-19] qualitatively attributes the change in ^{13}C chemical shift of the carbonyl group of acetone adsorbed onto an acidic solid as being due to protonation of this group and, hence, the presence of a partial positive charge on the carbonyl carbon. The threshold acid strength, corresponding to 30% SO_3/H_2SO_4, gives rise to a value of $\delta(^{13}C) = 246$ for adsorbed acetone. Yang *et al.*[14] observed two ^{13}C carbonyl resonances at values of $\delta(^{13}C) = 246$ and 235 for anhydrous $H_3[PW_{12}O_{40}]$ and assigned these to acetone adsorbed on two different isolated acidic protons. Furthermore, they demonstrated using REDOR experiments that the isolated acidic protons are located on both the bridging (O_c) and terminal (O_d) oxygen atoms in the Keggin unit (See Chapter 2, Section 2.2, Figure 2.2). The location of the acid sites had previously been associated with either the terminal (O_d) oxygen atom[20,21] or the bridging (O_c) oxygen atoms.[22] More recently, DFT calculations have indicated the protons are likely to be distributed amongst the various oxygen atoms.[23] The experimental observation by

Yang *et al.*[14] of two acid sites represents new information. The acid strengths of the two sites are high with one at the threshold of superacidity. Further NMR evidence also indicated that the isolated acidic protons and the adsorbed acetone were tightly bound together with restricted mobility.

In their studies of the hexahydrate $H_3[PW_{12}O_{40}]\cdot 6H_2O$ Yang *et al.*[14] observed a ^{13}C MAS NMR resonance at $\delta(^{13}C) = 219$. This was assigned to acetone adsorbed on hydrated proton species with an acid strength equivalent to that of zeolites.[19,24] The absence of spinning sidebands, and the relatively low cross-polarisation enhancement of this resonance in a ^{13}C CPMAS experiment, was taken as indicating considerable mobility of the adsorbed acetone and the hydrated proton. A resonance at $\delta(^{13}C) = 235$ (but not 246) was also observed for the hexahydrate so that both isolated acidic protons and hydrated protons are present. However, single crystal neutron diffraction data indicates that all the acidic protons are associated with a diaqua-hydrogen ion[25] and shows no evidence of an acidic proton on the Keggin unit. There is thus an apparent discrepancy between the NMR and structural investigations. Nonetheless, the use of ^{13}C solid-state NMR to study the behaviour of adsorbed isotopically labelled acetone on 12-heteropolyacids, although relatively new, offers a useful way of obtaining detailed information on the properties of acid sites particularly for well characterised samples with known hydration.

The adsorption of acetone onto solid acids and the measurement of the carbonyl ^{13}C chemical shift has been recognised for a number of years as a means of characterising acidity.[26] A range of chemical shifts has been observed between acetone (210 ppm) and 30% SO_3/H_2SO_4 (246 ppm) which is taken as the threshold

for superacidity. A selection of results are summarised in Table 7.3 and will be referred to in later discussion.

Table 7.3 ^{13}C MAS NMR chemical shift data measured from C-2-isotopically labelled acetone in various acidic media (modified from 26).

System	$\delta(^{13}C)$
CH_3COCH_3	210
$CF_3CH(OH)CF_3$	221
$MgCl_2$	221
HZSM-5	223
$MgBr_2$	223
ZnI_2	227
$ZnCl_2$	230
$TaCl_5$	237
AlI_3	238
$ScTf_3$	239
$AlBr_3$	243
$AlCl_3$	245
30% SO_3/H_2SO_4	246

7.3.1 Acetone adsorption studies

Isotopically-labelled 2-^{13}C-acetone (99% ^{13}C enriched) was introduced to the mixed compound $H_4[SiW_{12}O_{40}]/H_3[PW_{12}O_{40}]\cdot 6H_2O$ (1 : 1 molar ratio), $H_4[SiW_{12}O_{40}]\cdot 6H_2O$ and $H_3[PW_{12}O_{40}]\cdot 6H_2O$ in a closed system under vacuum; 3g of each material was

used. After three days, the resulting pale yellow solid from $H_3[PW_{12}O_{40}]\cdot 6H_2O$ was characterised using both ^{13}C MAS and ^{13}C CPMAS NMR spectroscopy. However, to observe a resonance in the ^{13}C MAS and ^{13}C CPMAS NMR spectra recorded from $H_4[SiW_{12}O_{40}]\cdot 6H_2O$ and $H_4[SiW_{12}O_{40}]/H_3[PW_{12}O_{40}]\cdot 6H_2O$ (1 : 1) it was necessary to leave these compounds to adsorb for a further day.

Two resonances in the carbonyl region are observed at $\delta(^{13}C) = 235.0$ and 218.2 in the ^{13}C MAS NMR spectrum recorded from 2-^{13}C-acetone (99% ^{13}C enriched) treated $H_3[PW_{12}O_{40}]\cdot 6H_2O$ as shown in Figure 7.9. The resonance for the methyl group occurs at $\delta(^{13}C) = 32.1$. The resonances observed at $\delta(^{13}C) = 205.1$ and 175.3 in Figure 7.6 are characteristic of mesityl oxide,[17] the formation of which was discussed in Chapter 2, see Figure 2.9. The results are consistent with the ^{13}C MAS NMR data recorded by Yang *et al.*[14] The resonance occurring at 235 ppm can be assigned to acetone interacting with an isolated acidic proton and the low-intensity resonance at 219 ppm must be due to a hydrated proton species.

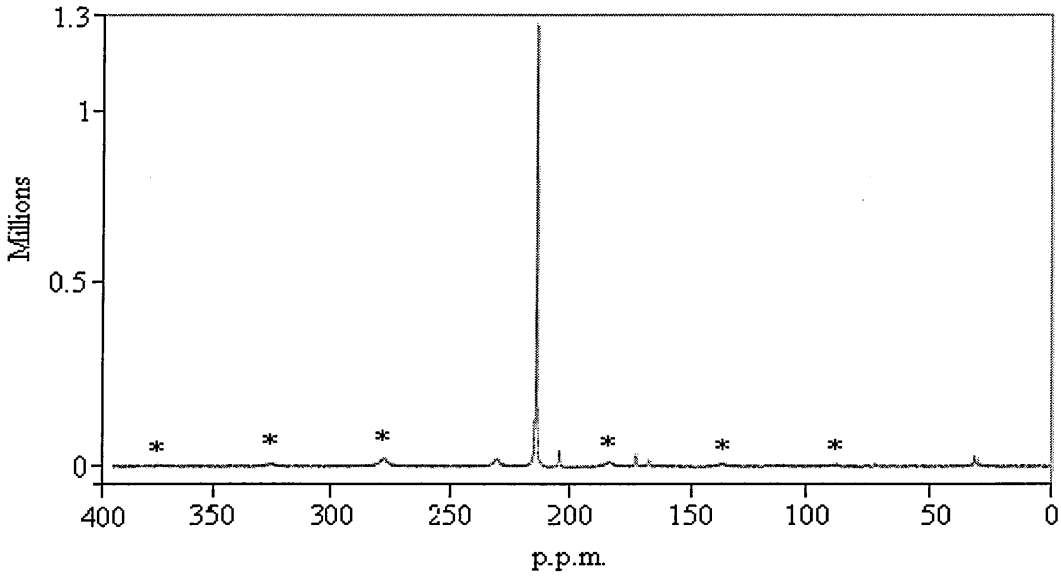

Figure 7.6 ^{13}C MAS NMR recorded from isotopically-labelled 2-^{13}C-acetone (99% ^{13}C enriched) adsorbed on to $H_3[PW_{12}O_{40}]\cdot 6H_2O$. Spinning sidebands are denoted by (*).

The ^{13}C MAS NMR spectra recorded from isotopically-labelled acetone adsorbed on $H_4[SiW_{12}O_{40}]\cdot 6H_2O$ and the mixed compound $H_4[SiW_{12}O_{40}]/H_3[PW_{12}O_{40}]\cdot 6H_2O$ in a 1 : 1 molar ratio both turned out to be very similar to that recorded from $H_3[PW_{12}O_{40}]\cdot 6H_2O$. The observed resonances are summarised in Table 7.4.

Table 7.4 Comparison of resonances observed in the ^{13}C MAS NMR spectra recorded from 12-heteropolyacids treated with isotopically-labelled acetone.

Compounds	^{13}C MAS NMR data / ppm (± 0.4)		
	$C^{\delta+}$=O-$H_{isolated}$	$C^{\delta+}$=O-$H_{hydrated}$	Methyl group
$H_3[PW_{12}O_{40}]\cdot 6H_2O$	235.0	218.2	32.1
$H_4[SiW_{12}O_{40}]\cdot 6H_2O$	235.0	220.6	32.1
$H_4[SiW_{12}O_{40}]/H_3[PW_{12}O_{40}]\cdot 6H_2O$ 1 : 1	234.6	220.1	31.8

The ^{13}C chemical shift of the resonance associated with the methyl group, within experimental uncertainty, remains constant. The ^{13}C chemical shift of the carbonyl group interacting with the isolated acidic proton has the same value, within experimental uncertainty (± 0.6 ppm), when adsorbed on the different 12-heteropolyacids. However, a small chemical shift difference (2.4 ±0.4 ppm, in the direction of increased acidity (see Table 7.3), observed for the resonance recorded from the carbonyl group associated with the hydrated acidic proton associated with $H_4[SiW_{12}O_{40}]\cdot 6H_2O$ compared to that recorded for $H_3[PW_{12}O_{40}]\cdot 6H_2O$. The ^{13}C chemical shift for this resonance is similar in value for both the 1 : 1 molar mixed compound and $H_4[SiW_{12}O_{40}]\cdot 6H_2O$.

The ^{13}C CPMAS NMR spectrum recorded from the isotopically-labelled acetone adsorbed on to $H_3[PW_{12}O_{40}]\cdot 6H_2O$ is shown in Figure 7.7.

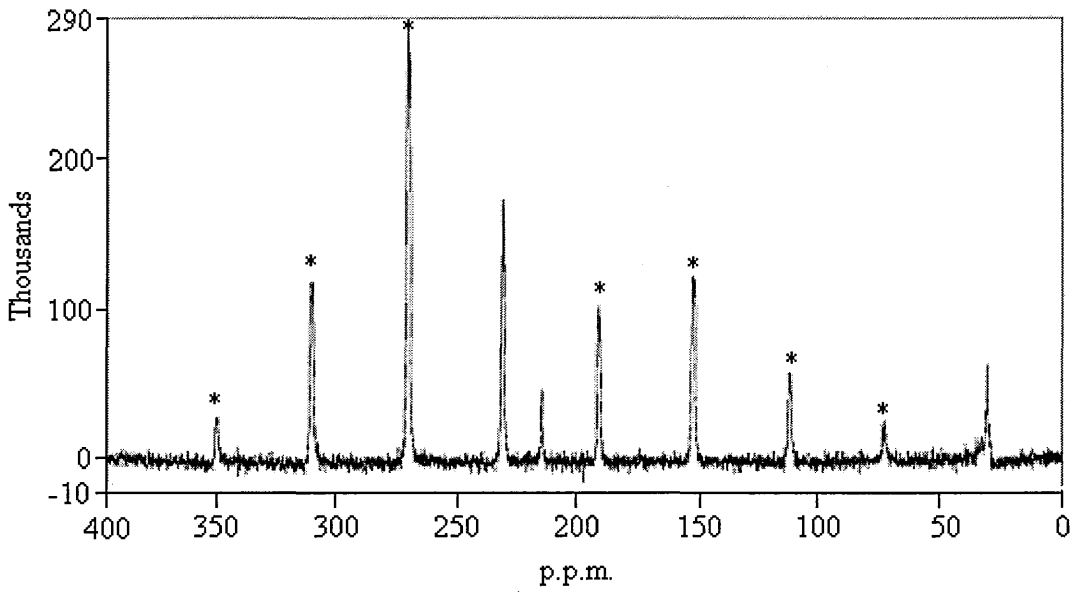

Figure 7.7 ^{13}C CPMAS NMR recorded from isotopically-labelled 2-^{13}C-acetone (99% ^{13}C enriched) absorbed on to $H_3[PW_{12}O_{40}]\cdot 6H_2O$. Spinning sidebands denoted by (*).

A significant increase in the sideband intensity of the resonance occurring in the region of 235 ppm, and corresponding to an isolated acid proton, is observed. This behaviour is consistent with the mobility of the acetone molecule associated with the isolated acidic proton being significantly restricted. By comparison, the acetone molecule associated with the hydrated proton species, which accounts for the resonance in the region 218 ppm, is relatively unrestricted in its mobility as indicated by the lack of spinning sidebands. Overall, the observed behaviour is consistent with the results observed by Yang *et al.*[14] under similar conditions.

The ^{13}C CPMAS NMR spectra recorded from isotopically-labelled acetone adsorbed on $H_4[SiW_{12}O_{40}]\cdot 6H_2O$ and the mixed compound $H_4[SiW_{12}O_{40}]/H_3[PW_{12}O_{40}]\cdot 6H_2O$ in a 1 : 1 molar ratio were both very similar to that recorded from $H_3[PW_{12}O_{40}]\cdot 6H_2O$. The observed resonances are summarised in Table 7.5, and, as

to be expected, are comparable with those in Table 7.4. However, it is noticable that there are larger differences for the methyl group resonances than those associated with the carbonyl groups. The latter, which reflect acidity values, are within experimental uncertanty consistent between the two types of ^{13}C NMR experiment.

Table 7.5 Comparison of resonances observed in the ^{13}C CPMAS NMR spectra recorded from 12-heteropolyacids treated with isotopically-labelled acetone.

Compound	^{13}C CPMAS NMR data / ppm (± 0.4)		
	$C^{\delta+}=O\text{-}H_{isolated}$	$C^{\delta+}=O\text{-}H_{hydrated}$	Methyl group
$H_3[PW_{12}O_{40}]\cdot 6H_2O$	235.1	217.9	31.1
$H_4[SiW_{12}O_{40}]\cdot 6H_2O$	234.5	220.7	31.6
$H_4[SiW_{12}O_{40}]/H_3[PW_{12}O_{40}]\cdot 6H_2O$	234.8	220.0	31.1

In terms of acidity, the ^{13}C MAS and CPMAS NMR results suggest that the isolated acidic protons associated with both $H_3[PW_{12}O_{40}]\cdot 6H_2O$ and $H_4[SiW_{12}O_{40}]\cdot 6H_2O$ possess the same acid strength. However, the observed chemical shift difference, associated with deshielding of the carbonyl carbon, indicates that the hydrated acidic protons of $H_4[SiW_{12}O_{40}]\cdot 6H_2O$ are slightly more acidic than those of $H_3[PW_{12}O_{40}]\cdot 6H_2O$. When compared with the data summarised in Table 7.3, the hydrated acidic protons of both hexahydrates have an acidity just lower than that of $CF_3CH(OH)CF_3$. Since the overall range of acidities covers 36 ppm the observed chemical shift difference in the region of 2.6 ppm is not insignificant.

Acidity studies carried out using temperature programmed desorption[27] and microcalorimetry[28] have, in contrast, shown hydrated $H_3[PW_{12}O_{40}]$ to be more acidic than hydrated $H_4[SiW_{12}O_{40}]$. These techniques, however, do not distinguish between the two acidic sites highlighted by the ^{13}C MAS NMR and give instead an overall acidity, and so direct comparisons are difficult to make.

Analysis of the spinning-side bands for the ^{13}C resonance associated with the isolated acidic proton in the CPMAS NMR spectra of the 12-heteropolyacid compounds gives a value for asymmetry parameter (η) equal to 0.45 in all three cases. This result is consistent with a similar type and geometry of acetone adsorption at the isolated acidic proton in all three compounds. It is also consistent with the similar values of $\delta(^{13}C)$.

Overall, the results indicate that a difference in the acidity of the hydrated acidic proton for the hexahydrates of $H_4[SiW_{12}O_{40}]$ and $H_3[PW_{12}O_{40}]$ can be detected using acetone absorption. It is feasible that the acidity of mixed compounds can be 'tuned' by varying the molar ratio, although this is an area for further investigation.

7.3.2 Silica-supported 12-heteropolyacids

Isotopically-labelled 2-^{13}C-acetone (99% ^{13}C enriched) was introduced to the silica-supported hexahydrates of $H_4[SiW_{12}O_{40}]$, $H_4[SiW_{12}O_{40}]/H_3[PW_{12}O_{40}]$ in a 1 : 1 molar ratio and $H_3[PW_{12}O_{40}]$ in the same way as described in the previous section. It was necessary to allow adsorption to occur over a period of four days in order to obtain ^{13}C NMR spectra with acceptable signal-to-noise ratios.

The ^{13}C MAS NMR spectra recorded from isotopically-labelled acetone adsorbed on silica-supported $H_3[PW_{12}O_{40}]\cdot 6H_2O$ is shown in Figure 7.8 (The broad resonance centred at approximately 105 ppm is due to signal from the NMR rotor caps). Table 7.6 summarises ^{13}C chemical shift values taken from this spectrum in comparison to those from the unsupported acid hexahydrate.

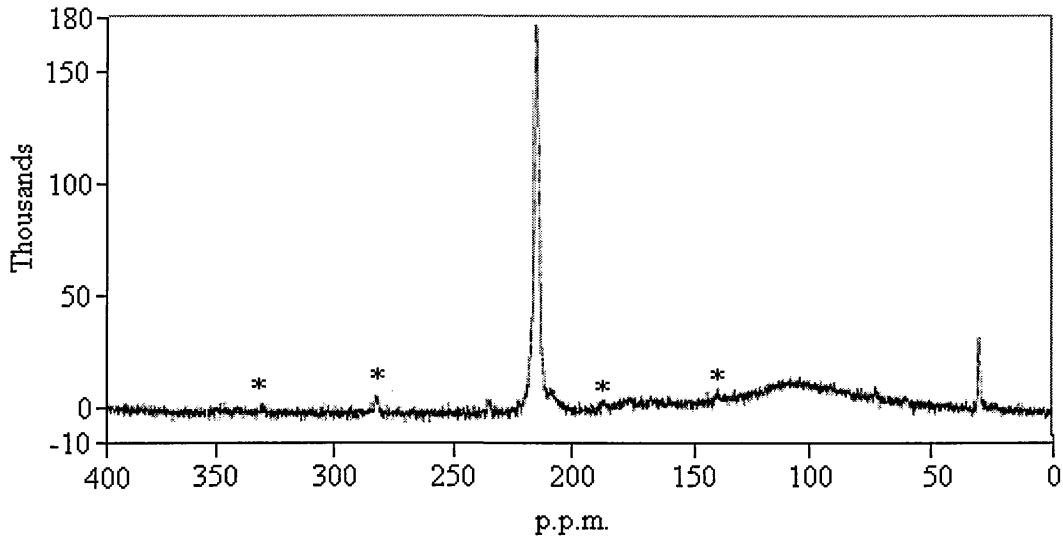

Figure 7.8 ^{13}C MAS NMR recorded from isotopically-labelled acetone adsorbed on silica-supported $H_3[PW_{12}O_{40}]\cdot 6H_2O$. Spinning sidebands denoted by (*).

Table 7.6 Comparison of ^{13}C chemical shift values derived from ^{13}C MAS NMR spectra recorded from isotopically-labelled acetone adsorbed on unsupported and silica-supported $H_3[PW_{12}O_{40}]\cdot 6H_2O$.

Compound	**^{13}C MAS NMR data / ppm (± 0.4)**		
	$C^{\delta+}=O\text{-}H_{isolated}$	$C^{\delta+}=O\text{-}H_{hydrated}$	Methyl group
$H_3[PW_{12}O_{40}]\cdot 6H_2O$	235.0	218.2	32.1
$H_3[PW_{12}O_{40}]\cdot 6H_2O/SiO_2$	235.0	215.4	29.8

The resonance associated with the hydrated acidic proton shows a 2.8 (± 0.6) ppm shift to lower frequency in comparison to $H_3[PW_{12}O_{40}]\cdot 6H_2O$; this corresponds to increased sheilding of the carbonyl group. On the basis of this result, it appears that the hydrated acidic proton becomes less acidic on interaction with the silica support. The result is consistent with microcalorimetric studies by Kapustin *et al.*[13] where 80% of the acid sites in unsupported, hydrated $H_3[PW_{12}O_{40}]$ were found to become weaker when supported on silica.

The ^{13}C CPMAS NMR spectrum recorded from $H_3[PW_{12}O_{40}]\cdot 6H_2O$ supported on silica and treated with isotopically-labelled acetone is shown in Figure 7.9. There is a reduction in signal-to-noise ratio due to the smaller amount of the solid acid available for acetone adsorption.

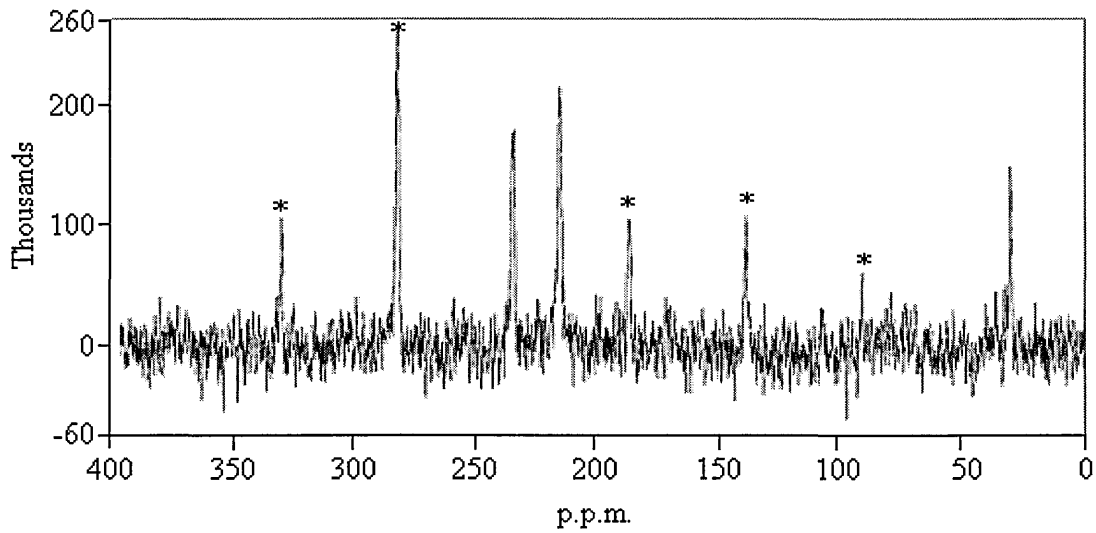

Figure 7.9 ^{13}C CPMAS NMR recorded from isotopically-labelled acetone adsorbed on to silica-supported $H_3[PW_{12}O_{40}]\cdot 6H_2O$. Spinning sidebands denoted by (*).

Once again there is an increase in the sideband intensity of the resonance occuring in the region of 235 ppm and the resonance observed in the region of 215 p.p.m does not have a sideband manifold. Table 7.7 compares the ^{13}C chemical shift values from this spectrum with those derived from the corresponding CPMAS NMR experiment for the unsupported hexahydrate. Overall, the results indicate that the isolated acidic proton still has restricted mobility, coupled with reduced acidity, when the hexahydrate is supported on silica. Analysis of the spinning sideband pattern for the resonance associated with the isolated acidic proton gives a value of 0.45 for the asymmetry parameter : a value the same as that observed for the unsupported 12-phosphotungstic acid. This indicates that the adsorption of acetone by the acid is not influenced by the presence of the silica support.

Table 7.7 Comparison of resonances observed in the ^{13}C CPMAS NMR spectra recorded from bulk and silica-supported acetone treated $H_3[PW_{12}O_{40}]\cdot 6H_2O$.

Compound	**^{13}C CPMAS NMR data / ppm (± 0.4)**		
	$C{=}O^{+}\text{-}H_{isolated}$	$C{=}O^{+}\text{-}H_{hydrated}$	Methyl group
$H_3[PW_{12}O_{40}]\cdot 6H_2O$	235.1	217.9	31.1
$H_3[PW_{12}O_{40}]\cdot 6H_2O/SiO_2$	235.1	215.4	30.1

On adsorption of acetone on to silica-supported $H_4[SiW_{12}O_{40}]\cdot 6H_2O$ or the hexahydrate of the silica-supported $H_4[SiW_{12}O_{40}]/H_3[PW_{12}O_{40}]$ (1 : 1) mixed compound, only resonances corresponding to the hydrated acidic proton were observed in both the ^{13}C MAS and CPMAS NMR spectra. The lack of resonances

corresponding to the isolated acidic proton for these two samples is most likely a result of insufficient acetone adsorbed on to the acid sites. It is not clear whether longer adsorption periods would resolve this problem or lead to unwanted side reactions involving acetone.

The ^{13}C chemical shift values recorded from silica-supported $H_4[SiW_{12}O_{40}]\cdot 6H_2O$ and the hexahydrate of the silica-supported $H_4[SiW_{12}O_{40}]/H_3[PW_{12}O_{40}]\cdot 6H_2O$ (1 : 1) mixed compound are shown in Table 7.8. For comparison, results for silica-supported $H_3[PW_{12}O_{40}]\cdot 6H_2O$ are also included in this table.

Table 7.8 Comparison of ^{13}C chemical shift values observed from ^{13}C MAS NMR spectra recorded from isotopicaly-labelled acetone adsorbed on silica-supported $H_4[SiW_{12}O_{40}]\cdot 6H_2O$, $H_3[PW_{12}O_{40}]\cdot 6H_2O$ as well as the mixed compound $H_4[SiW_{12}O_{40}]/H_3[PW_{12}O_{40}]\cdot 6H_2O$ in a 1 : 1 molar ratio.

Compounds	**^{13}C MAS NMR data / ppm (± 0.4)**	
	$C^{\delta+}$=O-$H_{hydrated}$	Methyl group
$H_3[PW_{12}O_{40}]\cdot 6H_2O/SiO_2$	215.4	30.1
$H_4[SiW_{12}O_{40}]\cdot 6H_2O/SiO_2$	215.3	29.9
$H_4[SiW_{12}O_{40}]/H_3[PW_{12}O_{40}]\cdot 6H_2O/SiO_2$ 1 : 1	216.0	30.0

The results show that the ^{13}C resonances recorded from the carbonyl group associated with the hydrated acidic protons of silica-supported $H_3[PW_{12}O_{40}]\cdot 6H_2O$

and $H_4[SiW_{12}O_{40}]\cdot 6H_2O$ are, within experimental uncertainty, identical. The resonance recorded from $H_4[SiW_{12}O_{40}]/H_3[PW_{12}O_{40}]\cdot 6H_2O$ is slightly greater in value than both of the parent 12-heteropolyacids but remains within experimental uncertainty. However, the difference in ^{13}C chemical shift values observed between silica-supported and unsupported 12-heteropolyacid compounds is significant, as shown in Table 7.9. The differences are based on values recorded in ^{13}C MAS NMR experiments. Similar results apply for the ^{13}C CPMAS experiments.

Table 7.9 Comparison of the difference in ^{13}C chemical shift values (recorded in ^{13}C CPMAS experiments) between unsupported and silica-supported 12-heteropolyacid compounds, in the form of hexahydrates.

Compound	**Δ(unsupported - silica-supported) / ppm (± 0.6)**
$H_3[PW_{12}O_{40}]\cdot 6H_2O$	2.8
$H_4[SiW_{12}O_{40}]\cdot 6H_2O$	5.3
$H_4[SiW_{12}O_{40}]/H_3[PW_{12}O_{40}]\cdot 6H_2O$ 1 : 1	4.1

These data indicate that the hydrated acidic protons of $H_4[SiW_{12}O_{40}]\cdot 6H_2O$ are affected to a greater extent, compared to those for $H_3[PW_{12}O_{40}]\cdot 6H_2O$, when these acids are supported on silica. This is possibly as a result of the extra acidic proton present on $H_4[SiW_{12}O_{40}]$, which is not thought to be involved in the structural $H_5O_2^+$ ion.[29] The 1 : 1 mixed compound gives an observed shift difference between that of the two parent 12-heteropolyacids. This suggests that varying the ratio of $H_4[SiW_{12}O_{40}]$ to $H_3[PW_{12}O_{40}]$ could change the acidity of the hydrated acidic proton

when the mixed compound is supported on silica. Although tentative, it is possible to suggest that the increase in activity of the silica-supported $H_4[SiW_{12}O_{40}]/H_3[PW_{12}O_{40}]$ (9 : 1) mixed compound observed by BP Chemicals may be due to a combination of fine-tuning of the acidity (Section 7.3.1.) and of the influence of the silica support.

7.4 Summary

The preparation and characterisation, particularly in terms of acidity, of mixed $H_4[SiW_{12}O_{40}]$ and $H_3[PW_{12}O_{40}]$ compounds has been carried out. Mixed compounds with different molar ratios were simply prepared by the evaporation of appropriate aqueous solutions to yield white crystalline materials. XRD analysis of the hexahydrates of these materials confirmed that they were single phases. The cubic unit cell parameters were found to vary in a non-linear manner with increasing molar ratio of $H_3[PW_{12}O_{40}]\cdot 6H_2O$ to $H_4[SiW_{12}O_{40}]\cdot 6H_2O$. This is interesting behaviour and suggests that the silico- and phospho- based Keggin units are not completely distributed at random in the cubic crystal structure of the mixed compounds. This is an area for further work.

The acidity of the bulk 12-heteropolyacids $H_4[SiW_{12}O_{40}]$ and $H_3[PW_{12}O_{40}]$ in their hexahydrate form has been investigated using isotopically-labelled acetone. Two acid sites were observed for both acids : one characteristic of an isolated acidic proton with restricted mobility and the other characteristic of a mobile hydrated acidic proton. The acidity of the isolated acidic proton was found to be the same in

both cases. However, the acidity of the hydrated acidic proton was found to be greater for $H_4[SiW_{12}O_{40}]$ than $H_3[PW_{12}O_{40}]$.

The fine-tuning of the hydrated acidic proton was attempted using a new approach. The secondary structure of the 12-heteropolyacids, as proposed by Misono[1] (see Chapter 2, Figure 2.10), was modified instead of the primary structure (the Keggin unit). The acidity of the $H_4[SiW_{12}O_{40}]/H_3[PW_{12}O_{40}]$ (1 : 1) mixed compound was found to occur between those of the pure 12-heteropolyacids used to prepare it; although the effect was not large.

When supported on silica, the acidity of the hydrated acidic proton of $H_3[PW_{12}O_{40}]$ was found to decrease in comparison with that of the unsupported acid. However, the acidity of the isolated acidic proton was found to remain the same.

The acidities of the hydrated acidic protons of $H_4[SiW_{12}O_{40}]\cdot 6H_2O$ and the mixed compound $H_4[SiW_{12}O_{40}]/H_3[PW_{12}O_{40}]\cdot 6H_2O$ (1 : 1) were both reduced when supported on silica, as was the case for $H_3[PW_{12}O_{40}]\cdot 6H_2O$. The reduction in acidity of the hydrated acidic protons was found to be in the order $H_4[SiW_{12}O_{40}]$ > $H_4[SiW_{12}O_{40}]/H_3[PW_{12}O_{40}]$ > $H_3[PW_{12}O_{40}]$ for the hexahydrates of these compounds.

References

(1) Misono, M. *Chemical Communications* **2001**, *1*, 1141-1152.

(2) Moffat, J. B. *Metal-Oxygen Clusters*; Kluwer Academic/Plenum Publishers: New York, 2001.

(3) Courtin, M. P.; Chauveau, F.; Souchay, P. *Comptes Rendus Chimie* **1964**, *258*, 1246.

(4) Essayem, N.; Coudurier, G.; Fournier, M.; Vedrine, J. C. *Catalysis Letters* **1995**, *34*, 223-235.

(5) Koyano, G.; Saito, T.; Hashimoto, M.; Misono, M. *Studies in Surface Science and Catalysis* **2000**, *130*, 3077-3082.

(6) Mioc, U. B.; Dimitrijevic, R. Z.; Davidovic, M.; Nedic, Z. P.; Mitrovic, M. M.; Colomban, P. *Journal of Materials Science* **1994**, *29*, 3705-3718.

(7) Vaughan, J. S.; O'Connor, C. T.; Fletcher, J. C. Q. *Journal of Catalysis* **1994**, *147*, 441-454.

(8) Thouvenot, R.; Rocchiccioli-Deltcheff, C.; Fournier, M.; Franck, R. *Inorganic Chemistry* **1983**, *22*, 207-216.

(9) Bielanski, A.; Datka, J.; Gil, B.; Malecka-Lubanska, A.; Micek-Ilnicka, A. *Catalysis Letters* **1999**, *57*, 61-64.

(10) Cheary, R. W.; Coelho, A. A.; deposited in CCP14 Powder Diffraction Library, Engineering and Physical Sciences Research Council, Daresbury Laboratory, Warrington, England. (http://www.ccp14.ac.uk/tutorial/xfit-95/xfit.htm), 1996.

(11) Dong, C.; Wu, F.; Chen, H. *Journal of Applied Crystallography* **1999**, *32*, 850-853.

(12) Laugier, J.; Bochu, B., pp WWW: http://www.inpg.fr/LMGP and http://www.ccp14.ac.uk/tutorial/lmgp/.

(13) Kapustin, G. I.; Brueva, T. R.; Klyachko, A. L.; Timofeeva, M. N.; Kulikov, S. M.; Kozhevnikov, I. V. *Kinetika i Kataliz* **1990**, *31*, 1017-1020.

(14) Yang, J.; Janik, M. J.; Ma, D.; Zheng, A. M.; Zhang, M. J.; Neurock, M.; Davis, R. J.; Ye, C. H.; Deng, F. *Journal of the American Chemical Society* **2005**, *127*, 18274-18280.

(15) Biaglow, A. I.; Gorte, R. J.; Kokotailo, G. T.; White, D. *Journal of Catalysis* **1994**, *148*, 779-786.

(16) Biaglow, A. I.; Gorte, R. J.; White, D. *Journal of Physical Chemistry* **1993**, *97*, 7135-7137.

(17) Biaglow, A. I.; Gorte, R. J.; White, D. *Journal of Catalysis* **1994**, *150*, 221-224.

(18) Biaglow, A. I.; Sepa, J.; Gorte, R. J.; White, D. *Journal of Catalysis* **1995**, *151*, 373-384.

(19) Haw, J. F.; Nicholas, J. B.; Xu, T.; Beck, L. W.; Ferguson, D. B. *Accounts of Chemical Research* **1996**, *29*, 259-267.

(20) Ganapathy, S.; Fournier, M.; Paul, J. F.; Delevoye, L.; Guelton, M.; Amoureux, J. P. *Journal of the American Chemical Society* **2002**, *124*, 7821-7828.

(21) Kozhevnikov, I. V.; Sinnema, A.; Vanbekkum, H. *Catalysis Letters* **1995**, *34*, 213-221.

(22) Lee, K. Y.; Mizuno, N.; Okuhara, T.; Misono, M. *Bulletin of the Chemical Society of Japan* **1989**, *62*, 1731-1739.

(23) Janik, M. J.; Campbell, K. A.; Bardin, B. B.; Davis, R. J.; Neurock, M. *Applied Catalysis A - General* **2003**, *256*, 51-68.

(24) Xu, T.; Munson, E. J.; Haw, J. F. *Journal of the American Chemical Society* **1994**, *116*, 1962-1972.

(25) Brown, G. M.; Noespirlet, M. R.; Busing, W. R.; Levy, H. A. *Acta Crystallographica Section B - Structural Science* **1977**, *33*, 1038-1046.

(26) Barich, D. H.; Nicholas, J. B.; Xu, T.; Haw, J. F. *Journal of the American Chemical Society* **1998**, *120*, 12342-12350.

(27) Izumi, Y.; Hasebe, R.; Urabe, K. *Journal of Catalysis* **1983**, *84*, 402-409.

(28) Liu-Cai, F. X.; Sahut, B.; Faydi, E.; Auroux, A.; Herve, G. *Applied Catalysis A - General* **1999**, *185*, 75-83.

(29) Kozhevnikov, I. V. *Catalysts for Fine Chemical Synthesis: Catalysis by Polyoxometalates*; John Wiley & Sons Ltd: West Sussex, 2002.

Chapter 8

Summary

8.1 12-Silicotungstic acid

The dehydration of the 12-heteropolyacid $H_4[SiW_{12}O_{40}]\cdot xH_2O$ has been investigated in detail using thermal analysis, XRD, ^{29}Si MAS NMR spectroscopy and FT-IR spectroscopy in the temperature range 25 - 900°C as the main characterisation techniques.

Three hydrated single phases with x = 24, 14 and 6 and an anhydrous phase are present in the temperature range 25 - 400°C. Decomposition of the anhydride $[SiW_{12}O_{38}]$ occurs at 550°C. The unit cells for x = 0, 6, 14 and 24 hydrates were determined by X-ray powder diffraction to be rhombohedral, cubic, triclinic and orthorhombic, respectively. XRD patterns recorded from hydrated phases occurring between two single phases could be interpreted in terms of mixtures of these phases.

A single, sharp, ^{29}Si resonance characteristic of the presence of a single silicon environment is observed in each single hydrated phase. Dehydration of $H_4[SiW_{12}O_{40}]\cdot 6H_2O$ to give the anhydrous form resulted in a 3.6 ppm shift of $\delta(^{29}Si)$ to high frequency.

No effect on the characteristic vibrations associated with the Keggin anion in the FT-IR fingerprint region was observed for the dehydration of $H_4[SiW_{12}O_{40}]\cdot xH_2O$. Vibrations characteristic of zeolitic type water molecules (3510 and 1620 cm^{-1}) were shown to decrease in intensity as x was reduced from 24 to 6. Further dehydration to x = 0 resulted in the loss of absorptions corresponding to water molecules interacting with acidic protons (3300 and 1720 cm^{-1}).

A more in depth study of the absorption process of anhydrous 12-silicotungstic acid would be of interest. However, this would require an environment allowing the gradual, quantitative and reproducible addition of water.

It would also be of direct interest to study any differences in the hydration and dehydration processes undergone by 12-silicotungstic acid using wide angle X-ray scattering (WAXS), for example. The recording of diffraction patterns on a timescale of seconds would allow detailed analysis of both processes. This type of investigation has not been carried out before, either for 12-silicotungstic acid or its analogues.

8.2 Silica-supported 12-silicotungstic acid

12-Silicotungstic acid has been shown to remain structurally unchanged and well-dispersed on the silica support on the basis of ^{29}Si MAS NMR and FT-IR spectroscopy results. However, a chemically distinct interfacial $H_4[SiW_{12}O_{40}]$ species is identified by XPS and is attributed to perturbed tungsten atoms within those Keggin anions in direct contact with the silica-support. The most extensive interactions were observed at low loadings.

XRD patterns characteristic of $H_4[SiW_{12}O_{40}]\cdot xH_2O$ (where x = 14, 6 and 0) have been observed on the silica support by varying the preparation method. However, broadening of the diffraction peaks is observed indicating a distinct reduction in the size of the crystallites; for example, for the hexahydrate a reduction from 89 nm (±4 nm) to 10 nm (±0.5 nm) is noted when supported on silica.

8.3 Coking and regeneration of silica-supported 12-silicotungstic acid

Two used catalysts have been characterised in an effort to gain information relevant to the deactivation of the catalyst and the extraction of valuable 12-silicotungstic acid. The used catalysts JM3 (which had a 1.5 year uneventful lifetime) and JM2 (which underwent a significant deactivation during its lifetime) were studied. TGA and DTA studies carried out under flowing air revealed two forms of coke deposited on JM2 and JM3 : hard and soft coke. The quantity of hard coke present on JM2 was found to be significantly higher than that found on JM3 (11.5 and 3% respectively). The removal of soft coke (TGA removal range 170-370°C) was achieved using dichloromethane extraction. Further extraction of both the catalysts by aqueous methods resulted in the removal of 12- silicotungstic acid which had been 'trapped' by the soft coke. However, 12-silicotungstic acid was still present on both JM2 and JM3 after the extraction process. Removal of hard coke was thus carried out using aerobic oxidation at 400°C. The majority of hard coke present on both JM2 and JM3 was oxidised after 6 hours heating. Following heat treatment, extraction by aqueous methods resulted in the removal of all 12-silicotungstic acid which was previously insoluble.

8.4 Mixed 12-heteropolyacid compounds

Fine-tuning of the acidity of the 12-heteropolyacid compounds was carried out through modification of the secondary structure of 12-heteropolyacids. The 12-silico- and 12-phospho-tungstic acids have been mixed in various ratios and shown to form a single phase compound. XRD analysis of these compounds found a

non-linear increase in cubic unit cell parameter as the percentage of 12-phosphotungstic acid was increased. This suggests that the distribution of the two types of Keggin anion in the mixed compound is not entirely random.

The preparation of further mixed compounds with different molar ratios to those already prepared would be useful to establish in more detail the exact form of the non-linear increase in cubic unit cell parameter with change in molar ratio. This experimental information would then form a basis to develop and evaluate structural models for the distribution of the different Keggin anions in the mixed structure.

8.5 Acidity of unsupported and silica-supported 12-heteropolyacids

Acidic strength and sites of silica-supported and non-supported hexahydrates of $H_4[SiW_{12}O_{40}]$, $H_3[PW_{12}O_{40}]$ and $H_4[SiW_{12}O_{40}]/H_3[PW_{12}O_{40}]$ in a 1 : 1 molar ratio have been studied using solid state ^{13}C NMR experiments for isotopically-labelled acetone adsorbed onto the compounds. Two acidic sites were found to exist in each of the solid acids under investigation. These sites were attributed to isolated (restricted mobility) and hydrated (mobile) acidic protons. The acidity of the isolated acidic proton was found to be the same for each of the solid acids, whereas the acidity of the hydrated acidic proton was found vary slightly.

The acidity of the hydrated acidic proton of $H_3[PW_{12}O_{40}]\cdot 6H_2O$ was found to decrease when the acid was supported on silica. The acidity of the isolated acidic proton, however, was found to remain the same. The hydrated acidic protons of $H_4[SiW_{12}O_{40}]\cdot 6H_2O$ and $H_4[SiW_{12}O_{40}]/H_3[PW_{12}O_{40}]\cdot 6H_2O$ (1 : 1) were also found to

have a reduced acidity when supported on silica. The difference in acidity between unsupported and silica-supported 12-heteropolyacids was found to increase in the order $H_4[SiW_{12}O_{40}]$ > $H_4[SiW_{12}O_{40}]/H_3[PW_{12}O_{40}]$ > $H_3[PW_{12}O_{40}]$ for the hexahydrates.

It would be of interest to carry out isotopically-labelled acetone adsorption experiments on silica-supported and non-supported $H_4[SiW_{12}O_{40}]/H_3[PW_{12}O_{40}]$ mixed compounds with varying ratios of the two acids. This could lead to the ratio of the two 12-heteropolyacids being optimised such that the reduction of acidity when supported on silica is minimised and the acidity of the hydrated acidic proton maximised.

It can also be noted that fine-tuning of the hydrated acidic proton by changing the secondary structure of 12-heteropolyacids need not be limited to mixing two different Keggin anions. Three or more heteropolyacids could be combined to alter the acidity of the proton. Modified Keggin anions such as $H_5[PW_{10}V_2O_{40}]$ could also be mixed with non-modified 12-heteropolyacids or Keggin anions modified differently.